10/6-6-96 95 (1)

AIM

Advanced Industrial Materials (AIM) Program
Office of Industrial Technologies
Energy Efficiency and Renewable Energy
U.S. Department of Energy (DOE)

Advanced Industrial Materials (AIM) Program

Annual Progress Report

FY 1995

Date Published: April 1996

Prepared by the
Oak Ridge National Laboratory
Oak Ridge, Tennessee 37831
managed by
Lockheed Martin Energy Research Corp.
for the
U.S. Department of Energy
under Contract No. DE-AC05-96OR22464

ORNL/TM-13225

Advanced Industrial Materials (AIM) Program
Office of Industrial Technologies
Energy Efficiency and Renewable Energy
U.S. Department of Energy (DOE)

ADVANCED INDUSTRIAL MATERIALS (AIM) PROGRAM

ANNUAL PROGRESS REPORT

FY 1995

Date Published: April 1996

Coordinated by Peter Angelini
Compiled by HSRD\BEIA\Information Management Technology Group
Oak Ridge National Laboratory

TABLE OF CONTENTS

ADVANCED CERAMICS AND COMPOSITES (Continued)

POLYMERS AND BIOBASED MATERIALS

NEW MATERIALS AND PROCESSES

INTRODUCTION

The Advanced Industrial Materials (AIM) Program
Office of Industrial Technologies
Fiscal Year 1995

C. A. Sorrell, Program Manager

In many ways, the Advanced Industrial Materials (AIM) Program underwent a major transformation in Fiscal Year 1995 and these changes have continued to the present. When the Program was established in 1990 as the Advanced Industrial Concepts (AIC) Materials Program, the mission was to conduct applied research and development to bring materials and processing technologies from the knowledge derived from basic research to the maturity required for the end use sectors for commercialization. In 1995, the Office of Industrial Technologies (OIT) made radical changes in structure and procedures. All technology development was directed toward the seven "Vision Industries" that use about 80% of industrial energy and generated about 90% of industrial wastes. These are:

- Forest Products
- Steel
- Aluminum
- Metal Casting
- Chemicals
- Refineries
- Glass

OIT is working with these industries, through appropriate organizations, to develop Visions of the desired condition of each industry some 20 or 25 years in the future and then to prepare Road Maps and Implementation Plans to enable them to reach their goals.

Recently, we began working with the forging, heat treating, and welding industries, which are cross-cutting industries to the seven. Each industry has decided to go through the process to develop a vision, road map, and implementation plan and OIT is working on ways to integrate them into the Industries of the Future, even though there will not be specific budget lines for them. We are pleased to have a part in this effort.

The mission of AIM has, therefore, changed to "Support development and commercialization of new or improved materials to improve productivity, product quality, and energy efficiency in the major process industries." Though AIM remains essentially a National Laboratory Program, it is essential that each project have industrial partners, including suppliers to, and customers of, the seven industries. Now, well into FY 1996, the transition is nearly complete and the AIM Program remains reasonably healthy and productive, thanks to the superb investigators and Laboratory Program Managers.

We were fortunate to have the foresight to begin the transition in 1993 when, at the suggestion of the AIM Guidance and Evaluation Board, we began to develop assessments of materials needs and opportunities, beginning with the pulp and paper industry, following with the glass industry. We are now engaged in assessments of the metal casting and chemical industries. These assessments identified real needs of these industries and we have been able to follow through with several new projects. In FY 1996, we can honestly say that every project addresses a need identified by one or more of the seven industries. The challenge to retain the cross-cutting benefits of materials not only remains, but is even more important now than before the changes in OIT. All seven industries understandably have identified materials as important, particularly for high temperature strength, corrosion resistant, and wear resistance and there are many common aspects to these industry needs that can best be addressed by a true cross-cutting materials program.

The same can be said of combustion, catalysts, separations, and sensors and controls, which also require materials development. Major advances in commercialization of new materials were made in 1995 and continue into 1996, particularly in iron and nickel aluminides and molybdenum disilicide, which are being tested in production environments of all seven industries, where they are proving to have remarkable high temperature fatigue resistance, strength, and corrosion resistance. Principal investigators for all the other projects are making excellent progress in the same direction. So far, we have been able to continue support for some of the more basic aspects of materials development that are required for applications engineering and development of new applications. This will become increasingly more difficult as budgets decrease and more funding is earmarked for specific industries, with rapid commercialization or near term problem solving as the major emphases.

This Annual Report for FY 1995 contains the technical details of some very remarkable work by the best materials scientists and engineers in the world. It is hoped that this introduction places that work in the proper context and adequately describes the challenges facing AIM over the next few years. Congratulations from the Program Manager to those who have actually done real work and made him look good.

ADVANCED METALS AND COMPOSITES

ADVANCED ORDERED INTERMETALLIC ALLOY DEVELOPMENT

C. T. Liu, P. J. Maziasz, J. H. Schneibel and D. S. Easton

Metals and Ceramics Division
Oak Ridge National Laboratory
P. O. Box 2008, Oak Ridge, TN 37831

INTRODUCTION

The need for high-strength, high-temperature, and light-weight materials for structural applications has generated a great deal of interest in ordered intermetallics, particularly in γ-based titanium aluminides. γ-based TiAl alloys offer an attractive mix of low density (~ 4g/cm^3), good creep resistance, and high-temperature strength and oxidation resistance. For rotating or high-speed components, TiAl also has a high damping coefficient which minimizes vibrations and noise. These alloys generally contain two phases, α_2 ($D0_{19}$ structure) and γ ($L1_0$), at temperatures below 1120°C, the eutectoid temperature. The mechanical properties of TiAl-based alloys are sensitive to both alloy compositions and microstructure. Depending on heat-treatment and thermomechanical processing, microstructures with near equiaxed γ, a duplex structure (a mix of the γ and α_2 phases) or a lamellar structure (mixtures of alternating plates of the γ and α_2 phases) can be developed in TiAl alloys containing 45 to 50 at. % Al. The major concern for structural use of TiAl alloys is their low ductility and poor fracture resistance at ambient temperatures. The purpose of this work is to improve the fracture toughness of TiAl-based alloys by controlling alloy composition, microstructure and thermomechanical treatment. This work is expected to lead to the development of TiAl alloys with significantly improved fracture toughness and tensile ductility for structural use.

TECHNICAL PROGRESS - FY 1995

Summary

1. Alloy Preparation and Fabrication:

Table 1 lists the alloy compositions and hot extrusion conditions of the TiAl alloys used in this study. The base composition Ti-47Al-2Cr-2Nb (at. %) was alloyed with 0.15 B, 0.2 W, and/or 0.3 Si. The boron and tungsten additions were added for refining *lamellar* structure and improving its stability. Tungsten and silicon were reported to have the beneficial effect of enhancing high-temperature properties and oxidation resistance. The five alloys containing 46 to 48 at. % Al were prepared by arc melting and drop casting into a copper mold (1" diam × 5" long), using high-purity charge materials. The alloy ingots were then canned in molybdenum billets and hot extruded at temperatures above T_α (the α transus temperature = 1320°C for Ti-47Al-2Cr-2Nb alloy). All alloys were successfully hot extruded, except that the alloy TIA-22 containing silicon had porosities in the extruded rod.

Table 1. Alloy Composition and Hot Extrusion Condition of TiAl Alloys

Alloy No.	Alloy Composition (at. %)	Hot Extrusion Temp (°C)[+]
TIA-20	Ti-47Al-2Cr-2Nb-0.15B	T_1
TIA-21	Ti-47Al-2Cr-1.8Nb-0.2W-0.15B	T_1
TIA-22	TI-47Al-2Cr-1.8Nb-0.2W-0.3Si-0:15B	T_1
TIA-23	Ti-46Al-2Cr-2Nb-0.15B	T_2
TIA-24	Ti-48Al-2Cr-2Nb-0.15B	T_2

[+] $T_2 > T_1 > T_\alpha$

2. Microstructural Features:

The cast alloy ingots of the five TiAl alloys (Table 1) were annealed for 1 h at 1400°C, followed by furnace cooling in a vacuum furnace. This heat treatment produced a nearly fully lamellar structure with a coarse grain size (~600 μm). Small equiaxed grains

are occasionally observed at lamellar colony boundaries. All the alloy ingots were successfully hot extruded at T_1 and T_2 above $T\alpha$ (i.e., $T_2>T_1>T\alpha$) without difficulty. Microcracks as well as cavities (located essentially at the ingot center) were observed mainly in the hot extruded TIA-22 but not noticeable in other alloys. It is believed that these defects originate in the cast ingot and that the silicon addition, even at a level of 0.3 at. %, has a detrimental effect on the castability of TiAl-base alloys.

The microstructure of the hot-extruded TiAl alloys in the as-extruded conditions and in the stress-relieved condition (2 h/900°C) was examined. The stress relief at 900°C did not cause any significant change in the optical microstructures. The hot extrusion at T_1 produced near full lamellar structures, with some equiaxed grains existing at colony boundaries. On the other hand, the hot extrusion of TIA-23 and -24 at T_2 resulted in a much smaller amount of equiaxed grains at colony boundaries.

The hot extruded alloys were heated below and above $T\alpha$(~1320°C) for 2 h in order to control lamellar features (such as colony size, grain-boundary equiaxed grains, interlamellar spacing, etc.) in these materials. Table 2 compares the grain size of the TIA alloys heat treated at 1320 and 1350°C. The heat treatment for 2 h at 1320°C (~$T\alpha$) gives a grain size of 30 to 33 μm for TIA-20, -21, and -24, 74 μm for TIA-22, and 258 μm for TIA-23. An increase in temperature from 1320 to 1350°C (i.e., 30°C increment) causes a sharp increase in grain size (by a factor of 5 to 8), as indicated in Table 2.

Table 2. Grain Size (μm) of TIA-20 to -24 in Hot Extruded (HE) and Heat Treated Conditions

Hot Extrusion at T_1			Hot Extrusion at T_2	
TIA-20	-21	-22	TIA-23	-24
(1) HE + 2 h/900°C				
			22	23
(2) HE + 2 h/1320°C				
33	31	74	258	30
(3) HE + 2 h/1350°C				
182	150	610		

Microstructural features in TIA-20 and -21 extruded at T_1 and stress relieved for 2 h at 900°C were examined by TEM. The hot extrusion at T_1 resulted in about 80 to 90% larger colonies that are fully lamellar, with 10 to 20% intercolony regions being a finer duplex structure. As shown in Table 3, the lamellar structure is quite non-uniform, with some grains having interlamellar spacing closer to 140 nm and others having a coarser spacing of about 325 nm in TIA-20. This difference is caused primarily by twinning within larger γ laths (i.e., γ/γ twin boundaries). The α_2-α_2 spacing also varies from area to area, but not as much (see Table 3). The heat treatment for 2 h at 1320°C coarsens the lamellar structure (Fig. 1) by about a factor of two and also eliminates the duplex structure along the intercolony boundaries. TIA-21 has a more uniform fine lamellar structure within the colonies, and some intercolony γ, but no duplex material. The heat treatment of 2 h at 1320°C also coarsened the lamellar structure of TIA-21, but not as much as it did for TIA-20.

Fig. 1a

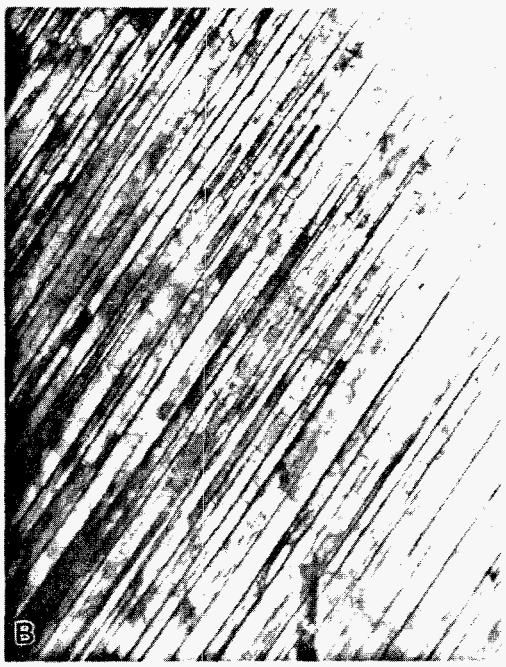

Fig. 1b

Fig. 1c

Fig. 1d

Fig. 1 The lamellar structure of larger colonies in as-extruded (a) TIA-20 and (b) TIA-21, both given a stress-relief heat-treatment of 2 h at 900°C, and (c) and (d) of those same alloys, respectively, given a heat-treatment of 2 h at 1320°C, which coarsens the lamellar structure significantly.

Table 3. Quantitative Lamellar Microstructural Data on Extruded and Stress-Relieved TiAl Alloys (all in nm)

Alloy/HT	Interlamellar Spacing	α_2-α_2 Spacing	γ-Width	α_2-Width
TIA-20				
2 h/900°C	140-325	400-500	95-870	30-60
2 h/1320°C	440	1000	160-1250	53-265
TIA-21				
2 h/900°C	160	460-500	74-635	21-53
2 h/1320°C	300	800	290-1100	53-210

3. Tensile Properties:

Mechanical properties are reported for TIA-20, -21, -23, and -24, but not for TIA-22. This is because TIA-22 alloy contains cast defects (cavities and microcracks) that cause

a large scattering of tensile data, particularly at room temperature. Table 4 lists the tensile data for TIA alloys hot extruded and stress relieved for 2 h at 900°C. TIA-23 and -20 alloys containing 46 to 47 % Al without W have the best tensile ductility at room temperature. TIA-23 with a refined fully lamellar structure (22 μm colony size) exhibited a room temperature tensile ductility of 5.5%, the highest tensile ductility ever reported for TiAl alloys with a fully lamellar structure. Comparison of the tensile data for TIA-20 and -21 hot extruded at T_1 indicates that adding tungsten at a level of 0.2% lowers the room-temperature elongation of the TiAl alloys.

Figure 2 compares the tensile properties for TIA-20 and -21 with a near fully lamellar structure produced by hot extrusion at T_1. The plot clearly shows that alloying with 0.2% W increases the yield strength (as well as tensile strength in Table 4) but lowers the tensile elongation at all tested temperatures. The tungsten addition actually reduces the tensile ductility of TIA-20 to about half at 800 and 1000°C. Figure 3 compares the tensile properties for TIA-23 and -24 with a fully lamellar structure produced by hot extrusion at T_2. This comparison shows that TIA-23 with 46% Al is significantly stronger at all test temperatures and more ductile at room temperature than those of TIA-24 with 48% Al. The

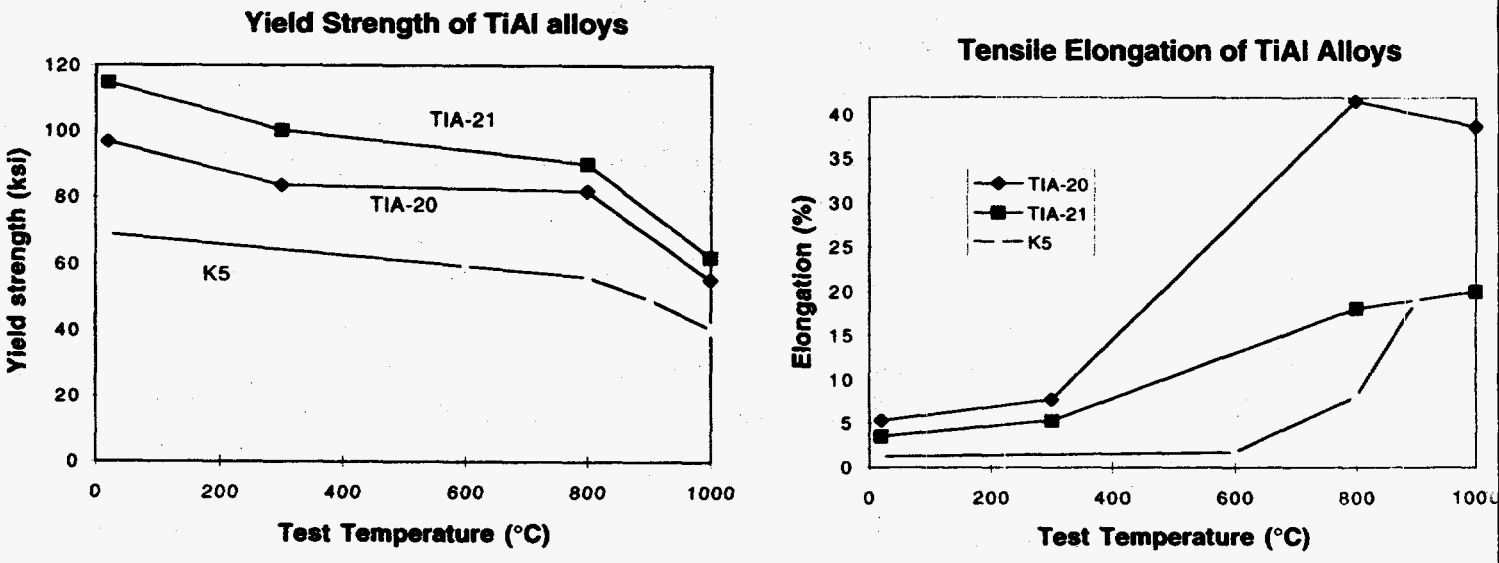

Fig. 2. Comparison of tensile properties of T_1 hot-extruded alloys TIA-20 and -21 with thermomechanically treated alloy K5 (Ti-46.5Al-2.1Cr-3Nb-0.2W at. %).

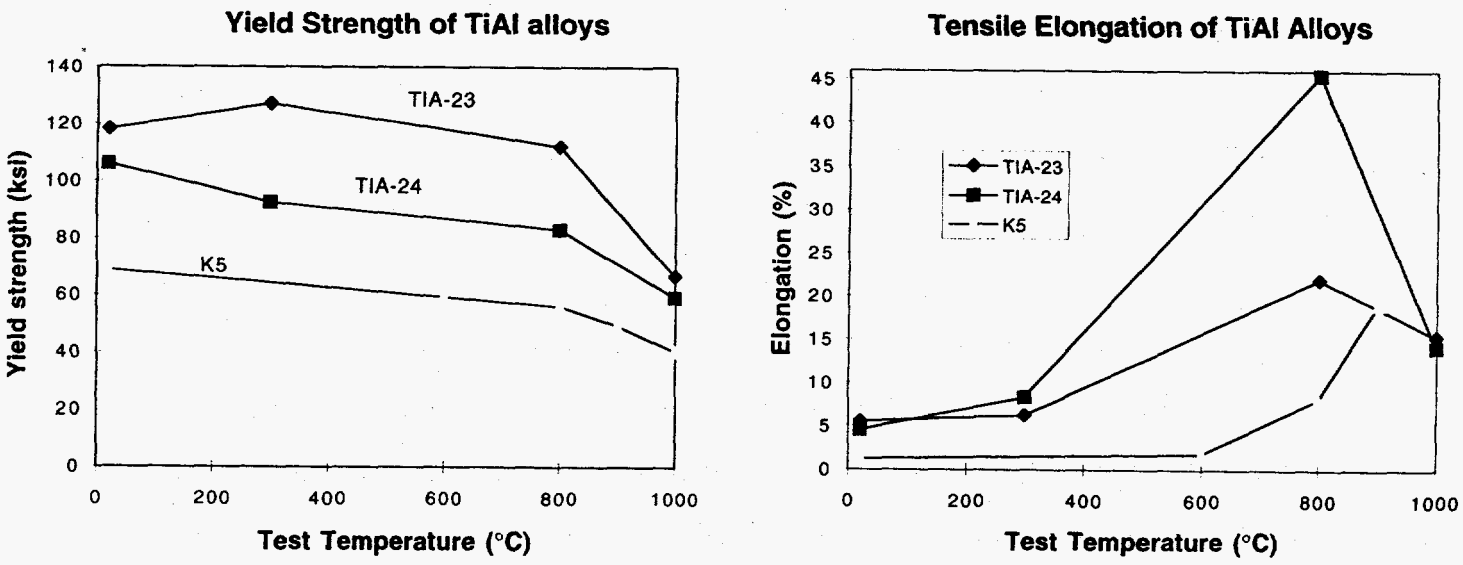

Fig. 3. Comparison of T_2 hot-extruded alloys TIA-23 and -24 with thermomechanically treated alloy K5 (Ti-46.5Al-2.1Cr-3Nb-0.2W at. %).

Table 4. Tensile Properties of Cast and Hot Extruded TiAl Alloys*
Tested in Air at a Strain Rate of 4.4×10^{-3}/min

Test Temperature (°C)	Yield Strength (MPa)	Ultimate Tensile Strength (MPa)	Tensile Elongation (%)
TIA-20: Ti-47Al-2Cr-2Nb-0.15B (HE/ T_1+ 900°C/2 h)			
RM	666(96.6)	844(123)	5.3
300	589(85.5)	816(118)	7.7
800	563(81.7)	639(92.8)	41.6
1000	380(55.1)	416(60.4)	38.6
TIA-21: Ti-47Al-2Cr-1.8Nb-0.2W+0.15B (HE/ T_1+ 900°C/2 h)			
RM	791(115)	915(133)	3.5
300	690(100)	887(129)	5.3
800	619(89.9)	735(107)	18.1
1000	426(61.9)	461(66.9)	20.0
TIA-23: Ti-46Al-2Cr-2Nb+0.15B (HE/ T_2 + 2 h/900°C)			
RM	811(118)	1010(146)	5.5
300	873(127)	1070(155)	6.2
800	774(112)	927(135)	21.9
1000	459(66.6)	497(72.2)	15.3
TIA-24: Ti-48Al-2Cr-2Nb+0.15B (HE/ T_2 + 2 h/900°C)			
RM	732(106)	884(128)	4.5
300	637(92.5)	866(126)	8.3
800	572(83.0)	721(104.6)	45.5
1000	407(59.1)	455(66.0)	14.1

*Stress relieved for 2 h at 900°C

data in Table 4 suggest that the alloys with a fully lamellar structures (TIA-23 and -24) are stronger than the alloys with near fully lamellar structures (TIA-20 and -21) at all test temperatures. The alloys with the fully lamellar structures show a maximum ductility around 800°C.

Table 5 lists the tensile data for TIA alloys hot extruded and heat treated at 1320°C. As compared with the data in Table 4 for hot extruded and stress relieved (2 h/900°C) materials, this heat treatment lowers the tensile strength of the alloys at room temperature and 1000°C. It also decreases the tensile ductility of hot extruded materials at room temperature, with the maximum decrease observed for TIA-23 (a decrease from 5.5 to 2.2%). The 1320°C treatment appears not to affect the 1000°C ductility of TIA-20, but substantially improves the 1000°C ductility of TIA-21, -23 and -24.

Table 5. Tensile Properties* of Cast and Hot Extruded TiAl Alloys Heat Treated for 2 h at 1320°C

Test Temperature (°C)	Yield Strength (MPa)	Ultimate Tensile Strength (MPa)	Elongation (%)
TIA-20 (HE/T_1)			
RM	500(72.6)	648(94.0)	4.5
1000	294(42.6)	314(45.6)	34.4
TIA-21 (HE/T_1)			
RM	545(79.1)	661(96.4)	3.2
1000	300(43.5)	336(48.8)	33.1
TIA-23 (HE/T_2)			
RM	532(77.2)	571(82.9)	2.2
1000	413(60.0)	448(65.2)	41.2
TIA-24 (HE/T_2)			
RM	545(79.1)	666(96.7)	3.5
1000	332(48.2)	352(51.1)	36.0

*Tested in air at a strain rate of 4.4×10^{-3}/min.

Table 6. Fracture Toughnesses Determined by Three-Point Bend Testing of Chevron-Notched TiAl Specimens

Specimen Number	Processing*	Fracture Toughness K_Q (MPa $m^{1/2}$)
TIA-20	Cast + 2h/1320°C	37.3
TIA-20	Cast + 2h/1350°C	45.2
TIA-21	Cast + 2h/1320°C	28.3
TIA-21	Cast + 2h/1350°C	50.4
TIA-20	HE + 2h/1320°C	52.3
TIA-20	HE + 2h/1350°C	60.9
TIA-21	HE + 2h/1350°C	43.0
TIA-21	HE + 2h/1320°C	26.3
TIA-23	HE + 2h/900°C	29.9
TIA-23	HE + 2h/1320°C	57.3

*HE=hot extrusion

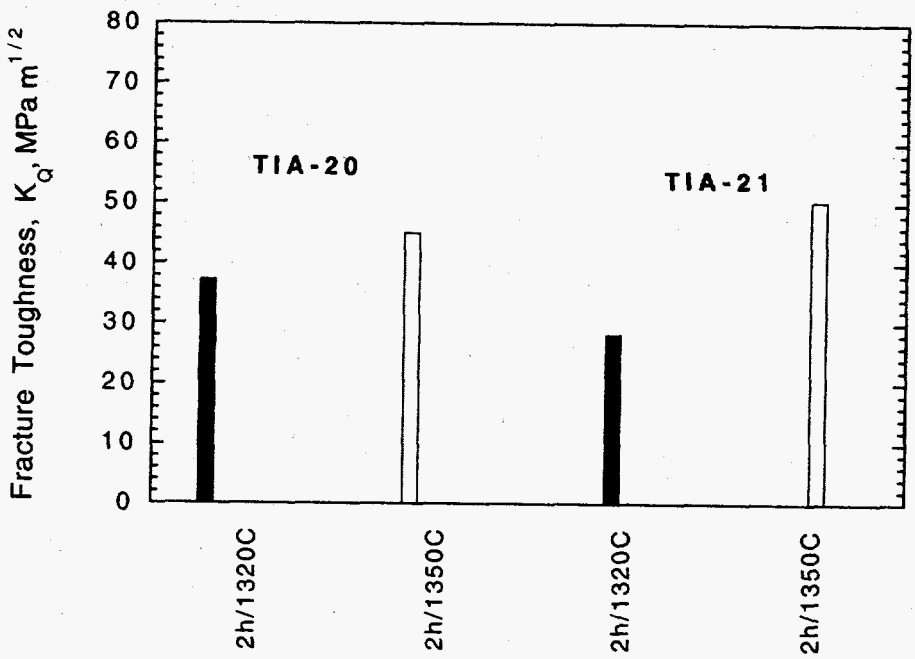

Fig. 4. Fracture toughness of cast TiAl alloys heat treated at 1320 or 1350°C for 2 h.

results than annealing at 1320°C. The data shows also that the heat treatment temperature is very critical, since a temperature increase of only 30°C may increase the fracture toughness

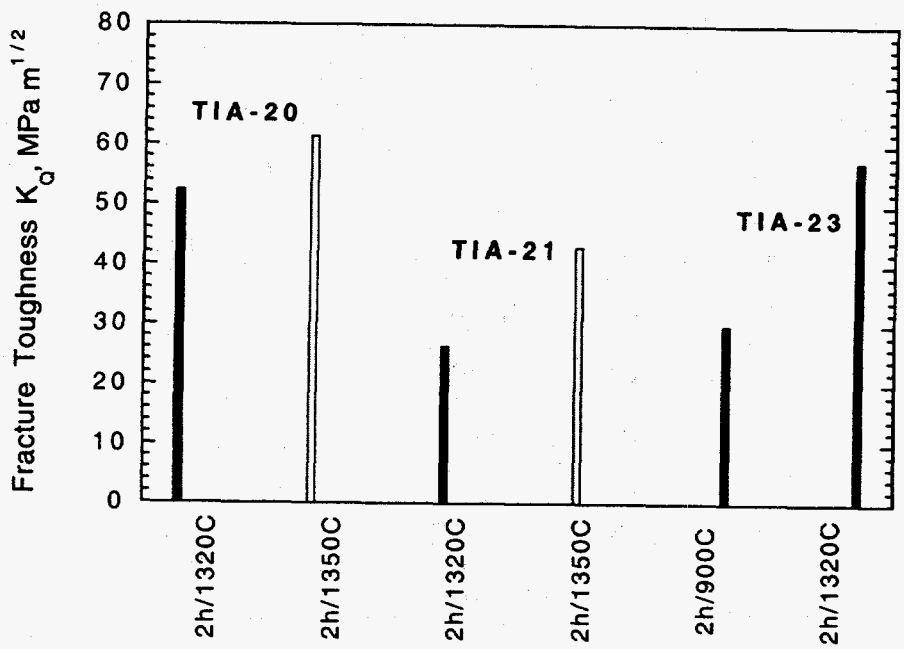

Fig. 5. Fracture toughness of hot extruded TIA alloys heat treated at 900 to 1350°C for 2 h.

by about 80% (alloy TIA-21). Figure 6 shows corresponding results for hot extruded materials. Extrusion of TIA-20 improves its fracture toughness. The tungsten-containing TIA-21 is relatively brittle, suggesting that W additions may have an embrittling effect. TIA-23 annealed at 1320°C is somewhat tougher than TIA-20 annealed at the same temperature. If the extruded TIA-23 is only annealed at 900°C, it still has a reasonably high fracture toughness of 30 MPa $m^{1/2}$.

The TiAl alloys fracture typically transgranularly at room temperature. This is illustrated in Fig. 6a, which shows the lamellar structure of extruded TIA-23 annealed for 2 h at 900°C. As seen in Fig. 6b, annealing extruded TIA-23 for 2 h at 1320°C increases the colony size significantly, from roughly 20 to 260 μm. Figure 7b shows also profuse γ/γ delamination perpendicular to the fracture surface. This delamination absorbs energy and significantly contributes to the increase in the fracture toughness caused by heat treating at 1320°C as opposed to 900°C (see Fig. 5).

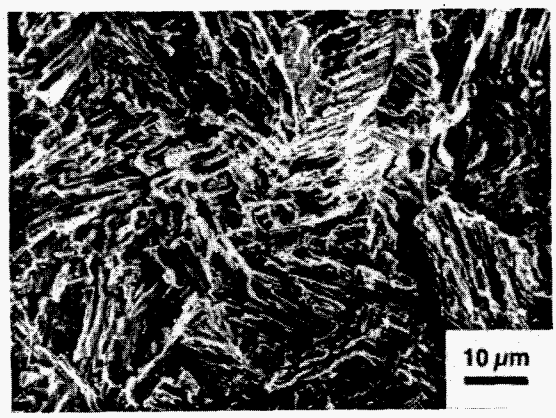

Fig. 6a

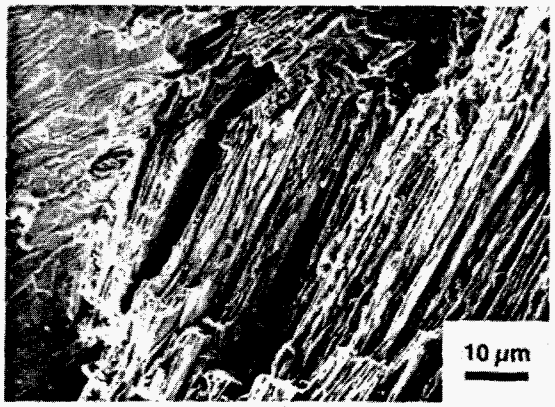

Fig. 6b

Fig. 6. Fracture surfaces of extruded TIA-23 annealed for (a) 2 h/900°C and (b) 2 h/1320°C.

MILESTONES DURING FY 1995

Milestone "modify TiAl alloys and evaluate correlation between fracture toughness and microstructure and prepare a draft report" was completed in August 1995. The abstract of the report "Tensile Property and Fracture Toughness of TiAl Alloys with Controlled Microstructures" is given below.

The objective of this study is to improve the mechanical properties by careful control of both microstructure and alloy additions in two-phase TiAl alloys based on Ti-47Al-2Cr-2Nb (at. %). Hot extrusion at temperatures above T_α produces refined lamellar structures in TiAl alloys, whose microstructural features can be further controlled by subsequent heat treatment at and above 900°C. The mechanical properties of the alloys with lamellar structures depend on three factors: colony size, interlamellar spacing, and alloying additions. The tensile elongation at room temperature is strongly dependent on lamellar colony size, with increasing ductility with decreased colony size. The strength at room and elevated temperatures is sensitive to interlamellar spacing, with increasing strength with decreased colony spacing. Fracture toughness at room temperature can be substantially improved by reheat treatment at 1320 and 1350°C. The tungsten addition at a level of 0.2% improves the tensile strength, whereas the silicon addition at a level of 0.3% reduces the castability of the TiAl alloys. The TiAl materials produced by hot extrusion are much superior to those produced by conventional thermomechanical treatments.

PUBLICATIONS

Journals

1. C.G. McKamey, S.H. Whang, and C.T. Liu, "Microstructural Characterization of a γ-TiAl-Ni Alloy Produced by Rapid Solidification Techniques," *Scr. Metall.*, 32, 383, 1995.

2. C.T. Liu and J.A. Horton, "Effect of Refractory Alloying Additions on Mechanical Properties of Near-Stoichiometric NiAl," *J. Mat. Sci. and Eng.*, A192/193, 170-78, 1995.

3. R.V. Ramanujan, P.J. Maziasz, and C.T. Liu, "The Thermal Stability of the Microstructure of γ-based Titanium Aluminides," accepted for publication in *Acta Metallurgica* (in press).

4. J.A. Horton, C.T. Liu, and E.P. George, "Shape Memory Properties of a Two-Phase NiAl Plus Fe Alloy," *J. Mat. Sci. and Eng.*, A192/193, 873-880, 1995.

Other Publications

1. C.T. Liu and J.O. Stiegler, "Aluminides-Nickel," pp. 1752-60 in *Encyclopedia of Advanced Materials*, ed. M.C. Flemings, Pergamon Press, 1994.

HONORS AND AWARDS

None

PATENTS/DISCLOSURES

None

LICENSES

We started to work on TiAl alloy development in September 1994, and no license agreements have been developed with industries as of yet. Pratt & Whitney, General Electric, Howmet, and Rolls-Royce of America are interested in the ORNL work on alloy development of NiAl. We had a few contacts with these companies for possible joint work on the TiAl development.

INDUSTRIAL INPUT and TECHNOLOGY TRANSFER

Based on our contact with Howmet, Pratt & Whitney, Rolls-Royce of America and other companies, one of a major concern for structural use of TiAl alloys is its poor tensile ductility and fracture toughness at ambient temperatures; in particular, after extensive services at elevated temperatures. Our program has been formulated based on the input from the industries. We are expecting to initiate technology transfer when the toughness problem is solved by this project. P. Angelini and C. T. Liu visited Howmet Corporation to discuss technical corporation and technology transfer with Dr. Neil Paton, Vice President, and his research staff on November 9, 1995. C. T. Liu gave a seminar on "Development of NiAl and TiAl Alloys for Structural Applications" during their visit.

DEVELOPMENT OF WELDABLE, CORROSION-RESISTANT IRON-ALUMINIDE (FeAl) ALLOYS

P.J. Maziasz, G.M. Goodwin, X.L. Wang, V.K. Sikka and D.J. Alexander

Metals and Ceramics Division
Oak Ridge National Laboratory
P.O. Box 2008, Oak Ridge TN 37831

INTRODUCTION

The initial alloy development phase to improve the weldability and mechanical properties (room-temperature ductility, high-temperature strength) of corrosion-resistant FeAl alloys was completed in FY 1994. The FeAl base-alloy for weldability, fabricability and mechanical properties is an Fe-36Al-0.2Mo-0.05Zr-0.13C (at.%) alloy. An optimized FeAl alloy with significantly better weldability and high-temperature strength, and better ductility at room-temperature due to resistance to hydrogen effects at room-temperature, is a boron micro-alloyed modification (100-400 at. ppm) of the base alloy. In FY 1995, this project entered a new industrial technology phase, to produce material suitable for industry testing and component fabrication. Two parallel paths were pursued. One was to explore FeAl coating/cladding technology for conventional structural steels and alloys in need of better corrosion and wear resistance. The other was to explore monolithic FeAl fabrication methods for making specimens or components for industrial testing. Previously, cast and hot-extruded ingot-metallurgy (I/M) FeAl materials were found to have good room- and high-temperature properties. In FY1995, it was further discovered that hot-extruded powder-metallurgy (P/M) FeAl material had outstanding strength, toughness and ductility at room-temperature and above. Industry contacts, particularly those related to DOE/OIT "Vision of the Future" Industries (ie. pulp and paper, glass, metal processing, etc) were made and pursued.

TECHNICAL PROGRESS - FY 1995

Summary

1. FeAl Welding and Weld-Overlay Applications:

FeAl weld consumables from commercial vendors were obtained in FY1994 and 1995, and their weld-

overlay performance on several different kinds of code-approved structural steels and alloys was completed. The compositions of FeAl aspiration-cast wires for shielded-metal-arc (SMA) and gas-tungsten-arc (GTA) welding processes obtained from Haynes International (Kokomo, IN) and others are summarized in Table 1. The results of weld-overlay deposit tests on 2¼Cr-1Mo, 9Cr-1MoVNb, and type 304L steels, including the cold-cracking behavior, for the first four sets of wires from Haynes are also given in Table 1. The FeAl Haynes batch IV-01 wires were selected based on previous weld-overlay test-pad data, and were received and tested during the year. The results were very good, with crack-free weld-deposits being made on all three kinds of steel substrates. Previously, FeAl (FA-385) weld-overlay deposits were made onto thin metal sheets of 253 MA (similar to type 308 austenitic stainless steel) supplied by Rolled Alloys (Temperance, MI). FeAl weld-overlays on thinner-section 253 MA and RA 85H alloys is an application of interest to Rolled Alloys, but this application requires eliminating the post-weld heat-treatment.

To facilitate commercial weld-overlay processes, smaller diameter solid- and powder-cored FeAl wires were ordered from Stoody Company, Bowling Green, KY. They were formulated to match the optimum FeAl alloy deposit compositions (36-39 at.% final FeAl overlay composition) obtained using the aspiration-cast FeAl wires. They were produced in coil form to enable automated gas-tungsten-arc (GTA) and gas-metal-arc (GMA) applications. Initial weld-overlay tests on a 2.25Cr-1Mo steel substrate produced good FeAl weld-deposits similar to those produced with the aspiration-cast wires (see Fig. 1).

Initial joining tests were made on centrifugically-cast FeAl pipes (0.75 in. thick, see following sections) using the Haynes III-01 and VI-01(higher Cr and more Al, intended to compensate for dilution effects on steels), and FAPY (lower Al) weld-wires because they were available. A crack-free joint was only obtained with the FAPY wires thus far. Hot-cutting (>100°C) of the FeAl was necessary to obtain a relatively crack-free surface prior to welding, because some micro-cracks were detectable metallographically in the 0.75 in. thick FeAl pipe. Characterization and process modification for such industrially-produced FeAl components will continue next year. Because processing/heat-treatment significantly affect the room-temperature mechanical

properties of FeAl, joining of FeAl in different metallurgical conditions will be tested. Moreover, the weld-overlay results suggest that dissimilar-metal welds between FeAl and lower-alloy-content steels may also be feasible.

2. P/M FeAl for Monolithic and for Coating Applications:

The FeAl base-alloy (FA-385) composition with good weldability was chosen for P/M studies. A large (400 lb) heat of nitrogen gas-atomized FeAl (FA-385) alloy powder was obtained from AMETEK (Eighty-Four, PA) in FY 1995. The powder was spherical (-100 mesh), with a bimodal size distribution (mainly 75-175 μm particles, with some finer 5-17 μm particles). The powder was consolidated by direct hot-extrusion at 950 to 1100°C to determine its properties for cladding applications. The P/M FeAl extrusions were all found to all be fully dense, but the properties and microstructure depended significantly on the extrusion temperature Fig. 2). PM/FeAl extruded at 1100°C had about 9% ductility, 500 MPa yield-strength (YS) and 930 MPa ultimate-tensile-strength (UTS) when tested at room-temperature in air. P/M FeAl extruded at 950°C had 12.5% ductility, 670 MPa YS and 1100 MPa UTS in air. Ductility of the P/M FeAl extruded at 1100°C was only sightly higher when tested in oxygen, whereas the material extruded at 950°C had almost 30% total elongation (all of it uniform elongation) and a UTS of 1500 MPa! Both these ductility and strength values are the highest ever reported for FeAl type alloys. The P/M FeAl extruded at 950°C was macroscopically more ductile in appearance, and SEM analysis showed a ductile fracture mode relative to the material extruded at 1100°C (Fig. 3).

As a follow-on to these outstanding tensile results, Charpy impact toughness (full-sized) specimens were machined of P/M FA-385. Previous toughness studies of hot-extruded I/M FA-350 (a very similar FeAl alloy) showed impact energies of only 4-5 J at 22-100°C. Charpy impact energies measured at room-temperature were about 105 J for P/M FA-385 extruded at 950°C, 85 J for material extruded at 1000°C and 25 J for material extruded at 1100°C (Fig. 4). The specimens retained their room-temperature levels of

toughness down to about -50°C. The Charpy specimens again a ductile appearance macroscopically after extrusion at 950 and 1000°C, but were more brittle-looking after extrusion at 1100°C (Fig. 5).

Next year, direct hot-extrusion of FeAl powder to produce cladding on type 316 stainless steel or other steel tubing will be tested. Additional heats of FeAl powder (including boron micro-alloying additions) will be ordered. General Electric Corporation (Dr. M. Lee, GE Corp. R&D Center, Schenectady, NY) has P/M FeAl specimens for fretting resistance, cavitation erosion resistance and abrasive wear resistance testing.

In FY 1995, FeAl coatings using thermal spray techniques were also made with the Ametek powder. Thermal spraying was done at the Thermal Spray Technology Center/Y-12 (R.D. Seals and C.J. Swindeman). In January 1995, Rocketdyne Division of Rockwell International Corp. (Canoga Park, CA) requested that FeAl coatings about 0.13 mm thick be applied to alloy 600 corrosion coupons for testing in molten $NaCl/NaCO_3$ salt at 900°C. Previous tests demonstrating the corrosion resistance of another very similar monolithic FeAl alloy (FA-350). The FeAl powder was sized to separate out the finer 20-40 μm particles, and plasma-spray tests varying the processing parameters were made on type 316 austenitic stainless steel coupons. FeAl coatings 0.13-0.26 mm thick adhered well at subsonic and at Mach II supersonic particle speeds. FeAl plasma-spray coatings (0.25 mm thick) were applied to the alloy 600 coupons from Rocketdyne with a 0.05 mm thick underlay of type 316 stainless steel for enhanced bonding. Sub-sonic and high-velocity (Mach II) FeAl coatings were applied, and the specimens were sent to Rocketdyne for corrosion testing in molten $NaCl/NaCO_3$.

3. As-Cast and Extruded FeAl for Monolithic Components and Cladding:

Last year 2-5% room-temperature ductility in air was found in as-cast FeAl, and 8-10% elongation was found when ingot-metallurgy (IM) materials were hot-extruded at 900°C to refine the grain size (0.025-0.080 mm). At higher temperatures of 600-800°C, however, the as-cast FeAl with coarser grain-size (0.25-0.67 mm) was found to be stronger, particularly in creep. Micro-alloying additions of boron were found to increase the room-temperature strength and resistance to moisture-induced embrittlement of as-cast FeAl, and

to dramatically improve the high-temperature strength (Fig. 6). Boron-doped as-cast FeAl is significantly stronger than solution-annealed type 316 austenitic stainless steel at 400-800°C (Fig. 6b). Charpy-impact properties of I/M extruded (900°C) FeAl alloys (FA-385 and FA-385M2 with added B) were also examined (Fig. 4). The I/M FA-385 had a toughness of about 25 J, similar to P/M FA-385 extruded at 1100°C, but the B-doped FA-385M2 had a significantly higher impact energy of 60 J at room-temperature (Fig. 4).

Based on the properties of smaller heats, a 600 lb heat of FeAl (FA-385 + 50 wppm B) was melted commercially in FY 1995. Radiant heating tubes (3.75 in. outer diameter, 96 in. length, with wall thicknesses of 0.25 - 0.75 in.) were centrifugally-cast and U-bends were sand-cast by Alloy Engineering & Casting Company (Champaign, IL) (Fig. 7). Radiant heating tubes with better performance in heat-treating furnaces with various atmospheres (oxidizing, carburizing, nitriding) are of interest to Ford Motor Co., General Motors and others. The FeAl was air-melted under an argon cover using the EXO-MELT™ developed at ORNL to mix the raw Fe, Al, Mo and Zr constitutents so that their exothermic heat of reaction reduces the melting time, saves energy, and reduces the erosion of the crucible material. Chemical analysis showed excellent agreement between the target and actual FeAl alloy compositions. These FeAl radiant heating tubes have been successfully pressure-checked, and are currently being sectioned for microstructural examination and mechanical specimen preparation. Successful behavior of as-cast FeAl will enable component fabrication for other industrial applications, such as pulp-and-paper (parts in Kraft black liquor recovery boilers), metals processing (ie., rolls for steel making or metal forming dies), and glass and metals heat-treating (glob cutters, heat-treating trays, natural gas burner nozzles).

4. Residual Stress Measurements in FeAl Cladding/Coating

Unique neutron diffraction methods at ORNL (neutron diffraction facility at the High Flux Isotope Reactor (HFIR), Z.L. Wang, C.R. Hubbard and S. Spooner) were used previously to measure residual stress distributions in FeAl weld-overlay cladding on a 2¼Cr-1Mo steel base-metal substrate. These unique data revealed compressive stresses in the steel substrate and high tensile stresses (about 400 MPa) in the FeAl weld

overlay. Finite-element-modeling showed that post-weld heat-treating relieved the initial stresses caused by the welding process, but that thermal expansion mismatch during cooling caused the stresses found in this specimen. Last quarter, a new specimen with one weld-overlay pass of a lower aluminum iron-aluminide alloy was deposited on 2¼Cr-1Mo steel with only preheat (350°C) and no post-weld heat-treatment. This specimen showed very large tensile residual stresses in the iron-aluminide cladding, ranging from 300-750 Mpa (Fig. 8), which revified the previous process modeling. Experiments and modeling analysis will continue next year.

MILESTONES

AIM Program FY 1995 Milestone 4 - Prepare FeAl coatings (weld-overlay and powder extrusion), complete properties and residual stress characterization of the materials, and provide materials for testing in industry and prepare draft publication (July 1995, ORNL-MAZIASZ)

This milestone was satisfied by the following:

a) "Residual Stress Distribution in FeAl Weld Overlay on Steel," by X.L. Wang, S. Spooner, C.R. Hubbard, P.J. Maziasz, G.M. Goodwin, Z. Feng and T. Zacharia, in High-Temperature Ordered Intermetallics VI, Part I, Mat. Res. Soc. Symp. Proc. Vol. 288, Materials Research Society, Pittsburgh, PA (1995) pp. 109-114.

b) "Overview of the Development of FeAl Intermetallic Alloys," by P.J. Maziasz, C.T. Liu and G.M. Goodwin, in Heat-Resistant Materials II, ASM-International, Materials Park, OH (1995) pp. 555-566.

c) I/M and P/M FeAl extrusion specimens, sent to General Electric for cavitation/erosion resistance testing (Dr. M. Lee, GE Research Center, Schenectady, NY)

d) FeAl plasma-spray coated Inconel 600 coupons sent to Rockwell International for corrosion testing in molten sodium nitrate/carbonate salts at 900°C (Dr. D.L. Grimmett, Rocketdyne Division, Rockwell International, Canoga Park, CA)

e) Centrifugally-cast radiant-heating tubes and sand-cast U-bends of FeAl using EXO-MELT process by Alloy Engineering and Casting

PUBLICATIONS

Journals

1. P.A. Ferguson and C.T. Liu, "Environmental Embrittlement and Cutting Cracks in FeAl(40% Al)." *Scripta Metallurgica et Materialia*, 26 (1992) 1669-1674.

2. P.J. Maziasz, G.M. Goodwin, C.T. Liu and S.A. David, "Effects of Minor Alloying Elements on the Welding Behavior of FeAl Alloys for Structural and Weld-Overlay Cladding Applications," *Scripta Metallurgica et Materialia*, 27 (1992) 1835-1840.

3. C.G. McKamey, P.J. Maziasz, G.M. Goodwin and T. Zacharia, "Effects of Alloying Additions on the Microstructures, Mechanical Properties and Weldability of Fe_3Al-Based Alloys," *Materials Science and Engineering,* A174 (1994) 59-74.

Other Publications

1. G.M. Goodwin, C.G. McKamey, P.J. Maziasz and V. Sikka, "Weldability of Iron Aluminides," Proc. of the 7th Annual Conference on Fossil Energy Materials, CONF-9305135, ORNL/FMP-93/1 (July, 1993) pp. 181-188.

2. G.M Goodwin, P.J. Maziasz, C.G. McKamey, J.H. DeVan and V.K. Sikka, "Weldability of Iron Aluminides," Proc. of the 8th Annual Conference on Fossil Energy Materials, CONF-9405143, ORNL/FMP-94/1 (August 1994) pp. 205-210.

3. X.L. Wang, S. Spooner, C.R. Hubbard, P.J. Maziasz, G.M. Goodwin, Z. Feng and T. Zacharia, "Residual Stress Distribution in FeAl Weld Overlay on Steel," in High Temperature Ordered Intermetallic Alloys, VI, Part I, Matls. Res. Soc. Symp. Proc. Vol. 288, eds. J.A. Horton, et al., MRS, Pittsburgh, PA (1995) pp. 109-114.

4. P.F. Tortorelli, J.H. DeVan, G.M. Goodwin and M. Howell, "High-Temperature Corrosion Resistance of Weld Overlay Coatings of Iron Aluminide," to be published in Proc. Symp. High-Temperature Coatings I, TMS, Warrendale, PA (1995).

5. P.J. Maziasz, C.T. Liu and G.M. Goodwin, "Overview of the Development of FeAl Intermetallic Alloys," in Heat-Resistant Materials II, eds. K. Natesan, P. Ganesan, and G. Lai, ASM-International, Materials Park, OH (1995) pp. 555-566.

6. P.F. Tortorelli, G.M. Goodwin, M. Howell and J.H. DeVan, "Weld-Overlay Iron-Aluminide Coatings For Use in High-Temperature Oxidizing/Sulfidizing Environments," in Heat-Resistant Materials II, eds. K. Natesan, P. Ganesan, and G. Lai, ASM-International, Materials Park, OH (1995) pp. 585-590.

PRESENTATIONS

Oral Presentations

1. G.M. Goodwin, C.G. McKamey, P.J. Maziasz and V. Sikka, "Weldability of Iron Aluminides," presented at the 7th Annual Conference on Fossil Energy Materials, sponsored by the Fossil Energy (AR&TD) Materials Program, US-DOE, held in Oak Ridge, TN on May 11-13, 1993.

2. G.M Goodwin, P.J. Maziasz, C.G. McKamey, J.H. DeVan and V.K. Sikka, "Weldability of Iron Aluminides," presented at the 8th Annual Conference on Fossil Energy Materials, sponsored by the Fossil Energy (AR&TD) Materials Program, US-DOE, held in Oak Ridge, TN on May 10-12, 1994.

3. P.J. Maziasz, S. Spooner, X.L. Wang, C.R. Hubbard and G.M. Goodwin, "Residual Stress Measurements in FeAl Weld-Overlay Cladding on Steel," presented at the TMS Symp. Interfacial Phases, Structure, and Properties, in conjunction with Materials Week 1994, Rosemont, IL, Oct. 2-6, 1994.

4. P.J. Maziasz, C.T. Liu and G.M. Goodwin, "Overview of the Development of FeAl Intermetallic Alloys,"

presented at the 2nd International Conference on Heat-Resistant Materials II, held 11-14 September, 1995 in Gatlinburg, TN, co-sponsored by ASM-International and NACE-International.

5. P.F. Tortorelli, G.M. Goodwin, M. Howell and J.H. DeVan, "Weld-Overlay Iron-Aluminide Coatings For Use in High-Temperature Oxidizing/Sulfidizing Environments," presented at the 2nd International Conference on Heat-Resistant Materials II, held 11-14 September, 1995 in Gatlinburg, TN, co-sponsored by ASM-International and NACE-International.

HONORS AND AWARDS

None

PATENTS/DISCLOSURES

1. C.T. Liu, C.G. McKamey, P.F.Tortorelli and S.A. David, "Corrosion Resistant Iron Aluminides Exhibiting Improved Mechanical Properties and Corrosion Resistance," U.S. Patent No. 5,320,802, granted June 14, 1994

2. P.J. Maziasz, G.M. Goodwin and C.T. Liu, "High-Temperature Corrosion-Resistant Iron-Aluminide (FeAl) Alloys Exhibiting Improved Weldability," invention disclosed to the ORNL Patent Section of Martin Marietta Energy Systems, Inc. on August 27, 1993. A U.S. Patent application has been prepared and was filed Sept. 1994, and office action responses are in progress.

LICENSES

None

INDUSTRIAL INPUT and TECHNOLOGY TRANSFER

Work began with Devasco International, Inc. of Houston, TX in FY 1993 for the development of shielded-metal-arc (SMA) electrode formulations for the FA-385 FeAl type alloy composition. Such production of weld-electrodes is an important step in enabling FeAl for weld-overlay cladding applications or any other application that involves welding. A CRADA to develop SMA electrodes was signed with Devasco in FY 1994.

Work began in FY 1993 with Haynes International (Kokomo, IN) to produce filler-metal weld wires via aspiration casting methods based on the most weldable FA-385 series alloy compositions. Weld wires of several compositional variants have been produced and weld-overlay cladding deposits have been made to test these alloys. Initial results were good, and analysis and evaluation of the weld-clad test pads continues. Production of coiled, smaller diameter solid- and powder-core weld wires began with Stoody Company (Bowling Green, KY) for gas-tungsten-arc (GTA) and gas-metal-arc (GMA) applications.

Commercial FeAl powder was produced by AMETEK Specialty Metal Products Division (Eighty-Four, PA) in FY 1995. The initial tensile and Charpy-impact data for extruded P/M FeAl were excellent. Thermal spray techniques were also used to deposit FeAl onto type 316 stainless steel. Good results have prompted Ametek to begin cost-share for new FeAl/FA-385M2 (200 appm B) powders. Ametek has expressed great interest in the properties that ORNL has obtained for P/M FeAl, and is will to purse further commercialization opportunities.

The successful centrifugal casting of FeAl pipes by Alloy Engineering and Casting (Champaign, IL) can be used for radiant-heating tube tests by Ford, GM and others. The centrifugal cast tubes can also be

extruded or co-extruded on 304/316 or other steels for chemical, petro-chemical or pulp-and-paper processing plant applications.

Rocketdyne-Rockwell International (Canoga Park, CA) is testing the FeAl coated alloy 600 coupons in molten sodium nitrate/carbonate salts at 900°C at their own expense, and is will to interact with us to determine how FeAl coatings or monolithic FeAl can best be applied to their project to develop corrosion resistant coatings at their Energy Technology Engineering Center (ETEC).

General Electric Corporate Research Center (Schenectady, NY) will test hot-extruded I/M FeAl specimens and new P/M FeAl specimens at their own expense for fretting, cavitation erosion and abrasive wear resistance, based on the work-hardening characteristics of FeAl. Some of the potential applications they are considering include large diesel engine fuel-injector nozzels, contact surfaces for some rolling elements, and high-traction contact components such as locomotive wheels. The lower density of FeAl is also attractive for advanced locomotive applications.

Rolled Alloys (Temperance, MI) (R.W Swindeman contact at ORNL) has expressed new interest in FeAl due to our success at making a crack-free FA-385 weld-overlay onto a sheet of their 253 MA stainless steel. They are willing to explore FeAl coatings on 253 MA and on RA 85H alloys for heat-treating, sulfidizing, oxidizing and incineration applications.

New industrial contacts made toward the end of this year include: PALL Trinity Micro Corporation (Cortland, NY) to consider using FeAl powders to produce sintered porous gas-metal filters for coal-gasification and clean-up of hot gases with high sulfur contents; Metallamics (Traverse City, MI) to consider FeAl for applications that are currently considering Fe_3Al or Ni_3Al; Thixomat, Inc. (Ann Arbor, MI) to consider FeAl as a material for critical components and hot-dies for injection-molding of thixotropic (semi-solid) aluminum, based on FeAl high-temperature strength and preliminary data on resistance to molten aluminum corrosion. All of these industrial interactions will be pursued further in FY 1996.

ESTIMATED ENERGY SAVINGS

The development of low-cost, low-density, corrosion-resistant, fabricable and weldable FeAl aluminide alloys will enable their application to a variety of high-temperature energy producing applications, to high-temperature materials processing, or to any aggressive corrosive high-temperature environment. All such applications will save energy through better operation at higher temperatures for better thermal efficiency or save money and down-time by having longer service lifetime. Some applications require a new material to enable the new energy/material efficient technology to develop (ie. Thixomat). Development of weld-overlay technology will enable FeAl alloys to be introduced for better corrosion/oxidation resistance and possibly better wear-resistance for existing systems components. Successful casting, extrusion or forging technology will also enable easy fabrication of many simple components for industry to test and evaluate. Heat-resistant iron-aluminide alloys can also be considered a "green technology" because iron and aluminum are not RCRA waste hazards like the nickel and chromium used in most heat-resistant alloys today (a primary consideration for the Rocketdyne application).

Table 1 - Compositions of Developmental FeAl Cast Filler-Metals

Wire and description		Composition (wt.%) Al	Cr	Nb	Ti	Mo	Zr	C	B	Comments
ORNL Weldable FeAl Alloy Reference Materials										
FA-385		21.1				0.42	0.1	0.03		
FA-385M1		21.1				0.42	0.1	0.03	0.0025	
FA-385M2		21.1				0.42	0.1	0.03	0.005	
FA-385M3		21.1	2.3			0.42	0.1	0.03		
FA-385M4		21.1		1.0		0.42	0.1	0.03		
Haynes Wires, aspiration-cast, 0.125 in. diam.										
I-01,	aim	30	5	0.5	0.5	0.25	0.2	0.1		
	actual	31.2	3.3	0.5	0.7	0.3	0.2	0.12	0.007	
	weld-deposit	21.2	2.9	0.4	0.4	0.5	0.2	0.13	0.007	no cracks
(1 layer, 2¼Cr-1Mo)										
I-02,	aim	30	5	0.5	0.5	0.25	0.2	0.1	0.0025	
	actual	31.3	3.2	0.5	0.7	0.3	0.2	0.12	0.009	
	weld-deposit	26.8	3.2	0.4	0.5	0.4	0.2	0.12	0.012	
(2 layers, 2¼Cr-1Mo)										
I-03,	aim	30	5	0.5	0.5	0.25	0.2	0.1	0.005	
	actual	31.5	3.5	0.5	0.6	0.3	0.2	0.11	0.017	
	weld-deposit	26.2	3.2	0.4	0.4	0.4	0.2	0.11	0.015	2nd layer cracked
(2 layers, 2¼Cr-1Mo)										
Haynes Wires, aspiration-cast, 0.156 in. diam										
III-01	aim	30	7	0.6	0.5	0.25	0.2	0.1		
	actual									
	weld-deposit									no cracks
(1 layer, 2¼Cr-1Mo steel)										
III-02	aim	30				0.4	0.1	0.03		FA-385 repeat
	actual									
	weld-deposit									no cracks
(1 layer, 2¼Cr-1Mo steel)										
Haynes Wires, aspiration-cast, 0.156 in. in diam.										
IV-01	aim	25	7			0.4	0.1	0.03	0.005	
	weld-deposit									no cracks
(1 layer, 2¼Cr-1Mo, 9Cr-1MoNbV, and 304L steels)										

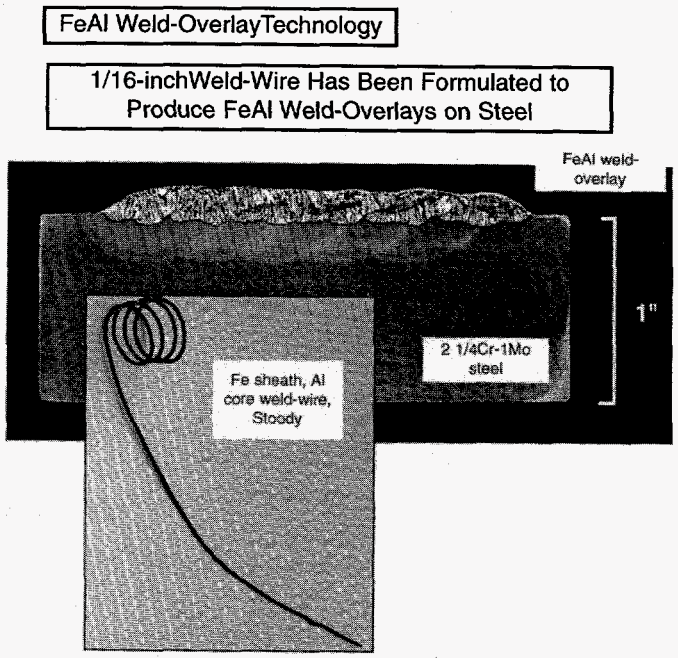

Fig. 1 - Fe sheath/Al core weld-wire (1.6 mm/0.0625 in) produced by Stoody and formulated to produce weld-overlays with FeAl composition on steel substrates.

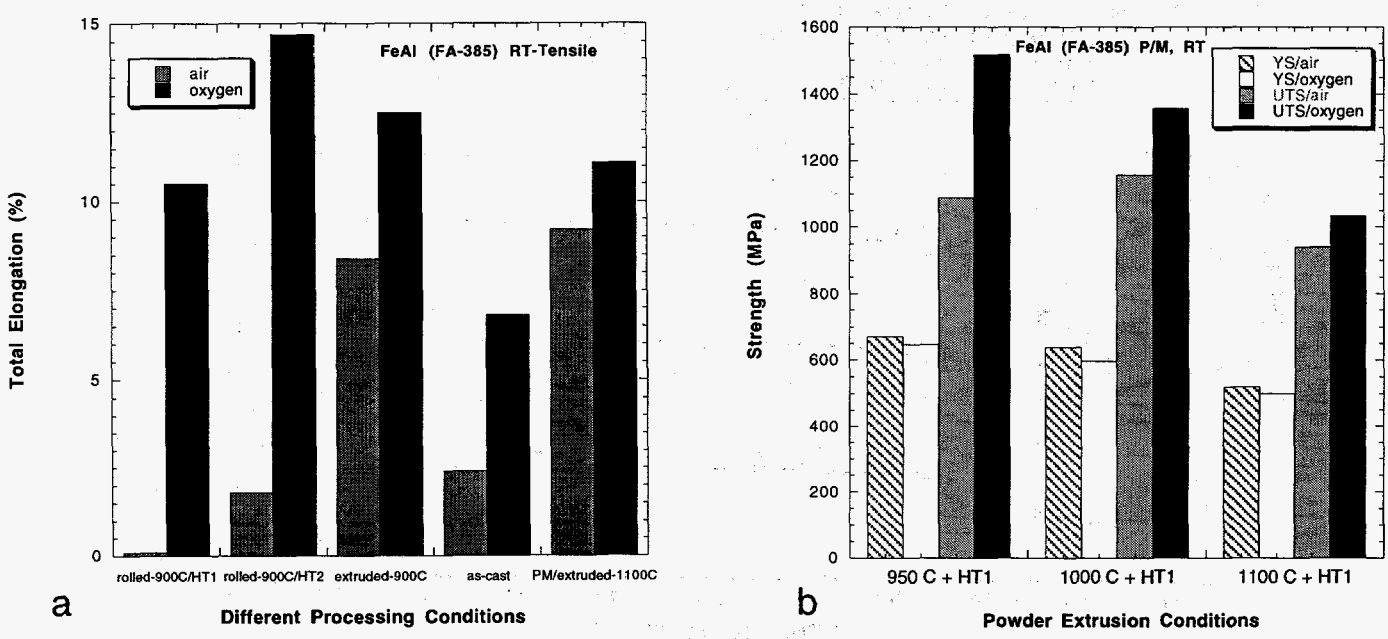

Fig. 2 - FeAl (FA-385) tensile properties at room-temperature for various different processing conditions. a) total elongation, and b) yield and ultimate tensile strength (YS and UTS, respectively).

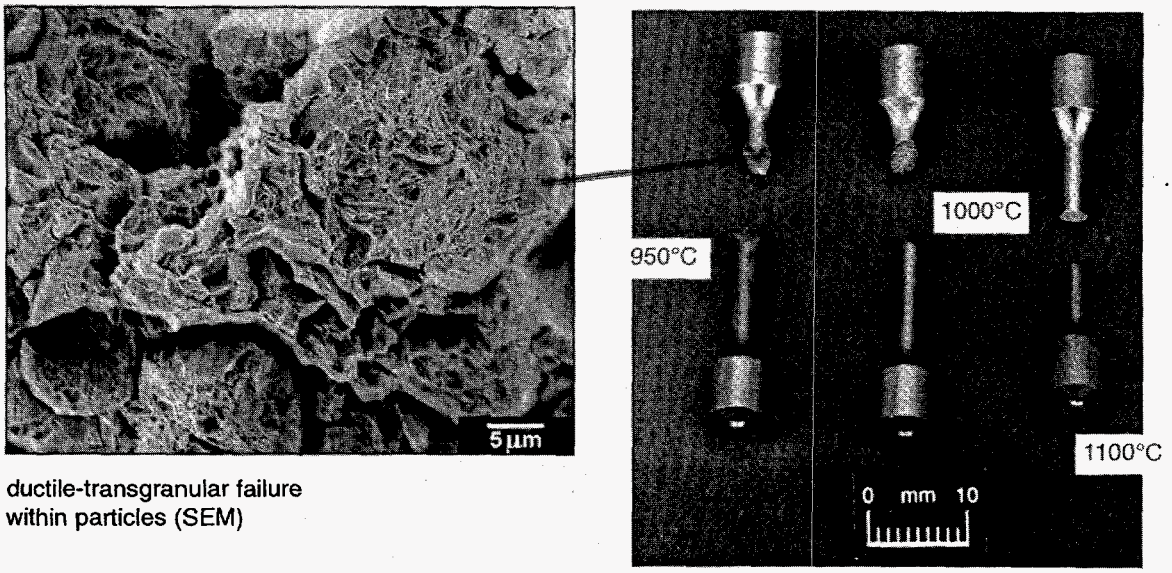

ductile-transgranular failure within particles (SEM)

tensile-tested in oxygen at room-temperature

Fig. 3 - Macro fractography of P/M FeAl (FA-385) extruded at different temperatures and tested in oxygen at room-temperature. SEM fracture surface analysis of P/M FeAl extruded at 950°C is also shown.

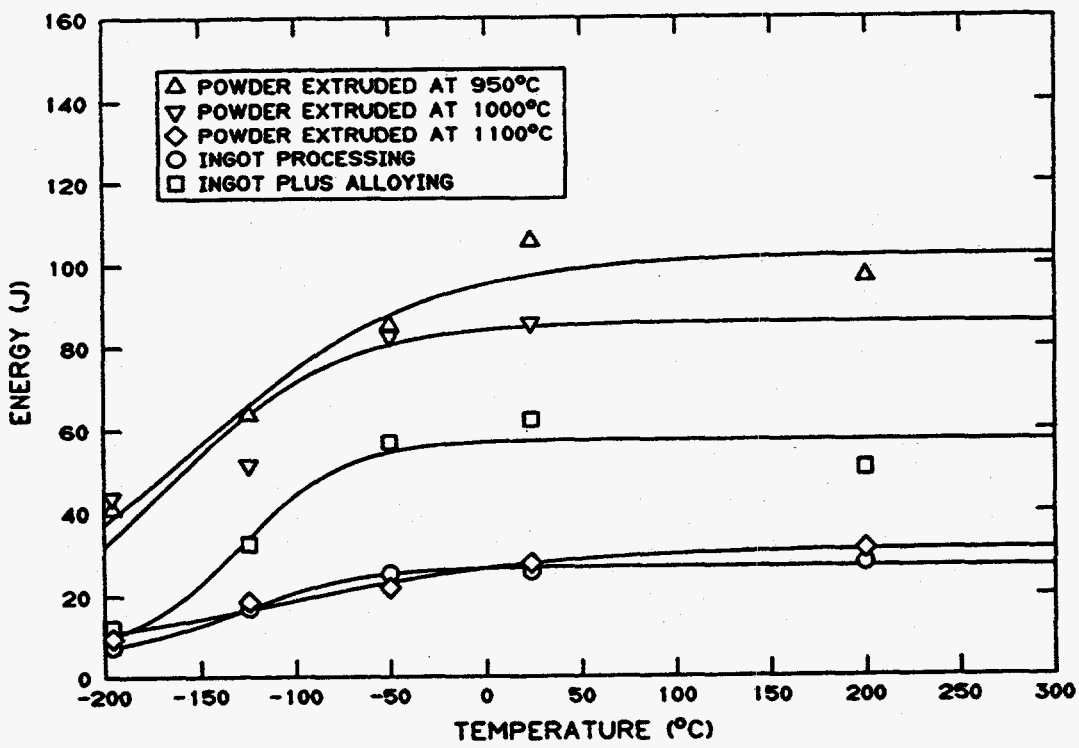

Fig. 4 - Charpy impact-toughness data for I/M and P/M FeAl specimens tested in air, showing absorbed energy as a function of test temperature. P/M FeAl (FA-385) specimens were extruded at different temperatures. I/M FeAl includes FA-385 and B-micro-alloyed FA-385, both extruded at 900°C.

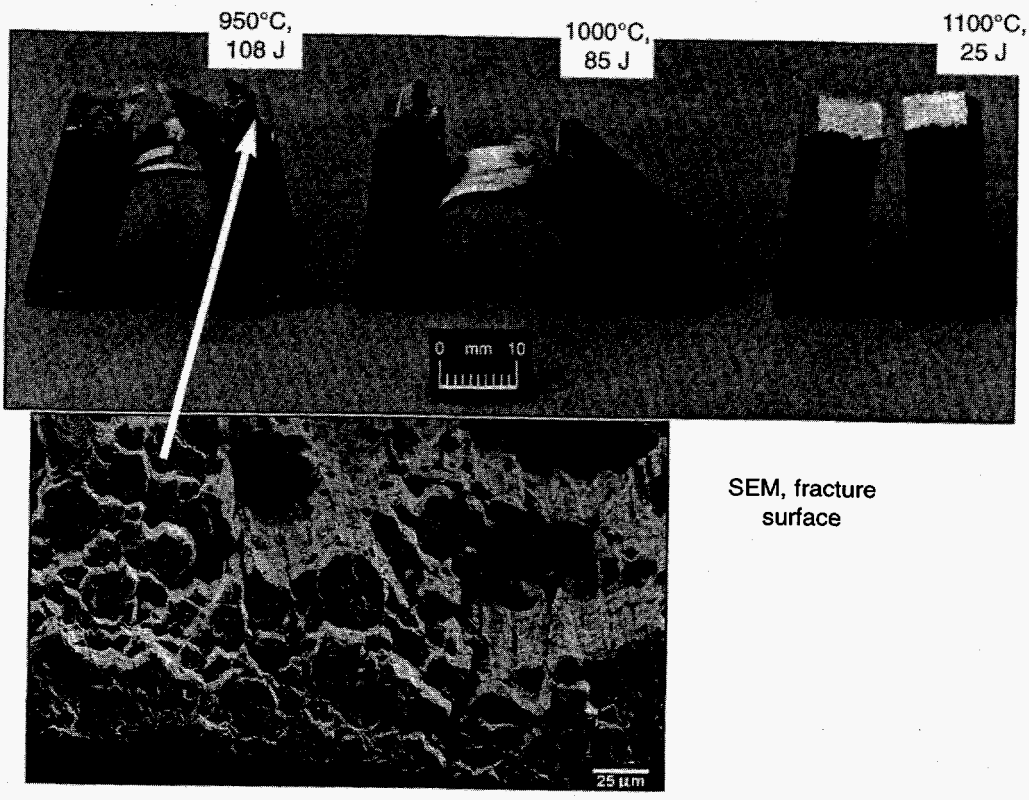

Fig. 5 - Macro fractography of P/M FeAl (FA-385) Charpy impact-toughness specimens, with SEM fracture surface analysis of the material extruded at 950°C.

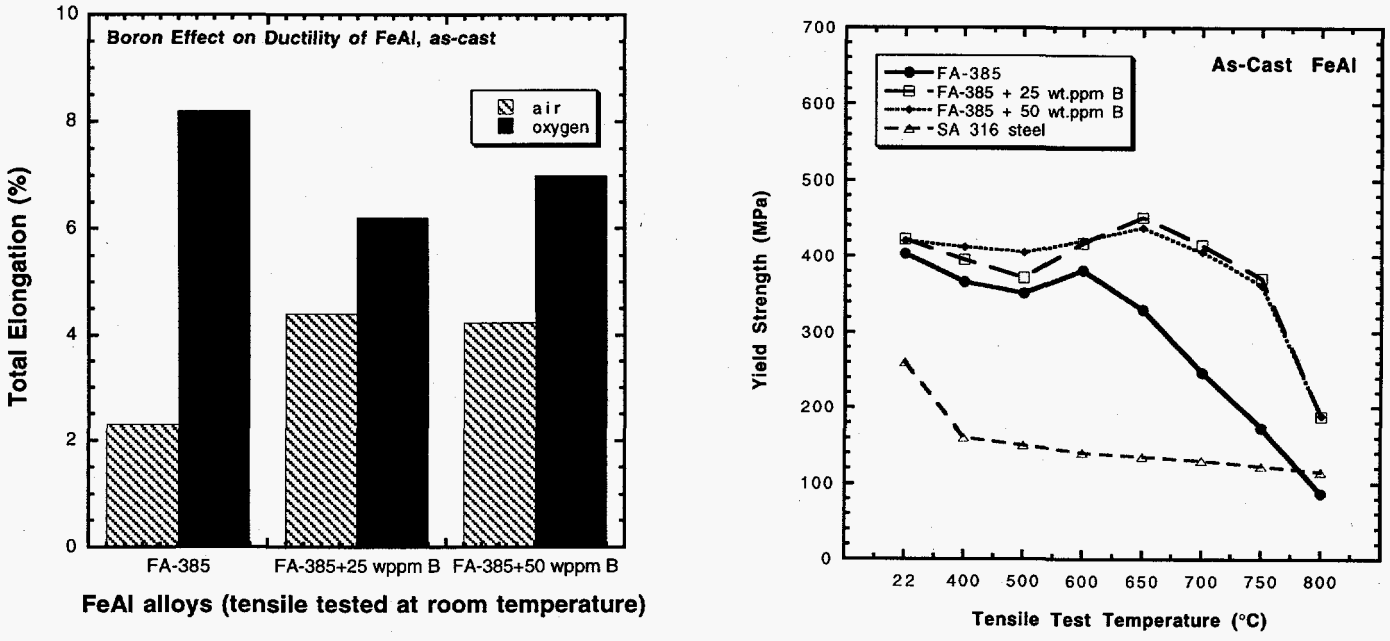

Fig. 6 - The effect of B micro-alloying on a) room-temperature total tensile elongation in air and in oxygen (the difference is a measure of environmental embrittlement resistance), and b) yield-strength (YS) as a function of test temperature up to 800°C, for as-cast FeAl (FA-385).

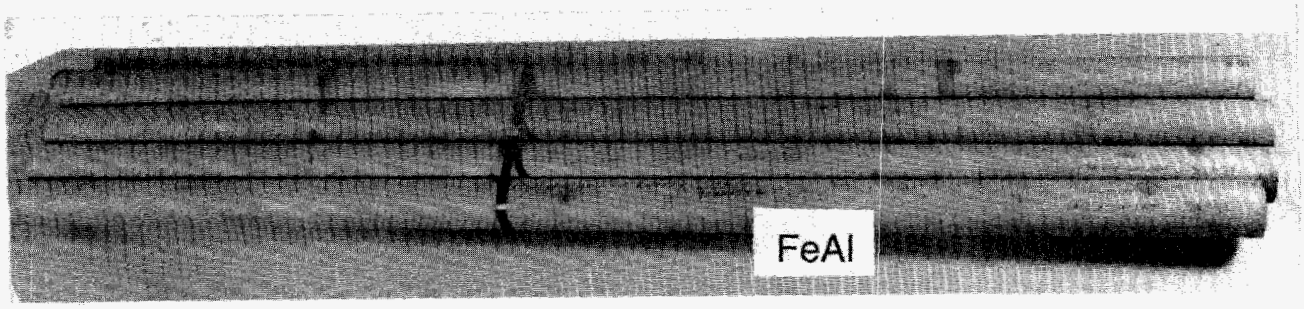

a

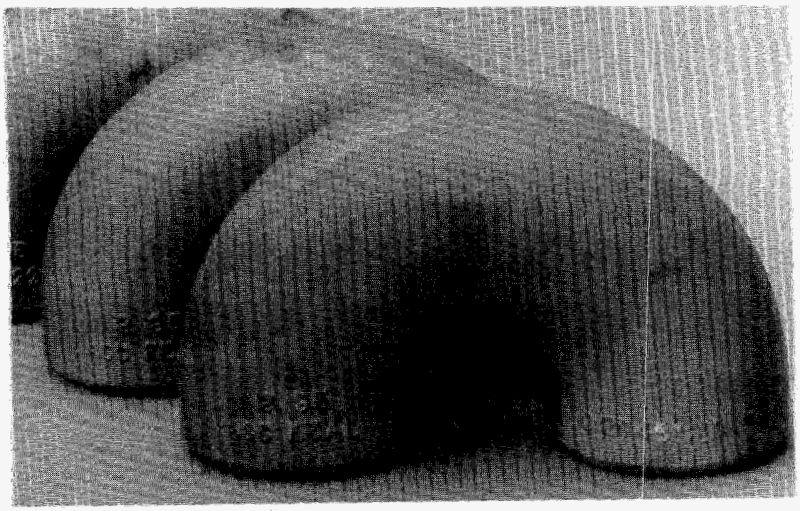

b

Fig. 7 - Commercial production of FeAl components by Alloy Engineering & Casting Company using the EXO-MELT technology, including a) centrifugally-cast radiant heating tubes, and b) sand-cast U-bends.

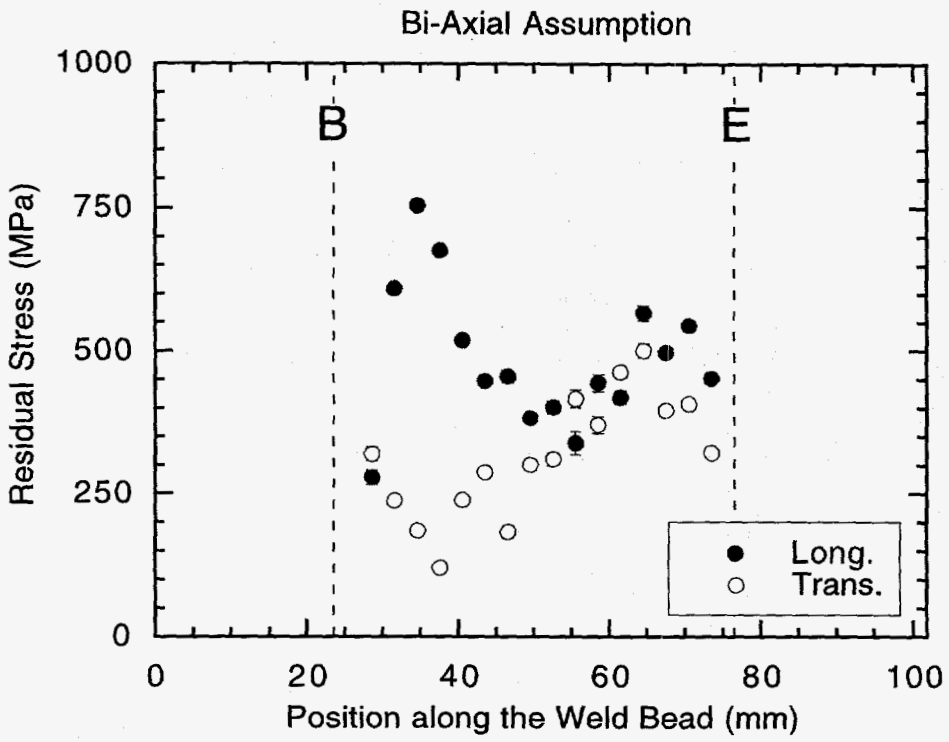

Fig. 8. - Residual stresses measured by neutron diffraction techniques in an FeAl weld-overlay deposit (single-pass) on 2.25Cr-1Mo steel, with preheat (350°C), but no post-weld heat-treatment. B indicates the beginning and E indicates the end of the weld-deposit. Stresses are fairly high and tensile in nature.

MATERIALS FOR THE PULP AND PAPER INDUSTRY

Section 1: DEVELOPMENT OF MATERIALS FOR BLACK LIQUOR RECOVERY BOILERS

J.R. Keiser, Z. Feng, C.R. Hubbard, S. Spooner, R.W. Swindeman,
B. Taljat, R.L. Thomas, X.L. Wang and T. Zacharia

Metals and Ceramics Division
Oak Ridge National Laboratory
P.O. Box 2008, Oak Ridge, TN 37831

and

D.L. Singbeil and R. Prescott

Pulp and Paper Research Institute of Canada
3800 Wesbrook Mall, Vancouver, BC, Canada V6S 2L9

INTRODUCTION

Black liquor recovery boilers are critical components of kraft pulp and paper mills; they provide the means to recover the pulping chemicals required in the kraft process, and they provide electrical power for the mill. Recovery boilers require the largest capital investment of any individual component of a paper mill, and they are probably the major source of materials problems in a mill. In particular, cracking into, or through, the stainless steel outer layer of co-extruded or composite tubing used in recovery boilers is a critical problem. Almost invariably, the cracks have been located in wall tubes which form openings for the smelt spout close to the boiler floor or in the floor tubes themselves. These cracks pose considerable risk to the boiler if they penetrate the tube, because water leaking into the smelt bed can cause a smelt-water explosion capable of destroying the boiler. Since neither the cause of the cracking nor an effective solution has been identified, this program was established to develop a thorough understanding of the degradation that occurs in the composite tubing used for walls and floors. This is being accomplished through a program that includes collection and review of technical reports, collection and analysis of smelt samples, collection and tabulation of temperature data, microstructural characterization of composite tubing, measurement

of residual stresses in both as-produced and as-formed composite tubing, computer modeling to predict residual stresses under other conditions, and operation of laboratory corrosion tests. From this work it is anticipated that alternate materials will be identified and these will be tested in recovery boilers.

TECHNICAL PROGRESS - FY 1995

Summary

1. Compilation of Information on Composite Tube Cracking

The Pulp and Paper Research Institute of Canada (Paprican) has the lead role in production of a state-of-the-art report on co-extruded or composite tubing used in kraft recovery boilers. Work on this portion of the program began in mid-summer 1995 and will continue through the second quarter of FY 1996. Information sources that were consulted include:

- tube manufacturers
- boiler manufacturers
- public domain literature
- companies operating kraft recovery boilers
- consultants and failure analysis laboratories
- failure analyses conducted specifically for this project

In addition to obtaining written documentation from these sources, visits were made by members of the research team to manufacturing facilities for the tubes and boilers, mill sites during operation of the boilers and on shutdowns when the equipment was available for inspection. University laboratories and consultants offices were also visited. An overview of information obtained to date from each of these sources is outlined below.

Tube manufacturers: There are two principal manufacturers of composite tubes worldwide; these are Sweden's Sandvik AB and Japan's Sumitomo Metals. Other, smaller manufacturers also exist but they

sell very little material into the pulp and paper market. There are no North American suppliers of this type of tubing. The bulk of composite tubes sold in North America come from Sumitomo, largely as a consequence of marketing agreements with the North American boiler manufacturers. Sandvik does have a significant presence in North America, but sells most of its product into Europe.

Composite tube manufacture generally consists of preparing and mating two billets of material, one inner and one outer. The combined billet is then co-extruded through a die at high temperature to form a continuous tube. For recovery boilers, the inner layer is composed of SA-210 Gd A1 carbon steel or equivalent and is used to provide the strength and pressure handling capabilities of the tube. The outer layer has usually been made from 304 or 304L austenitic stainless steel. The alloy used for the outer layer was chosen for its resistance to sulfidation, a common form of corrosion encountered in these boilers. More recently, tubes with an outer layer of Alloy 825 or equivalent composition have been introduced into service. Other alloy combinations have also been made, both for pulp and paper and applications in other industries. Regardless of the alloys, typical tube thicknesses used in the pulp and paper industry are about 0.25 in. (6.4 mm) total thickness, with the outer corrosion resistant layer being about 0.07 in. (1.8 mm) thick. Tubes for the pulp and paper industry are produced with external diameters of either 3 or 2½ in. (76.2 or 63.5 mm), with the latter being standard for more modern boilers. The source of the tube (Sandvik or Sumitomo) appears to have no influence on the tendency to crack or severity of cracking.

Boiler Manufacturers: Six boiler manufacturers compete for most of the worldwide recovery boiler sales. In North America, the principal suppliers are ABB Combustion Engineering and Babcock & Wilcox. Kvaerner produces recovery boilers in Sweden while Ahlstrom and Tampella are based in Finland. Mitsubishi is a prominent Japanese boiler manufacturer. The European manufacturers were the earliest to adopt the use of composite tubes for wall and floor construction (1972 and 1978 respectively). The North American boiler manufacturers were about 5 years behind their European counterparts in using composite tubes. Cracks in composite tubes were first observed in Europe in

1984 in spout opening tubes, and in floor tubes by 1986. By 1992, cracks had also been reported in the tubes installed in some North American boilers (principally in spout openings). Most current reports of composite tube cracking in North America are for floor tubes. General facets of boiler construction are similar across all manufacturers. Fine details vary, but there is no apparent relation to incidences of cracking.

Boiler design plays a role in the location and severity of cracking, but no design has proven immune to composite tube cracking. The time from installation to first cracking for floor tubes has been reported to vary from 4 to 48 months. Higher pressure boilers (1200-1500 psi steam pressure) were the first to report cracks, but are also more likely to have been constructed with composite tubes. Many low pressure boilers (600-900 psi) also report cracked floor tubes. Initial reports in North America led to the mistaken belief that cracking was restricted to boiler designs with a sloped floor. This early report of incidences of cracked floor tubes was due in part to the greater ease with which sloped floor boilers are inspected and to the fact that the preponderance of composite floor tubes used in North American were supplied to sloped floor boilers. Boilers designed with spouts which butt up against the outside of the boiler wall are clearly at much greater risk of developing cracks in the tubes which form the spout openings. The total number of boilers reporting cracked tubes continues to increase as inspection techniques mature and information on the problem circulates among the operating companies.

Public Domain Literature: A number of strategies have been employed to search the public domain databases. The principal engineering and science databases have been used, as well as specialized databases like Paperchem and that at the Electric Power Research Institute. General search strategies have been: composite or clad tubes; fatigue, corrosion fatigue or stress corrosion cracking of 304, 304L and alloy 825 alloys; cracking of 304, 304L and alloy 825 alloys at high temperatures, cracking and fracture of clad or composite materials, residual stresses in clad or composite materials. Additional references are being added to the list from the files of the research team, and those of

steering committee members for the project. This activity is still in progress, and relevant literature will be summarized for the final report.

Companies Operating Kraft Recovery Boilers: Operating information, inspection data, failure analyses, and other information has been sought from companies which operate kraft recovery boilers. One key finding from this source is that the total number of tubes which have been subjected to a complete metallographic failure analysis is very few relative to the total number of cracked tubes identified in boilers. Most cracked tubes are returned to service or repaired in place rather than being removed. This issue is of particular concern because only a detailed failure analysis can confirm whether or not cracks have propagated through the interface between the outer stainless steel layer and the inner carbon steel. There is currently widespread belief that this is unlikely, despite the fact that one or two incidents of crack propagation through the interface have been documented.

Consultants And Failure Analysis Laboratories: Information and advice have been sought from consulting companies and failure analysis laboratories with experience of recovery boiler operation and repair. Client confidentiality or the desire to maintain business trade secrets has generally restricted the information obtained from these sources.

Failure Analyses Conducted Specifically For This Project: Samples of cracked tubes have been solicited from all companies contacted by researchers in this project. Failure analyses are conducted at Oak Ridge National Laboratory as these samples are received.

A draft report is scheduled for completion by the end of February, 1996. The final report will be prepared and issued after comments on the draft report have been received from members of the project steering committee.

2. Residual Stress Measurements

Residual stresses are thought to be a very significant factor in the initiation and propagation of cracks in composite tubes used in kraft recovery boilers. To characterize the residual stresses in

composite tubes and panels constructed of composite tubes, a systematic study utilizing neutron and X-ray diffraction methods has been undertaken. The study will extend over several years. During the first year, two tasks were undertaken; use neutron diffraction to determine the residual stress distribution (depth profile) in straight composite tubes of various diameters and with various clad materials and apply X-ray diffraction to determine the surface stress state of these composite tubes. The experimental data obtained for straight composite tubes will serve as a baseline for understanding the residual stresses in tube panels and will provide input to the modeling task.

Composite tube specimens used for neutron and X-ray residual stress measurements were obtained from Sandvik Steel and Babcock & Wilcox (B & W). Sandvik Steel provided samples of their tubing while B & W provided samples of tubing produced by Sumitomo Metals. The composite tubes tested were composed of a SA-210 grade A1 (Sandvik 4L7) carbon steel core with a corrosion-resistant clad layer of either 304L (Sandvik 3R12) or alloy 825 (Sanicro 38).

The neutron diffraction experiments were performed using a residual stress mapping system at the High Flux Isotope Reactor of Oak Ridge National Laboratory. Masking slits were positioned before and after the specimen to define a sampling volume, and strain mapping was accomplished using a three-dimensional translation stage mounted on the sample table of the neutron spectrometer. All strain measurements were made at the mid-length of the tube specimens. From the diffraction peaks measured at each location residual strains were calculated, and then residual stresses were calculated from this information using Hooke's law.

Figure 1 shows the residual stress data at room temperature as a function of radius for the four Sandvik tubes and one Sumitomo tube. For all Sandvik tubes, the residual stresses are small throughout the carbon steel layer (within ± 100 MPa). Larger residual stresses were found to be present in the clad layers. These stress values are considered significant especially when compared with the yield strength of the clad materials. For example, in composite tubes with 304L clad, the maximum stresses are approximately ± 150 MPa, which is just below the yield strength of 304L

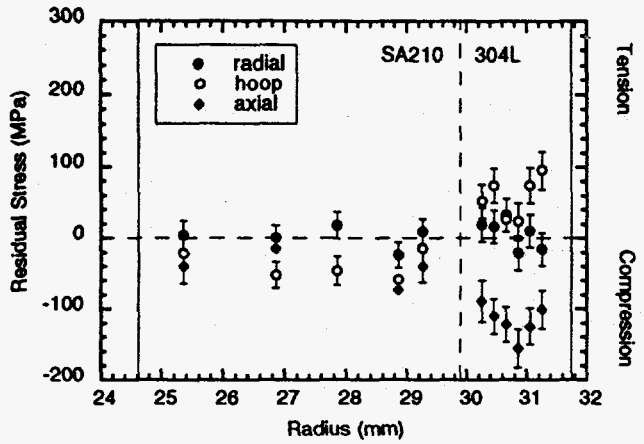

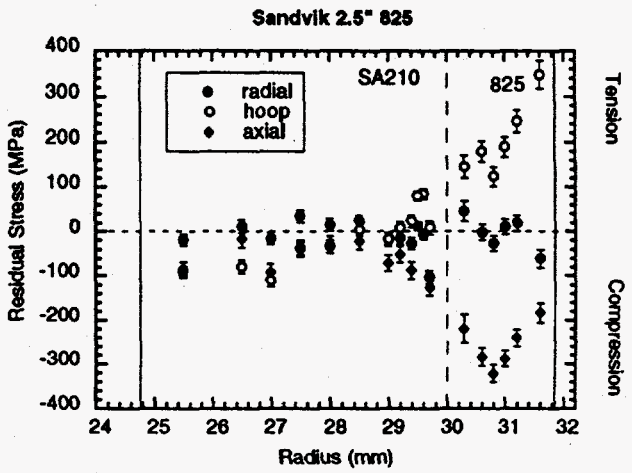

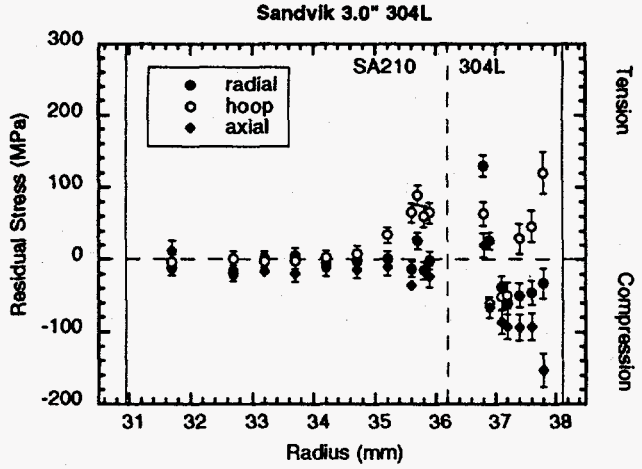

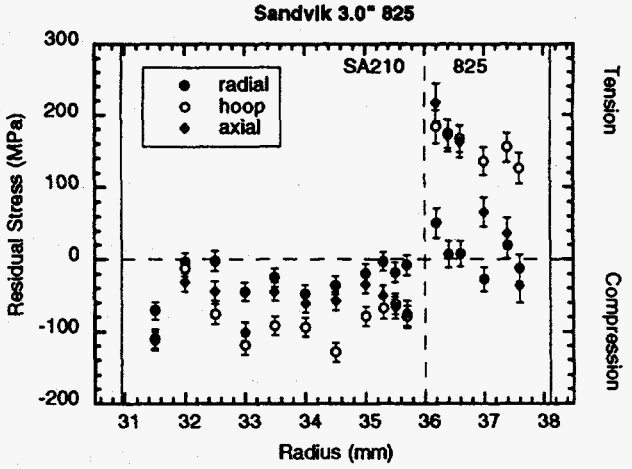

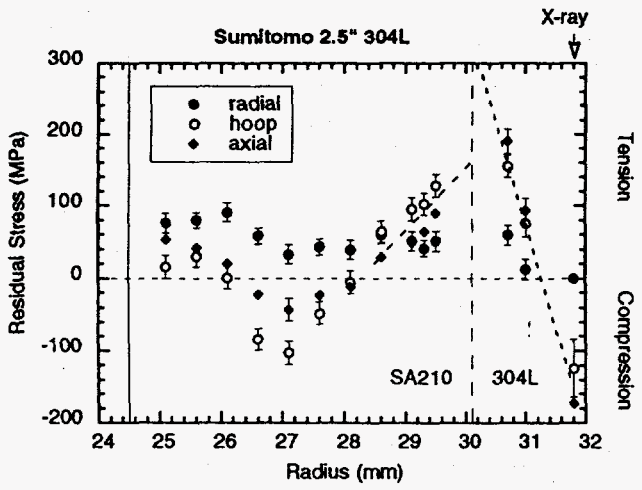

Figure 1 Residual stress versus tube radius for five composite tube sections. The residual stresses are tensile for positive values and compressive for negative values. Neutron diffraction was used to determine stresses through the thickness of the tube, and X-ray diffraction was used on one sample to measure residual stress at the tube surface.

(180 MPa at room temperature). In composite tubes with 825 clad, the maximum residual stresses are even greater, reaching as much as ± 350 MPa. For comparison, the yield strength of alloy 825 is 450 MPa at room temperature. In all Sandvik tubes, the axial stress is compressive and the hoop stress is tensile near the outer surface of the clad layer. This similarity suggests that the residual stress in as-manufactured Sandvik tubes arises from similar forming processes. However, the observed residual stress pattern in Sandvik tubes is quite different from that determined for a Sumitomo tube (also shown in Figure 1), where both axial and hoop stresses were found to be compressive. This difference likely arises from a different forming process utilized by each manufacturer. In order to fully understand these residual stress data, especially the difference between them, complete knowledge of the forming process at each manufacturer would be needed.

In parallel with the neutron diffraction, progress has also been made for surface stress measurements using X-ray diffraction. Portable X-ray instruments are available and can be used to determine residual stresses in composite tubes under service conditions. However, before taking a portable X-ray unit into a boiler for field measurements, it is necessary to establish the relationship between the residual stress state measured by X-ray and neutron diffraction and determine the potential for cracking. The present study aims at comparing the surface stress measured by X-ray diffraction with the extrapolation of neutron diffraction data obtained from an identical composite tube. Fig. 2 compares the depth profile of hoop and axial strain components in the clad layer of a Sumitomo tube obtained by neutron and X-ray diffraction. As can be seen, within the experimental precision, the neutron and X-ray data are in agreement. There are, however, significant experimental errors (50 MPa) associated with the X-ray data. Two factors contribute to the uncertainties in the X-ray data: (1) large grain size (30-40 μm) of the clad layer and (2) preferred orientation due to pilgering (cold working). The latter was confirmed by recent X-ray texture measurements on a ring cut from the same sample tube. To reduce the effects due to preferred orientation, the X-ray source was oscillated ±6° during data collection. To overcome the grain size problem, a linear translation

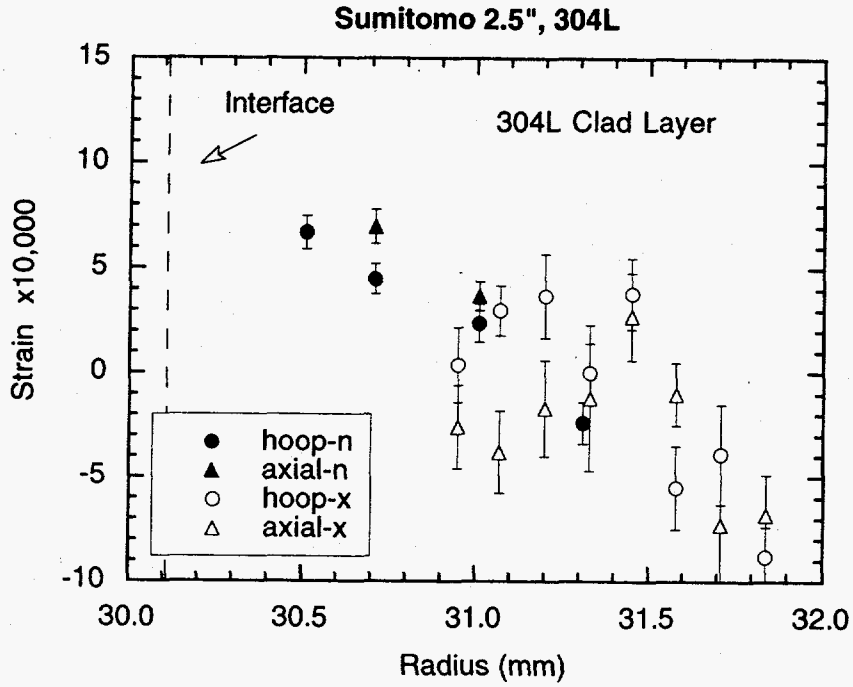

Figure 2 Comparison of the hoop and axial strain components in the stainless steel layer of a Sumitomo tube as obtained from X-ray and neutron diffraction data.

stage was built and tested. With this system, the specimen can be oscillated so that a large number of grains can be sampled during data collection. Preliminary measurements indicate that by oscillating over a range of 20 mm along the axial direction, the uncertainties in the X-ray stress data were reduced by half. This translation stage should greatly facilitate the characterization of the near surface stress state using the X-ray diffraction method.

3. Residual Stress Modeling

The mechanisms which are proposed as potential causes of cracking in composite tubes all involve residual and/or applied stresses. The magnitude and type of stresses that exist in composite tubes at room temperature are being determined by means of neutron and X-ray diffraction studies as described in the previous section. The purpose of this task is to incorporate the room temperature residual stress data collected from the diffraction studies in a model that is designed to determine the

stresses in composite tubes under boiler operating conditions.

The first effort in this study was to develop a computational model for establishing a baseline for the thermal stress evaluation. A simple finite element (FE) model of the tube-membrane cross section was developed, assuming that there exists a generalized plane strain condition along the cross section. Due to symmetry, only one half of the composite tube and a half of the membrane plate were included in the FE model. The connecting welds between the tube and the plate were also included in the model, but the welding residual stresses were neglected.

A simple thermal analysis was performed assuming a uniform temperature of 343°C everywhere in the tube-web assembly. The extrusion residual stresses, obtained from the neutron diffraction (ND) measurements, were imposed in the composite tube as initial stresses. From the analysis, it was clear that the mismatch in thermal expansion coefficients between the 304L stainless steel and the carbon steel is a dominant factor for the thermal stress build up at the service temperature. This mismatch causes the stainless steel overlay to be in compression while the carbon steel base material is in tension.

Further development of the model addressed uncoupled thermo-mechanical analysis for calculating the stress distribution caused by temperature gradients in the tube cross section and study of residual stresses introduced by welding the tubes and membranes and their contribution to the overall in-service stress distribution. The model for analyzing the stress distribution due to temperature gradients across the tube cross section was developed in order to study the effect of different temperatures on the fireside versus the insulated (outside) of the tube.

Welding the tubes and membranes together may introduce large residual stresses in the tube-membrane assembly. Temperature gradients, which exist during the heating and cooling associated with welding, are calculated by the thermal analysis and are the basis for the residual stresses.

The ability of the models to accurately represent what actually occurs in the tubing is limited by the quality of the mechanical properties data attributed to the materials. The best available data

is used, and updating of this data base is done whenever it is warranted.

The ND measurement results for both the Sandvik and Sumitomo type 304L SS/SA210 tubes were available for inclusion in modeling studies, but the results for alloy 825/SA210 tubes were not available during the initial portions of this work. In order to generate room temperature residual stress data for 825/SA210 it was assumed that the materials in the composite tube were at equilibrium when the tube was annealed at 920° C. Cooling of the tube was simulated, and the resulting room temperature stress distribution was considered as representative of the residual stress distribution resulting from tube fabrication. For comparison, the effect of cooling on a composite tube composed of 304L SS/SA210 was also calculated. Also, the calculated von Mises stress during cooling was compared to the temperature dependent yield strength for both tube types; 304L SS/SA210 and alloy 825/SA210. In the former tube, it was found that the stainless steel overlay starts yielding around 900° C and is yielding almost all the time during cooling. Alloy 825 is a higher strength material, and therefore it does not yield during cooling, but some yielding was calculated to occur on the carbon steel side between 780 and 870° C.

Since the extrusion and welding residual stresses are calculated in two separate analyses, a program which joins the two residual stress fields into a common residual stress distribution was developed. This allowed the calculated residual stress distribution to be introduced as an initial stress field to the in-service stress analysis. Welding residual stresses may make an important contribution to the overall in-service stress distribution. Figure 3 shows the hoop and axial residual stress due to welding in the 304L SS/SA210 tubing. Graphs are made such that the abscissa represents the tube circumference with "0" near the membrane attachment and "+90" at the fireside crown of the tube. The tube outer surface (designated out-surface) experiences tensile hoop residual stresses, which are higher in the region of the welding (see Fig. 3a). Residual stresses in the axial direction were calculated to be very high tensile stresses in the region of the welds, but are rather compressive at the +90 and -90 locations (see Fig. 3b). The behavior of alloy 825/SA210 tube is similar, except the

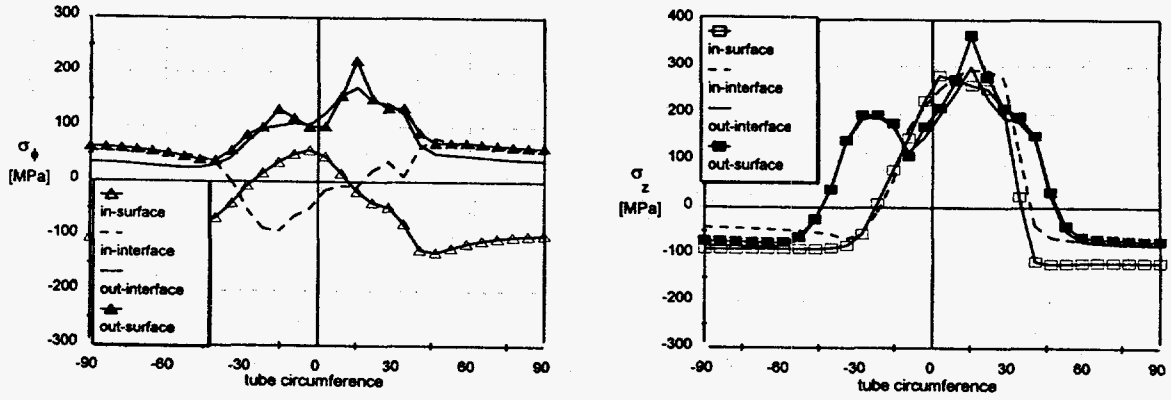

Figure 3 Welding residual stresses in 304L SS/SA 210 composite tubing; a) hoop stresses, b) axial stresses.

stresses are considerably higher.

The residual stress data for the effects of tube formation and membrane welding were used with an improved thermal model. Three different temperature load cases were analyzed. For the first case, the fireside of the tube was assigned a temperature of 343°C (650°F) while the inside of the tube was 287°C (550°F). The other two cases have the same temperature distribution but a hot spot of 550°C (1022°F) at the crown of the tube or a hot spot of 550°C in the valley where the tubes are welded to the membrane. To complete the simulation of actual conditions, an internal tube pressure of 8.62 MPa (1250 psi) is applied in addition to the temperature load for all three cases.

Figure 4 shows the effect of hot spots on the hoop stress distribution at the tube's inside surface (designated in-surface) and outer surface for the Sumitomo 304L SS/SA210 tube. It can be seen that the hot spots add a tensile stress component in the region of the hot spot. The effect is more pronounced on the inner surface than on the outer surface. The hot spots have almost no effect on the axial stresses in the membrane overlay, but, as shown in Figure 5, the valley hot spot considerably changes the stress state in the carbon steel part of the membrane.

Figure 6 shows the hoop stress comparison for the Sandvik and Sumitomo 304L SS/SA210 tubes and for an alloy 825/SA210 tube whose room temperature residual stresses were defined by assuming

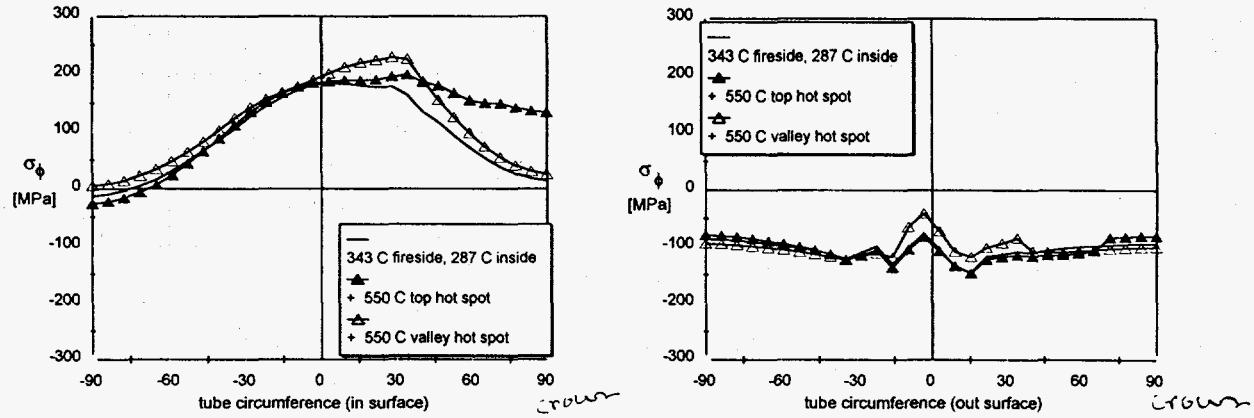

Figure 4 In-service hoop stress in Sumitomo tube - hot spot effect on the inside service and the outside surface. The 0 point represents the membrane attachment point and +90 is the crown of the tube.

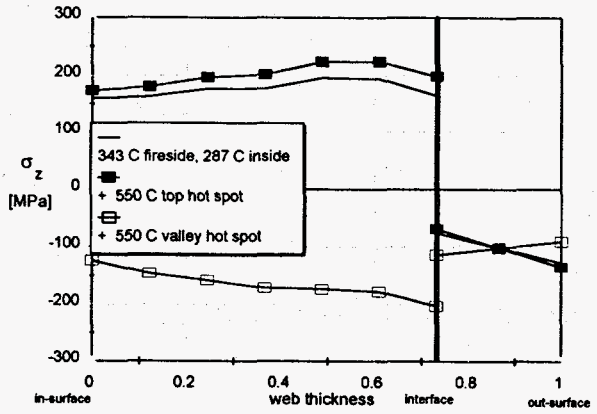

Figure 5 In-service axial stress in membrane of Sumitomo tube assembly - hot spot effect

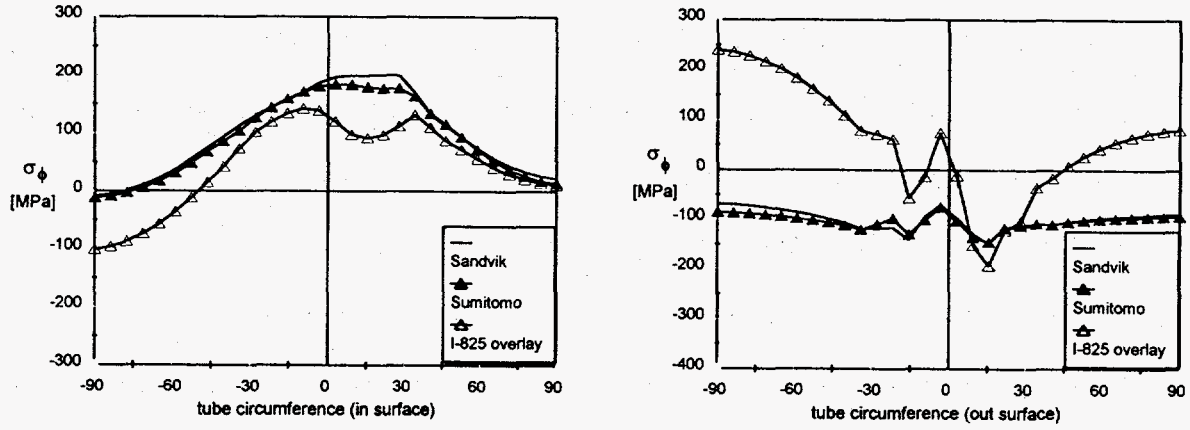

Figure 6 In-service hoop stresses on the inside and outside surfaces of three different tubes.

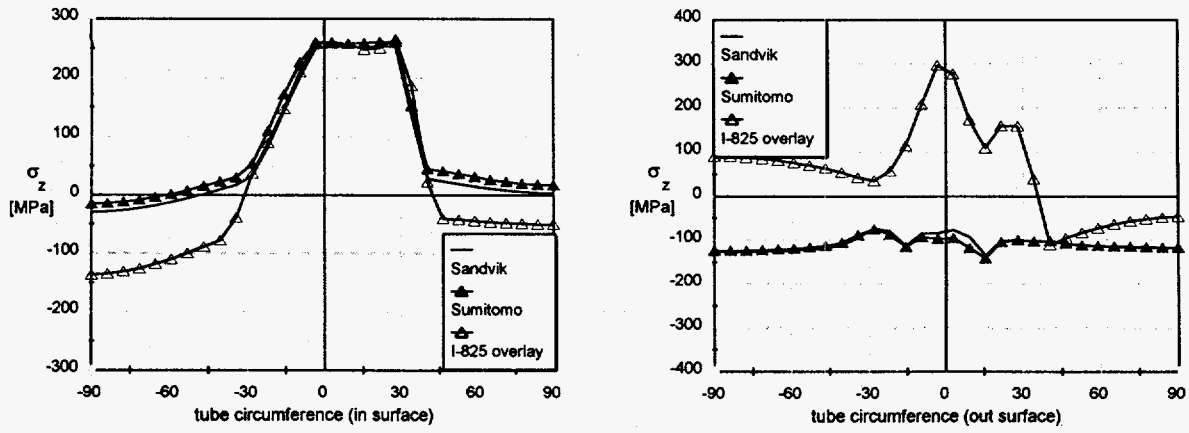

Figure 7 In-service axial stresses on the inside and outside surfaces of three different tubes.

cooling of such a tube from an equilibrium condition at 920°C. The same comparison for axial stresses is shown in Fig. 7. There is not a significant difference in the stress state in the carbon steel side. However, due to the difference in the thermal expansion coefficients among these three materials, there is a significant difference in the overlay hoop and axial stresses. The 304L SS experiences compressive stresses, while the axial and hoop stresses in the alloy 825 overlay are tensile almost everywhere. The same can be observed for the membrane, except the carbon steel is always in tension in all three cases.

The results presented should give a fairly reasonable representation of the stresses if no lateral constraints are applied to the tubes. Based on information from boiler fabricators and from observations during mill visits, it is clear that no constraints are intentionally added that would impede the thermal expansion of the boiler. The assumption to neglect the boiler dead weight seems to be reasonable also. According to the boiler construction the effect might be important for the tubes at the upper level of the boiler, while it can easily be neglected for the lower level, which is the portion of the boiler currently being analyzed. However, it is always a possibility for various tube-tube stresses to be generated as a result of the assembly process or which are caused by temperature non-uniformity in a certain wall or floor section. The results described in this report might also be

changed as properties, especially the weld material properties, are updated.

Although the overall expansion of the boiler walls is not constrained, local areas in the floor or wall panel, where the temperature is higher or lower than the temperature of the surroundings, may be subject to high constraints from the neighboring tubes. This is a case which could introduce tensile stresses in normal operation (no lateral constraints), so this is one of the major tasks that needs to be addressed in future studies.

4. Microstructural Characterization

There are several objectives to this portion of the program. One objective is to document the microstructural features of unexposed, as-fabricated composite tubing both as a function of the material and as a function of the tube fabricator. Another objective is to characterize a significant number of samples from composite tubing that had been exposed in a recovery boiler. Exposed samples are generally taken from tubing that was removed from service because of cracking or other degradation. A third objective is to collect information that might help differentiate between environmentally assisted stress corrosion cracking and a fatigue mechanism as the cause of cracking on the composite tubes and the membranes.

The microstructures of four unexposed composite tubes were studied; special attention was given to the structure in the vicinity of the interface between the carbon steel and the austenitic steel. The microstructure along the interface was characterized photographically for all four tubes, and microhardness measurements were made in the vicinity of the interface for all four. Electron microprobe measurements were made on one tube to define the carbon and nitrogen concentration variations in the vicinity of the interface. The microstructures of the Sumitomo 825-SA210 2½ in. tube are shown in Fig. 8, while Fig. 9 shows the structure in the vicinity of the interface for the Sandvik 3R12/4L7 (304L-SA210) 3 in. tube. These micrographs show an apparent carbide depleted region in the carbon steel adjacent to the carbon steel-austenitic alloy interface, and they show a

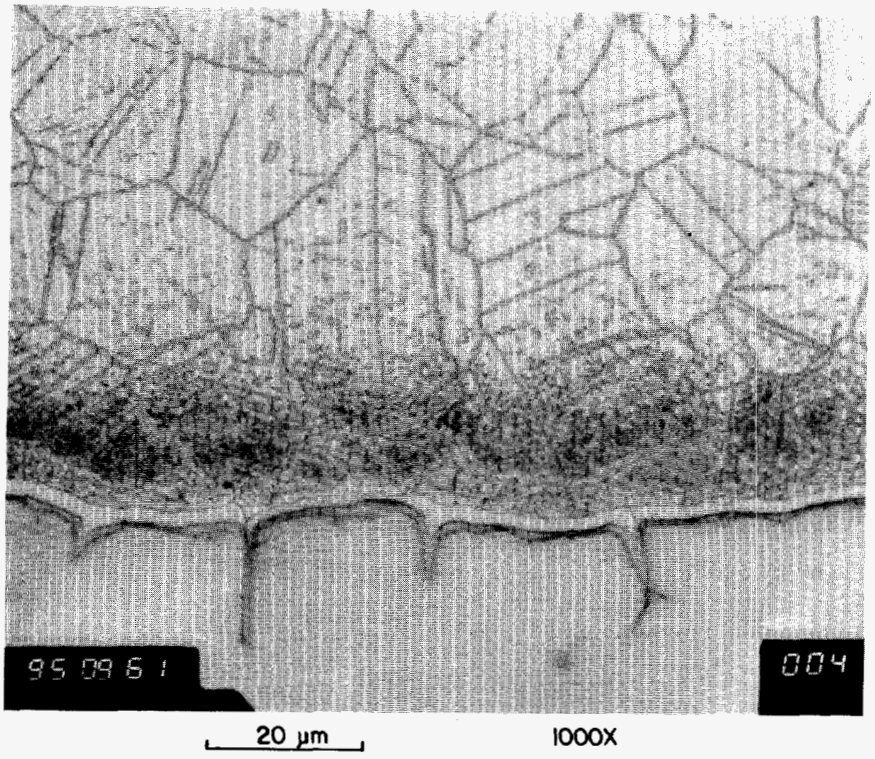

Figure 8 Microstructure of Sumitomo 825/SA210 2½ in. tube

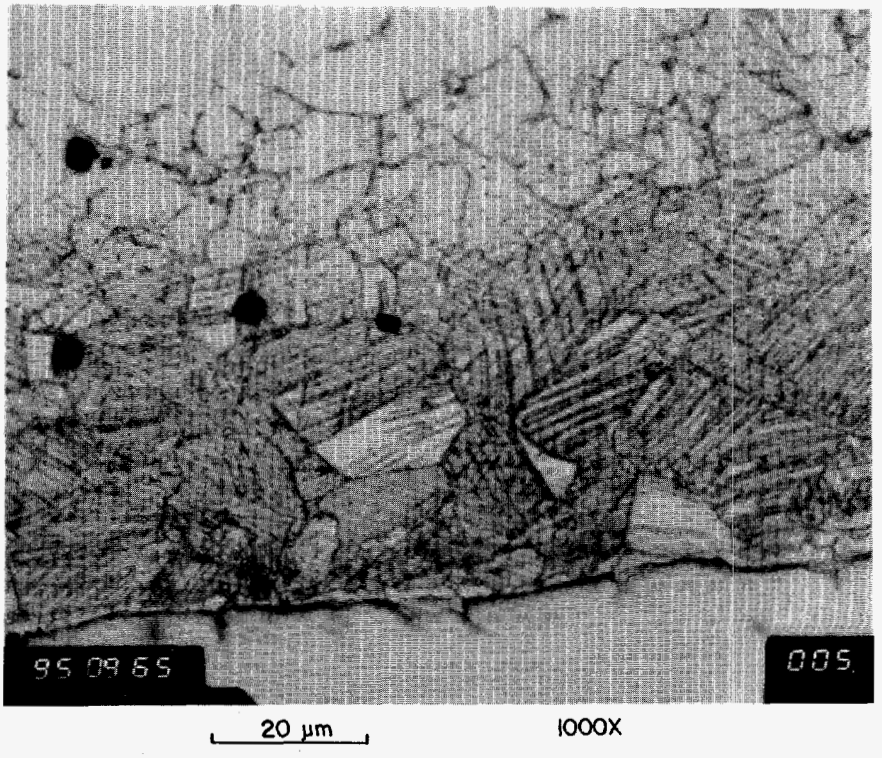

Figure 9 Microstructure of Sandvik 3R12/4L7 (304L/SA210) 3 in. tube.

precipitate-rich region adjacent to the interface in the austenitic alloy. The results of microhardness measurements, shown in Fig. 10, indicate the austenitic alloy is considerably harder in the precipitate-rich region adjacent to the interface. The data presented in Fig. 10 show the hardness results for each sample as measured using both a 100 gm load and a 10 gm load. The 100 gm load results are taken over a wider area and represent more of an average of the hardness. The results from tests with the 10 gm load give a better indication of short range variations in hardness because the hardness indent covers a much smaller area and thus samples a smaller volume of material. Comparison of the results from all four samples show the results are qualitatively similar. Close examination shows that the hardness of the tube materials away from the interface is slightly lower in the Sandvik tubes than in the Sumitomo tubes; this hardness difference may be due to relatively small differences in composition.

Reported or measured compositions of the alloys are within the nominal range for the all the alloys. Measurement of the carbon and nitrogen concentrations for one sample, the Sumitomo 825-SA210 2½ in. tube, indicates that the nitrogen composition shows essentially no variation across the interface, but carbon shows a significant concentration adjacent to the interface in the austenitic alloy.

Microstructural characterizations have also been completed on composite tube samples that are cracked as a result of recovery boiler exposure. Figures 11-14 shows cracking in the 304L stainless steel cladding on such composite tubes. As can be seen, these cracks generally, but not always, have some common features. The cracks are fairly wide and unbranched in the outermost region of the cladding. Cracks that progress through the cladding often show branching in the innermost part of the cladding, and the cracks invariably stop at the interface or turn and run parallel to the interface. Any penetration into the carbon steel is in the form of corrosion pits which only go a limited distance.

An exception to this pattern was seen in a tube which exhibited intergranular cracking which proceeded a short distance into the carbon steel. Cracking in the stainless steel was transgranular,

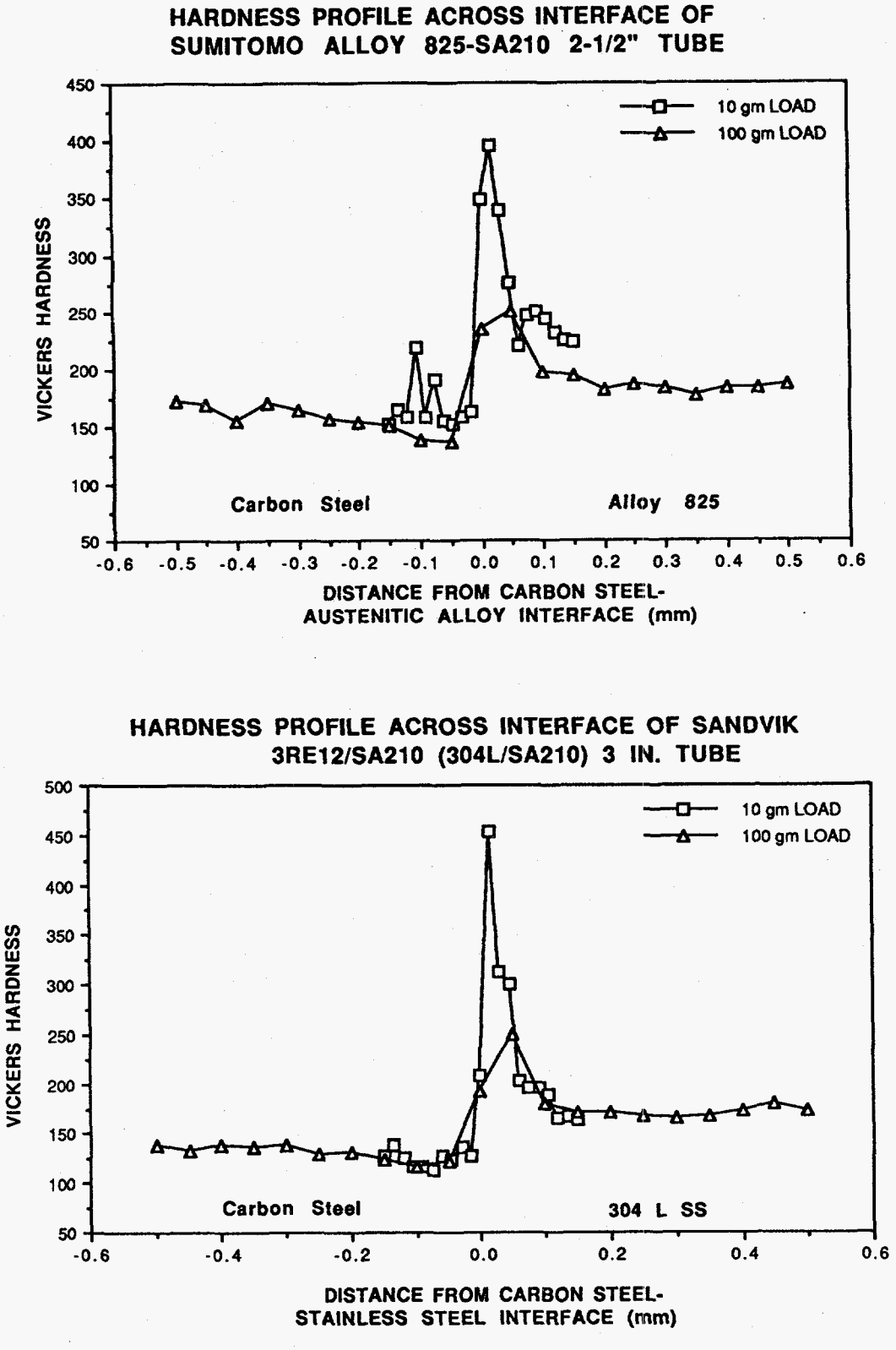

Figure 10 Hardness measurements in the vicinity of the interface for the Sumitomo 825/SA210 2½ in. tube and the Sandvik tube 3R12/4L7 3 in. tube

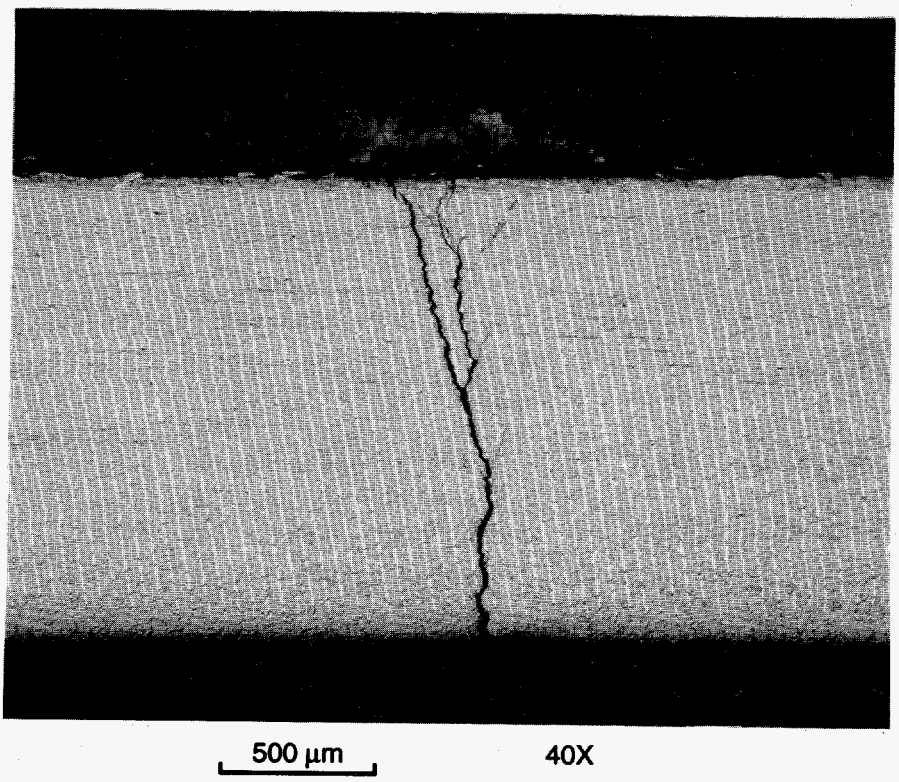

Figure 11

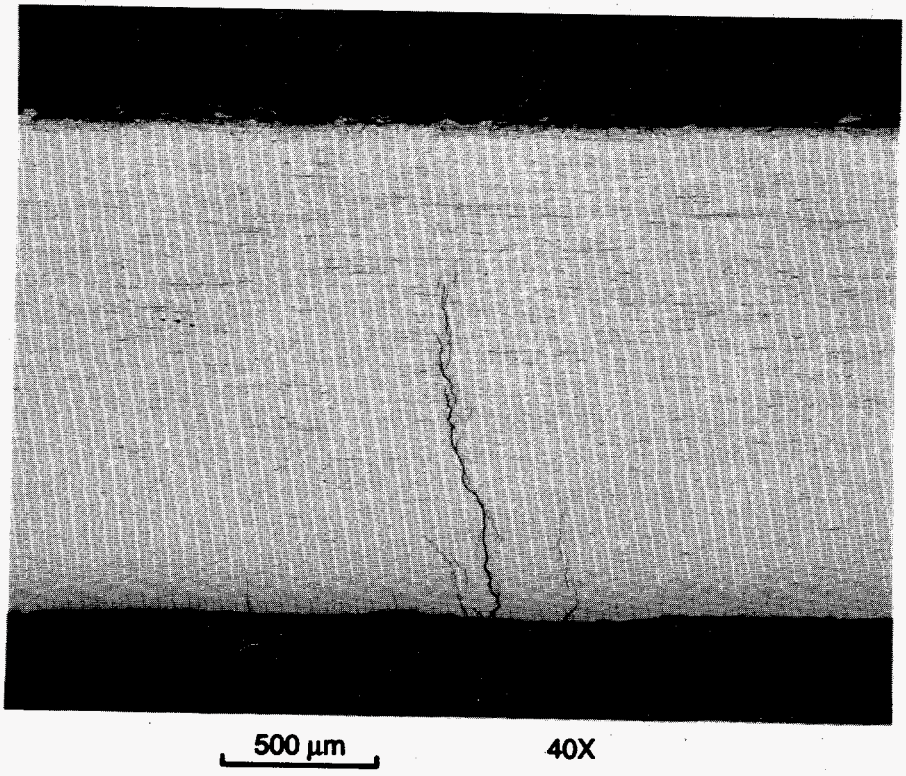

Figure 12

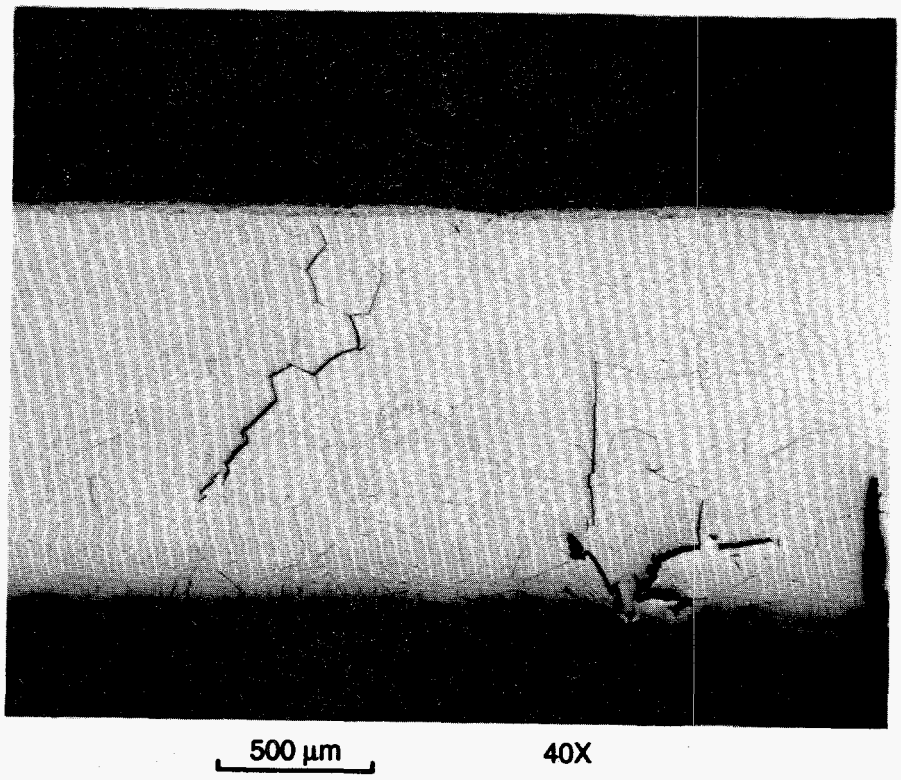

Figure 13

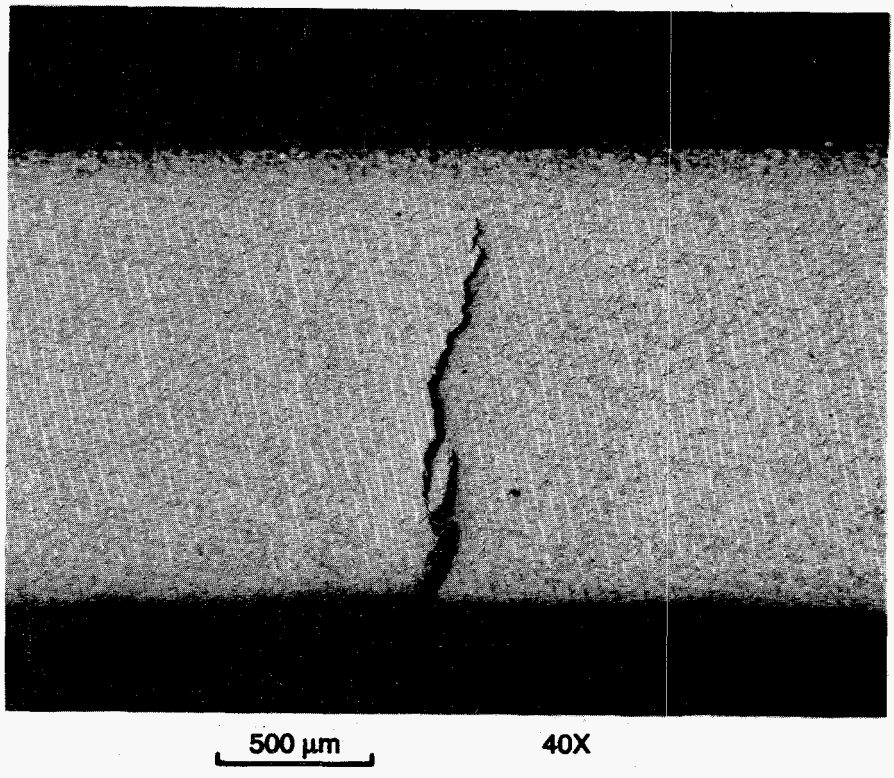

Figure 14

and a crack had advanced a significant distance along the stainless steel/carbon steel interface. It was below this interfacial crack that the intergranular cracking occurred in the carbon steel. As seen in Figure 15, the cracking did not extend past the decarburized region of the carbon steel. Further study of this cracking is underway.

The electron microprobe has been used to determine the composition of the material that is present in cracks like those shown in Figs. 11-15. The analyses indicate that oxygen and sulfur are essentially always a part of any foreign material found in such cracks. From these semiquantitative measurements, the oxygen concentration is generally a factor of ten greater than the sulfur concentration. Chlorine is sometimes found in the cracks, but only a portion of the time, and, when it is present, chlorine is always accompanied by oxygen and sulfur.

To provide information that could help differentiate between cracking that occurs through a fatigue mechanism versus cracking related to environmentally driven stress corrosion cracking, transmission electron microscopy studies are planned. These studies will investigate the dislocation structure in the vicinity of cracks to determine if that structure has the characteristics of material that has been subjected to fatigue.

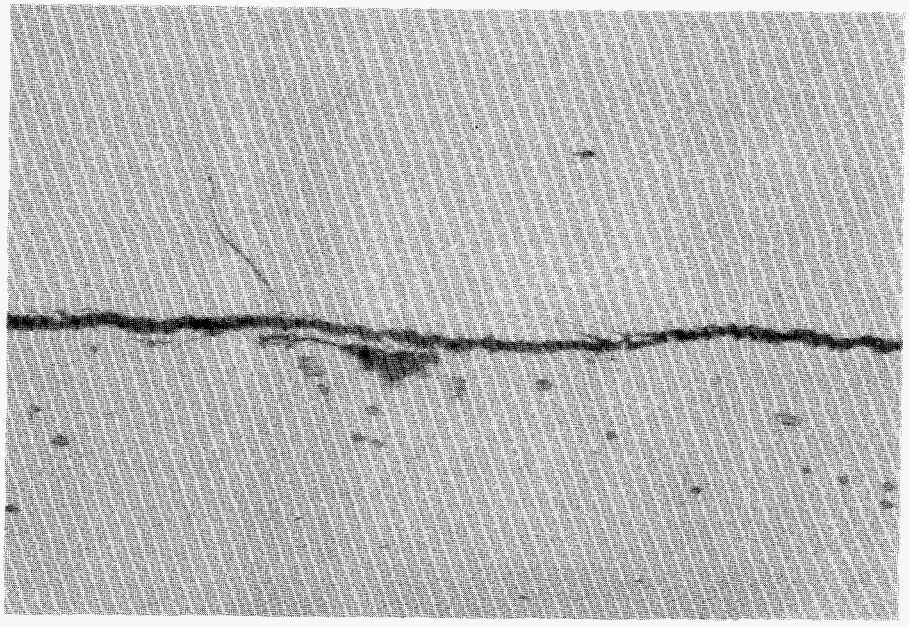

Figure 15

5. Thermal Fatigue of Composite Tubes

Tasks that are related to the assessment of thermal fatigue in composite tubes include a review of fatigue in constituent alloys, the collection of physical and mechanical properties data needed for the development of deformation and damage models, fatigue tests on tubes and the constituent alloys used to manufacture composite tubing panels, and evaluation of damage mechanisms in the cladding and weldments.

During this reporting period, the collection was completed of literature data on mechanical and thermal fatigue of constituent materials. Alloys for which isothermal fatigue data were available included type 304L stainless steel, type 308 stainless steel filler metal, alloy 625, alloy 825, Sanicro 38, and carbon steels whose compositions were comparable to SA-210. Thermal fatigue data were found for type 304L stainless steel, carbon steels, and composite tubes. A report summarizing the findings is being prepared.

The physical and mechanical properties provided in ASME Boiler and Pressure Vessel Code Sect. VIII, Div. 2 were recommended as the reference properties to be used in the modeling work. Properties such as thermal expansion coefficients, thermal conductivity and diffusivity, and elastic moduli were found in Sect. VIII, Div. 2 for temperatures to 815°C (1500°F) for some alloys. When needed, Code data were supplemented by information obtained from the alloy vendors. No physical and mechanical properties data were found for as-deposited filler metals (309L stainless steel and 312 stainless steel). Welds were produced for specimen preparation to obtain the needed properties. Tabulated yield strengths and ultimate strengths were obtained for base and cladding materials. It was found that the physical and mechanical properties of SA-516 Gr 55 were similar to SA-210, so data for SA-516 Gr-55 were selected for use on an interim basis when needed for analysis in the temperature range of 427 to 927°C (800 to 1700°F).

Alloys were obtained for mechanical testing. These included fine-grained 304L stainless steel (similar to tube cladding), coarse-grained 304L stainless steel (similar to web cladding), type 312

stainless steel filler metal (used for joining the tubes to webs), fine-grained alloy 625 (similar to a candidate tube cladding), and AISI 1027 carbon steel (similar to pressure tubing). Exploratory tensile and relaxation testing of the fine-grained 304L stainless steel was begun to provide data on which to estimate the level of residual stress that could be retained in composite tubing. Testing was performed in the temperature range of room to 650°C (1200°F). At the upper limit of the composite tube operating temperature (316°C), it was found that the fine-grained 304L stainless steel had a high yield strength, relative to the yield strength one would select from design and construction codes, but the flow strength of the annealed 304L stainless steel was substantially less than that observed for the carbon steel.

The design and assembly of a thermal fatigue testing apparatus was begun. A 50,000 pound universal testing system was selected for mechanical loading, and radiant lamp heaters were chosen as the heat source.

Section 2: CORROSION AND FAILURE ANALYSIS STUDIES IN SUPPORT OF THE PULP AND PAPER INDUSTRY

J. R. Keiser, S. J. Pawel, and R. W. Swindeman

Metals and Ceramics Division
Oak Ridge National Laboratory
P.O. Box 2008, Oak Ridge, TN 37831

INTRODUCTION

Technical support is being provided to various pulp and paper companies and related industries to help determine the cause of material degradation problems and to identify alternate materials to prevent such degradation. During the past year, examinations included repair welds on six recovery boiler water-wall tubes, severely thinned lime kiln chains, a failed economizer tube from

a recovery boiler, a cracked alloy 253MA tubing from a black liquor fluidized bed combustor, and samples of tubing and studs from floors of black liquor recovery boilers. The results of the analyses were communicated to the plant operators, and, in some cases, recommendations of alternate materials were made.

TECHNICAL PROGRESS

Summary

1. Repair Welds on Carbon Steel Water-Walls

Six water-wall tube specimens of unknown history, each about ½ m (1½ ft) in length and including portions of adjacent tubes and the interconnecting membrane material, were available for this examination. The buildup associated with the weld repair on each tube was readily visible and two specimens representing each tube repair were selected for this study. Cross sections including the weld repair and adjacent base material were mounted and polished using standard metallographic specimen techniques.

Optical microscopy of the as-polished specimens revealed no cracking, porosity, or obvious contamination (slag or inclusions) associated with the weld. A very minor lack of fusion - a segment about 0.13 mm (0.005 in.) long at the extreme edge of a weld buildup region - was observed on only one of the twelve cross sections examined.

Some type of metal spray coating was observed covering large portions of the tubing. No attempt was made to identify the coating type (not relevant to this investigation). However, it was apparent that the coating exhibited widely varying degrees of adherence to the substrate. In some regions, the coating was absent all together, while in others, small regions where the coating was adjacent - but not bonded - to the substrate were observed. Other regions revealed apparently intimate contact/bonding of the coating and substrate. It is possible that the metallographic procedure itself contributed to some loss of adhesion of the coating, but regions of poor coating

adhesion (chipping and flaking) were readily apparent in the as-received material.

Etching of the cross sections revealed a very nominal weld/heat affected zone (HAZ) appearance. The weld metal appeared as variable-sized ferrite grains with carbide particles and the usual residual signs of solidification pattern in multiple pass welds. The HAZ immediately adjacent to the weld exhibited typical grain coarsening and a microstructure of ferrite and (probably) some bainite. A typical grain refinement gradient (to smaller grains) was observed as distance from the weld increased. The base metal exhibited a typical pearlitic structure consistent with a low carbon content steel.

Hardness profiles across the weld bead, through the HAZ, and into the base metal revealed very little hardening associated with the weld. Maximum hardness in the HAZ varied among the specimens from HRB 90-99 (HRC 10-22) compared to a base metal hardness of about HRB 75. The low values of maximum hardness are not indicative of a material particularly susceptible to cracking.

Based on this examination, it appears that the quality of the weld repair/overlay is good and nominal in appearance in every way. There does not appear to be any inherent limitation on the number of times a tube may be repaired in this fashion, as hardening and related cracking does not seem to be a significant factor. No attempt to measure the residual stress associated with the weld repair was performed, but the general wastage corrosion mechanism is not substantially influenced by this factor and therefore tube life/performance may not be limited by the residual stress pattern due to the weld repair.

2. Lime Kiln Chains

Links from two lime kiln chains were examined after, respectively, three months and seven months service. Sections of both links showed significant reductions in cross section, likely a result of oxidation, and both were distorted, one more severely than the other, from the service stresses. Based on microstructural observations and hardness measurements, it was concluded that neither

section had not seen sustained service temperatures above 816°C (1500°F). On the basis of these observations, it was recommended that a higher strength alloy with higher chromium content to improve corrosion resistance should be used.

3. Economizer Tube Examination

An examination was conducted on a carbon steel tube from a black liquor recovery boiler economizer. The tube had a hole about 6 mm x 2 mm in the vicinity of a bend along with a number of circumferentially oriented cracks near the hole. A metallurgical consulting company was concluding their examination at the time ORNL was asked to provide supplementary information. Assistance from ORNL was requested in the form of Auger surface analysis of the face of one of the cracks. The Auger analysis was conducted along with metallographic and XPS analyses. In addition, checks of the hardness, ovality, and wall thickness were made.

The Auger analysis was conducted on a fresh fracture that was nearly 100% cleavage with only small patches showing ductile tearing. The surface analysis showed only Fe, C, and O, and the primary source of C and O was determined to be contamination from contact with the air. Examination of a pre-existing crack showed the presence of significant chlorine and sulfur, but sputtering showed this to be predominately surface contamination rather than a significant chloride or sulfide phase. The tube ovality, the orientation of the cracks, and hardness measurements are not consistent with nominal fabrication stresses but rather indicate a difficult fabrication history. There is likely a substantial and complicated stress pattern in the tubes at the bend location that is capable of contributing to a cracking problem that potentially is limited to this region. Environmental cracking is consistent with the data collected, but the constituents present on the process side of the tubing are not consistent with intergranular cracking, and the materials typically associated with intergranular cracking of carbon steel were not found.

4. Black Liquor Fluidized Bed Combustor Analysis

An examination was conducted on sections from two heat exchangers that had been used for a limited duration operation at about 650°C (1200°F) in an indirectly fired combustor used to process black liquor from a paper mill. The heat exchangers had been inspected immediately following shutdown and no cracking was found. A subsequent inspection a few weeks later revealed cracking in the exchanger constructed of 253MA alloy while the exchanger constructed of 310S stainless steel had no cracking. Microscopic examination showed that the cracking in the 253MA pipe originated on the exterior surface and was totally intergranular. Because of the intergranular nature of the cracking, samples of both materials were subjected to an oxalic acid etch to check for the presence of a sensitized microstructure. Both materials showed preferential attack by the acid along grain boundaries, an indication of chromium depletion. Analysis of the corrosion products at and near the surface of the 253MA sample showed significant concentrations of sulfur.

Cracking of the pipe was attributed to polythionic acid stress corrosion cracking (PA SCC). To avoid such problems during future operations, recommendations were made for alternate tube materials that would not be as prone to sensitization, shutdown procedures that could be used to prevent PA SCC, and operating conditions that would lessen the possibility of PA SCC.

5. Black Liquor Recovery Boiler Studded, Carbon Steel Floor Tubes

The operation of black liquor recovery boilers is critical to the operation of pulp and paper mills both from the aspect of recovery of chemicals used in the pulping process as well as for the production of electrical power. A large proportion of boilers have floors constructed of carbon steel tubes, the majority of them with tube studs for promoting heat transfer and for holding a refractory in place. A failure of a floor, waterwall, or heat exchanger tube can release water that could reach the molten salt bed creating the potential for a serious explosion. A significant number of boilers have experienced such tube failures, so failed tubes from the floors of three boilers have been

examined at ORNL.

There are several features that seem to be common to failed floor tubes. Generally, extreme wastage of studs has occurred in the region around the tube rupture. In addition, tube wall thinning is usually found in the vicinity of the tube rupture. Microstructural examination of the carbon steel tubes in the vicinity of the failures showed that the tubes had reached temperatures much in excess of 538°C (1000°F), sometimes the structures indicate temperatures in excess of 732°C (1350°F). Most likely, molten smelt reached the tube surface causing the stud and tube wastage along with the temperature excursions. Tube wall thinning reduced the amount of load-bearing material, and during the time of temperature excursions the yield strength of the carbon steel tube would be lower. The result would eventually be for the load from internal presurization to exceed the load-bearing capability of thinner, weaker tube.

Development Of Materials For Service In Kraft Recovery Boilers

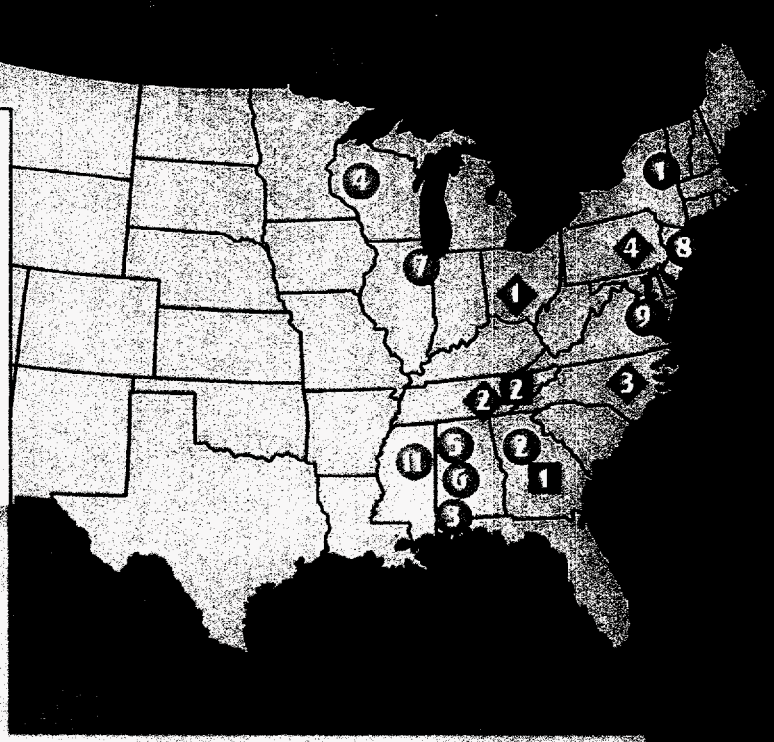

The Project Incorporates a Strong Team Effort

Pulp and Paper

1. Champion International
2. Georgia-Pacific
3. International Paper
4. James River
5. MacMillan Bloedel
6. Parsons & Whittemore
7. Stone Container
8. Union Camp
9. Westvāco
10. Weyerhaeuser
11. Weyerhaeuser

Suppliers

1. Babcock & Wilcox
2. Combustion Engineering
3. Kvaerner
4. Sandvik

Research Sites

1. Institute for Paper Science and Technology
2. Oak Ridge National Laboratory
3. Pulp and Paper Research Institute of Canada

Approach

- Identification of degradation mechanisms, and selection of improved technologies/materials
- Evaluation of alternative design/materials
- Manufacturing and testing of components

The project is a direct result of the "Materials Needs And Opportunities" assessment of the AIM Program.

Research and Development Sponsored by

Advanced Industrial Materials (AIM) Program, Office of Industrial Technologies, Energy Efficiency and Renewable Energy, U.S. Department of Energy

Ni_3Al TECHNOLOGY TRANSFER

V. K. Sikka, S. Viswanathan, M. L. Santella, and R. W. Swindeman

Metals and Ceramics Division
Oak Ridge National Laboratory
P. O. Box 2008
Oak Ridge, Tennessee 37831

INTRODUCTION

Ductile Ni_3Al and Ni_3Al-based alloys have been identified for a range of applications. These applications require the use of material in a variety of product forms such as sheet, plate, bar, wire, tubing, piping, and castings. Although significant progress has been made in the melting, casting, and near-net-shape forming of nickel aluminides, some issues still remain. These include the need for (1) high-strength castable composition for many applications that have been identified; (2) castability (mold type, fluidity, hot-shortness, porosity, etc.; (3) weld reparability of castings; and (4) workability of cast or powder metallurgy product to sheet, bar, and wire.

All of the issues listed above can be "show stoppers" for the commercial application of nickel aluminides. This report describes the work completed to address some of these issues during the fourth quarter of FY 1995.

TECHNICAL PROGRESS - FY 1995

Summary

The chemical composition of Ni_3Al-based alloys and its competitor materials are presented. The oxidation and carburization resistance data on Ni_3Al-based alloys are compared with Alloy 800. The creep data of Ni_3Al-based alloys are compared with that of the HU material. The Exo-Melt™ process developed for melting of nickel and iron aluminides was chosen as a R&D 100 winner for 1995. The cumulative amount of Ni_3Al-based alloy melted by the Exo-Melt™ process reached nearly 20,000 lb through July 1995.

Mold filling and solidification analyses were completed for the base tray. A video animation output of the results was completed.

Tensile properties were completed from room temperature to 1100°C on base metal and weldments in 95-mm-diam centrifugally cast pipe of alloy IC-221M. Most of the weldment failures were in the base metal. In order to understand the weld-induced cracking, Gleeble testing was carried out on alloys IC-221M and IC-396M.

The technology transfer activities including the progress of the Cooperative Research and Development Agreement (CRADA) work with Delphi Saginaw and Metallamics are described.

1. High-Strength Castable Compositions, Start 10/94, End 9/95:

The Ni_3Al-based compositions compete strongly with commercially available nickel- and iron-based alloys. The chemical composition of Ni_3Al-based alloys and commercial alloys such as Haynes 214, HU, and Alloy 800 are shown in Table 1. The oxidation, carburization, tensile, and creep data of Ni_3Al-based alloys were compared with the commercial alloys in the last two quarterly reports. Comparisons clearly showed the following:

1. Oxidation and carburization resistances of Ni_3Al-based alloy IC-221M are significantly better than iron-based high-nickel alloys, HU and Alloy 800.
2. Tensile strength properties of IC-221M are five times better than HU in the temperature range of interest (800 to 1000°C).
3. The creep rupture strength of IC-221M is nearly three times higher than the cast HU alloy.

Based on the above listed improvements in properties, we have worked several commercial producers including the latest licensee (United Defense) in developing cast components for the following furnace furniture applications:

1. Trays and fixtures for carburizing furnaces: This activity is currently under way with Delphi Saginaw under a CRADA. Six base trays for the batch furnace and two

Table 1. Composition of Ni_3Al-based alloys and commercially available competing alloys

Element	Weight percent						
	IC-50[a]	IC-218LZr[b]	IC-396M[c]	IC-221M[d]	Haynes 214[e]	HU[f]	Alloy 800[e]
Al	11.3	8.7	7.98	8.0	4.5	--	0.4
Cr	--	8.1	7.72	7.7	16.0	18.0	21.0
Mo	--	--	3.02	1.43	--	--	--
Zr	0.6	0.2	0.85	1.7	--	--	--
B	0.02	0.02	0.005	0.008	--	--	--
C	--	--	--	--	0.03	0.55	0.05
Fe	--	--	--	--	3	42.45	45.5
Ti	--	--	--	--	--	--	0.4
Ni	88.08	83.1	80.42	81.1	76.35	39.0	32.5
Si	--	--	--	--	0.1	--	--
Y	--	--	--	--	0.02	--	--

[a]Cold workable.
[b]Hot and cold workable.
[c]Castable alloy for static applications (some microporosity).
[d]Castable alloy for dynamic application (minimum microporosity).
[e]Wrought alloy.
[f]Cast alloy.

assemblies for the pusher furnace were in production heat-treating furnaces. After casting, the trays and fixtures were received at ORNL where they were weld repaired as needed. Three of the batch-furnace trays and one assembly of the pusher-furnace trays were given a preoxidation treatment of for 3 h at 1100°C. The preoxidation treatment was carried out to see if the excellent carburization resistance of IC-221M can be even further improved because Al_2O_3 film is known to be an excellent barrier to carbon penetration. Trays and assemblies are currently setting at GM awaiting installation.

2. Trays for oxidizing heat-treating furnaces: At least three companies have been identified for this application. United Defense and ORNL are working closely with these companies to identify their needs and get the components into test at the earliest possible time. In fact, one set of trays has been cast at United Defense for use in the oxidizing furnace at United Defense. The data developed at United Defense can be used to further strengthen the identified applications.
3. Hot-forging dies: In this application, the IC-221M alloy was sand cast into a near-net-shape die, machine finished, and tested on a production hammer forge press at United Defense. The preliminary data have shown nearly two times the life of the current die material being used. Savings resulting from longer life, better shape retention, less down time, less loss time to change dies, and less inventory of dies will easily exceed the lower cost of the current material.
4. Grate bars for calcination furnaces: These are bars of special shape with use in calcination of ores. The grate bars are exposed to temperatures in the range of 1000 to 1150°C and to environments containing high-carbon activity. Sixteen of the grate bars were cast and have been operating in a calcination furnace for the last five months. If the grate bars show no distortion or corrosion product after six months of service, we expect a demand for replacing over 15,000 of them. This level of application will clearly make the Ni_3Al-based alloy truly commercial.

5. Furnace support structures: These are components of special shape and are used for supporting billets and plates during their heating period prior to heat treatment. These components are also called bucks. One of the companies is currently working with United Defense through ORNL to get these parts cast and put into service.
6. Tube hangers for oil industry application: Heat recovery boilers in the oil industry require hangers that can support the superheater tubes. These hangers operate at temperatures approaching 1100°C. Several of these hangers were cast at United Defense and installed at one of the oil companies. After a few months of service, a decision will be made as to their use in other plants. This is potentially a very large application in the oil industry.
7. Transfer rolls: In this application, the IC-221M rolls are used to transfer steel plates during heat treating. The rolls are nominal 14 in. OD × 1 in. wall × ~ 14 ft long. Two roll assemblies of Ni_3Al-based alloy have been in operation at one of the steel companies for almost two years. Based on this experience, other steel companies are also becoming interested. A major hurdle for this application is the ability to successfully weld the rolls to the trunnions. Significant progress to this problem has been made and reported in the next section.
8. Others: Many other applications are currently being identified. These include: roll guides, mixing spokes, nuts and bolts, and radiant burner tubes. ORNL is working with United Defense and Alloy Engineering & Casting Company to fulfill the potential demands for the newly identified components.

2. Castability of Nickel Aluminides, Start 10/94, End 9/95:

Work under this milestone has continued on two aspects. The first one is the development of a cost-effective method for melting the alloy. The second aspect is the modeling of solidification behavior. Significant progress continued in both areas.

The newly developed Exo-Melt™ process, developed for melting of Ni_3Al-based alloys won the *Research & Development* magazine's R&D 100 award. This award is given

to the top 100 innovations each year. Based on the publicity from this award, 47 requests for information were received. Thirty-two requests were fulfilled during this reporting period.

The Exo-Melt™ process use continues to grow. A bar chart showing the accumulative quantity of the Ni_3Al-based alloy melted during FY 1995 is shown in Fig. 1.

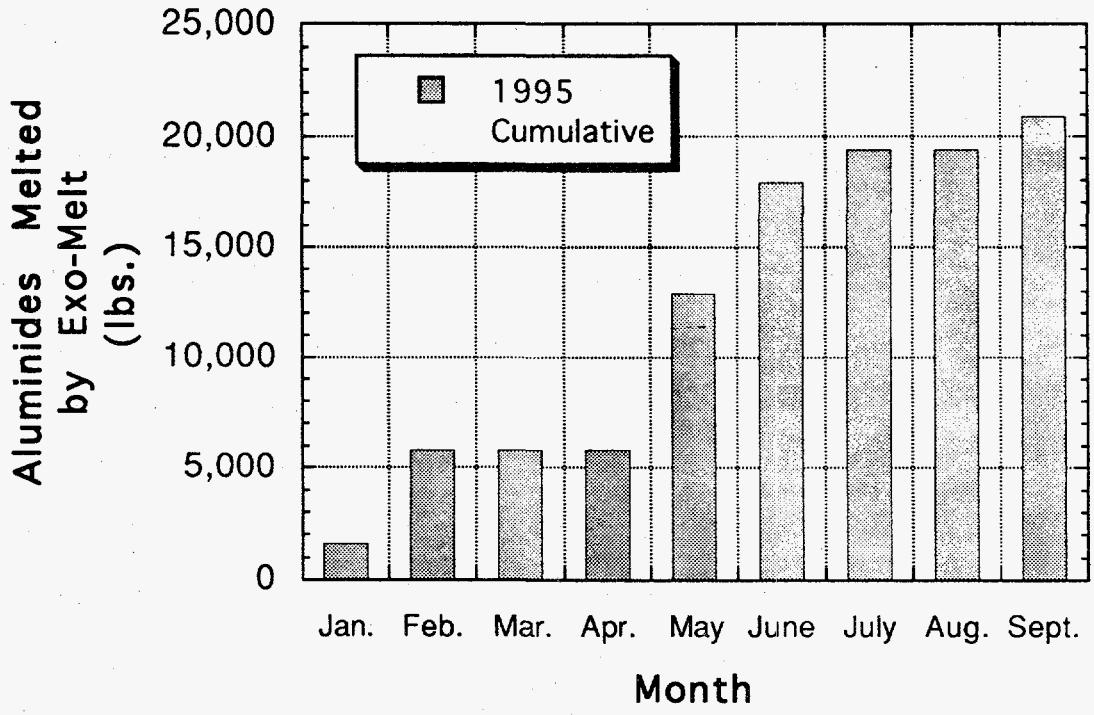

Fig. 1. Nickel aluminides melted in FY 1995 by the Exo-Melt™ process.

Mold filling and solidification analyses were completed for the base tray. A video animation output of the results is under preparation. The mesh contained approximately 110,000 nodes. Since the tray configuration was symmetric about the center of the tray, only half the tray was modeled, allowing a smaller mesh size than used earlier. Since the tray was poured at a tilt (as opposed to being poured flat), the filling simulation was conducted for two tilt angles. For both tilt angles, the filling was fairly turbulent, consistent with the observation that tray quality was not greatly affected by the tilt angle. Some shrinkage was observed at the riser closest to the sprue. This may suggest the

reason for folds being observed in that area in the casting. Modifications are being made to the gating to allow for a smoother fill.

3. Weld Repairability of Castings, Start 10/94, End 9/95:

Efforts continued in the areas of: (1) evaluating the mechanical properties of welds, (2) assessing the possible effects of ingot composition on weld-induced cracking, and (3) developing a procedure to evaluate the susceptibility of alloys to weld-induced cracking.

a. Mechanical Properties of Welds. Four welded plates were prepared to conduct initial stress-rupture testing. The plate material used was actually sections of webs cut from a sand-cast heat-treating tray of the IC-221M composition. The approximate nominal plate dimensions were 50×75 to 100×9.5 mm. Weld edge preparation consisted of a double-vee groove with a root gap opening of 2 to 4 mm. The gas tungsten arc (GTA) welding process was used with argon cover gas. Gas shielding was also provided on the back side of the root pass so that grinding was not necessary. Two sets of welded plates were made using either metal-powder-cored filler metal purchased from Ametek Specialty Metal Products Division, or solid wire made at ORNL. Both filler metals had the nominal composition of IC-221LA. One set of plates was welded along the 50-mm edge to yield specimens with the welds oriented transverse to their axes. For the second set, the weld axes were oriented with the specimen axes. Test specimens were machined from the welded plates and tested in air at 871°C (1600°F) with a stress level of 103 MPa (15 ksi). The test results are given in Table 2. In specimens 94W01 and 94W02, the weld was transverse to the specimen axis. Because the IC-221LA filler metal has lower strength and higher ductility than the IC-221M base metal alloy, this orientation concentrates the applied stress in the weld. As expected, both of these specimens failed along the weld centerlines. These data are not conclusive, but the longer life of the 94W02 specimen suggests that weld deposits made with conventionally processed filler metal could have better creep resistance than those made with powder-cored wire.

Table 2. Results from stress-rupture tests of specimens of IC-221M welded with IC-221LA filler metal[a]

ID	Time to failure (h)	Nominal strain (%)	Remarks
94W01	37.1	0.50	Transverse weld, powder-cored wire
94W02	338.7	0.86	Transverse weld, solid wire
94W03	748	3.97	Longitudinal weld, powder-cored wire
94W04	190.1	1.44	Longitudinal weld, solid wire

[a]Stress = 103 MPa, temperature = 871°C.

Examination of the 94W03 and 94W04 specimens indicated that the creep behavior of the IC-221M base metal was the dominating factor in their failure. There were numerous crack initiation sites in both of these specimens, but the weld metal was not a preferred crack initiation site. The difference in time-to-failure appears to be related to variability in the behavior or microstructure of the sand-cast IC-221M.

In another case, a double-vee groove joint geometry was used to weld 25-mm-thick plates of IC-221M. These plates were made by air melting and casting into a 100 × 150 × 25-mm chill mold. The IC-221LA powder-cored wire was used to produce the GTA weld. The plates were restrained during welding, and radiography indicated that, except for some crater cracks, the welds were defect-free. A macroetched, cross-sectional view of this welded plate is shown in Fig. 2. Five full cross-section stress-rupture test specimens were machined from the plate. Two specimens were used for tensile testing at room temperature and 871°C. The remaining three specimens were used for stress rupture testing. The rupture data are plotted in Fig. 3.

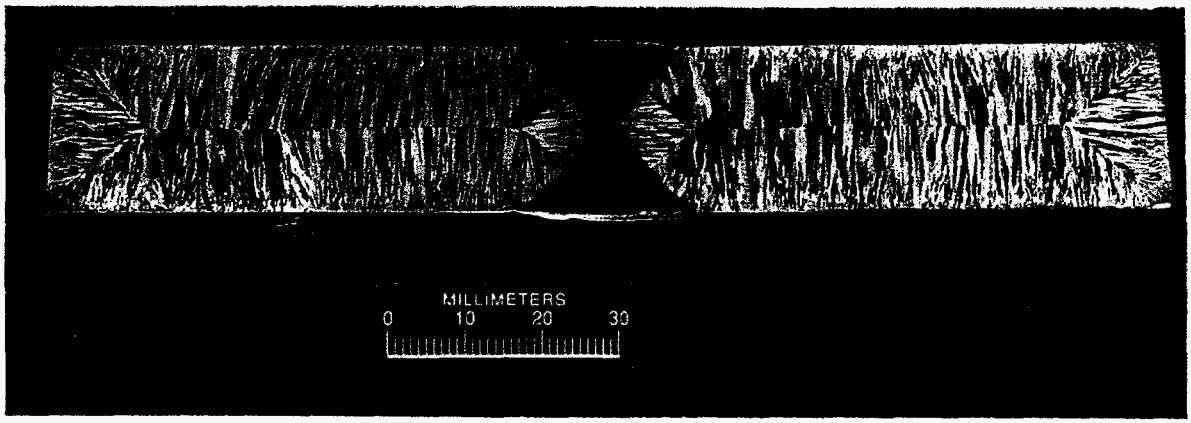

Fig. 2. Macroetched cross section of 25-mm-thick IC-221M plates welded together with IC-221LA filler metal.

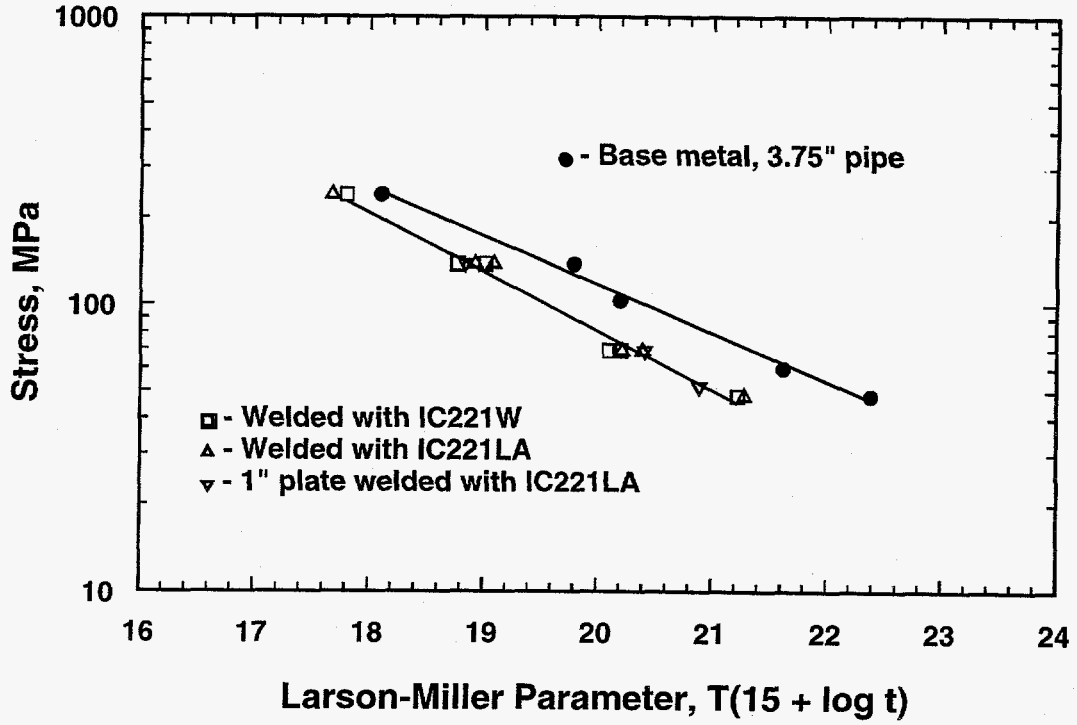

Fig. 3. Larson-Miller plot of stress rupture test results from 3.75-in.-OD centrifugally cast IC-221M pipe and welds of IC-221M castings made with either IC-221 or IC-221LA filler metal (right).

Two welds were also made on sections of 95-mm OD (3.75-in.) centrifugally cast IC-221M pipe using the same processing as for the 1-in.-thick plate. The wall thickness of the cast pipe is 6 to 7 mm (about 0.25 in.). The pipe sections were welded entirely from

the outside using a single-vee-groove joint design. One weld was made with the IC-221LA. The second weld was made using an IC-221LA root pass, but was welded to completion using IC-221W filler metal. Both of the filler metal wires were metal-powder cored. These welds were also radiographed and judged to be acceptable. A photograph showing both welded pipes is given in Fig. 4.

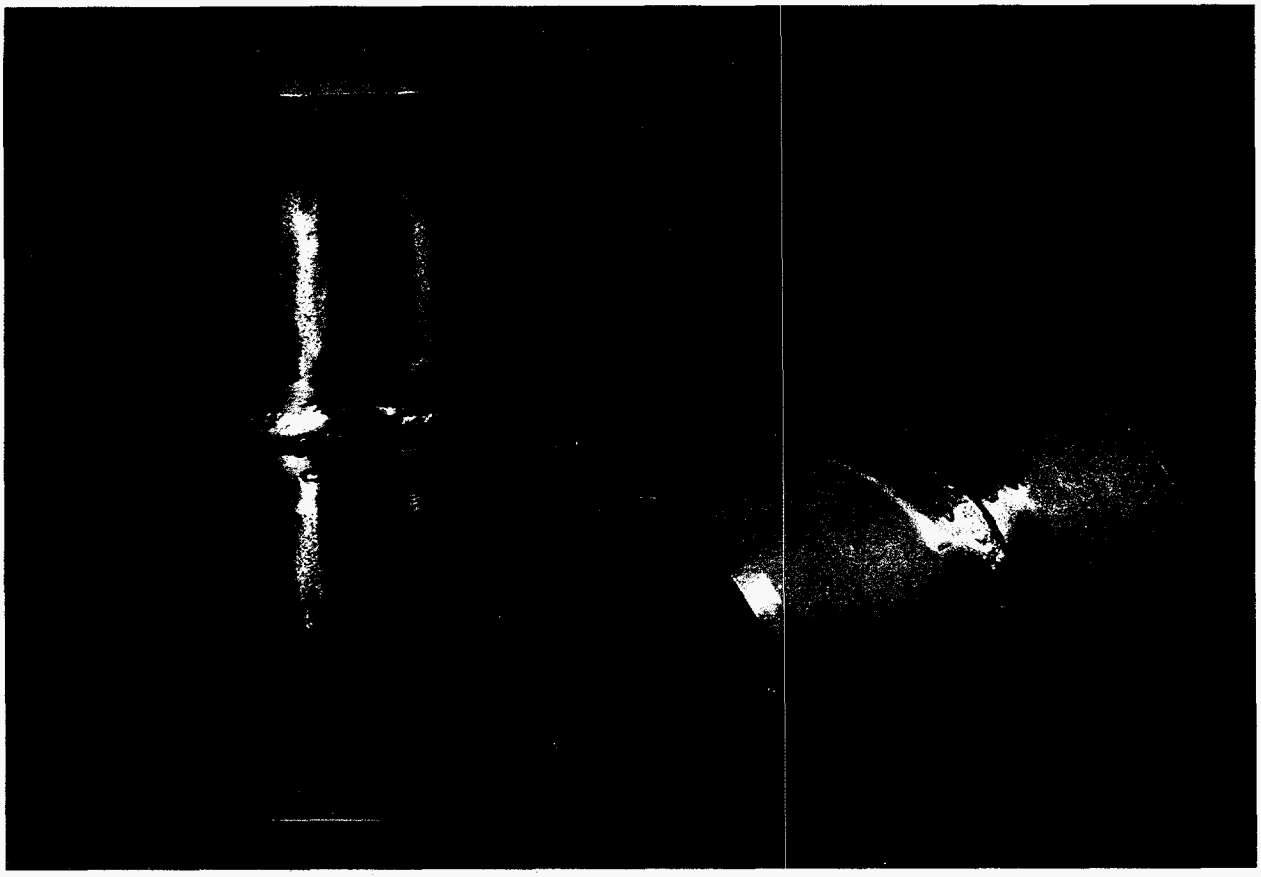

Fig. 4. Centrifugally cast IC-221M pipe sections welded together with either IC-221LA filler metal (left) or with a combination of IC-221LA and IC-221W filler metals.

A series of tensile specimens with gauge dimensions of 28.6 mm long by 3.2 mm diam were machined from each weldment and from the base metal of the pipe. The weld was centered in the gauge length of the weldment specimens. The tensile tests were done in air at room temperature, 600, 800, 900, 1000, and 1100°C using a cross-head speed of 0.085 mm/s, and the results are presented in Table 3. These data shown that

Table 3. Results for tensile test specimens made from base metal and weldments in 95-mm-OD centrifugally cast pipe of IC-221M

Specimen identification	Test temperature (°C)	Condition	Yield strength (MPa)	Tensile strength (MPa)	Elongation (%)	Failure location
1B	23	Cast	673	673	0.7	NA[a]
1W1	23	IC-221LA filler	679	687	1.8	Base
1W2	23	IC-221W filler	675	687	1.2	HAZ[b]
2B	600	Cast	649	649	0.2	NA[a]
2W1	600	IC-221LA filler	637	637	1.4	Base
2W2	600	IC-221W filler	666	666	1.5	Base
3B	800	Cast	562	562	0.5	NA[a]
3W1	800	IC-221LA filler	618	618	1.0	Base
3W2	800	IC-221W filler	482	482	0.8	HAZ[b]
4B	900	Cast	511	511	0.4	NA[a]
4W1	900	IC-221LA filler	454	454	1.9	Base
4W2	900	IC-221W filler	513	513	1.0	Base
5B	1000	Cast	257	257	0.0	NA[a]
5W1	1000	IC-221LA filler	217	221	5.8	Weld
5W2	1000	IC-221W filler	337	337	0.9	Base
6B	1100	Cast	168	168	0.4	NA[a]
6W1	1100	IC-221LA filler	92	94	17.4	Weld
6W2	1100	IC-221W filler	167	172	1.2	Base

[a]NA = not applicable.
[b]HAZ = heat-affected zone.

the yield strength of the base metal decreased with temperature, but that it was still quite high (168 MPa) even at 1100°C. The base-metal alloy showed very little ductility throughout this temperature range.

The weldment tensile properties compared favorably with those of the base metal. The yield strengths of specimens from the IC-221LA weld were comparable to the base metal up to 900°C. As expected, the IC-221LA weld specimens show reduced yield strength above this temperature, and this is due to the lower intrinsic strength of the IC-221LA alloy as compared to IC-221M. The tensile specimens from the IC-221W weld had properties comparable to those of the base metal up to 1100°C. As Table 3 shows, the failure initiation sites for weldment specimens were mainly in the base metal or heat-affected zone (HAZ) of the welds. Only the IC-221LA specimens tested at 1000 to 1100°C clearly broke through the weld metal. The better high-temperature ductility of IC-221LA compared to IC-221M and IC-221W is also illustrated by the data of Table 3.

Also, some of the specimens from the pipe welds were used for stress-rupture testing, and these data are plotted in Fig. 3. The rupture life of the welded specimens was less than that of the base metal for the range of conditions tested. Failure of the specimens was primarily in the weld metal or heat-affected zone (HAZ).

Effects of Ingot Composition on Weld-Induced Cracking. A series of 25 × 25 × 75-mm ingots were prepared to examine whether an elevated concentration of B, Fe, or Si had a noticeable effect on the resistance of IC-396M to weld cracking (see Table 4). Bars of the same nominal dimensions and composition of one of the small ingots (No. 15712) that were machined from a centrifugal casting (made by Sandusky International) and an air-melted drop casting (No. 15758) were also evaluated. The groove preparation and welding procedures were identical to those described in previous reports. Two grooves were made in each casting. One was welded with metal-powder-cored wire, and the other was welded with solid wire.

Table 4. Nominal compositions of experimental heats based on IC-396M

Melt no.	Composition (weight percent)							
	Ni	Al	Cr	Mo	Zr	B	Si	Fe
15711	*a*	8	7.7	3	0.90	0.008	--	--
15712	*a*	8	7.7	3	0.90	0.035	0.12	0.23
15713	*a*	8	7.7	3	0.90	0.035	--	--
15714	*a*	8	7.7	3	0.90	0.008	0.12	--
15715	*a*	8	7.7	3	0.90	0.008	--	0.23
15716	*a*	8	7.7	3	0.90	0.035	0.12	--

[a]Balance.

Each of the initial root pass weld beads made in the SI material cracked extensively, and no further welding of this casting was attempted. For ingot 15758, the root passes made with both filler metals also cracked. No further welding was done on this casting either. Both slots on each of the remaining drop-cast ingots (Nos. 15711 to 15716) were welded to completion. There was no visual indication of cracking in any of these welds. However, metallographic examination of specimens cut from these ingots showed that several of the welds did contain cracks.

The observations made on these welded ingots formed the basis for the following conclusions:

1. Most of the cracking observed in all of the test specimens from these three ingot types occurred near the weld fusion lines. The cracks often extended into both the weld metal and the HAZs of the base metal. This observation indicates that the composition of the various IC-396M castings and their microstructures influence cracking behavior.

2. For alloys of identical IC-396M composition [SI material (Nos. 15758 and 15712)], the tendency for welds made with the IC-221LA filler metal to crack was lowest in an arc-melted drop-cast ingot and highest in a centrifugally cast ingot. Differences between the three castings include: grain size, scale of the solidification microstructure, and distribution of shrinkage defects. The arc-melted drop casting had the finest microstructure, lowest amount of shrinkage defects, and the fewest cracks after welding. The centrifugal casting had the coarsest solidification microstructure and the most shrinkage, and it had a very high tendency for cracking of the welds. Processing in air under argon cover also appears to increase the tendency for cracking.
3. For alloys of identical processing listed in Table 4, the addition of up to either 0.12 wt % Si or 0.23 wt % Fe did not significantly increase the tendency for cracking.
4. For alloys of identical processing, increasing the boron concentration to the range of 0.030 to 0.036 wt % did increase the tendency for cracking.
5. For the technique and parameters used for these welds, the deposits made with the powder-cored wire were more likely to contain relatively large cracks and other defects associated with incomplete melting of the filler metal.

During the last quarter, two additional centrifugal castings of IC-221M were received from Sandusky International. One objective of these castings was to evaluate whether centrifugal castings of the IC-221M composition would be more resistant to weld cracking than those made from IC-396M. Two additional castings were made, and based on visual and metallographic examination, they contained more shrinkage porosity and scale than the IC-396M castings. Eight 14-in.-OD × 1-in.-wall × 4-in. rings were cut from the end of each casting for evaluation of welding behavior. One edge of each ring was machined to a 37.5° single-vee bevel to enable full-penetration circumferential welds to be made from the outer diameter side of the castings. After the welding trials were under way, it was discovered that one of the castings contained an excessive copper addition, and further work on it was halted. The second casting was relatively close to the target for

IC-221M except for elevated levels of carbon (0.1 wt %) and boron (0.014 wt %). This casting was welded in several different conditions: (1) as-received, (2) as-received and remachined to remove highly defective material from the inside diameter of the casting, (3) remachined and stress relieved for 1.5 h at 950°C, (4) as-received and cut into 6-in. segments, and (5) as-received and machined into approximate 1 × 1 × 3-in. bars for comparison to existing data on similarly sized cast specimens. The welds on all of these pieces contained cracks, typically along the weld centerlines.

Test for Weld-Induced Cracking. The need exists for a systematic, quantitative method of evaluating the susceptibility of various nickel-aluminide ingots and weld deposits to HAZ cracking. One approach evaluated for this purpose was the use of a Gleeble thermomechanical simulator to measure the high-temperature tensile properties of several IC-221M and IC-396M alloys. The intention of this testing was to correlate the results to observations about the cracking response of the alloys during welding. Three alloys have been tested: (1) the IC-396M centrifugally cast roll shell material made by Sandusky International, (2) arc-melted and chill-cast material of the same nominal IC-396M composition (melt 16046), and (3) arc-melted and chill-cast IC-221M (melt 16048). Specimens were tested in argon atmosphere at a nominal strain rate of 0.016 s^{-1}. Data from tests conducted after heating directly to the test temperature, referred to as the "on-heating" condition, are summarized in Figs. 5 and 6. There is little difference in the on-heating tensile strength of the three cast alloys (see Fig. 5). Figure 6 shows that of these three alloys, the IC-221M composition had the best tensile elongation, and that the centrifugal casting had the worst. The low ductility of the centrifugally cast IC-396M at temperatures above 900°C is indicative of an alloy, which is difficult to weld without cracking. In this case, the hot-ductility data and the observations about actual welding are consistent. Further analysis of these data and additional testing are planned.

The evaluation of the creep and strength of samples machined from commercial static castings of IC-221M has been extended to the temperature range of 815 to 1038°C

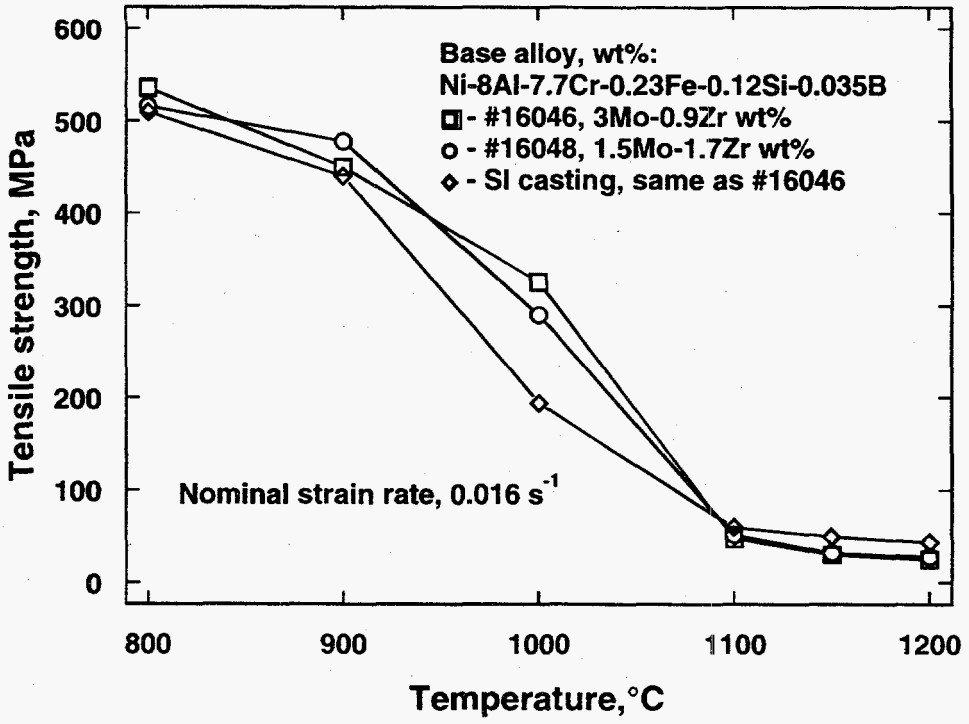

Fig. 5. Variation of tensile strength with temperature as determined from Gleeble testing of specimens from nickel-aluminide castings.

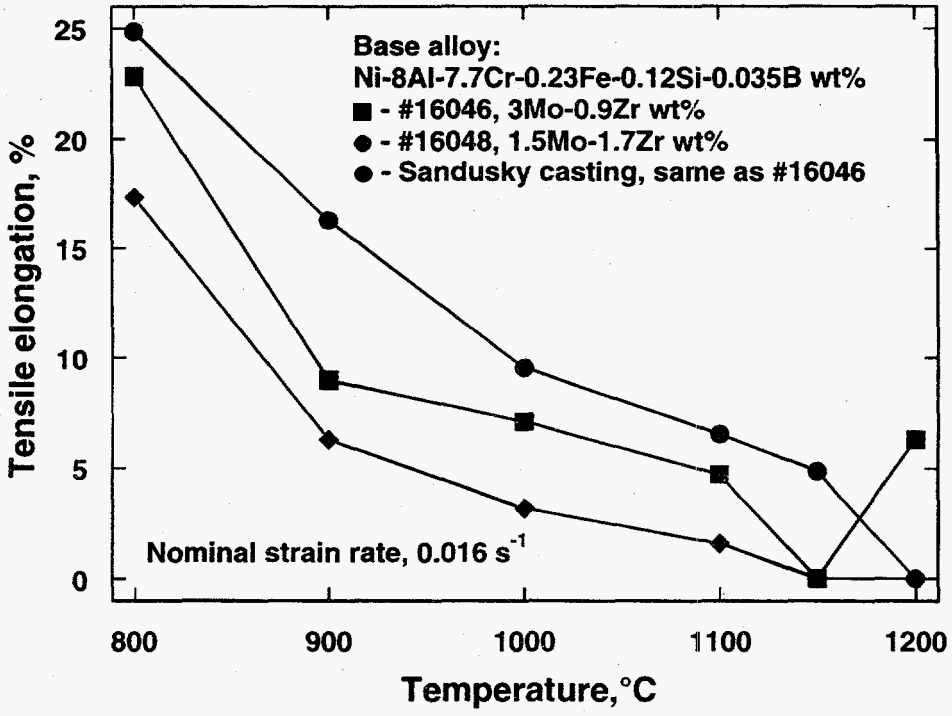

Fig. 6. Variation of tensile elongation with temperature as determined from Gleeble testing of specimens from nickel-aluminide castings.

(1500 to 1900°F). Testing times approaching 10,000 h have been achieved. Comparisons are being made to the performance of similar castings made from the HU alloy. Data are summarized in Fig. 7 which shows the log stress versus the Larson-Miller parameter (LMP) for rupture life. At lower values of the LMP, corresponding to temperatures of 815°C, the intermetallic IC-221M has about three times the strength of the HU alloy. At higher values of the LMP, corresponding to 1038°C, IC-221M has nearly twice the strength of the HU alloy. Variability in the rupture life of IC-221M for repetitive tests occurs as a result of the influence of casting defects on creep crack initiation and growth. The data shown in Fig. 7 result from testing specimens machined from cast bars with relatively sound cross sections. Efforts are being made now to evaluate the behavior of more representative casting configurations. For example, plate-type specimens were machined from web-type casting sections. It was found that machining sections from products often removed much of the sound material, and specimens suitable for testing could not be produced. Alternate methods to test castings at high temperature are being examined.

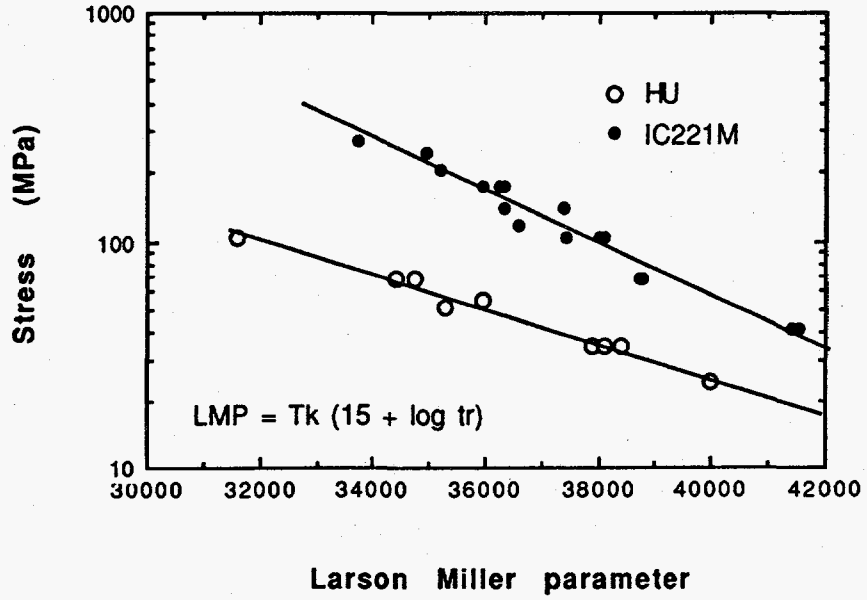

Fig. 7. Comparison of the stress versus Larson-Miller parameter for rupture life of IC-221M and heat-resistant casting HU alloy.

4. Workability of Cast or Powder Metallurgy Product to Sheet, Bar, and Wire, Start 10/94, End 9/95:

This task has been looking at the production of wrought product through both powder metallurgy and near-net-shape methods. Sheet is one of the products that is expected to be in great demand. The sheet of up to 60 mil thickness can be produced by direct casting from liquid phase. Such a process has been carried out by Allegheny Ludlum Steel Corporation. However, the company refuses to produce it because they believe that it competes with some of the products they currently produce. In the meantime, we have examined the potential use of a direct powder rolling process. In this process, elemental or prealloyed powders are directly compacted into sheet. Such a sheet is followed by binder burn-out and rolling and annealing cycles to reach the final thickness. This process has recently been demonstrated for an Fe-Al alloy and is expected to be extendible to the Ni_3Al-based alloy. It should also be noted that the water-atomized powder seems to work better for the roll compacting process and, thus, has the potential of using low-cost powders.

5. Technology Transfer Activities, Start 10/94, End 9/95:

The purpose of this milestone is to undertake activities that will promote the transfer of nickel-aluminide technology to industry. These activities include visiting potential producers and users of materials and describing the technology in detail, training industry personnel either at ORNL or at the industrial facilities, and holding technology transfer meeting at ORNL. As a result of these activities, several additional applications have been identified for these materials.

The technology transfer approach described above has generated strong interest from the following companies:

- General Electric: nickel aluminide for use as extrusion dies.
- Lindberg Heat Treating: for use of various components in heat-treating furnaces.

- Steeltech: strong interest in sand casting of components. Personnel has been trained in using the Exo-Melt™ process. However, they cannot manufacture unless a license has been negotiated.
- Rapid Technologies: continued interest in furnace applications as conveyors. A completed report of work with Rapid Technologies was prepared and submitted for their approval.
- FMC Corporation: United Defense, a part of FMC, has signed a license from ORNL for the castings of nickel aluminides.
- PCC Airfoils: interested in using nickel-aluminide trays for heating of ceramic shells; testing of trays in the production furnace continued since March 1995. Testing has reflected that the additional trays should be from IC-50 rather than from IC-221M.
- Alcon Industries, Inc.: interested in pursuing the casting of furnace components of nickel aluminide; melting of a 500-lb heat was planned at Alcon during May and June 1995, however, it has not happened because of licensing concerns. Still no progress has been made because Alcon has not responded to ORNL's proposal.
- BCast: interested in machining and manufacture of nickel-aluminide nuts and bolts; a set of molds for this task has been prepared and castings will be made during the next quarter.
- Ford Motor Company: Ford has a strong interest in trying Ni_3Al-based alloys for radiant burner tubes. Sketches of their tubes, plan for testing, and requirements have been received at ORNL. The major hurdle in the use of Ni_3Al-based alloys for radiant burner tubes was their weldability. This issue has been put to rest by successfully welding several pieces of the tubes. The welds in the tubes have also been tested for their tensile properties from room temperature to 1100°C.

  During the next quarter, we plan to purchase the different sizes of the tubes required by Ford and work with them to get the tubes into test. The successful testing of the tubes

at Ford will open up the potential for the subject application in many different manufacturing companies.

- Weirton Steel: for furnace rollers and radiant tubes. This interest continues. However, no further action has been taken.

Activities are under way in support of all of the companies listed above.

This list continues to grow, and the following are the new additions:

- A. Finkl & Sons: for furnace supports known as "bucks" and also potentially for cutters for hot cutting of billets.
- Chevron Oil: for tube hangers.
- Shell Oil: for pyrolysis process.
- Lukens Steel: for furnace rolls.
- Wyman-Gordon: for heat-treating trays and potentially isothermal forging dies.
- Latrobe Steel: for guide rolls.
- The Timken Company: for heat-treating furnace components.

PERSONNEL INFORMATION

Visits were made to the following companies: United Defense, Wyman-Gordon, A. Finkl & Sons, and Anchor Glass Container.

INDUSTRIAL INPUT AND TECHNOLOGY TRANSFER

The coupons of Ni_3Al-based alloy exposed in batch and pusher carburizing furnaces at Delphi Saginaw continued to be evaluated by metallography, SEM, and microhardness. A report summarizing the results of this study were prepared and sent to Delphi Saginaw for their approval.

Six batch-furnace trays and two pusher-furnace assemblies were shipped to Delphi Saginaw for installation in commercially operating carburizing furnaces. One-half of the parts were in the as-cast condition, and the other half were in the preoxidized condition.

The transfer furnace rolls of nickel aluminide have continued to operate at Bethlehem Steel Company. The total operating time has now reached nearly two years. The welding issue to assembling the two additional rolls is nearly complete. The information gained from the welding studies will be used in the assembly of two additional rolls for installation in a commercial operating furnace at Bethlehem Steel.

A final report detailing the work carried out under Metallamics was prepared.

PUBLICATIONS

V. K. Sikka and R. Cooper, "Synthesis of Ni3Al and NiAl Intermetallics," in *Novel Techniques in Synthesis and Processing of Advanced Materials*, ed., J. Singh and S. M. Copley (The Minerals, Metals & Materials Society: Warrendale, Pennsylvania, 1994), pp. 23-35.

J. E. Orth and V. K. Sikka, "Commercial casting of nickel aluminide alloys," *Advanced Materials & Processes* **148**(5) (1995) 33-34.

S. C. Deevi and V. K. Sikka, "Reaction Synthesis of Heat-Resistant Materials," in *Heat-Resistant Materials II*, ed., K. Natesan, P. Ganesan, and G. Lai (ASM International: Materials Park, Ohio, 1995), pp. 275-286.

V. K. Sikka and S. C. Deevi, "Intermetallics for Structural Applications," in *Heat-Resistant Materials II*, ed., K. Natesan, P. Ganesan, and G. Lai (ASM International: Materials Park, Ohio, 1995), pp. 567-578.

V. K. Sikka, S. C. Deevi, and J. D. Vought, "Exo-Melt: A Commercially Viable Process," *Advanced Materials and Processes*, **147**(6) (1995).

E. K. Ohriner, V. K. Sikka, and S. C. Deevi, "Processing and Properties of Ni_3Al-Based Composites," in *P/M in Aerospace Defene and Demanding Applications - 1995*, ed., F. H. Froes (Metal Powder Industries Federation: Princeton, New Jersey, 1995), pp. 197-203.

HONORS AND AWARDS

1995 R&D 100 Award entitled "Exo-Melt Process" by Vinod K. Sikka, Joseph D. Vought, and Seetharama C. Deevi.

PATENTS/DISCLOSURES

M. L. Santella and G. M. Goodwin, "Nickel Aluminide Alloys with Improved Weldability," No. 5,413,876, May 9, 1995.

LICENSES

A license was negotiated and executed with United Defense, a company owned by FMC. The license is for the melting, casting, and marketing a wide range of components from nickel-aluminide compositions.

Since the signing of the license, United Defense has placed a two-page advertisement in a technical journal. They have also placed a marketing team. Because of our assistance and their aggressive efforts, United Defense has already delivered some components to a range of companies.

COST INFORMATION

None.

SYNTHESIS AND DESIGN OF SILICIDE INTERMETALLIC MATERIALS

ANNUAL REPORT
AND
QUARTERLY PROGRESS REPORT
July-September 1995

J.J. Petrovic, R.G. Castro, D.P. Butt, H.H. Kung, K.J. Hollis, A. Bartlett

Los Alamos National Laboratory
Los Alamos, NM 87545

EXECUTIVE SUMMARY

INTRODUCTION:

The objective of this program is to develop structural silicide-based composite materials with optimum combinations of elevated temperature strength/creep resistance, low temperature fracture toughness, and high temperature oxidation resistance for applications of importance to the U.S. processing industry. A further objective is to develop silicide-based prototype industrial components. The ultimate aim of the program is to work with industry to transfer the structural silicide materials technology to the private sector in order to promote international competitiveness in the area of advanced high temperature composite materials and important applications in major energy-intensive U.S. processing industries. The program presently has a number of developing industrial connections, including a CRADA with the advanced materials company Advanced Refractory Technologies Inc., and a soon to be finalized CRADA with Schuller International Inc. targeted at the area of $MoSi_2$-based components for fiberglass melting/processing applications.

Current experimental emphasis is on the development and characterization of SiC reinforced-$MoSi_2$ matrix composites, plasma sprayed $MoSi_2$-based materials and microlaminate composites, and $MoSi_2$ reinforced-Si_3N_4 matrix composites. We are developing processing methods for $MoSi_2$-based materials, such as plasma spraying/spray forming and electrophoretic deposition. We are also pursuing the fabrication of prototype components for fiberglass processing, as well as prototype industrial gas burner and injection tube components of these materials. The joining of $MoSi_2$ materials to metals is also being investigated.

SUMMARY OF TECHNICAL PROGRESS IN FY-1995:

Impending CRADA with Schuller International:

Significant efforts have been expended to develop a CRADA with Schuller International in the area of $MoSi_2$ materials for fiberglass manufacturing components. Numerous discussions took place with Schuller personnel to develop the technical aspects of the CRADA, as well as the wording and procedural aspects of the CRADA documentation. The objectives of this CRADA are to develop, design, and fabricate silicide and/or oxide-based materials which will be used for specific glass melting applications at Schuller International. These applications include, but are not limited to, the following: coatings for molybdenum components and refractory linings used in glass melting, fabrication of near net shape components such as spinner disc inserts, redesign or replacement of precious metal components, and the development of a performance database for silicide and oxide-base materials in molten glass. This CRADA is of a three-year duration.

At the present time, the CRADA with Schuller International is nearly completed and should be signed in the near future.

CRADA with Advanced Refractory Technologies:

The objective of the CRADA with Advanced Refractory Technologies (ART) is to develop and commercialize SiC-$MoSi_2$ matrix composites, using both the approaches of SiC whisker reinforcement as well as in-situ SiC reinforcement. In this CRADA, ART has developed SiC-$MoSi_2$ composite blends, and Los Alamos has consolidated these composite blends and evaluated the properties of the composites.

ART developed an improved blending technique, termed the Aqueous Dispersion/Flocculation (ADF) process. This ADF process lead to improved blend homogeneity, as well as lower cost processing, for both SiC whisker-$MoSi_2$ composites and carbon-$MoSi_2$ (in-situ SiC formation) composites. Due to its importance for industrial applications, the wear behavior of ART SiC-$MoSi_2$ composites was evaluated in a collaboration with the U.S. Bureau of Mines. The wear resistance was found to increase significantly with increasing SiC content.

The CRADA with ART commenced in February 1993 and is scheduled to end in December 1995.

$MoSi_2$-Al_2O_3 Microlaminate Composites:

Net-shape microlaminates of $MoSi_2$-Al_2O_3 composites have been produced by plasma spray forming, and subsequently tested in four-point bending at various temperatures, strain rates, and heat treatments. The microlaminate composites exhibit non-linear stress-strain behavior at elevated temperatures, with significant overall deformation observed. An important result is that interfacial debonding is not a necessary requirement for obtaining a layered composite that can exhibit a large work of fracture. While some of the results have shown that debonding can occur under certain circumstances, the production of a strain-tolerant layered beam is equally dependent on the geometry of the layered structure, and the stress-strain behavior of the ductile phase.

$MoSi_2$-Si_3N_4 Composites:

The fabrication, microstructures, and mechanical properties of hot pressed $MoSi_2$ reinforced-Si_3N_4 matrix composites were investigated as a function of $MoSi_2$ phase size, volume fraction, and amount of MgO densification aid. No reactions were observed between $MoSi_2$ and Si_3N_4 at the fabrication temperature of 1750 °C. Composite microstructures varied from particle-matrix to cermet morphologies with increasing $MoSi_2$ phase content. The MgO densification aid was only present in the Si_3N_4 phase. An amorphous glassy phase was observed at the $MoSi_2$-Si_3N_4 phase boundaries, the extent of which decreased with decreasing MgO level. No general microcracking was observed in the $MoSi_2$-Si_3N_4 composites, despite the presence of a substantial thermal expansion mismatch between the $MoSi_2$ and Si_3N_4 phases. $MoSi_2$-Si_3N_4 composites generally exhibited improved room temperature fracture toughness and good strength levels at both room temperature and elevated temperatures.

$MoSi_2$-SiC and $MoSi_2$-Si_3N_4 SHS Materials:

Self-propagating high temperature synthesized (SHS) powders of $MoSi_2$-SiC and $MoSi_2$-Si_3N_4 produced by the Exotherm Corporation have been investigated for potential plasma spray coating and structural use in glass melting applications. Both plasma sprayed composites and hot pressed composites from these Exotherm powders have been fabricated. The elevated temperature bend strength of these composites was determined to be in the range of 100-200 Mpa at 1200 °C. Electron microscopy investigations of the deformed composites indicate dislocation generation at the composite interfaces.

Electrophoretic Deposition of $MoSi_2$ and $MoSi_2$ Composites:

Electrophoretic deposition is a means to obtain both coatings and free-standing shapes, by depositing powders onto an electrode from liquid suspensions, followed by consolidation. Three general areas of emphasis have included powder surface characterization and modification, deposition medium and dispersant optimization, and deposition process optimization. Powders of $MoSi_2$, Si_3N_4, modified Si_3N_4, and $MoSi_2$-Si_3N_4 have all been deposited from several different solvent systems, including acetone, ethanol, and non-polar solvents such as cyclohexane and dodecane. $MoSi_2$ deposits were dense (60% of theoretical) and deposition rates from acetone and ethanol were fast relative to the deposition of alumina and zirconia. Small, monolithic $MoSi_2$ closed-end tube shapes were successfully formed by electrophoretic deposition, and sintered to 95% theoretical density. Electrophoretic deposition was also employed for the application of $MoSi_2$ coatings onto Mo substrates.

Mechanical Property Characterization of Plasma-Sprayed $MoSi_2$ Composite Tubes:

The thermal, elastic, and mechanical properties of plasma-sprayed $MoSi_2$ tubes for high temperature burner and heat exchanger applications were characterized at Penn State University. Powder x-ray diffraction was used to determine phases present in the as-

sprayed and heat treated rings. Microstructural examinations of both the as-sprayed and heat treated rings were performed by SEM. A quantity of C- and O-ring specimens were mechanically tested at room temperature, and strength distributions and Weibull parameters measured.

Corrosion of $MoSi_2$-Based Components and Coatings in Molten Glass:

In collaboration with Schuller International, an investigation was begun to evaluate the corrosion resistance of $MoSi_2$ components and $MoSi_2$-coated refractories in molten alkali-borosilicate glass used in the manufacture of fiberglass. Both static and dynamic corrosion tests were performed. Initial results showed that $MoSi_2$ corrosion below the molten glass line is quite slow. Corrosion at the glass line is more rapid, but is comparable to that of the refractory brick oxide material AZS (alumina-zirconia-silica). Plasma sprayed $MoSi_2$ coatings were observed to be extremely adherent to the refractory AZS material.

Joining of $MoSi_2$-Based Components:

A Partial Transient Liquid Phase (PTLP) method has been pursued to join $MoSi_2$ to stainless steel, as will be required by many industrial applications. This method involves metal interlayers of different melting points at the joint, some of which melt and then interdiffuse with higher melting point species, producing a strong solid-state joint. Joint interlayers have employed Nb, Ta-Ti, and Ta high melting point refractory metals, and lower melting point Cu-Ag and Al metals. Joints of $MoSi_2$ to stainless steel which are of good quality and reproducibility have been obtained. Joint strengths are of the order of 200 Mpa.

10. Publications, Presentations, Patents, Honors/Awards:

Publications:

1. H. Kung, R.G. Castro, A.H. Bartlett, and J.J. Petrovic, "The Structure of Plasma Sprayed $MoSi_2$-Al_2O_3 Microlaminate Tubes", Scripta Met. et. Mater., 32, 179-183 (1995).

2. D.E. Alman, J.A. Hawk, and J.J. Petrovic, "Abrasive Wear Behavior of $MoSi_2$/SiC and $MoSi_2$/ZrO_2 Composites", Scripta Met. et. Mater., 32, 1765-1770 (1995).

3. D.E. Alman, J.A. Hawk, and J.J. Petrovic, "Abrasive Wear Behavior of a Si_3N_4 Matrix-$MoSi_2$ Particulate Composite", submitted to the Journal of the American Ceramic Society, 1995.

4. J.J. Petrovic, "Mechanical Behavior of $MoSi_2$ and $MoSi_2$ Composites", Mat. Sci. Eng., A192/193, 31-37 (1995).

5. L.J. Neergaard and J.J. Petrovic, "Fracture Behavior of $MoSi_2/Si_3N_4$ Composite", Ceram. Eng. Sci. Proc., 16, 137-146 (1995).

6. D.P. Butt, T. Taylor, H. Kung, and M. Sandlin, "Kinetics of Thermal Oxidation of Silicon Nitride Powders", submitted to the Journal of the American Ceramic Society, 1995.

7. D.P. Butt, D.A. Korzekwa, S.A. Maloy, H. Kung, and J.J. Petrovic, "Impression Creep Behavior of SiC Particle-$MoSi_2$ Composites", submitted to the Journal of Materials Science, 1995.

8. M. Sandlin, T. Taylor, D.P. Butt, and J.J. Petrovic, "Aqueous Zeta Potential of Molybdenum Disilicide", submitted to the Journal of the American Ceramic Society, 1995.

9. M. Sandlin, D.P. Butt, and J.J. Petrovic, "Electrophoretic Deposition of $MoSi_2$", to be submitted to the Journal of the American Ceramic Society, 1995.

10. A. Bartlett, R. Castro, H. Kung, D.P. Butt, and J.J. Petrovic, "Corrosion of Plasma Sprayed $MoSi_2$-Alumina Laminate Tubes in Molten Metals", in print, Industrial Heating Journal of Thermal Technology, 1995.

11. S.D. Conzone, A. Bartlett, and D.P. Butt, "Joining $MoSi_2$ to 316L Stainless Steel Using the Partial Transient Liquid Phase Method", submitted to the Journal of Material Science, 1995.

Presentations:

1. M.S. Sandlin, D.P. Butt, and J.J. Petrovic, "Electrophoretic Forming of Non-Oxide Ceramics", presented at the 97th Annual Meeting of the American Ceramic Society, Cincinnati, Ohio, April 1995.

2. M.S. Sandlin, D.P. Butt, and J.J. Petrovic, "Laminated and Functionally Graded Microstructures by Electrophoretic Deposition", presented at the Fall Meeting of the American Ceramic Society, Basic Science Division, New Orleans, November 1995.

3. S. Conzone, A.D. Bartlett, and D.P. Butt, "Partial Transient Liquid Phase Joining of $MoSi_2$ to Stainless Steel", presented at the Fall Meeting of the American Ceramic Society, Basic Science Division, New Orleans, November 1995.

4. J.J. Petrovic, M.I. Pena, M.S. Sandlin, and H.H. Kung, "Silicon Nitride-Molybdenum Disilicide Composites", presented at the Fall Meeting of the Materials Research Society, Boston, Massachusetts, November 1995 (Invited Presentation).

Patents:

1. U.S. Patent No. 5,382,553, "Molybdenum Disilicide Composites Reinforced with Zirconia and Silicon Carbide", Inventor: John J. Petrovic, Issue Date: January 17, 1995.

2. R. Castro, W. Johnson, D.P. Butt, and S. Leonard, "Molydisilicide Coatings for Refractories in Glass Melts", U.S. Patent Application in Process, Record of Invention Filed, 1995.

3. John J. Petrovic and Joel D. Katz, "Method of Joining Sintered Silicon Carbide Using Molybdenum Disilicide", U.S. Patent Application in Process, Record of Invention Filed, 1995.

Awards and Honors:

1. Los Alamos National Laboratory Distinguished Performance Award, Silicides Intermetallic Composites Team, R.G. Castro, J.J. Petrovic, D.P. Butt, H.H. Kung, K.E. Elliott, C.D. Kise, August 1995.

2. Los Alamos National Laboratory Technology Transfer Recognition Award, R.G. Castro and J.J. Petrovic, October 1995.

3. J.J. Petrovic selected as one of "50 R&D Stars to Watch" for the development of High Temperature Structural Silicides, Industry Week Magazine, December 19, 1994 Issue, Pgs. 60-64.

4. J.J. Petrovic selected as a Fellow of ASM International, for "Pioneering Contributions to the Science and Technology of Advanced Structural Silicides and Ceramics", October 1995.

5. J.J. Petrovic selected as a Fellow of the Los Alamos National Laboratory, July 1995.

TECHNICAL PROGRESS: July-September 1995

Schuller International CRADA Activities:

On September 29th, Dr. Ted Michelson, Senior Director of Corporate Research Development at Schuller Mountain Technical Center visited LANL to meet with representatives of the Industrial Partnership Office (Randy Tremper, Susanne Charlton, Molly Birely, and Ray Wilson) and the project leaders (Richard Castro and John Petrovic) to discuss details associated with the CRADA agreement. The major topic of discussion was the specific wording associated with the standard DOE CRADA document. The concerns of Dr. Michelson/Schuller were addressed by the representative of the IPO who tried to clarify the wording in the CRADA document as well as modifying the standard CRADA document to reflect Schullers concerns. Changes in the CRADA document have been complete and have been drafted into the final document for routing through LANL. Accompanying these changes are the Environmental, Safety and Health information and NEPA documentation. The final CRADA document is expected to be delivered to DOE for final approval in the next few weeks. Following the CRADA discussions, a tour of the Sigma facility and the new Materials Science Laboratory at LANL was given by R. Castro and J. Petrovic

During this quarter, a Project Benefits Analysis Spreadsheet was also completed on the development of MoSi2 coatings for improving the lifetime of refractory chrome bricks which are currently used in the melting of glass. Information was provided jointly by Schuller International (Dr. Walter Johnson) and LANL (Richard Castro) on the project benefits of developing advanced coatings for refractory bricks. The data which was provided included the operations and energy savings benefits, the systems lifetime, installation costs, the potential market impact and the commercialization timetable. Also include in this Benefits Analysis was a Commercial Risk Assessment which included the commitment of the commercializing agent, the impact of government regulations on commercialization, the market infrastructure, the proof of concept, the complexity of the process, and the technology gaps and difficulties for commercialization. It was estimated that the coating of an existing glass melter used in the fiberization process would cost approximately $2500 assuming specific materials and operating costs for the coating process.

Facilities:

The upgrade to the vacuum system on the low pressure plasma spray chamber has been completed. This upgrade was done in anticipation of the CRADA activities which will involve the coating of molybdenum electrodes with the oxidation resistant $MoSi_2$-based materials. Molybdenum electrodes are typically used in the melt of glass before fiberization. This upgrade will provide faster pump down times of the vacuum chamber and improve the operating atmosphere for depositing materials on the molybdenum surface.

An acceptance test was performed at Sulzer Metco in Irvine, CA on the CNC controlled X-Y plasma torch manipulator and spindle which will be used when coating the 30" long molybdenum electrodes which will be provided by Schuller under the CRADA agreement. This capability will enable the coating of full scale electrodes before on-site testing of the electrodes at Schuller's glass melting facilities. The X-Y manipulator and spindle have been received at LANL and are currently being installed. The transferred arc power supply which was purchased with FY1994 capital equipment funds, will also be installed on the special designed spindle. This capability will allow the simultaneous cleaning of the molybdenum electrode surface while depositing the oxidation resistant $MoSi_2$ coatings.

Operation and testing of the 5-axis robot has been completed. The robot will be used for controlling the plasma spray process for coating the chrome refractory bricks with $MoSi_2$-based material. A Plasmadyne SG-1B atmospheric plasma torch has been installed on the robot arm and has been successfully tested. Investigations are currently focusing on programming the robot to spray uniform patterns of $MoSi_2$ onto the surface of the chrome refractory brick. Coating thickness on the order of 5 to 25 mils are being applied to 1.00" x 1.00" sections of the refractory brick for glass compatibility studies up to 1600 C. Following these investigations, $MoSi_2$ coatings will be deposited directly onto the surface of full scale bricks for on-site glass testing at Schuller.

Technical Activites:

An 18" fiber glass spinner disc was provided to LANL to investigate the laser drilling of smaller diameter holes (less than .010") to improve the operation and efficiency of the fiberization process. Machined sections of the fiberglass spinner disc have been provided to the main machine shop at LANL for laser drilling studies. Initial trials have shown that a special operational setup may be required to laser drill holes in the spinner disc below .008" in diameter. Investigations to optimize the laser drilling process will continue in FY1996.

Mechanical Properties Characterization of Kanthal $MoSi_2$ Tubes
R. C. Lutz and J. R. Hellmann, Pennsylvania State University:

Super Kanthal $MoSi_2$ tubes were provided to Penn State to characterize the thermal, elastic and mechanical properties of commercially available $MoSi_2$ tubes as part of a subcontract to Pennsylvania State University to evaluate the characteristic strength of tubular $MoSi_2$-based materials. The tubes were sectioned into C- and O-ring test geometryis, for strength testing in diametral compression at room temperature. The different geometries are employed to assess the role of flaws and microstructural characteristics resident on the inside and outside surfaces on determining the strength of the tubes. Fractography, x-ray diffraction, and qualitative chemical analyses were performed to correlate microstructural features and crystalline phase content with measured strengths and fracture characteristics.

Preliminary characterization of the tubes revealed that they are comprised of primarily tetragonal $MoSi_2$ (a-$MoSi_2$), with Mo_5Si_3 in minor concentrations,

accompanied by metastable hexagonal b-$MoSi_2$ and crystalline silica (cristobalite) present in minor (<1 weight percent) concentrations. Energy Dispersive Analysis by X-rays (EDAX) revealed that the outer surfaces of the tubes were silicon-rich (relative to stoichiometric $MoSi_2$), and contained a substantial concentration of iron which was not observed in the bulk of the sample. The outer surface of the tube was covered with a 15-20 μm thick silica-rich layer, but no such layer was observed on the inner surface of the tube. After removal of the silica glass with a HF acid etch, the sample surface was molybdenum-rich, in qualitative agreement with the presence of Mo_5Si_3, which forms during the oxidation of the disilicide. A significant volume fraction (12%) of alumino-silicate glass particles were observed in the bulk of the samples, and appears to be a deliberately added second phase. Archimedes density analyses revealed that the samples are approximately 93% dense, with approximately 6% closed porosity, and the balance open porosity, after correcting for the density of the glass inclusions. Acoustic resonance spectroscopy was employed for determining the room temperature Young's modulus (323 GPa), shear modulus (140 GPa) and Poisson's ratio (0.155); these values were in good agreement with the Vioght/Reuss bounds for a composite body comprised of $MoSi_2$ and 12 volume percent aluminosilicate glass.

Dimensions, failure loads, and fracture stresses for thirty-four o-rings and nineteen c-rings are given in Appendix A. Fractographic analysis revealed that the majority of the c-rings failed from porosity within the wall of the tube; however, a substantial fraction failed from flaws resulting from differential shrinkage of agglomerates during processing (4 failures) and from silica glass inclusions (1 failure). The o-ring specimens in all cases failed from glassy inclusions very near, or at, the inner surface of the tube. No edge failures were observed. Weibull moduli and characteristic strengths of the Kanthal tube sections are given in Table 1. The c-rings (KCR) were substantially stronger, and possessed a narrower strength distribution than the o-rings (KOR). No evidence of residual stress contributing to the higher c-ring strength was observed (no change in diameter of the rings were observed upon sectioning into c-ring geometries); therefore it is likely that the strength difference is solely attributed to differences in flaw type between the inner (o-ring) and outer (c-ring) surfaces of the tube. Fractographic analysis revealed the presence of a nearly dense, glassy layer on the outer surface of the tubes, and a measurable difference in Mo:Si stoichiometry at the outer surface relative to the bulk of the tube. Furthermore, significant evidence of processing-induced microstructural artifacts (axial striations and alignment of $MoSi_2$ grains and silica particles on the inner surface of the tubes) which could contribute to lower o-ring strengths was observed. These were most likely a direct consequence of the extrusion process employed in the manufacturing of the tubes.

References

1. R.G. Castro, J.R. Hellmann, A.E. Segall, and D.L. Shelleman, "Fabrication and Testing of Plasma-Spray Formed $MoSi_2$ and $MoSi_2$ Composite Tubes," in the Proceedings of the Symposium on High Temperature Silicides and Refractory

Alloys, 1993 Fall Meeting of the Materials Research Society, Boston, MA December, 1993.

2. D.L. Shelleman, J.R. Hellmann, and A.E. Segall, "Room Temperature Strength Behavior of $MoSi_2$ Tubes," report to R. Castro, Los Alamos National Laboratories, October 1993.

Mechanical Behavior:

Composite $MoSi_2/Si_3N_4$ and $MoSi_2$/SiC powders have been supplied by Exotherm Corporation. These powders have been prepared by combustion synthesis methods, and have been analyzed in this and previous quarterly reports. Test beams for high temperature mechanical testing have been fabricated from these powders by two methods: hot-pressing, and vacuum plasma spray. Mechanical tests were done in four-point bending in air, at various temperatures and strain rates. Most of the testing has to now focused on the behavior of the hot-pressed materials. Both the $MoSi_2/Si_3N_4$ and $MoSi_2$/SiC beams were tested under all combinations of the following temperatures and nominal cross-head displacement rates: 1200°C, 1300°C, 1400°C ; .01"/minute and .001"/minute. The strain rates for the given displacement rate depend on the beam geometry, but in all cases approximately correspond to $O(\mathbf{e},) = 5x10^{-4}$ and $5x10^{-5}$, respectively. The only plasma sprayed material tested was the $MoSi_2/Si_3N_4$, at 1200°C and .001"/minute. The $MoSi_2$/SiC was not tested because severe cracking during spray forming prevented obtaining specimens of sufficient size. In addition, a 50-50 $MoSi_2/Si_3N4$ composite hot pressed from blended $MoSi_2$ and Si_3N_4 powders was tested to compare the mechanical response as a function of microstructure, specifically the distribution of the reinforcing phase.

Stress-strain curves of $MoSi_2/Si_3N_4$ tested at .001"/minute and .01"/minute, and $MoSi_2$/SiC tested at .001"/minute and .01"/minute are shown in Figs. 1-4 respectively. In all cases, higher cross-head speeds and lower temperatures led to higher yield strengths, higher ultimate strengths, and in general, lower strains to failure. This is consistent with the mechanical response of the composite being dependent upon the matrix properties.

The effect of damage, however, is best seen in Fig. 5, in which the stress-strain response of the Exotherm materials are compared to that of unreinforced hot-pressed $MoSi_2$. The unreinforced material exhibits temperature dependent power law behavior, while the reinforced material consistently shows lower strength and lower elongation to failure. Fig. 6 is a low magnification SEM micrograph of the Exotherm $MoSi_2/Si_3N_4$ material after testing at 1400°C and .001"/minute. The Si_3N_4 reinforcing phase (dark) can be seen to have agglomerated and almost completely covered all grain boundaries. Failure originates within these large agglomerations and leads to premature failure before the theoretically predicted power law hardening benefits can be realized.[1] Figure 7 shows the $MoSi_2$/SiC microstructure; similar agglomerations of the SiC phase (dark) led to early damage and premature failure of this composite as well.

While the Exotherm powder microstructures can be seen to be less than ideal for mechanical property optimization, comparison can be made with the behavior of the blended $MoSi_2/Si_3N_4$ materials. Figure 8 shows stress-strain curves for the Exotherm and

blended powders, both tested at 1200°C and .001"/minute. The blended and hot pressed materials have a nominally higher loading of the Si_3N_4 reinforcing phase, but fail at even lower stresses than the Exotherm powders. Figure 9 shows the microstructure of the blended composite after testing, showing damage developing within the ductile $MoSi_2$ phase (light). High triaxial constraint led to failure of the ductile phase, as compared to the Exotherm materials in which this constraint led to failure either at the matrix/reinforcement interface or within the reinforcement itself. Differences in failure modes is likely due to the blended composites consisting of two completely interpenetrating phases, while the Exotherm materials behaved more as particulate reinforced materials. The implication is that a more finely dispersed reinforcing phase would lead to a more damage resistant composite; more carefully tailored starting powders, in which the reinforcing phase is contained within the $MoSi_2$ grains, could yield much improved behaviors.

Stress-strain behavior of the plasma sprayed $MoSi_2/Si_3N_4$ composite, compared to unreinforced plasma sprayed $MoSi_2$, is shown in Figure 10. Also shown are the predictions of Bao *et al.*[1] for a particle reinforced material. Material parameters for the model were taken from the stress-strain curve of the unreinforced $MoSi_2$; Ramberg-Osgood power law behavior was assumed, and the particles were assumed spherical and homogeneously distributed. Model predictions suggest an included volume fraction of Si_3N_4 approximately equal to 40%. However, TEM investigations have indicated that the volume fraction is much lower. High resolution SEM is underway to better characterize the volume fraction. It may be that significant amounts of included Mo_5Si_3 contribute to hardening; TEM work suggests that the tri-silicide is associated with high dislocation densities. Future work will investigate the hardening mechanisms, and will attempt to optimize spray conditions so as to maximize the volume fraction of the Si_3N_4.

References:

1. G. Bao, J.W. Hutchinson, R.M. McMeeking, *Acta Metall. Mater.*, **39**, [8],1871-1882 (1991).

Impression Creep:

Impression creep tests were performed on hot pressed samples of Exotherm, Inc. $MoSi_2/SiC$ (30 vol. % SiC) powder. Ultra-high creep resistant ($e_{SS}<10^{-9}$ sec^{-1}) SiC indenters were used for all impression creep testing. Tests were performed at a single temperature (1200°C) with three different loads to determine the stress exponent. Additionally, for a given load (109.5 MPa), three test temperatures were utilized to determine the creep mechanism activation energy. The resultant steady state creep rates for these tests are shown in Figures 11 and 12 respectively. The creep rates observed ranged from a high of 1.7e-6 sec^{-1} to a low of 9.2e-8 sec^{-1}.

The data shown in Figure 11 was used to determine the stress exponent of creep. Curve fitting the data gave a stress exponent of 5.00 with a Pearson's R of 0.9995. This

value of the stress exponent was used to calculate the dividend factor for cylindrical geometry impression load correction (B) to be 3.29. The load values reported here are all geometry corrected. The data shown in Figure 12 was used to determine the creep mechanism activation energy. Curve fitting the data gave an activation energy of 64.4 kJ/mole with a Pearson's R of 0.99995. This value is approximately an order of magnitude lower than other values reported previously for $MoSi_2$/SiC (30 vol. % SiC) composites.[1] Future microscopy of the creep test samples may reveal reasons for the unexpectedly low activation energy.

1. D. P. Butt, S. A. Maloy, H. Kung, D. A. Korzekwa, and J. J. Petrovic, Mat. Res. Soc. Symp. Proc., Vol. 322 (1994).

Microstructural Characterization:

In this quarter, structural characterization of three 4-point bend tested $MoSi_2$-based composites, two reinforced with Si_3N_4 and one with SiC, was performed using conventional and high resolution transmission electron microscopy (TEM). A Philips CM30 analytical TEM and a JEOL 3000F high resolution TEM equipped with a field emission gun were used. The synthesis and mechanical testing of the composites were conducted by Rich Castro and Andy Bartlett, and the experimental details and results will be reported in this quarterly report as well. In general, the different processing route (plasma spraying vs. hot pressing) has resulted in very different mechanical behavior. The main effort in this quarter is to characterize the deformation mechanisms in the three different composites under the 4-point bend testing condition. It was found that the different deformation mode is mainly governed by their microstructures. A summary of the structural characterization is attached.

In this quarter, efforts were also spent in the characterization of Si_3N_4 powders oxidized at 700°C and 1100°C, respectively. The oxidation treatment was conducted by Darryl Butt and the two powders have shown very different oxidation kinetics. For the 1100°C oxidized Si_3N_4 powders, a thin layer (<1 nm) was observed on the surface of the Si_3N_4 powders. The surface layer is crystalline in nature but has a different crystal structure than the Si_3N_4 matrix. It is suspected that the surface layer could be silicon oxy-nitride. Future nanoprobe chemical analysis has been planned to characterize the composition of the surface layer. Furthermore, characterization of the 700°C oxidized powders will also be conducted and compared with the 1100°C oxidized powders in order to unveil the intrinsic difference between the two oxidation treatments. A complete summary will be reported in the next quarterly report.

Deformation Mechanisms in $MoSi_2$/Si_3N_4 and $MoSi_2$/SiC Composites:

Electron microscopy observations from the tensily strained regions of plasma sprayed $MoSi_2$/Si_3N_4 composites after four point bending testing at 1200°C reveal that an unusual 2% tensile strain ductility is mainly attributed to the dislocations generated at $MoSi_2$/ Mo_5Si_3 and $MoSi_2$/Si_3N_4 heterophase interfaces. Using the same testing

condition for two other $MoSi_2$ ceramic composites, hot pressed $MoSi_2$/SiC composites and hot pressed $MoSi_2$/Si_3N_4 composites, higher strengths were obtained and typical intermetallic ceramic composite behaviors when mechanically strained, interface debonding and cracking, were observed in the tensily strained regions of both composites. The two different deformation mechanisms observed were explained by different microstructures of the composite and, suggested by this, the mechanical properties of a $MoSi_2$/SiC or $MoSi_2$/Si_3N_4 composite could be tailored by changing its microstructure to obtain optimum strength and ductility.

It was addressed that molybdenum disilicide, $MoSi_2$, has been considered a potential candidate structural material for high temperature applications because of its high melting point and good oxidation resistance at elevated temperatures[1]. However, lack of adequate high temperature strength and low temperature ductility hinders its potential structural applications. Extensive studies have been concentrated on adding reinforcing second ceramic phases to improve its strength at high temperatures. Among them, SiC and Si_3N_4 were chosen due to their structural stability and thermal compatibility with most ceramics and intermetallic compounds.

Three $MoSi_2$-based composites, plasma sprayed $MoSi_2$/Si_3N_4 composites, hot pressed $MoSi_2$/SiC composites and hot pressed $MoSi_2$/Si_3N_4 composites were used in this study. Different mechanical properties using four point bend testing were observed for differently processed composites, where plasma sprayed $MoSi_2$/Si_3N_4 composites showed an unusual 2% tensile strain ductility and have a low strength of ~90 MPa, and hot pressed $MoSi_2$/SiC composites and hot pressed $MoSi_2$/Si_3N_4 composites showed poor ductility yet have higher strength of ~130 MPa and ~170 MPa respectively. It is important to understand why these differently processed composites show different mechanical properties, which may lead to help control and optimize the mechanical properties of $MoSi_2$-based composites.

Three $MoSi_2$-based composites, plasma sprayed $MoSi_2$/Si_3N_4 starting with a $MoSi_2$-46 vol.% Si_3N_4 powder mixture, hot pressed $MoSi_2$/SiC starting with a $MoSi_2$-30 vol.% Si_3N_4 powder mixture and hot pressed $MoSi_2$/Si_3N_4 starting with a $MoSi_2$ 46 vol.% Si_3N_4 powder mixture, were tested using four point bending method at 1200°C with a crosshead rate of 0.001 in/min. The processing conditions and their mechanical properties are listed elsewhere[2].

After mechanical testing, up to the strain before samples break, the tensily deformed regions were cut from the samples for transmission electron microscopy study. TEM specimens were prepared by mechanical polishing, dimpling and ion milling. The thin areas of these TEM specimens for electron microscopy investigation are ~ 100 mm from the top surfaces of tested samples. Characterization of the specimens was carried out using a Philips CM30 analytical electron microscope and a JEOL 3000F high resolution transmission electron microscope.

The microstructure of plasma sprayed $MoSi_2$/ Si_3N_4 composites is shown in Figure 13(a), which consists of Mo_5Si_3 and Si_3N_4 particles embedded either in $MoSi_2$ grains or at $MoSi_2$ grain boundaries. It has been shown previously that, due to the high partial pressure, $MoSi_2$ lost Si preferentially during plasma spraying[3], which explain the

presence of the Mo_5Si_3 particles. In addition, Si_3N_4 particles sublime before going through the melting process, therefore only particles that are surrounded by $MoSi_2$ grains will be preserved after the spraying condition. It also explains that instead of big Si_3N_4 agglomerates, only isolated Si_3N_4 grains can be found embedded in the $MoSi_2$ matrix. No glassy phases, as reported in [4], were observed either at grain boundaries or triple junctions, with a typical example shown in figure 13(b). Dislocations were often observed near $MoSi_2/Mo_5Si_3$ and $MoSi_2/Si_3N_4$ interfaces as shown in Figures 14(a) and (b).

Hot pressed $MoSi_2/Si_3N_4$ composite has a very different microstructure than its plasma sprayed counterpart with big Si_3N_4 agglomerates and large $MoSi_2$ grains. The grain boundaries and triple junctions are free of glassy phases. Dislocations were rarely found in either $MoSi_2$ or Si_3N_4 grains. Interface debonding and cracking were commonly seen as shown in Figures 15(a) and (b).

Hot pressed $MoSi_2$/SiC composites exhibit a microstructure similar to $MoSi_2/Si_3N_4$, which consists of large regions of SiC agglomerates and large $MoSi_2$ grains. The grain boundaries and triple junctions are free of glassy phases, and dislocations are also rarely found in this composite after testing. Interface debonding and cracking can be seen commonly as shown in Figures 16(a) and (b).

From Figures 14(a)&(b) it is suggested that the dominant deformation mechanism in plasma sprayed $MoSi_2/Si_3N_4$ composites is dislocation slip, where $MoSi_2/Mo_5Si_3$ and $MoSi_2/Si_3N_4$ interfaces provide heterogeneous nucleation sites for dislocation generation. Behaving differently, hot pressed MoSi/SiC and $MoSi_2/Si_3N_4$ composites deform by interface debonding and cracking, as can be seen in Figures 15(a)&(b) and 4(a)&(b). The different deformation mechanisms result from different composite microstructures, where small ceramic particles embedded $MoSi_2$ composites, Figure 13(a), deform by dislocation slip and composites with big agglomerates of ceramics, Figures 15(a) and 4(a), deform by interface debonding and cracking, which relieve stress before dislocations nucleate.

Suggested by the observations in this study, it is possible to design a $MoSi_2$-based composite of desired strength and ductility by varying composite microstructure. Big grains of ceramic reinforcements are needed to reinforce $MoSi_2$ for higher strength while small ceramic particles are needed to nucleate and generate dislocations for better ductility. Systematic studies on the influence of the amount of ceramic additions and the ceramic grain sizes on the composite microstructure will be valuable for an optimum design of $MoSi_2$-ceramic composites for high temperature applications.

References:

1. J.J. Petrovic, MRS Bulletin, Vol. XVIII, p.35, July 1993.
2. A.G. Bartlett, this quarterly report.
3. H. Kung, 1994 October-December Quarterly Report.
4. H. Kung, 1995 January-March Quarterly Report.

Oxidation Studies on $MoSi_2$, $MoSi_2$/SiC and $MoSi_2/Si_3N_4$:

Oxidation studies were completed this quarter on several $MoSi_2$-based powders. Pure $MoSi_2$ powder with a mean particle size of 1.6 microns was obtained from H.C. Starck Inc. (Newton, MA 02161). $MoSi_2$/SiC (30 vol.% SiC) and $MoSi_2/Si_3N_4$ (42 vol.% Si_3N_4) composite powders with mean particle sizes of 3.3 microns and 26.2 microns, respectively were obtained from Exotherm Inc. (Canton, NJ 08103). The isothermal oxidation behavior of all three of the powders was studied at temperatures of 500, 600, 800, 900, 1000, and 1100 °C for up to 48 hours. Our interest in the oxidation kinetics of these powders stemmed primarily from the need to grow extremely thin oxide layers to enable control of zeta potential and powder mobility in aqueous and non-aqueous suspensions. The bulk of the results of these studies was reported in the previous quarter and will not be repeated here. We plan to put together a short monograph on the work, which will likely be submitted for publication in Oxidation of Metals.

This quarter we initiated a study of the pesting behavior of hot pressed samples prepared from the Exotherm $MoSi_2/Si_3N_4$ and $MoSi_2$/SiC powders. Both materials have exhibited some degree of pesting at 500 °C, times up to 400 hours. However, it is clear that the $MoSi_2/Si_3N_4$ material is significantly more resistant to pesting than other $MoSi_2$ materials we have looked at. The pesting of this material appears to be limited to its surface and, thus, is not catastrophic. These studies are continuing.

Samples of plasma sprayed Exotherm powders have been prepared for high temperature oxidation studies in simulated combustion environments. These studies will begin in the next quarter.

Studies of the Corrosion of $MoSi_2$-Based Materials in Molten Glass:

Glass corrosion tests continued this quarter. Most of our investigations focused on dynamic corrosion tests. In the previous quarter we reported having set up an apparatus for studying the corrosion of $MoSi_2$ in flowing glass (i.e. the specimen rotates). Much of this past quarter was spent optimizing this apparatus. The system is now operable. Tests are currently being conducted on Kanthal tubes at 1065 °C under a glass flow rate of approximately 150 cm/min.

This quarter we procured and set up a new high temperature (1750 °C) bottom loading furnace that will be dedicated to static glass corrosion tests. We recently conducted tests to 1500 °C on AZT refractory brick with plasma-sprayed $MoSi_2$ coatings. Specimens were removed from the glass by quenching. Unlike previous tests done at 1100 °C, the refractory cracked severely. However, the coating remained intact and showed lower corrosion rates compared with the refractory.

In the next quarter, we will continue dynamic glass corrosion tests at 1100 °C on Kanthal tubes, and static tests at 1200-1550 °C focusing on coated refractories and $MoSi_2$ components that have been plasma sprayed in air. Additionally, we will begin designing and procuring the necessary components that will allow us to do high temperature ac/dc electrochemical measurements of the corrosion of $MoSi_2$ in molten glass.

Studies of the Corrosion of Plasma Sprayed $MoSi_2$, $MoSi_2$/SiC and $MoSi_2/Si_3N_4$ in Simulated Sea Water:

Plasma spray formed samples of Exotherm $MoSi_2/Si_3N_4$ and $MoSi_2$/SiC have been prepared for electrochemical measurements of corrosion. We will use our state of the art facilities in the Materials Corrosion and Environmental Effects Laboratory to do a limited number of dc and impedence spectroscopy measurements in simulated sea water to determine, in particular, the corrosion rates and pitting tendencies of these materials. These studies are scheduled to begin in November.

Joining $MoSi_2$ to 316L Stainless Steel Using the PTLP Method:

The recently developed partial transient liquid phase (PTLP) method (a modification of the transient liquid phase method) is an attractive candidate for many types of ceramic/ceramic and ceramic/metal joining. The PTLP method involves the use of a metallic interlayer system composed of a refractory metal core and two thin non-refractory outer layers. During PTLP bonding, the less refractory layers liquefy, forming diffusion zones which promote interfacial bonding. PTLP processing is expedient because refractory joints can be attained at relatively low processing temperatures, surface preparation requirements are not stringent, and interlayers with various thermal expansion coefficients can be used to minimize residual stresses. The last two quarters we have been developing PTLP methods for joining $MoSi_2$ to stainless steel. A $MoSi_2$/stainless steel joint is industrially desirable because 316L stainless steel is a material commonly used (in the form of housings, fittings, and supports) in many applications where $MoSi_2$ may also be used.

We have had success joining $MoSi_2$ to 316L using a niobium interlayer and 28 wt.% Cu/72 wt.% Ag eutectic composition. This particular joint would be useful only at temperatures below approximately 300 °C. Thus, in many applications the joint would need to be water cooled. This quarter, we prepared joined specimens for mechanical testing. The samples are currently being machined; therefore, mechanical testing will begin soon. The results of our work to date have been submitted for publication (1).

In addition to the planned work described above, in the next quarter, we will continue development of higher temperature joints. In addition, we will also investigate means for joining $MoSi_2$ to brass. Brass is another material used in housings and fittings.

References:

1. S.D. Conzone, A. Bartlett, and D.P. Butt, "Joining $MoSi_2$ to 316L Stainless Steel", submitted to J. Mater. Sci., 1995.

Table 1: Weibull modulus and characteristic strength of O-rings and normalized C-rings determined by linear regression and maximum likelihood analyses.

	LR		ML	
Sample	m	σ_0	m	σ_0
KOR	11.5	276	9.70	277
KCR	18.9	413	20	414

Appendix A. Strength Data for Kanthal Ring Sections Broken at Room Temperature

Table A.1: Data for O-rings broken in diametral compression

Test: Compression of O-rings at Room Temperature
Material: Kanthal MoSi2
Equipment: Instron 4202 Universal Testing Machine
Hewlett Packard 9121 Computer Attachment

Samples Tested: 34

Test Parameters: 2000 lb Load Cell
X-head Speed: 0.002"/min

Sample	Outer Diameter(mm)	Thickness (mm)	Width(mm)	Load(lbs)	Stress(MPa)
KOR1	12.22	4.74	3.64	498.5	255
KOR2	12.19	4.75	3.73	433.6	215
KOR3	12.16	4.72	3.75	455.3	227
KOR4	12.22	4.74	3.71	475.7	239
KOR5	12.21	4.63	3.71	459.1	241
KOR6	12.24	4.67	3.69	475.2	247
KOR7	12.17	4.70	3.72	433.8	220
KOR8	12.19	4.62	3.72	489.4	257
KOR9	12.17	4.63	3.71	507.6	266
KOR10	12.17	4.65	3.71	529.9	275
KOR11	12.21	4.66	3.74	506.3	260
KOR12	12.18	4.66	3.74	518.4	266
KOR13	12.16	4.65	3.72	585.0	303
KOR14	12.17	4.61	3.64	556.8	299
KOR15	12.20	4.65	3.74	502.8	259
KOR16	12.20	4.71	3.74	541.5	273
KOR17	12.19	4.68	3.88	540.7	265
KOR18	12.25	4.61	3.86	484.8	247
KOR19	12.18	4.68	3.68	539.9	279
KOR20	12.16	4.63	3.62	606.7	325
KOR21	12.17	4.64	3.73	476.8	247
KOR22	12.18	4.64	3.72	578.3	301
KOR23	12.20	4.68	3.75	520.5	265
KOR24	12.18	4.64	3.72	506.3	263
KOR25	12.14	4.61	3.68	412.0	219
KOR26	12.19	4.62	3.72	530.7	278
KOR27	12.19	4.62	3.70	454.8	240
KOR28	12.21	4.67	3.71	601.9	311
KOR29	12.17	4.65	3.68	541.2	283
KOR30	12.22	4.63	3.71	585.0	307
KOR31	12.18	4.61	3.72	452.1	238
KOR32	12.16	4.57	3.71	543.9	292
KOR33	12.19	4.59	3.62	511.9	280
KOR34	12.18	4.60	3.69	440.8	235
AVERAGE	12.19	4.65	3.72	508.7	264
ST. DEV.	0.02	0.04	0.05	49.9	28

Table A.2: Data for C-rings broken in diametral compression

Test: Compression of C-rings at Room Temperature
Material: Kanthal MoSi2
Equipment: Instron 4202 Universal Testing Machine
Hewlett Packard 9121 Computer Attachment

Samples Tested: 19

Test Parameters: 2000 lb Load Cell
X-head Speed: 0.016"/min

Sample	Outer Diameter(mm)	Thickness (mm)	Width(mm)	Load(lbs)	Stress(MPa)	Normalized Stress(MPa)
KCR1	12.18	4.62	3.57	542.8	300	378
KCR2	12.18	4.62	3.60	511.4	257	324
KCR3	12.18	4.64	3.55	498.0	341	430
KCR4 (incl)	12.20	4.57	3.74	526.2	326	411
KCR5 (aggl)	12.17	4.65	3.39	473.0	335	422
KCR6	12.17	4.61	3.53	472.2	343	433
KCR7 (aggl)	12.21	4.60	3.58	516.8	331	417
KCR8	12.22	4.61	3.58	445.4	327	412
KCR9	12.18	4.67	3.73	524.6	332	419
KCR10	12.16	4.58	3.73	526.2	326	412
KCR11	12.17	4.64	3.70	505.8	285	359
KCR12	12.19	4.64	3.67	498.0	332	419
KCR13	12.17	4.63	3.59	528.1	301	379
KCR14	12.19	4.60	3.59	402.4	299	377
KCR15	12.21	4.57	3.56	516.2	303	382
KCR16	12.19	4.58	3.72	527.2	309	389
KCR17 (aggl)	12.20	4.61	3.41	502.0	302	381
KCR18	12.18	4.60	3.56	509.8	318	402
KCR19 (aggl)	12.18	4.65	3.51	456.9	284	358
AVERAGE	12.19	4.62	3.60	499.1	313	395
ST DEV	0.02	0.03	0.10	34.0	22	28

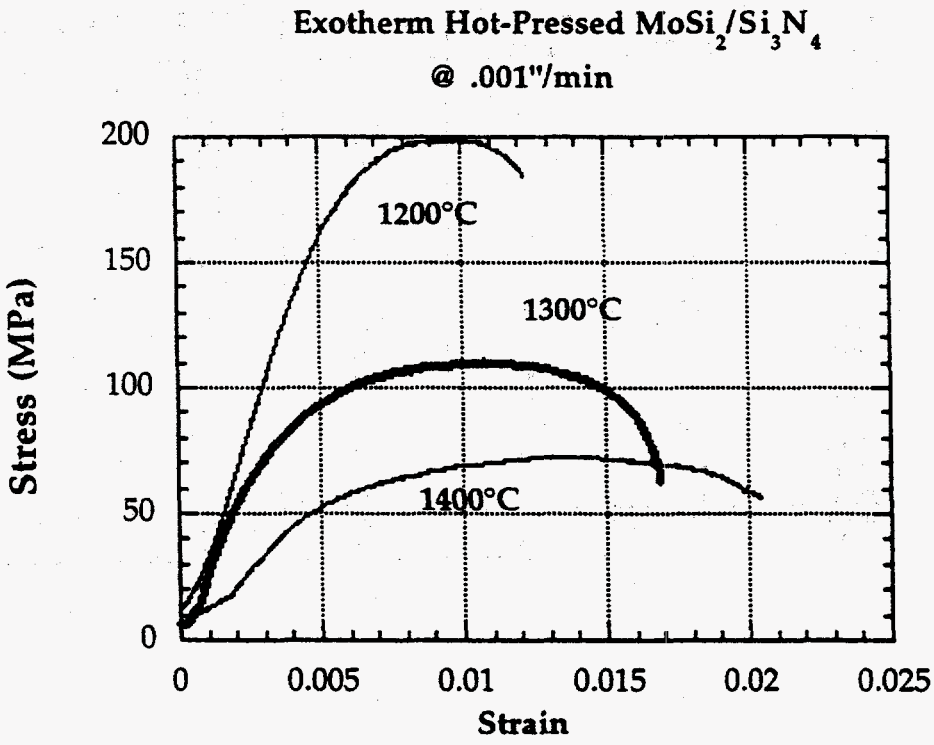

Figure 1: Stress-strain curves of $MoSi_2/Si_3N_4$ tested at .001"/minute.

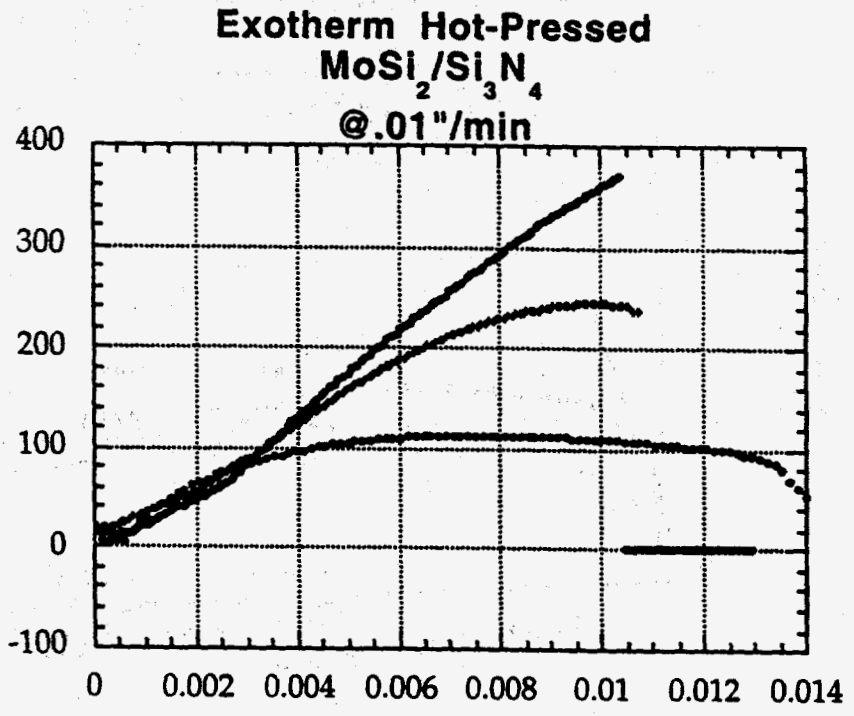

Figure 2: Stress-strain curves of $MoSi_2/Si_3N_4$ tested at .01"/minute.

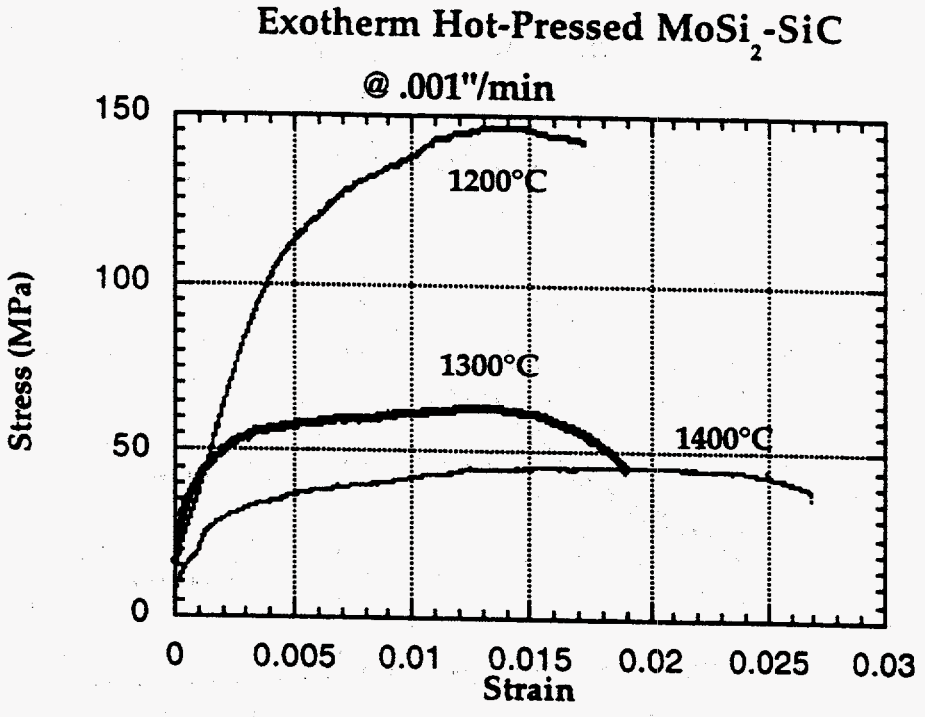

Figure 3: Stress-strain curves of $MoSi_2$/SiC tested at .001"/minute.

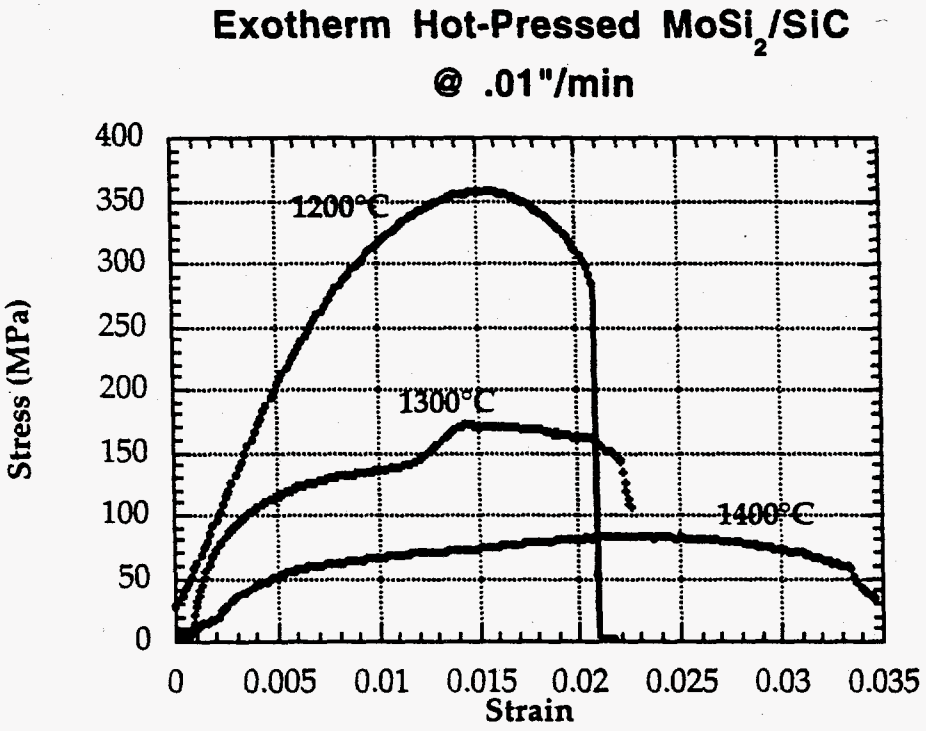

Figure 4: Stress-strain curves of $MoSi_2$/SiC tested at .01"/minute.

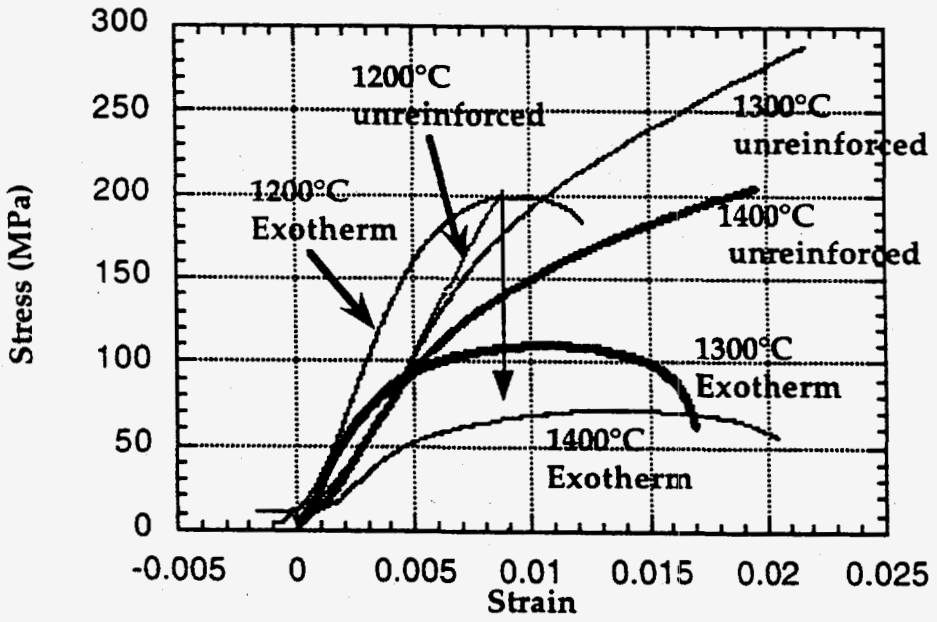

Figure 5: Comparison of stress-strain response of Exotherm materials to that of unreinforced hot-pressed $MoSi_2$.

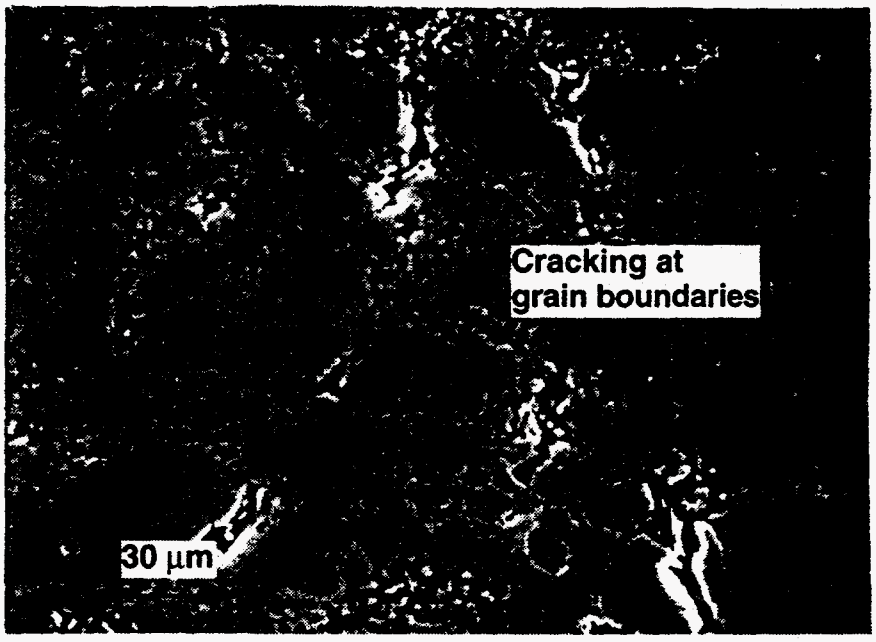

Figure 6: Low magnification SEM micrograph of the Exotherm $MoSi_2/Si_3N_4$ material after testing at 1400 °C and .001"/minute.

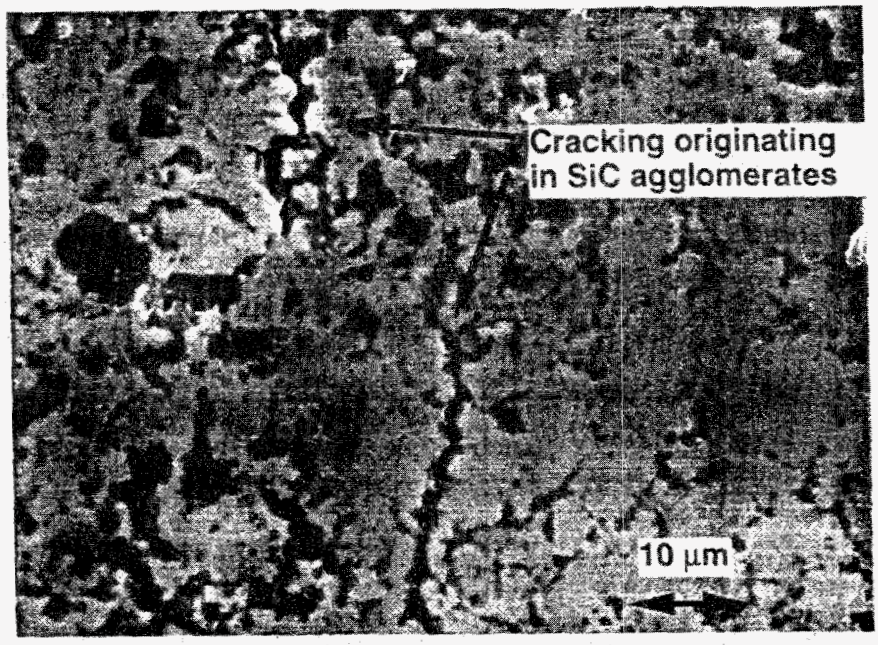

Figure 7: $MoSi_2$/SiC microstructure after mechanical testing.

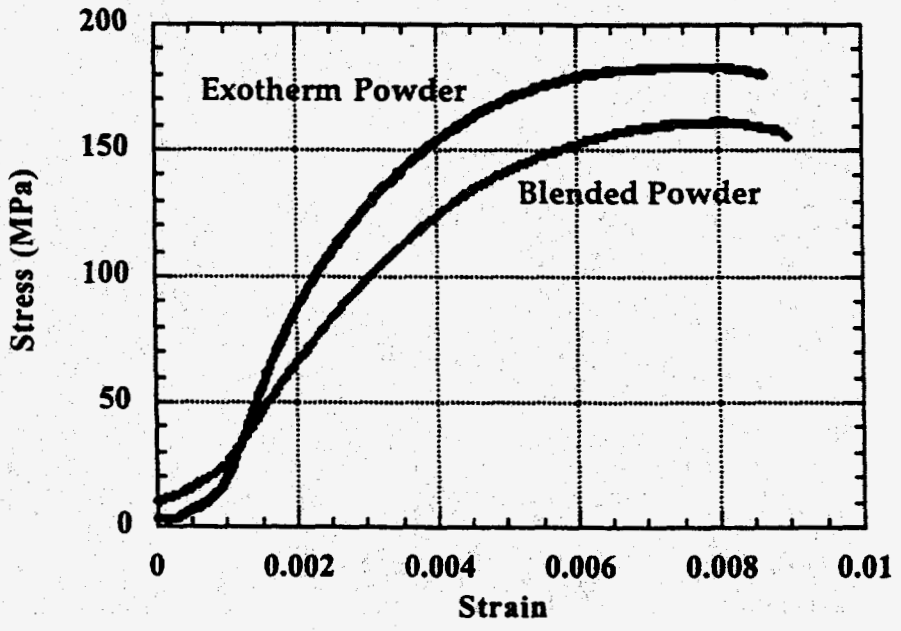

Figure 8: Stress-strain curves for Exotherm and blended powders, both tested at 1200 °C and .001"/minute.

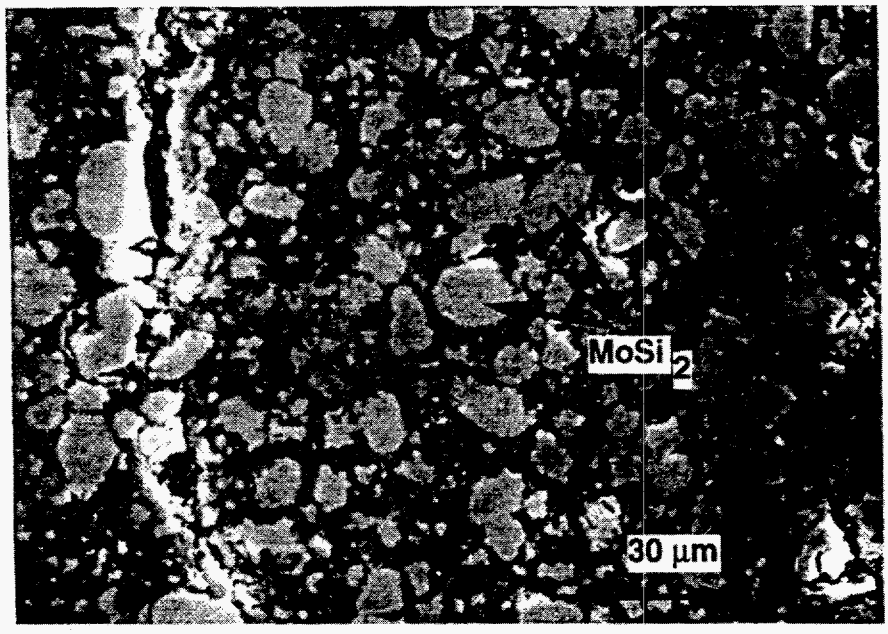

Figure 9: Microstructure of the blended composite after testing, showing damage developing within the ductile $MoSi_2$ phase.

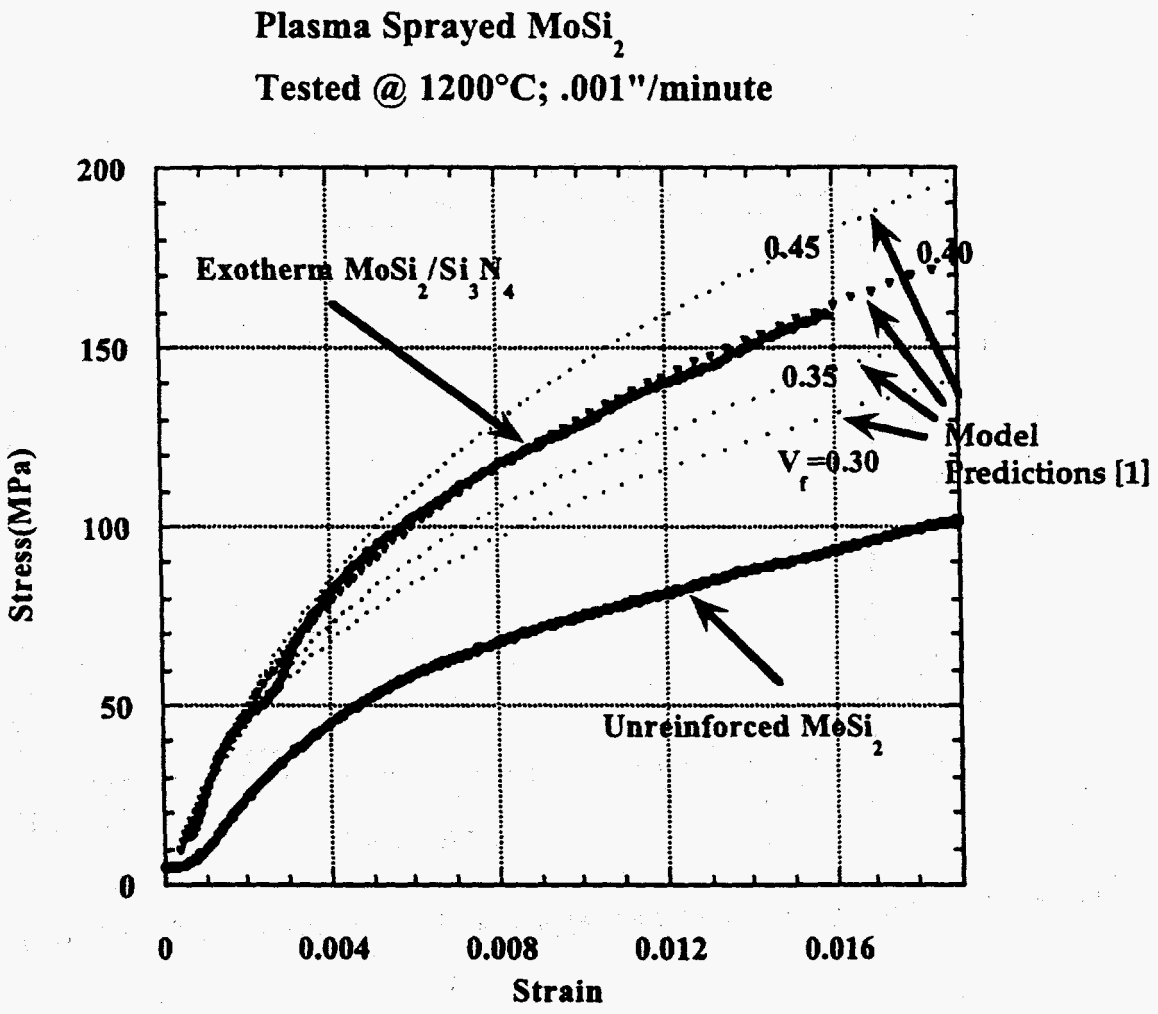

Figure 10: Stress-strain behavior of plasma sprayed $MoSi_2/Si_3N_4$ composite, compared to unreinforced plasma sprayed $MoSi_2$.

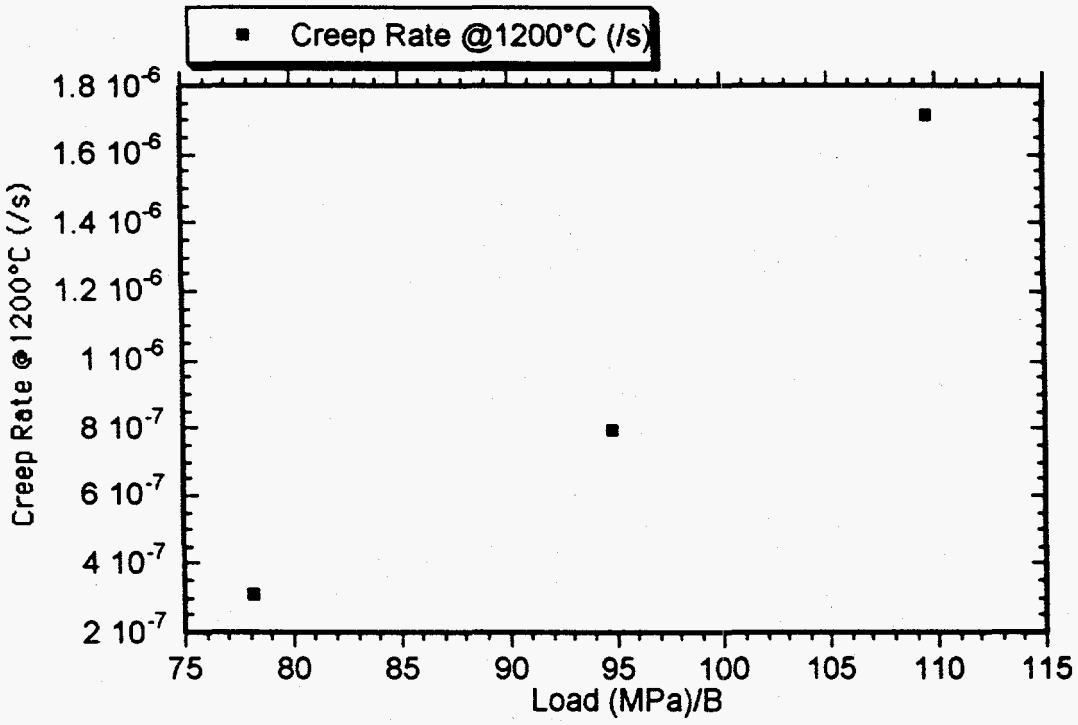

Figure 11: Creep rate versus corrected applied load for hot pressed $MoSi_2$/SiC samples.

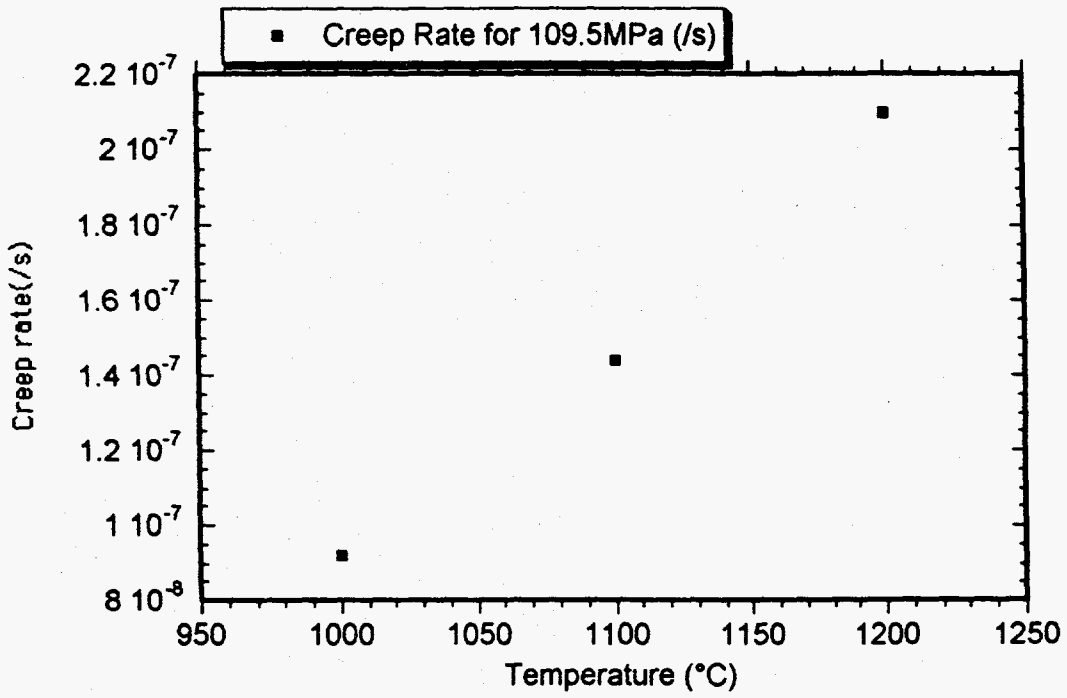

Figure 12: Creep rate versus test temperature for hot pressed $MoSi_2$/SiC samples.

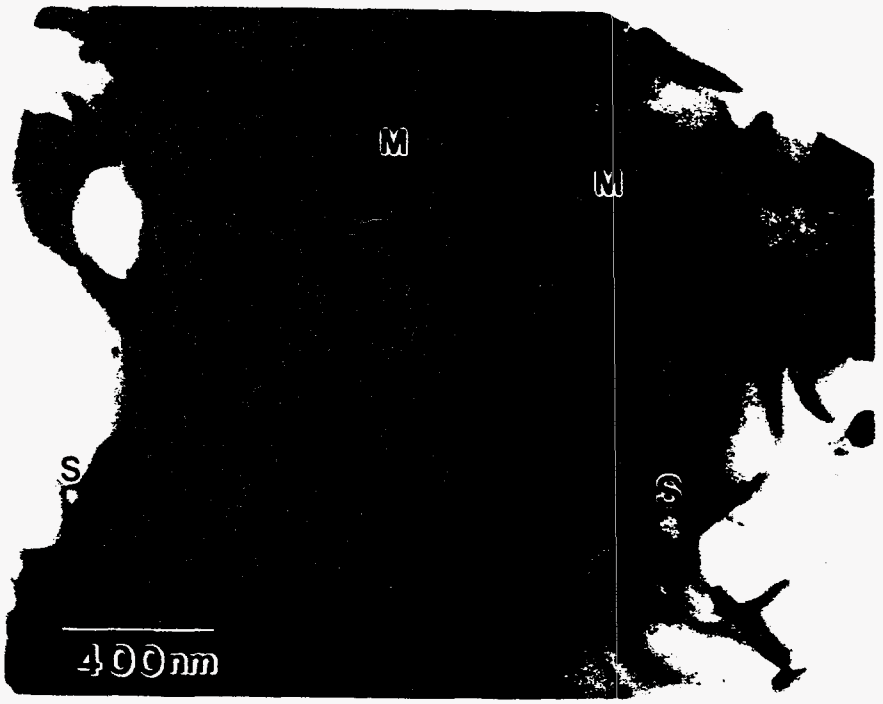

(a)

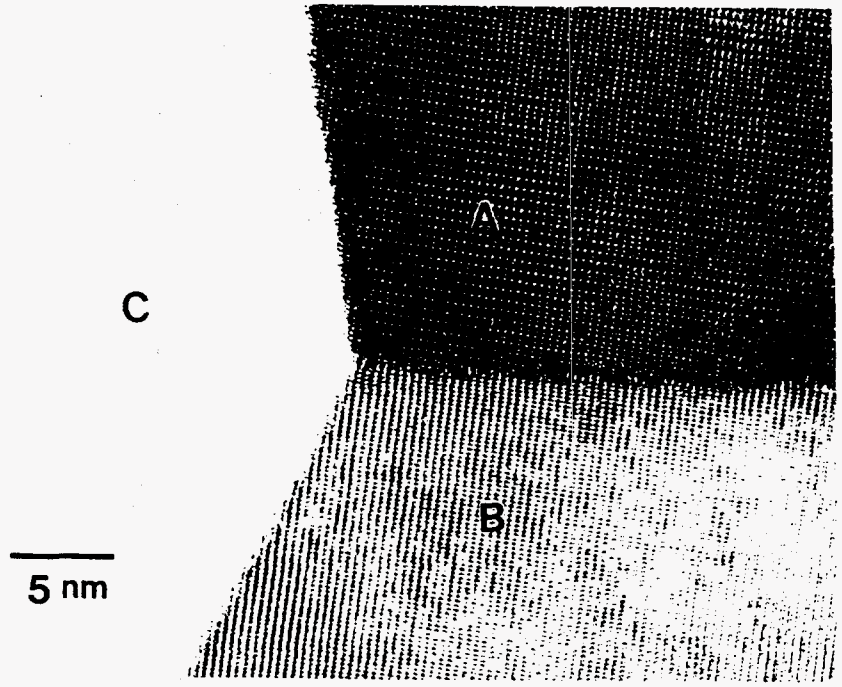

Figure 13: (a) Microstructure and (b) HREM image of a $MoSi_2$ triple junction in plasma sprayed $MoSi_2/Si_3N_4$ composites. In (a) M stands for Mo_5Si_3 and S stands for Si_3N_4. In (b) C grain is not oriented for lattice imaging; nevertheless, it shows that there is no glassy phase present at the triple junction.

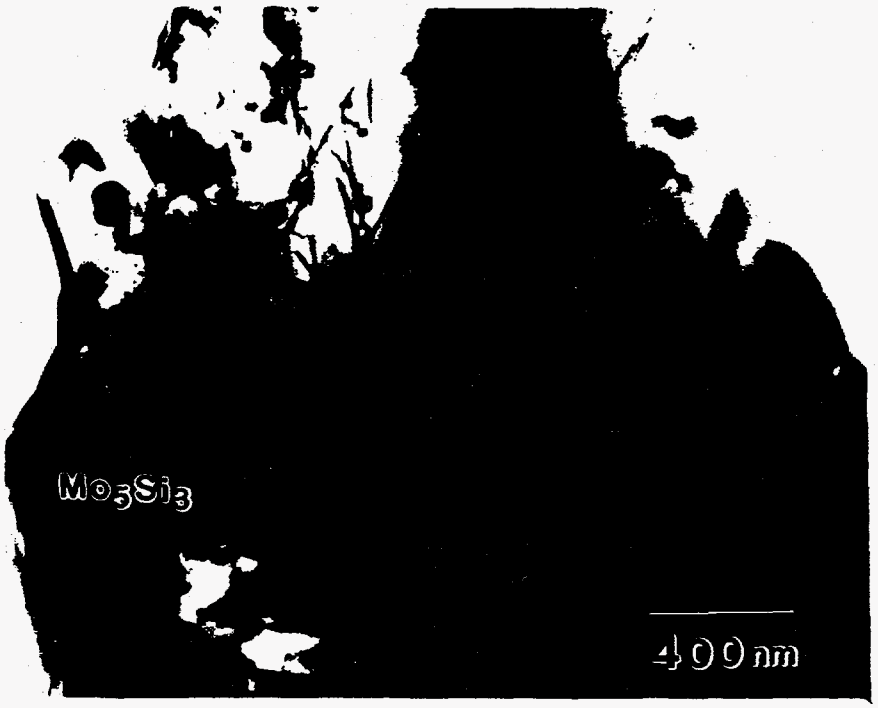

(a)

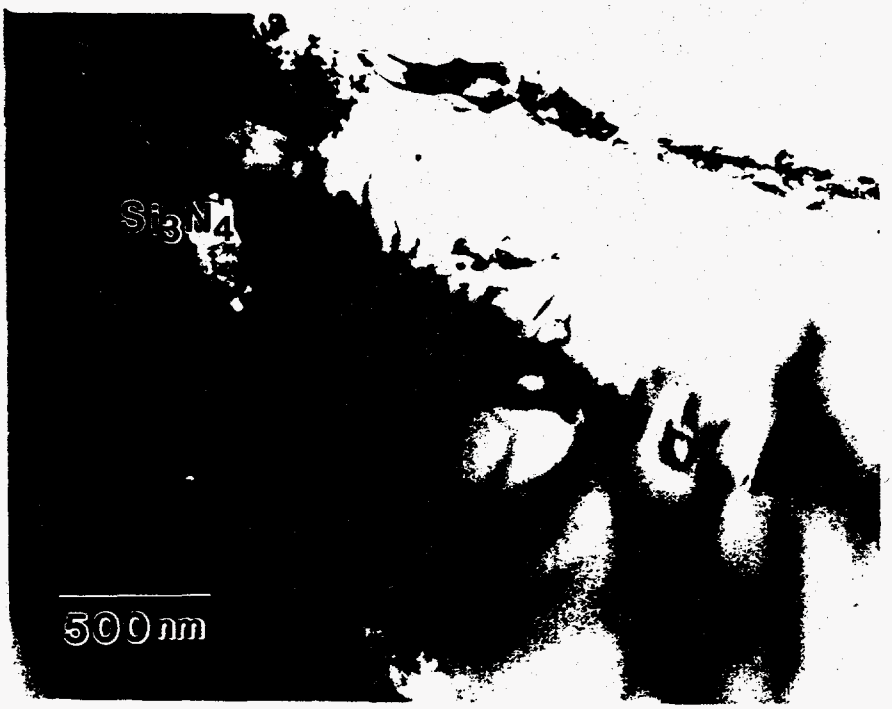

Figure 14: Dislocations were often observed at (a) $MoSi_2/Mo_5Si_3$ and (b) $MoSi_2/Si_3N_4$ interfaces in plasma sprayed $MoSi_2/Si_3N_4$ composites after four point bend testing.

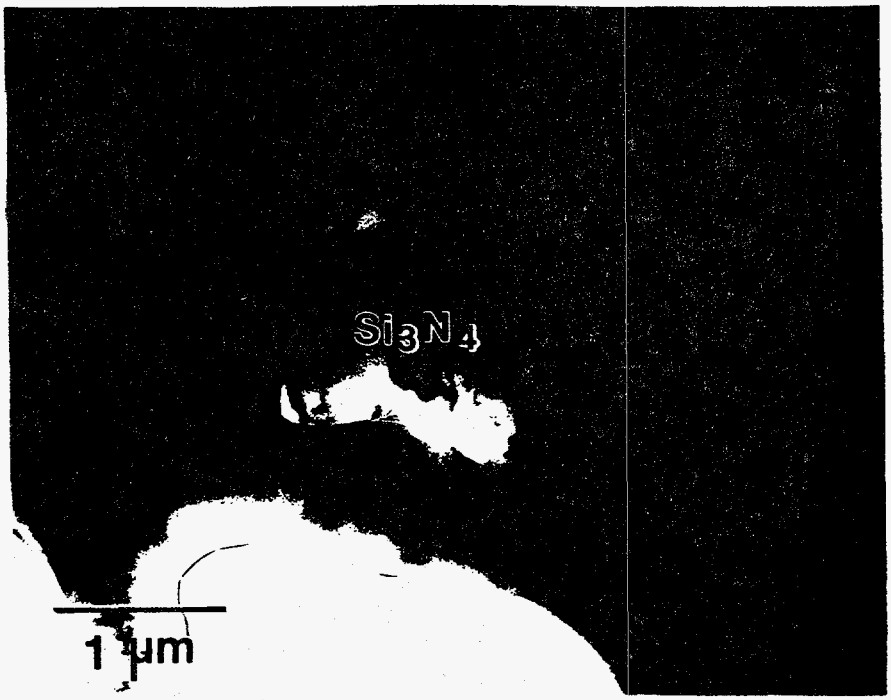

(a)

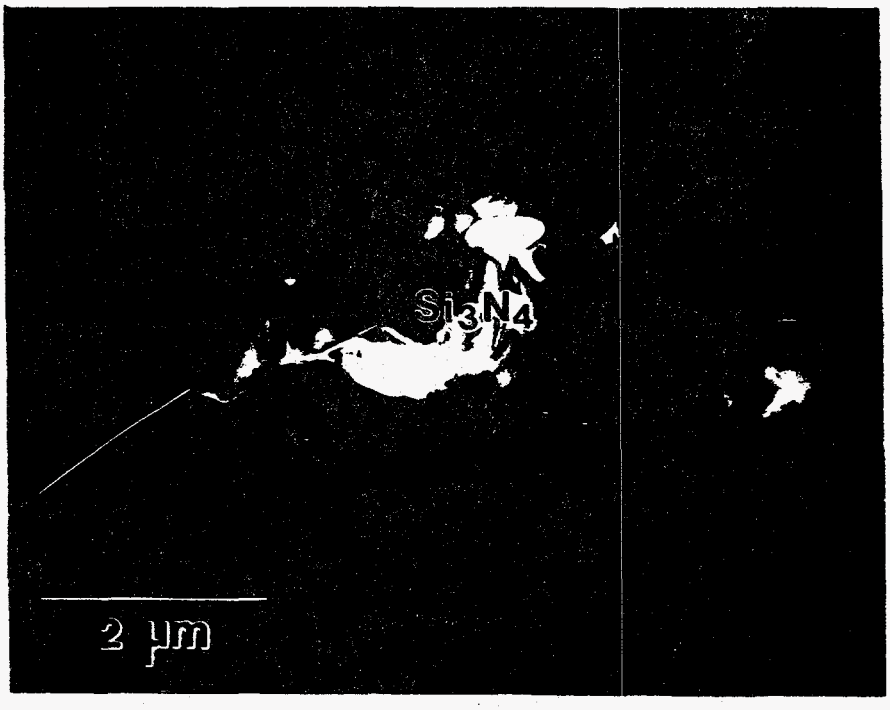

Figure 15: (a) Interface debonding and (b) cracking were often observed in hot pressed $MoSi_2/Si_3N_4$ composites after four point bend testing.

(a)

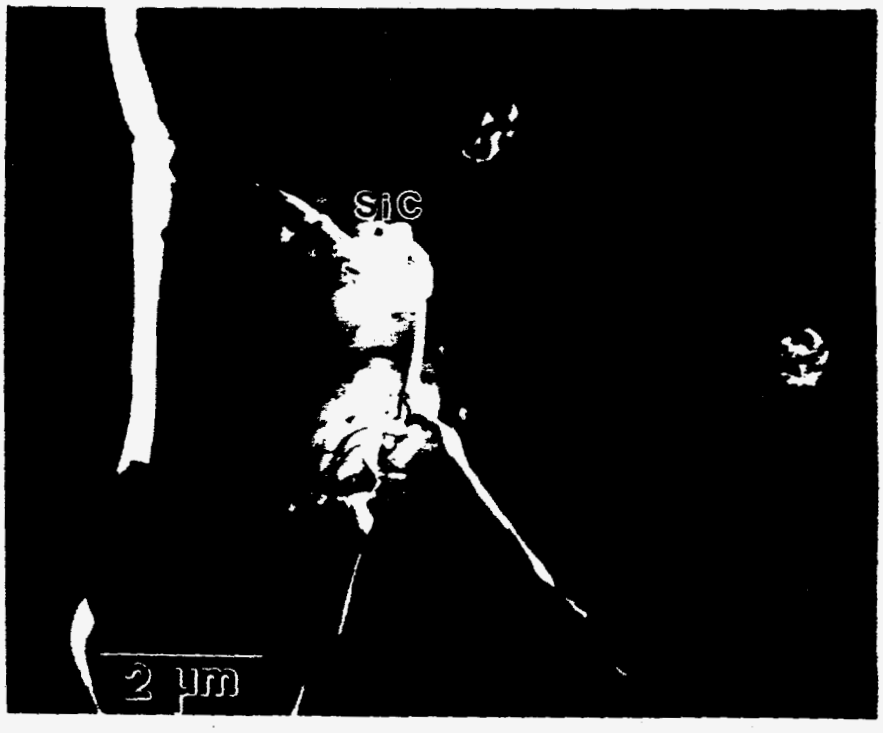

Figure 16: (a) Interface debonding and (b) cracking were often observed in hot pressed $MoSi_2$/SiC composites after four point bend testing.

construction of a low-temperature UDS system. Craig A. Blue visited MIT on April 5-6, 1995, in order to learn the various aspects of the UDS system. The design of the low-temperature system was completed within one week of his return from MIT. Procurement and fabrication of necessary parts for the low-temperature system followed. The apparatus consists of a vacuum chamber, melt furnace for the crucible, melt temperature control system, pressure control system, melt vibration system, droplet charging assembly, jet monitoring system, and supporting structures.

Construction at ORNL of the low-temperature UDS system was completed in June 1995, and a picture of the system is shown in Fig. 1. Over 30 runs have been completed to date and further tailoring of this system is ongoing. The tailoring of the system includes elimination of orifice clogging, completed, and large diameter uniform droplet formation (> 750 mm). The large diameter work was accomplished in line with the possible development of a new/additional funding source.

Preliminary, Low-Temperature System Results

All the initial experimentation with the low-temperature system utilized tin as the material of choice. Figure 2 shows a scanning electron micrograph of tin powder produced. The operating parameters for the experiment include: 300°C melt temperature, 103-kPa crucible/chamber pressure difference, 10-kHz perturbation frequency, 100-mm orifice diameter, and a d.c. charge plate voltage of 400 V. Preliminary-size distribution data revealed an average diameter of 168 μm and a standard deviation of 2 μm. As can be seen by the scanning electron micrograph and the size distribution data, the powder produced is very uniform.

Medium-Temperature System

The medium-temperature apparatus has been assembled, and preliminary testing is in progress. This system will allow for the fabrication of uniform droplet of materials with melting points as high as 1250°C. Also, this system was designed for higher volume melts (15 to 20 lb/materials dependent). Therefore, this system will aid in the development of the UDS system for industrial practices. The successful and timely construction of both the low- and medium-temperature systems allowed the meeting of milestones and set the stage for the design and construction of the high-temperature system.

MASSACHUSETTS INSTITUTE OF TECHNOLOGY*

Optimization of Process Parameters for the Development of the Uniform-Droplet Spray Process

Technical Progress (FY 1995)

The first quarter FY 1995 was utilized to transfer the UDS process technology developed in the Laboratory of Manufacturing and Productivity at MIT to the collaborating teams at ORNL and Tufts University. In early April, Dr. Craig Blue, investigator at

---

*Personnel at MIT are Prof. Jung-Hoon Chun, Principal Investigator, and two M.S. students, Jean-Pei Cherng and Ho-Young Kim.

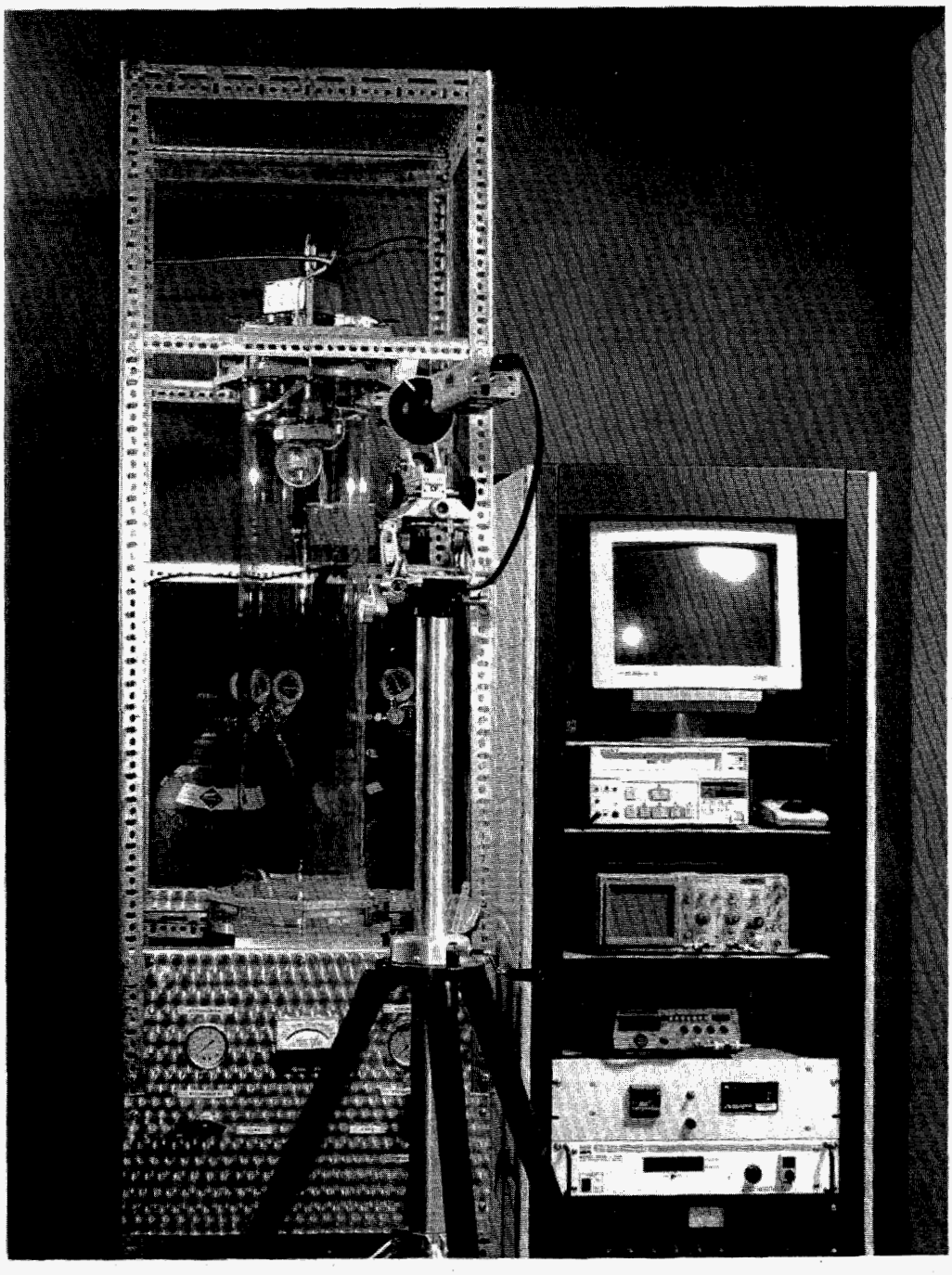

Fig. 1. Low-temperature uniform-droplet spray system located at the Oak Ridge National Laboratory.

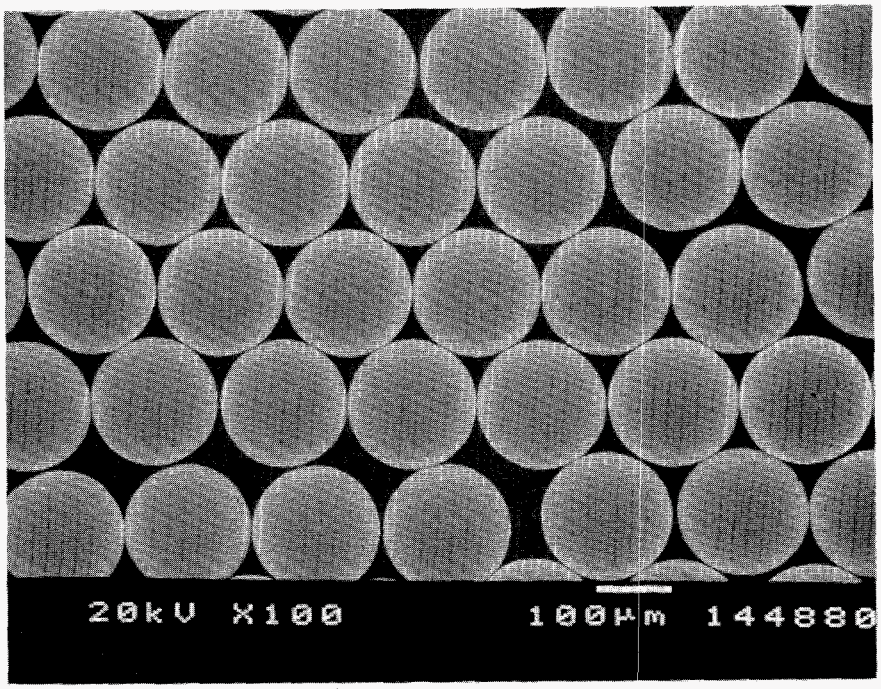

Fig. 2. Scanning electron micrograph of tin powder produced at the Oak Ridge National Laboratory.

ORNL, visited MIT to become familiar with the UDS system and its operation in order to proceed with the design and construction of a similar system at ORNL. Common research efforts have been discussed to optimize the UDS process parameters and modify the system for higher temperature metals such as aluminum and ferrous alloys. We began to modify the UDS apparatus to spray higher melting-point metals such as aluminum alloys. Crucible and filter materials were selected which would not chemically react with the aluminum melt at operating temperatures near 800°C.

Our objective for the current quarter is to collect uniform powders of aluminum alloy. Preliminary attempts made to spray aluminum with a 100-µm orifice showed erratic stream behavior. The jet of molten aluminum wandered back and forth from a vertically stable position, causing jet break-up to be unsteady. It appeared that the orifice became partially blocked with contaminate particles that passed through and deflected the stream. However, stability of the droplet stream was observed with increasing orifice diameter. The strong affinity of aluminum to oxidize is a major source of nonideal processing conditions. Oxidation causes abundant inclusions to form in the melt, and aluminum oxide, whose density closely matches that of pure aluminum, is difficult to separate from the melt. These oxides and other contaminate particles could be affecting jet stability. Furthermore, oxidation can prevent uniform jet break-up by forming an oxide skin around the stream of aluminum after it exits the orifice.

During this quarter, we focused on developing an effective filtration system to stabilize the aluminum stream. Aluminum filtration is commonly practiced in cast shops to improve product quality. However, conventional applications do not require very fine filter pore sizes (< 400 µm). To improve filter efficiency, different commercial filters were investigated to determine the effect of experimental parameters including: + filter pore size, + filter height, and + filter strength. The orifice used is 100 µm in diameter. With a

ceramic foam filter made from phosphate-bonded alumina at 45 pores per linear inch (ppi) and 5 mm in height, the aluminum stream was unsteady and uniform break-up could not be sustained. Experiments using a silicon-carbide, chemical vapor deposition (CVD) foam, at 100 ppi and 3 mm in height, showed no improvement in stream behavior. Inspection of the crucible contents after an experiment shows an oxide skin that remains on top of the filter. However, it is hypothesized that the high-crucible pressure applied on top of the melt during an experiment may force oxide particles through the filter. This implies that a thin filter is an ineffective barrier between the oxide film and the aluminum. Increasing the height of the SiC CVD foam to 15 mm successfully stabilized the aluminum stream. Uniform jet break-up was achieved and sustained as shown in Fig. 3.

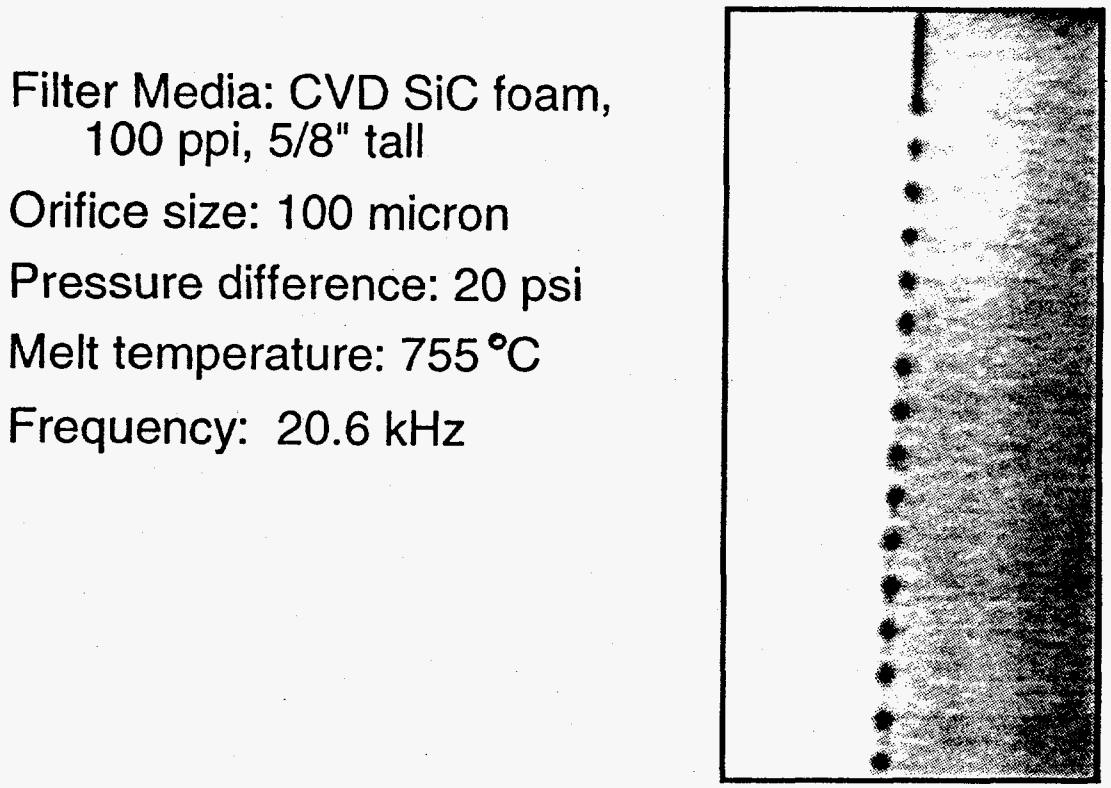

Fig. 3. Uniform jet break-up of aluminum.

However, the SiC CVD foam filter does not give consistent results. Orifice clogging is still a recurrent problem. Composition spectral analysis of a sample clogged orifice showed silicon-carbide particles contaminating the aluminum melt below the filter. Particles of the filter material may be detaching and clogging the orifice. Although inexpensive, ceramic foam filters have a structure with relatively low-mechanical strength and are easily damaged in handling or while in use. Another type of filter currently being tested is a bonded, silicon-carbide grit filter. Its grit construction provides more strength and a more tortuous filtration path.

Further investigation is being carried out to determine the optimal parameters for a consistent and repeatable uniform jet break-up. It is important to eliminate uncertainty in the processing conditions to maintain a stable jet. Then, the aluminum jet will be characterized by mass flow rates. In addition, the stream of droplets will be charged to

prevent droplet merging. The aluminum powders will be collected to confirm uniformity in size and shape.

Proposed work for the next quarter includes spraying droplets of larger size (200 to 400 μm) in order to increase robustness of the process against instability as well as to increase mass flow rate. Jet stability is observed to increase with larger orifice size.

A model to determine the thermal state and solidification behavior in the deposit has recently been developed and experimentally validated for lead-tin eutectic alloy [15]. The model assumes one-dimensional heat transfer through the top surface of the deposit and bottom of the substrate. Explicitly solving for enthalpy and temperature in the deposit using the Scheil equation, the deposit thermal model has shown acceptable agreement with experimental results. Furthermore, the simulations and experiments revealed the sensitivity of the deposit thermal state to mass flux variations. Therefore, care must be taken to ensure correct mass flow rate and spray radius from charging are maintained. This model can be modified and tested for spraying aluminum alloys. Using the modified model, relationships between the desired microstructure of a sprayed deposit to the process parameters can be established for applications in spray-forming technology.

TUFTS UNIVERSITY*

Process-Structure Relationship in the Uniform-Droplet Spray Process

Objective

The objective of the work at Tufts University is to characterize the solidification and microstructural evolution in the UDS process through experimentation and modeling, with the eventual goal of developing novel microstructures by the UDS process in a controlled manner. The first year of the study is focused on the solidification of the traveling uniform droplets, although the solidification and microstructural evolution in the spray deposit are also to be investigated.

Technical Progress (FY 1995)

Summary

The first half-year period was mainly spent for the following:

- Acquisition of lab space in the Bray Laboratory at Tufts University.
- Design and construction of a UDS apparatus for experiments with low-melting-point alloys (completed).
- Preliminary experiments to process low-melting-point alloys with the completed UDS apparatus (in progress).

---

*Personnel at Tufts are Prof. Teiichi Ando, Principal Investigator, Rajesh Shingavi, Alfred DiVenuti, and Charles Tuffile (three M.S. students), Tina Notosoehardjo and Mona Masghati (two B.S. students), and Prof. Anil Saigal, who participates in the project through advising the students. Partial support for Shingavi, DiVenuti, and Tuffile is provided through this grant from the Advanced Industrial Materials (AIM) Program of the U.S. Department of Energy.

- Design and fabrication of a calorimeter for droplet enthalpy measurements (completed).
- Acquisition of an Al-Fe alloy and 30 lb of an Al-Cu-Zr alloy (completed).

Concurrently, work has begun in the areas of:

- Design of a furnace and a crucible for processing higher melting-point alloys.
- Nonadiabatic calorimetry for droplet enthalpy measurements.
- Modeling of the solidification in traveling droplets.

UDS Apparatus

Following the progress made in the first quarter ending July 15, 1995, we continued and completed the construction of the low-temperature UDS apparatus. Due to delays in machining of the stainless-steel melting crucible and the top plate of the UDS chamber, for which off-campus machine shops had to be used, the assembling of the apparatus was completed in late September 1995, as opposed to our initial estimated completion time of August. Figure 4 shows Tufts' UDS apparatus.

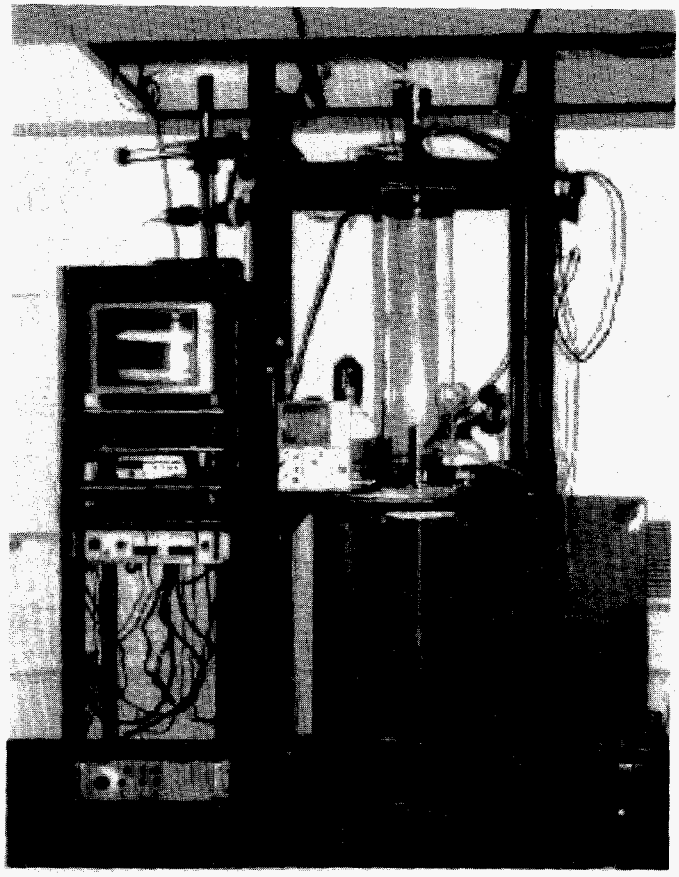

Fig. 4. Uniform-droplet spray apparatus at Tufts University.

The basic design of our low-temperature UDS apparatus was adopted from the one developed by the Laboratory for Manufacturing and Productivity at MIT. The main features of the apparatus include a 9-in.-diam by 1-m-high Pyrex glass chamber, a melting crucible with band heaters, a melt vibrating system, a gas supply system, a droplet charging system, a jet break-up monitoring system, a melt temperature control system, and supporting structures that hold the chamber and the control panels.

A 1-m-long chamber is utilized to accommodate the flight distances necessary for the complete solidification of droplets up to 200 μm diam in an inert gas atmosphere. The melting furnace is constructed of AISI 304 stainless steel and can accommodate approximately 0.5 kg of low-melting temperature alloys — up to a maximum temperature of about 600°C. A graphite crucible is being manufactured for use with aluminum and other alloys with high-melting points up to 1200°C. The droplet monitoring system consists of a CCD video camera, a VCR monitor, and a stroboscope, which is synchronized with the piezoelectric transducer through a function generator.

Modifications were made to facilitate specific experiments and also to make the UDS apparatus robust. The principal modifications made are listed below:

- The base plate was modified to incorporate the supporting fixtures for the calorimetric measurement device. This is to be used for experiments to determine the droplet enthalpy.
- The top plate was modified for incorporation of safety valves.
- Use of "Quick-Connects" for top-plate inlets to reduce preparation time.
- Modification of the evacuation channel to facilitate the evacuation of the crucible prior to evacuating the chamber. This sharply reduces the level of oxygen present in the crucible which might inhibit subsequent jet break-up.
- A frequency reducer was build to facilitate synchronization of the strobe and the piezoelectric transducer. Frequency reduction by one, two, and three decades is available for a wide range of input frequencies.
- A voltage reducer circuit which goes to a two-channel oscilloscope was made for measuring and controlling the exact voltage going to the piezo.
- An O-ring design for the piezo assembly was incorporated in order to minimize the heat flow to the piezo.

Alloy Acquisition

We have purchased 10 lb of pure tin for use in the preliminary experiments. Orders have been placed for 30 lb each of Sn-5Pb and Sn-37Pb alloys for further preliminary studies and droplet enthalpy measurements. We have also received about 50 lb of an Al-Fe alloy and 30 lb of an Al-Cu-Zr alloy from Alcoa as gifts. These alloys will be used in our study, with and without compositional modifications, as soon as the planned preliminary experiments with low-melting-temperature alloys are completed. Two pounds of the Al-Fe binary alloy have been shipped to ORNL, and yttrium will be added, thereby producing a ternary alloy to be used in our joint future work.

Preliminary Experiments

Using the low-temperature UDS apparatus, we have begun preliminary experiments with pure tin. We have been able to produce both droplets and fiber of tin. At present, however, we have not been able to reduce the oxygen content in the chamber in a controlled manner due to the use of an old, ill-functioning mechanical pump. A new pump has been ordered to rectify this problem. The new pump will arrive by October 20, 1995. As soon

as the new pump has been placed in our system, more experiments using tin and tin-lead alloys will follow. Important experiments to be performed with the low-temperature UDS apparatus include direct measurements of the droplet enthalpy as a function of flight distance using a nonadiabatic calorimetric method developed at Tufts and MIT. A brief explanation of the planned experiments is give in the next section.

Work in Progress

Higher-Temperature Melting Capability

To permit processing of higher melting-point alloys, particularly aluminum alloys, we have designed and will soon start fabrication of a graphite crucible and a melting furnace. These components will be mounted directly on the current UDS apparatus for the study of in-flight solidification of aluminum-alloy droplets. The provision of this higher temperature capability is a vital step in the study of microstructural control in spray-deposited aluminum alloys, which is planned, primarily, for the second year of this project. Concurrently, we have assigned Rajesh Shingavi, a graduate student, to work in collaboration with the Laboratory for Manufacturing and Productivity at MIT on the characterization of aluminum alloys.

Nonadiabatic Calorimetry

Charles Tuffile, a graduate student, has been assigned to this work. We have purchased the necessary components and fabricated a calorimeter to be used in a calorimetric study of uniform droplets to experimentally determine the droplet enthalpy as a function of flight distance. A supporting fixture and a low-energy input, magnetic stirring system have also been fabricated. The newly devised calorimeter is based on the concept of nonadiabatic calorimetry in which the rate of heat loss from the calorimeter is accounted for as a function of the temperature of the oil bath. This approach is necessary for experiments in which a large opening has to be provided to permit the entry of the droplets into the calorimeter. We are programming the heat balance equation developed previously by Tufts and MIT to facilitate in-process data acquisition.

The experimentally determined droplet enthalpy values will be compared with values computed by the solidification model being developed and to further facilitate accurate prediction of the thermal state and the microstructure evolution in the spray deposit.

Modeling of the Solidification in Traveling Droplets

Alfred DiVenuti and Rajesh Shingavi, two graduate students, are assigned to this work. The modeling of the solidification of traveling droplets, assuming no undercooling and local equilibrium, has been conducted at MIT. It is further assumed that the Scheil equation describes the solute partitioning during solidification. While such a treatment enables us to predict the thermal states of the droplets reasonably accurately and permits systematic spray -forming experiments with controlled liquid fractions, it is not necessarily capable of predicting the actual solidification of the traveling droplets and the resultant microstructures, particularly when undercooling is not negligible. Substantial undercoolings are expected to be present in uniform droplets. We are modeling the droplet solidification, accounting for the prior undercooling, by applying an appropriate existing model for droplet solidification in conjunction with the droplet motion equation. The particular model we are currently adopting in our modeling is one developed by Lipton, Glicksman, and Kurz [16] which takes into account the thermal, constitutional, and curvature undercoolings. The interface is still assumed to be at local equilibrium (i.e., a

constant value of the equilibrium partition coefficient is used). The use of the Lipton, Glicksman, and Kurz model is justified for cases in which undercooling is relatively small. We have programmed the Lipton, Glicksman, and Kurz model. This program will be incorporated in the droplet motion model that has been developed at MIT. We plan to extend our modeling effort to incorporate another solidification model, such as the one presented by Boettinger, Coriell, and Trivedi [17], which takes into account not only the three components of undercooling but the fourth term (the kinetic undercooling) so as to cover higher ranges of undercooling where the interface compositions deviate from conditions of local equilibrium.

References

1. P. Acquaviva et al. "Thermal Modeling of Deposit Solidification in Uniform-Droplet Spray Forming" submitted and accepted to ASME Intelligent Manufacturing and Material Processing Symposium Proceedings, San Francisco, November 12-17, 1995.

2. C. H. Passow, M.S. Thesis, Department of Mechanical Engineering, Massachusetts Institute of Technology, 1990.

3. C. H. Passow, J.-H. Chun, and T. Ando, *Metall. Trans.* **24A** (1993) 187.

4. T. Ando, J.-H. Chun, and S. Sahu, Proc. '93 Powder Metallurgy World Congress, Part II., (Kyoto, Japan: *Jap. Soc. of Powder and Powder Metall.*, 1993), p. 971.

5. C.-A. Chen, S. Sahu, J.-H. Chun, and T. Ando, *Science and Technology of Rapid Solidification and Processing, Series E-Vol. 278* , NATO ASI Series, (Dordrecht: Kluwer Academic Publishers, 1994) p. 123.

6. C.-A. Chen, J-H. Chun, and T. Ando, Proc. 1994 Powder Metallurgy World Congress, Toronto, 1994.

7. A. R. E. Singer, *Met. Mater.* **4** (1970) 246.

8. A. R. E. Singer and R. W. Evans, *Met. Technol.* **10** (1983) 61.

9. A. G. Leatham, R. G. Brooks, and M. Yaman, *Modern Developments in Powder Metallurgy, Vol. 15*, ed. E.N. Aqua et al., (Princeton, New Jersey: APMI, 1985) p. 157.

10. E. J. Lavernia and N. J. Grant, *Int. J. Powder Metall.* **2**(2) (1986), 93.

11. Y. Ikawa, K. Kumagai, H. Hamabe, Y. Ozaki, and S. Yamauchi, *J. Jap. Inst. Met.* **30**(6) (1991) 548.

12. S. Matsuo, T. Ando, M. C. Zody, and N. J. Grant, *Advances in Powder Metall., Vol. 5*, ed. L. F. Pease III et al., (Princeton, New Jersey: APMI, 1991), p. 161.

13. P. Mathur, D. Apelian, and A. Lawley, *Acta Metall.* **37**(2) (1989) 429.

14. B. P. Bewlay and B. Cantor, *Metall., Trans.* **20B** (1990) 899.

15. X. Liang, J. C. Earthman, and E. J. Lavernia, *Acta Metall. Mater.* **40** (1992) 3003.

16. J. Lipton, M. E. Glicksman, and W. Kurz, *Metall. Trans. A* **18A** (1987) 341.

17. W. Boettinger, S. R. Coriell, and R. Trevedi, *Rapid Solidification Processing-Principles and Technologies, IV*, eds. R. Mehrabian and P. A. Parrish, Claitor's Publishing Division, 1988.

Publications

1. P. Yim, J.-H. Chun, T. Ando, and V. K. Sikka, "Production and Characterization of Mono-Sized Sn-38 wt. % Pb Alloy Balls," 1995 International Conference on Powder Metallurgy and Particulate Materials (PM2TEC'95), May 14-17, 1995, Seattle, Washington.

2. P. Yim, J.-H. Chun, T. Ando, and V. K. Sikka, "Production and Characterization of Mono-Sized Sn-38 wt. % Pb Alloy Balls," to appear in International Journal of Powder Metallurgy, 1995.

3. P. Acquaviva, C.-A. Chen, J.-H. Chun, and T. Ando, "Thermal Modeling of Deposit Solidification in Uniform-Droplet Spray Forming," ASME Symposium on Intelligent Manufacturing and Material Processing, ASME International Mechanical Engineering Congress and Exposition, November 12-17, 1995, San Francisco, California.

4. P. Acquaviva, C.-A. Chen, J.-H. Chun, and T. Ando, "Thermal Modeling of Deposit Solidification in Uniform-Droplet Spray Forming," submitted to ASME *Transactions Journal of Engineering for Industry*, 1995.

5. C.-A. Chen, P. Acquaviva, J.-H. Chun, and T. Ando, "Effects of Droplet Thermal State on Deposit Microstructure in Spray Forming," to appear in *Scripta Metallurgica et Materialia*, 1995.

Interaction with Industry

The Droplet-Based Manufacturing Research Program Meeting was held on September 29, 1995, at MIT to foster collaboration with industry and review current progress. Industry participation in the meeting included: Dr. Badreddine Ahtchi, Senior Engineering Scientist, Unilever Research U.S., Edgewater Laboratory; Mr. Richard Aubin, Manager of Rapid Manufacturing, United Technology Research Center; Dr. Craig Blue, Oak Ridge National Laboratory; Dr. Men , Technical Specialist, Molten Metal Processing Division of Alcoa; Ms. Sara Dillich, Program Manager, Advanced Industrial Concept Division, U.S. Department of Energy; Mr. John Fischer, Principal Engineer, Boeing Company; Mr. Richard Foulke, President, Ultra Clean International Corp.; Mr. Tim Garner, Senior Engineering Supervisor, Delco Electronics; Dr. Kesh S. Narayanan, Program Director, Division of Design, Manufacturing, and Industrial Innovation, National Science Foundation.

Research for this work was sponsored by the U.S. Department of Energy, Assistant Secretary for Energy Efficiency and Renewable Energy, Office of Industrial Technologies, Advanced Industrial Materials Program, under contract DE-AC05-84OR21400 with Lockheed Martin Energy Systems.

ADVANCED CERAMICS AND COMPOSITES

ADVANCED METHODS FOR PROCESSING CERAMICS

W.B. Carter
School of Materials Science and Engineering
Georgia Institute of Technology
Atlanta, GA 30332-0245

Research sponsored in part by the U.S. Department of Energy, Assistant Secretary for Energy Efficiency and Renewable Energy, Office of Industrial Technologies, Advanced Industrial Materials (AIM) Program, under contract DEAC05-84OR21400 with Martin Marietta energy Systems, Inc.

INTRODUCTION

Combustion chemical vapor deposition (combustion CVD) is being developed for the deposition of high temperature oxide coatings. The process is being evaluated as an alternative to more capital intensive conventional coating processes. The thrusts during this reporting period were continued work on the deposition of zirconia-yttria coatings, the development of the oscillating capillary nebulizer for performing combustion CVD (ceria deposition), and the design, construction and evaluation of a substrate holder for controlling substrate temperature.

TECHNICAL PROGRESS - FY 1995

Summary

1. Zirconia-Yttria Coatings:

Zirconia coatings containing yttria were deposited onto sapphire substrates using liquid fuel combustion chemical vapor deposition. Toluene solutions, containing 2.5 and 7.5 mole percent Y 2-ethylhexanoate (Y 2-EH) (balance Zr 2-EH) and total metal concentrations (Zr + Y) of 0.005 M and 0.02 M, were used.

The thermal stability of the coatings was investigated by heat treating one half of each specimen in air at 1,200°C for 24 hours.

SEM examination indicated that the coatings are polycrystalline. Coating morphologies vary with the deposition conditions. Marked differences exist between coatings before and after annealing and between coatings deposited from solutions with different Y content.

The coatings deposited from the lower Y content solutions (2.5 mole % Y 2-EH) are nodular and dense. Figure 1 displays the effect of the 24 hour, 1,200°C anneal on the morphology of the coatings deposited from the 2.5 mole percent Y 2-EH solutions. The smoothing and neck formation in the post annealed coating is evidence that substantial diffusion occurred during heat treatment.

The coatings deposited from the higher Y content solutions (7.5 mole % Y 2-EH) display more complex consisting of a dense layer of material surrounding tall columnar grains extending through it.

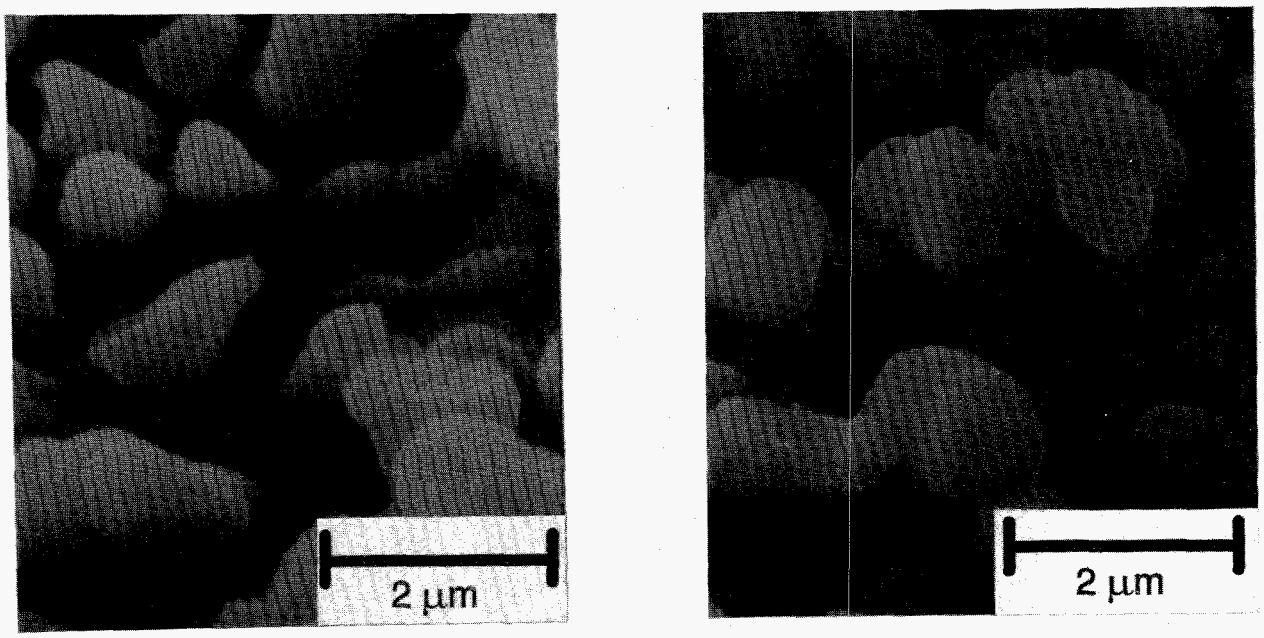

Figure 1 - SEM plan view micrographs of coatings produced from a 2.5 mole % Y 2-EH solution of 0.02 M total cation concentration prior to annealing (left) and after annealing (right).

Figure 2 shows a coating produced from a 7.5 mole percent Y 2-EH solution at 0.02 M concentration. The coral-like morphology of these coatings is displayed on the left. Annealing causes these coatings to densify as shown on the right.

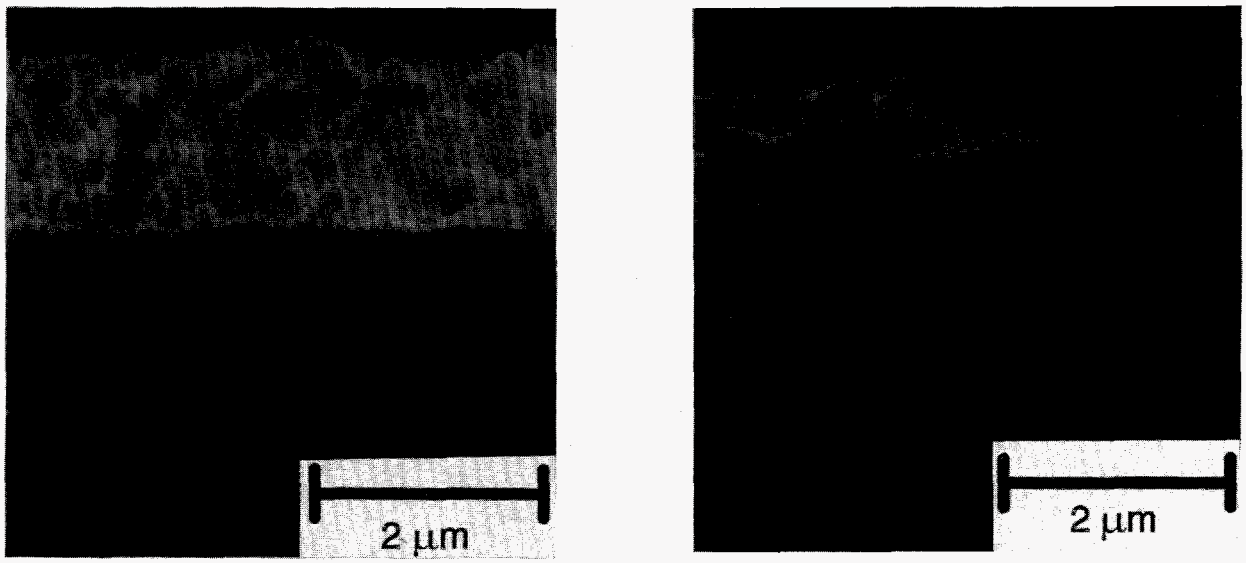

Figure 2 - SEM micrographs of fracture cross sections of coatings produced from a 7.5 mole % Y 2-EH solution of 0.02 M total cation concentration prior to annealing (left) and after annealing (right).

The complex microstructures seen in the coatings deposited from the high Y content solutions are believed to be due to the simultaneous growth of two phases. Assuming that the coatings have Y contents similar to the solutions from which they were deposited, the ZrO_2/Y_2O_3 phase diagram (H.G. Scott, J. Mater. Sci., 10 (1975), 1527) indicates that these coatings were grown in the tetragonal + cubic two phase field. Those coatings deposited from low Y content solutions were grown in the tetragonal phase field (assuming growth temperatures of at least 1,000°C).

The x-ray diffraction (XRD) patterns of all the coatings differ significantly from random powder patterns, indicating large amounts of preferred orientation. XRD data suggest that the coatings deposited from the 2.5 mole percent Y 2-EH solutions contain monoclinic and tetragonal/cubic phases. The XRD data is ambiguous regarding whether cubic or tetragonal is present and electron diffraction has confirmed only the presence of the monoclinic phase. Consideration of the phase diagram of this system suggests that monoclinic material should be present if one assumes that coating compositions are similar to those of the precursor solutions and that near equilibrium conditions exist during deposition.

Coatings produced from the 7.5 mole percent Y 2-EH solutions contain monoclinic and tetragonal/cubic material. The XRD data is ambiguous regarding whether cubic or tetragonal material is present. Electron diffraction has detected only monoclinic and tetragonal. The presence of tetragonal and cubic phases is expected from naive considerations of the phase diagram. Upon cooling to room temperature, some of the tetragonal material would be expected to transform to monoclinic.

Thermal aging produced marked changes in the XRD patterns. The coatings produced from low Y 2-EH solutions show significant differences in peak intensities (both absolute and relative) before and after annealing. Coatings produced at both concentrations display these changes.

As these coatings are highly textured, quantitative phase content information cannot be derived from the Bragg-Brentano diffraction patterns. The changes mentioned above suggest that relaxation processes are active at 1,200°C that induce either the transformation or realignment of unfavorably oriented grains.

Coatings produced from high Y 2-EH solutions at both concentrations also show a regular variation between the before and after anneal XRD patterns. In these coatings, XRD peaks associated with cubic material decreased in intensity (both absolute and relative) after the.

Electron diffraction and energy dispersive spectroscopy work in the TEM is being conducted in order to resolve the ambiguities in the phase composition of the coatings.

2. Ceria Deposition:

Gaseous fuel combustion chemical vapor deposition was utilized to deposit ceria (CeO_2). A standard Bunsen burner with a one inch diameter burner head was modified to allow an atomized solution of water and dissolved coating precursors to be entrained in the oxidant and fuel gas flow inside the mixing barrel. Methane was used as the fuel gas. Air and oxygen (diluted with argon) was used as the oxidant.

The ceria coating was nodular and crystalline with a cubic unit cell. Grain size was less than 0.5 μm and the coating thickness was about 0.8 μm.

Ceria was also deposited with the use of an oscillating capillary nebulizer (OCN) using liquid fuel combustion chemical vapor deposition. The OCN was developed by Wang for sample introduction for ICP-AES and ICP-MS (L. Wang, Ph.D. Dissertation, School of Chemistry and Biochemistry, Georgia Institute of Technology, 1995). The OCN consists of two concentric silica capillary tubes. Liquid is fed through the inner capillary and oxidizing gas through the outer tube. Different droplet size distributions are obtained by varying the diameters of the inner and outer capillaries, the pressure of the oxidizer, and the liquid feed rate. The OCN produces an aerosol with a droplet size distribution that is narrower than that produced by a conventional perfume sprayer-type pneumatic nebulizer. By varying the configuration of the OCN, aerosols with different Sauter mean diameters can be produced.

Ceria coatings were produced using liquid fuel combustion chemical vapor deposition and two different OCN configurations. Figure 3 displays SEM micrographs of CeO_2 coatings deposited with these two different sets of OCN. The coating shown on the left was produced with a larger size aerosol and higher temperature than the coating shown on the right (11 μm Sauter mean diameter vs. 2.3 μm, 1,250-1,300°C vs. 1,100-1,150°C). The coating produced with the larger size aerosol is powdery and non-adherent. The coating produced with the smaller size aerosol is dense, nodular, and adherent.

It has been found that higher deposition temperatures usually produce dense, adherent coatings whereas lower deposition temperatures often produce powdery deposits (solution concentration and other deposition parameters constant). The ability to produce higher quality coatings at lower temperatures is a distinct advantage of the OCN over the perfume sprayer-type nebulizer. This ability will be particularly important when deposition temperatures must be kept low to avoid tempering substrates.

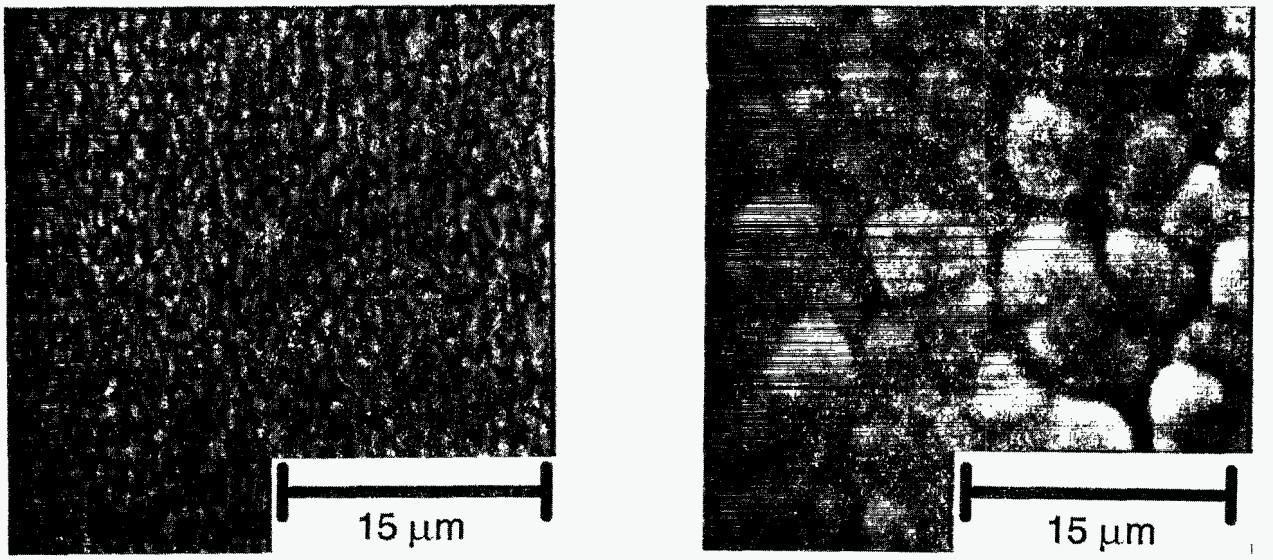

Figure 3 - SEM plan view micrographs of CeO_2 coatings deposited on alumina substrates with 11μm Sauter mean diameter aerosol (left) and 2.3 μm Sauter mean diameter aerosol (right).

3. Substrate Holder:

A substrate holder was designed and built that allows greater temperature stability and control than the wire substrate supports used previously. It consists of a copper rod, threaded on one end, and a copper block with a threaded hole to receive the rod. Cooling water circulates through the copper block. Substrates are mounted on the flat, upper surface of the copper rod and held and held in place by spring loaded clips. A thermocouple is mounted in a hole in the upper end of the rod just beneath the substrate. Another thermocouple can be pressed against the upper surface of the substrate. Temperature control is obtained by varying the distance the rod is inserted into the copper block, the water flow rate, flame characteristics, and flame position with respect to the substrate.

MILESTONES DURING FY 1995

The oscillating capillary nebulizer (OCN) was utilized in performing combustion chemical vapor deposition. The use of the OCN allows greater control over deposition conditions by producing a narrower droplet size distribution than a perfume type pneumatic nebulizer. By using small size aerosols, lower deposition temperatures can result in higher quality coatings.

PUBLICATIONS

Conference Proceedings

1. W.B. Carter, G.W. Book, and A.T. Hunt, "Combustion Chemical Vapor Deposition of Ceramic Coatings," Novel Techniques in Synthesis and Processing of Advanced Materials, eds. J. Singh and S.M. Copley, TMS, pp. 79-89, 1995. Proceedings of a Symposium held at Materials Week '94 in Rosemont, IL, Oct. 2-6, 1994.

2. W.B. Carter and S. Godfrey, "Combustion Chemical Vapor Deposited Partially Stabilized Zirconia Coatings," Elevated Temperature Coatings: Science and Technology I, eds. N.B. Dahorte, J.M. Hampikian, and J.J. Stiglich, TMS, 103-111, 1995. Proceedings of a Symposium held at the TMS Fall Meeting, Rosemont, IL, Oct, 2-6, 1994.

3. W.B. Carter, J.M. Hampikian, S.H. Godfrey, and T.A. Polley, "Thermal Aging of Combustion Chemical Vapor Deposited Coatings," Proceedings of the Symposium on Coatings and Substrate Integrity of High Temperature Materials, sponsored by TMS-MSD Flow and Fracture Committee and SMD High Temperature Alloys Committee, TMS Annual Meeting, Las Vegas, NV, Feb. 12-16, 1995.

PRESENTATIONS

1. W.B. Carter, G.W. Book, and A.T. Hunt, "Combustion Chemical Vapor Deposition of Ceramic Coatings," International Symposium on Novel Techniques in Synthesis and Processing of Advanced Materials, sponsored by ASM-MSD Structures Committee and TMS-EMPMD Electronic and Photonic Device Materials Committee, ASM Materials Week / TMS Fall Meeting, Rosemont, IL, Oct. 2-6, 1994. Invited.

2. W.B. Carter and S. Godfrey, "Combustion Chemical Vapor Deposited Partially Stabilized Zirconia Coatings," Symposium on High Temperature Coatings I, sponsored by TMS-MDMD Surface Modification and Coatings Committee, ASM Materials Week / TMS Fall Meeting, Rosemont, IL, Oct, 2-6, 1994.

3. W.B. Carter, J.M. Hampikian, S.H. Godfrey, and T.A. Polley, "Thermal Aging of Combustion Chemical Vapor Deposited Coatings," Symposium on Coatings and Substrate Integrity of High Temperature Materials, sponsored by TMS-MSD Flow and Fracture Committee and SMD High Temperature Alloys Committee, TMS Annual Meeting, Las Vegas, NV, Feb. 12-16, 1995.

HONORS AND AWARDS

None

PATENTS/DISCLOSURES

None

LICENSES

None

INDUSTRIAL INPUT AND TECHNOLOGY TRANSFER

A collaboration with Dow Corning on the coating of ceramic fibers with weakly bonding material for incorporation into continuous fiber ceramic composites (CFCCs) was initiated. Andy Szweda is the technical contact at Dow Corning.

COST SHARING

None

ESTIMATED ENERGY SAVINGS

The combustion chemical vapor deposition process being developed promises to reduce energy consumption for certain coating applications currently being performed by conventional methods. The consumption of inexpensive organic solvents and gases should more than offset the elimination of furnace and vacuum hardware and their concomitant energy requirements. Often, less expensive reagents can be used with combustion CVD than are required for conventional CVD processes. The substantially smaller capital investment anticipated for the combustion CVD process relative to conventional techniques will also entail less energy expenditure up front in equipment production. As the process is presently in the early stages of development and those applications to which it may ultimately be applied are uncertain, it is not possible to produce a quantitative estimate of potential energy savings.

HIGHLIGHTS

OSCILLATING CAPILLARY NEBULIZER YIELDS HIGHER QUALITY COATINGS - The Oscillating Capillary Nebulizer (OCN) has shown the ability to produce flames in which combustion CVD can be performed at lower flame temperatures, and yet yield coatings with superior properties.

AEROGEL NANOCOMPOSITE MATERIALS

A. J. Hunt, M. Ayers, P. Stevens, and S.Q. Zeng

Energy and Environment Division
Lawrence Berkeley Laboratory
Berkeley, CA 94720

INTRODUCTION

Aerogels materials are porous, low density, nanostructured solids with many unusual properties including very low thermal conductivity, good transparency, high surface area, catalytic activity, and low sound velocity. This research is directed toward developing new nanocomposite aerogel materials for a number of applications. An important focus of the work has been to further increase the thermal resistance of silica aerogel by producing a composite material containing infrared opacification agents. The resulting aerogel composites enable a number of new industrial applications for aerogel-based thermal insulation. Three primary benefits accrue from the development of composite aerogel insulation; extending the range of applications to higher temperatures, providing a more compact insulation for space sensitive-applications, and lowering the cost of the aerogel by as much as 30%. Superinsulating aerogel can replace existing CFC-containing polyurethane insulation in low temperature applications to reduce heat losses in hot and cold piping, significantly improve the thermal efficiency of refrigeration systems, and reduce energy losses in a variety of industrial applications. Enhanced aerogel insulation can also replace steam and process pipe insulation in higher temperature applications to substantially reduce energy losses and provide much more compact insulation. The aerogel insulation research has been extended to the much wider area of nanostructured aerogel composites. A number of new composite materials were prepared with unusual properties. These properties arise from their very fine dimensions can produce enhanced or unusual behavior such as superplasticity in metal matrix composites and quantum size effects. These materials may be useful for light weight metals, magnetic cooling cycles, or electroluminescent displays, and optical devices.

TECHNICAL PROGRESS FY 1995

Summary

Development and Testing of Enhanced Aerogel Insulation

Thermally enhanced aerogel insulation based on silica/carbon composites was produced and evaluated for insulating applications. Infrared radiation is responsible for a substantial portion of the thermal conductivity in aerogel at ambient and higher temperatures. Reducing the radiant transfer substantially improves the thermal performance of aerogel insulation. At higher temperatures (200° to 500°C), the radiative component of heat transfer in aerogel becomes dominant and must be suppressed. This radiation is blocked by adding material with a high absorption coefficient in the infrared. Theoretical and experimental research established that carbon was found to be the one of the best additives for applications not requiring visual transparency.

We have developed a new method to add carbon to silica aerogel that has many advantages over the particle addition methods. Chemical vapor infiltration (CVI) is used to produce nanocomposite aerogel. A silica or other composition aerogel is infiltrated with a gas that is catalytically decomposed by the aerogel. The decomposition product is left inside the aerogel as a solid deposit at a nanometer scale. Using the CVI method increases the strength of the aerogel composite and allows for much higher doping levels of carbon. Infrared transmission and nitrogen adsorption surface area and pore distribution measurements as well as high resolution transmission electron microscopy (HREM) were used to characterize the composites. Patent applications covering the CVI-aerogel nanocomposite production process were filed in FY 1994.

An precision instrument to measure the thermal conductivity of aerogel as a function of pressure and temperature was built and tested. The instrument is a Vacuum Insulation Conductivity Tester (VICTOR) that utilizes a thin film heater and is

equipped with a vacuum chamber for variable pressure capabilities. Thermal resistance measurements with VICTOR showed an increase of more than 50% in thermal resistance at temperatures from 20 C to 100° Opacified aerogel will be an outstanding insulating material for temperatures up to 500° C.

The thermal behavior of aerogel is very complex due to the presence of and the interaction three different modes of heat transfer. Heat transfer calculations accounting for the interaction between radiation, conduction, and gas conductivity inside aerogel were carried out to predict opacified aerogel's thermal conductivity as a function of temperature, and gas pressure. The calculations predict dramatic effects of carbon doping on the thermal performance of aerogel at temperatures from 200° to 500° C.

New composite silica aerogels containing iron, iron oxide, iron/carbon, and silicon were prepared and tested. The photoluminescent response of silicon/silica composites was characterized. The magnetic and optical properties of the iron- and iron oxide-silica aerogels were characterized. Transmission electron microscopy was used extensively to characterize the nanostructure and crystallinity of the new composites.

Milestones

We have carried out measurements on a new family of unusual nanoporous composite materials based on CVI-aerogel using VICTOR the Vacuum Insulation Conductivity tester. Measurements confirmed the improved thermal conductivity and improved strength of the opacified aerogel.

Develop New composite Materials

Silicon-silica and silicon rich composites exhibit photoluminescence that our measurements confirm is due to quantum well confinement effects. These materials were used to develop a new oxygen and pressure sensor based on photoluminescence quenching

by the oxygen. An instrument sensitive to oxygen content from less than one millibar to ambient was built and tested.

PUBLICATIONS

Journals

A.J. Hunt, M.R. Ayers, and W.Q. Cao, "Aerogel Composites using Chemical Vapor Infiltration," J. of Non-Crystalline Solids, 185, 227-232, 1995.

X.Y. Song, W.Q. Cao, M.R. Ayers, and A.J. Hunt, "Carbon Nanostructures in Silica Aerogel composites," J. Materials Research *10* 251-254, 1995.

A.J. Hunt and W.Q. Cao, ''New Routes to Nanocomposite Materials Using Aerogels," Better Ceramics Through Chemistry VI, A. K. Cheetham, C.J. Brinker, M.L. Mecartney, and C. Sanchez Eds., Materials Research Society, Pittsburg, *346* 451-455, 1994.

D. Lee, P.C. Stevens, S.Q. Zeng and A.J. Hunt "Thermal Characterization of Carbon Opacified Silica Aerogels," J. Non-Crystalline Solids, 186, 285-290, 1995.

J.E. Ludman, J.J. Ludman, H. Callahan, J. Caulfield, D. Watt, J. Sampson, J. Robinson, S. Davis, and A.J. Hunt, "Interferometeric Atmospheric Refractive-Index Environmental Monitor," Applied Optics *34* 3267-3273, 1995.

S.Q. Zeng, A.J. Hunt, R. Greif, and W.Q. Cao, "Approximate Formulation for Coupled Conduction and Radiation Through a Medium with arbitrary Optical thickness," J. of Heat Transfer, 117, 797-799, 1995.

S.Q. Zeng, A.J. Hunt, R. Greif, and W.Q. Cao, "Mean Free Path and Apparent Thermal Conductivity of a Gas in a Porous Medium," J. of Heat Transfer, 117, 758-761, 1995.

S.Q. Zeng, A.J. Hunt, and R. Greif, "Transport Properties of Gas in Silica Aerogel," in press, Journal of Non-Crystalline Solids 1995.

S.Q. Zeng, A.J. Hunt, and R. Greif, "Theoretical Modeling of Carbon Content to Minimize the Heat Transfer in Silica Aerogel," Journal of Non-Crystalline Solids, 186, 271-277, 1995.

S.Q. Zeng, and A.J. Hunt, "Mean Free Path and Apparent Thermal Conductivity of Gas in Aerogel," Accepted for publication in J. of Heat Transfer, 1995

PATENTS/DISCLOSURES

"Aerogel Composites and Method of Manufacture," Wanqing Cao and Arlon Hunt, patent pending.

LICENSES

A license was given to Aerojet Corporation CRADA for the infrared opacification process to improve the thermal properties of aerogel. for the commercialization of aerogel

INDUSTRIAL INPUT AND TECHNOLOGY TRANSFER

A CRADA was completed in FY 1996 with Aerojet Corporation to commercialize the production of silica aerogel using the carbon dioxide substitution process developed at LBL. The CRADA has several industrial partners to evaluate potential applications; included are General Motors, Cadillac Division, and Boeing, Maytag, Benteler, and Glacier Bay Corporations.

COST SHARING

None

HIGHLIGHTS

We are developing a new oxygen sensor

We designed built and tested a new oxygen sensor based on the photoluminescence properties of microwave treated silica aerogel

Characterization of Three-Way Automotive Catalysts

E.A. Kenik, K.L. More
Oak Ridge National Laboratory
Metals ad Ceramics Division
Oak Ridge, TN 37831-6376

W. LaBarge, R.F. Beckmeyer, J.R. Theis
Delphi Automotive Systems
Flint, MI 48556

INTRODUCTION

This has been the third year of a CRADA between Delphi Automotive Systems (DAS; formerly General Motors - AC Delco Systems) and Martin Marietta Energy Systems (MMES) aimed at improved performance/lifetime of platinum-rhodium based three-way-catalysts (TWC) for automotive emission control systems. While current formulations meet existing emission standards, higher than optimum Pt-Rh loadings are often required. In addition, more stringent emission standards have been imposed for the near future, demanding improved performance and service life from these catalysts. Understanding the changes of TWC conversion efficiency with ageing is a critical need in improving these catalysts. Fresh specimens of different TWC formulations can have very different catalytic performance even for similar levels of noble metal (Pt, Rh) loading and relative ranking can change with even mild ageing. The efficiency, selectivity, and robustness of a catalyst system reflects the state of the chemically active material; including morphology, structure, elemental and chemical form. The ageing behavior and lifetime of the catalyst are determined by the evolving state of the catalyst, which in turn is a function of the chemical environment (both reactants and poisons) and exposure time and temperature. In addition, changes in the formulation and processing of the catalytic/support materials can impact the performance and lifetime of the convertor. Reactivation of a catalyst requires at least partial reversal of the microstructural evolution responsible for the degradation in catalytic performance. Initially in a fresh catalyst, the active material is often distributed on a very fine scale, approaching single atoms or small atomic clusters.

As such, a wide range of analytical techniques have been employed to provide high spatial resolution characterization of the evolving state of the catalytic material.

TECHNICAL PROGRESS

Summary

Technical progress meetings between DAS and MMES were held in Flint, MI on April 10, 1995 and in Oak Ridge on December 12, 1994 and September 6, 1995 to report current results on characterization of as-prepared, thermally aged, and dynamometer- and vehicle- aged catalyst monoliths received at ORNL during the latter half of FY 1994 and FY 1995. The results reported included fresh and dynamometer-aged convertors from both a ceria level variation study and a process variation study. Characterization emphasized the application of scanning electron microscopy (SEM), electron probe microanalysis (EPMA), analytical electron microscopy (AEM), and X-ray diffraction.

Milestones

1. Ceria Variation Study

This study was concerned with the microstructural characterization of a series of convertors with different levels of ceria in the washcoat that had been dynamometer-aged to exposures equivalent to ~300,000 miles. DAS had extensive data on the relative performance of these convertors for comparison with the observed microstructural evolution of both the washcoat and the heavy metal clusters (HMC). Figure 1 shows the microstructure of the aged 20 and 40% ceria washcoats. Significant sintering of the ceria and the $\gamma \rightarrow \alpha$ transformation and growth of the alumina component of the washcoat occurred. Both the sintered ceria and the α-alumina exhibited low dislocation density. During grain growth the large (0.5-2 μm) α-alumina grains generally engulfed adjacent ceria and HMCs, resulting in loss of oxygen storage capacity and catalyst surface area. More α-alumina was observed in the aged 40% ceria washcoat (Figure 1), which was confirmed with

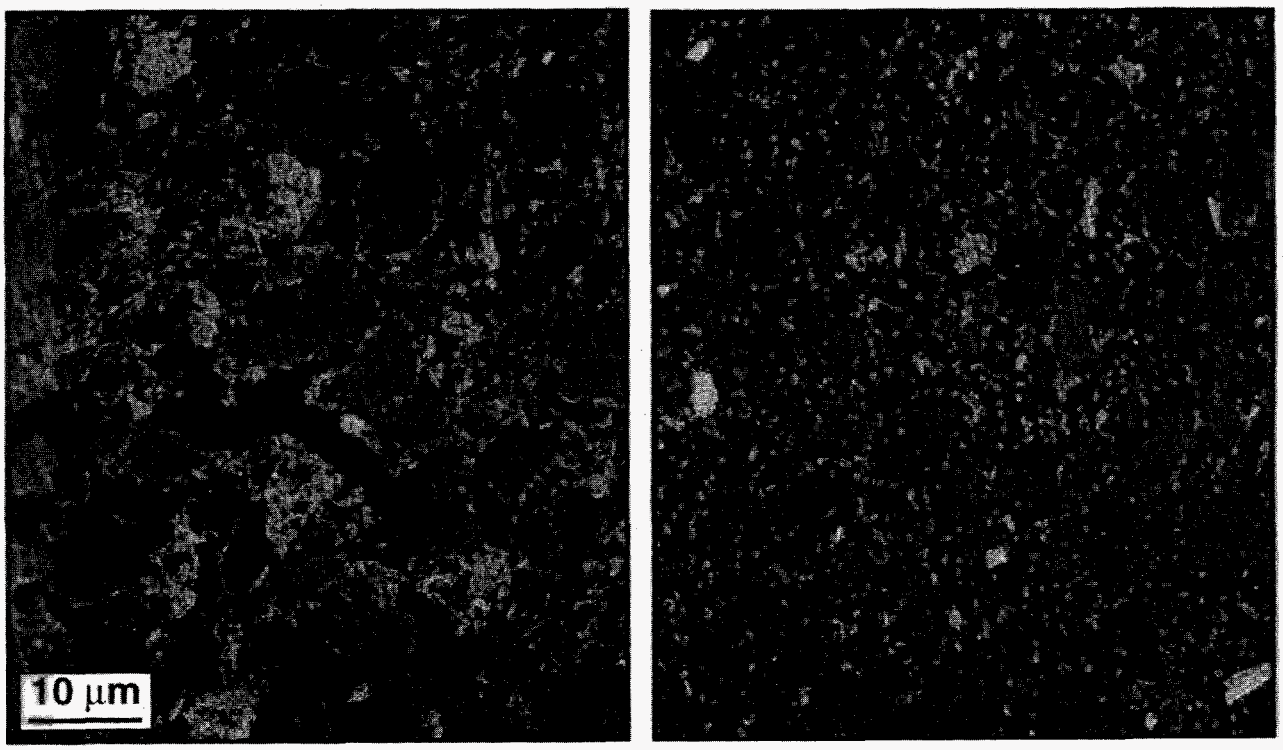

Figure 1: The microstructure of the dynamometer-aged 20 and 40% ceria washcoats. Note the significant sintering, $\gamma \rightarrow \alpha$ alumina transformation, and the larger amount of α-alumina present in the 40% ceria washcoat.

quantitative X-ray diffraction of scraped washcoat powders.

Both AEM and SEM indicated that formation of α-alumina appeared to be associated with the presence of ceria particles; no α-alumina formed in the center of alumina aggregates where no ceria was present. High levels of phosphorus (up to 12 wt%) were observed via both AEM and SEM in association with some, but not all, ceria particles. These ceria particles were present at the free surface of the washcoat exposed to the exhaust gas stream and the source of the phosphorus was presumed to be zinc dialkyl phosphate (ZDP), an oil additive. This phosphorus poisoning of the ceria

particles could result in reduced catalytic and oxygen storage activity of the washcoat.

The Pt/Rh ratio of the HMCs in both the 20% and 40% ceria aged washcoats was an increasing function of the cluster diameter (Figure 2). The Pt/Rh for HMCs in the 40% ceria washcoat exhibits a weaker size dependence than the 20% ceria material. For the smaller HMCs (<15 nm) in the 20% ceria washcoat, the average Pt/Rh was ~4; whereas for the larger HMCs (>15 nm) the Pt/Rh was ~8. The corresponding Pt/Rh values for the 40% ceria material were ~8 (<15 nm) and ~15 (>15 nm). In general, there was a strong association of the smaller HMCs with

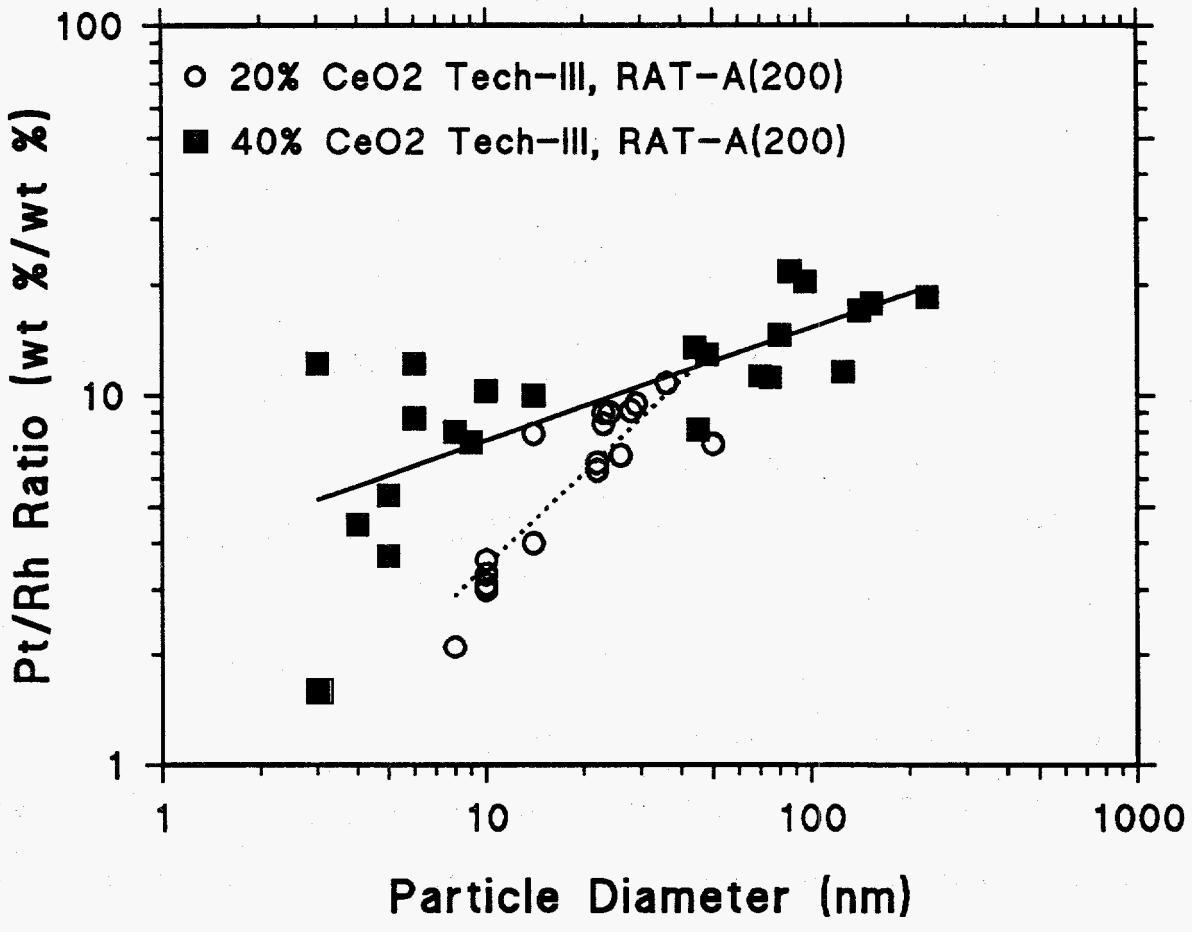

Figure 2: Pt/Rh ratio of the heavy metal clusters in the 20% and 40% ceria dynamometer-aged washcoats as a function of cluster diameter. Note the weaker dependence on cluster size for the 40% ceria material.

one phase of the washcoat; whereas the larger HMCs exhibited less preferential association. High resolution SEM indicated that smaller, rhodium-enriched HMCs were present on the surface of the washcoat oxide particles. X-ray diffraction indicated that the average HMC in the aged 40% ceria material contained slightly more rhodium than that in the 20% ceria material.

A high degree of scatter is often observed in the Pt/Rh versus HMC size data. At least a portion of this variation can be attributed to the inhomogeneous distribution of platinum versus rhodium. It was observed that the Pt/Rh values for HMCs from one area exhibit a similar slope as a function of size relative to overall data set, but at a lower or higher Pt/Rh level. Slight differences in the relative amounts of platinum versus rhodium deposited locally would result in such different Pt/Rh values. Such variations also have been observed in the CRADA both for other dynamometer- and vehicle-aged monoliths.

The inlet and outlet microstructures of the aged 20% and 40% ceria monoliths were compared. The washcoat structures were qualitatively similar with both sintering and $\gamma \rightarrow \alpha$ alumina transformation and growth apparent in all four materials. Quantitative X-ray diffraction measurements of the relative amount of $\gamma \rightarrow \alpha$ transformation for these materials are underway. Average Pt/Rh and size of HMCs in these specimens have been measured by AEM and will be compared with "average" Pt/Rh values based on lattice parameters from X-ray diffraction.

2. Process Variation Study

The revised program for this CRADA included parallel microstructural characterization and dynamometer-testing of a series of monoliths prepared under different process variations, including the chemistry and pH of the loading solution and the drying/calcining procedures. Both as-prepared and dynamometer-aged monoliths were prepared at DAS and the associated microstructures were characterized. Several processing parameters were identified which permitted significant differences in precious metal loading and uniformity of distribution. It was found that certain processing conditions resulted in excess or preferential adsorption of one of the heavy metals. Two step loading

sequences were studied in order to provide flexibility in distributing the heavy metals. However, it was found that the precise drying/calcination sequence influenced the heavy metal loading. Further dynamometer-ageing of specific process variation monoliths is underway to determine if such variations and associated precious metal distributions result in improved catalytic performance and/or lifetime.

3. Vehicle-Aged Monolith

In order to compare and benchmark microstructural evolution observed in the washcoat and HMCs for various dynamometer-ageing schedules, the vehicle-aged microstructure of the same catalyst formulation was characterized for a monolith that had been field tested for 110,000 km. There were many similarities in the microstructures observed in several dynamometer-aged washcoats with those observed in various locations of the vehicle-aged monolith. Sintering and the $\gamma \rightarrow \alpha$ transformation were observed for both inlet and outlet washcoat samples; however, there was a difference of degree. The inlet washcoat was heavily sintered with little porosity and exhibited only α-alumina, whereas the outlet exhibited less severe sintering and was a mixture of fine-grained γ and coarse α aluminas. The inlet structure was similar to that of dynamometer-aged washcoats that had been exposed to severely over-temperature conditions; whereas the outlet structure was similar to that of washcoats dynamometer-aged to simulate 50,000-100,000 miles exposure.

Both AEM and microprobe (EPMA) indicated the presence of poisons on the surface of the washcoat, which included calcium, phosphorus, and oxygen with smaller amounts of iron, zinc, aluminum, and, in at least one case, lead. The calcium, phosphorus, and zinc could all arise from the oil or oil additives. Discontinuous particles of this calcium phosphate glaze (~0.5 μm diameter) were observed on the inlet washcoat surface; whereas continuous surface enrichment of calcium and phosphorus was observed for both ends. The discontinuous glaze was present in sufficient amounts in the inlet washcoat to be identified by X-ray diffraction. In addition, the presence of PtO in the inlet washcoat also was indicated by X-ray diffraction.

4. Future Directions

The program plan for future CRADA research was reviewed at the April 10, 1995 review meeting and currently includes completion of the microstructural characterization and dynamometer-testing under the process variation study and characterization of monoliths from the ceria level variation, the vehicle-ageing, and the stabilized washcoat studies. The exact level of effort on each of these projects depends on the availability of funds. Several factors have delayed progress on this CRADA, including the unavailability of the DAS engine dynamometer facility and stabilized washcoat specimens and delays in the preparation and dynamometer-ageing of monoliths. However, Delphi has indicated their satisfaction with the productivity of the CRADA and their desire to extend the period of the CRADA. A no-cost extension of the CRADA to the end of FY 96 was jointly requested by both Delphi and MMES and approved by DOE.

PUBLICATIONS

Three CRADA related publications have been submitted at this time.

1. K.L. More, D.W. Coffey, and T.S. Geer, *Microbeam Analysis - 1995* (Proc. 29th Ann. Conf. of Microbeam Analysis Soc., ed. E.S. Etz, VCH Publishers, New York, pp. 137-138 (1995).

2. E.A. Kenik, K.L. More, W. LaBarge, and R. Beckmeyer, *Proc. Microscopy and Microanalysis 1995* (Proc. 53rd Ann. Mtg. Microscopy Soc. of Amer., eds. G.W. Bailey et al., Jones and Begell Publishing, New York, pp. 430-431 (1995).

3. K.L. More, D.W. Coffey, and T.S. Geer, *Proc. Microscopy and Microanalysis 1995* (Proc. 53rd Ann. Mtg. Microscopy Soc. of Amer., eds. G.W. Bailey et al., Jones and Begell Publishing, New York, pp. 412-413 (1995).

PRESENTATIONS

Eleven presentations have been made at periodic progress report meetings between Delphi and MMES personnel working on this CRADA. Posters have been presented at the last two AIM annual information and review meetings. A presentation of goals and results from this CRADA was

made by Delphi personnel at the PNGV CRADA review meeting held on March 6-9, 1995. Two presentations on the preparation techniques developed for TEM specimens from catalytic convertor monoliths have been made this year (regional American Vacuum Society meeting and annual Catalysis Society meeting). Two presentations (one invited) were presented on CRADA related material during the last quarter of FY 1995 (Microbeam Analysis Society and Microscopy Society of America meetings).

HONORS AND AWARDS

None for CRADA at this time.

PATENT/DISCLOSURES

A record of invention has been prepared by Delphi Automotive Systems for a joint patent application on the Delphi process for preparing catalyst monoliths, which should be filed before the end of CY1995. The application utilizes microstructural characterization from the CRADA to support the record of invention.

LICENSES

None for CRADA at this time.

INDUSTRIAL INPUT AND TECHNOLOGY TRANSFER

Joint work proceeding under CRADA titled "Improved Catalyst Materials and Emission Control Systems" between Delphi Automotive Systems (formerly General Motors Corporation, AC Delco Systems) and Martin Marietta Energy Systems.

HIGHLIGHTS

1. No-cost extension until end of FY 96 approved for CRADA between Delphi Automotive Systems and Martin Marietta Energy Systems on "Improved Catalyst Materials and Emission Control Systems", CRADA No. ORNL92-0115.

2. Microstructural characterization of as-produced catalyst materials from process variation study completed and presented to Delphi at quarterly progress meetings before the end of the first quarter of FY 1995. Dynamometer ageing of process variation monoliths to provide comparison of conversion efficiencies. Microstructural characterization of initial dynamometer-aged process variation monoliths presented mid FY 1995.

3. Microstructural characterization of 20% and 40% ceria catalysts after extended dynamometer-ageing completed and presented to Delphi before the end of the first quarter of FY 1995. Additional characterization of 30% and 60% ceria catalysts aged as a function of time in order to understand the microstructural evolution of washcoat during ageing of catalysts.

4. Initial microstructural characterization of vehicle-aged catalyst completed and presented to Delphi before the end FY 1995. Similarity and differences in microstructural evolution relative to dynamometer-aged catalysts noted; including sintering of washcoat and $\gamma \rightarrow \alpha$ alumina transformation/growth, differences between inlet and outlet washcoat structures, and presence of both a discontinuous calcium phosphate glaze at inlet and surface enrichment of calcium and phosphorus at both ends of monolith.

CHEMICAL VAPOR INFILTRATION OF TiB_2 COMPOSITES

T. M. Besmann

Metals and Ceramics Division
Oak Ridge National Laboratory
P.O. Box 2008, MS 6063
Oak Ridge, TN 37831-6063

INTRODUCTION

This program is designed to develop a Hall-Heroult aluminum smelting cathode with substantially improved properties. The carbon cathodes in current use require significant anode-to-cathode spacing in order to prevent shorting, causing significant electrical inefficiencies. This is due to the non-wettability of carbon by aluminum which causes instability in the cathodic aluminum pad. It is suggested that a fiber reinforced-TiB_2 matrix composite would have the requisite wettability, strength, strain-to-failure, cost, and lifetime to solve this problem. The approach selected to fabricate such a cathode material is chemical vapor infiltration (CVI). This process produces high purity matrix TiB_2 without damaging the relatively fragile fibers. The program is designed to evaluate potential fiber reinforcements, fabricate test specimens, and scale the process to provide demonstration components.

TECHNICAL PROGRESS - FY 1995

Summary

Efforts this period were devoted to the scale-up of the CVI process for preparing TiB_2 matrix composites in the anticipation of testing within a DOE/Alcoa program on wettable cathodes for the Hall-cell production of aluminum.

Previous efforts in the development of TiB_2 composites were confined to disk shapes having diametral dimensions of 4.5 cm. In order to provide specimens for test at the Alcoa

Technical Center in their inert prototype cathode program it was necessary to develop larger components of the order of several hundred square centimeters. The object of the current phase of the work has therefore been to develop such a scale-up component.

A forced chemical vapor infiltration (FCVI) system capable of preparing disk-shaped composites was designed, constructed and successfully operated as part of an Air Force Wright Laboratory program in 1992. This unit was made available to the AIM project to produce TiB_2 composites for the AIM project. The effort to scale-up the process for fabrication of TiB_2 composites has involved the development of a new precursor feed system for the large FCVI unit, development of a fixturing system for the component, modification of the system exhaust, and the development of processing protocols to uniformly densify the composite.

A new precursor feed system was required because the existing feed system on the large FCVI unit is designed exclusively for a SiC precursor. The feed system for $TiCl_4$ used in the smaller-scale FCVI unit required the evaporation of the reagent into the hydrogen stream via a heated bubbler. For the substantially larger flows required of the scale-up process this was not possible. As a result, a new feed system utilizing a peristaltic pump for metering liquid into an evaporator was designed. Monitoring of the feed rate was afforded by a balance which continually weighted the $TiCl_4$ reservoir. The system was constructed and operated as designed.

Fixturing to prepare a 20x20 cm plate 0.5-1 cm in thickness was designed. Several experimental and design iterations were necessary to produce components of the required dimensions due to leakage problems with the initial design, to accommodate unexpected shrinkage in the Thornel P-25 carbon fiber fabric, and to sufficiently uniformly distribute the precursor vapor over the entrance surface of the preform. As a result, gas entrance ports at the periphery of the holder needed to be blocked to prevent the precursor stream from flowing around the part

due to preform shrinkage. In addition, channels were machined connecting the remaining gas entrance ports to allow the precursor stream to directly contact much larger and uniform areas of the preform entrance surface.

The FCVI exhaust had previously flowed through an oil trap and a second safety trap. For the $TiCl_4$ and BCl_3 precursors utilized in TiB_2 deposition this was problematic. The chlorides react on contact with air to form solid products which clogged the lines. The exhaust system needed to be replumbed to avoid clogging, and a scrubber needed to be recommissioned to process the effluent.

Several samples were prepared under differing conditions to obtain appropriately densified material. This empirical approach, coupled with first-state modeling utilizing the FCVI model developed with Georgia Institute of Technology (GTCVI), allowed development of appropriate processing parameters. This resulted in preparation of a final sample plate having adequate uniformity and density.

The product composite provided in early August 1995 to Alcoa Technical Center for evaluation measured 19x19 cm by 0.95 cm in thickness. The density of the plate was 87-90% of theoretical, with 40 v% fibers loading.

MILESTONES:

1. Demonstrate scale-up of TiB_2 matrix composites to 8-in^2 plates, supply specimens to Alcoa for Hall-cell evaluation, and prepare letter report (August 1995)

PUBLICATIONS

1. Letter report on scale-up of TiB_2 matrix composites fabrication.

PRESENTATIONS:

1. "Chemical Vapor Infiltration of Fibrous TiB_2 Composites," T. M. Besmann and J. C. McLaughlin, Advanced Industrial Materials Program Annual Meeting, Washington, DC, June 14-16, 1995.

HONORS AND AWARDS

None.

PATENTS/DISCLOSURES

None this period

LICENSES

Refractory Composites, Inc. has executed a non-exclusive license on the U. S. patent "Titanium Diboride Ceramic Fiber Composites for Hall-Heroult Cells," No. 4,929,328.

INDUSTRIAL INPUT AND TECHNOLOGY TRANSFER

The Alcoa Technical Center has performed bench-scale Hall cell at tests of small-scale specimens and has tested a sample prepared from a scale-up specimen.

COST SHARING

HIGHLIGHTS

Scale-up specimens of TiB_2 have been successfully prepared and provided to Alcoa Technical Center for evaluation. See figure on next page.

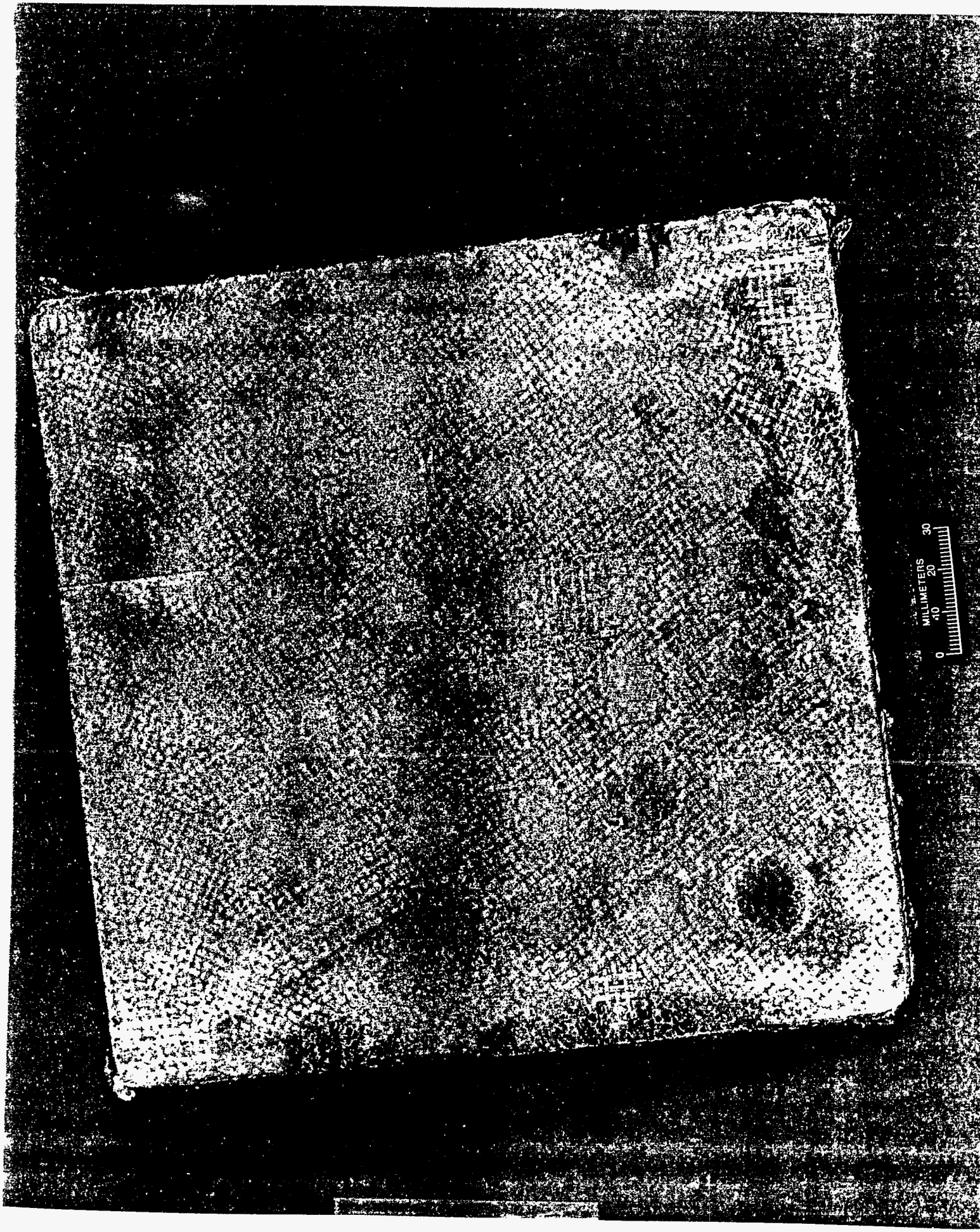
MILLIMETERS
0
10
20
30

CRACK RESISTANT COMPOSITES
METALLIC AND INTERMETALLIC-BONDED CERAMIC COMPOSITES

K. P. Plucknett, T. N. Tiegs, P. F. Becher, S. B. Waters, and P. A. Menchhofer
Metals and Ceramics Division, Oak Ridge National Laboratory
P. O. Box 2008, Oak Ridge, TN 37831-6068

INTRODUCTION

The purpose of this task is to establish a framework for the development and fabrication of metallic-phase-reinforced ceramic matrix composites with improved fracture toughness and fatigue resistance. The incorporation of metallic phases that plastically deform in the crack-tip region, and thus dissipate strain energy, will result in an increase in the fracture toughness of the composite as compared to the monolithic ceramic. It is intended that these reinforced ceramic matrix composites will be used over a temperature range from 20°C to 800-1200°C for advanced applications in the industrial sector. In order to systematically develop these composites, a combination of experimental and theoretical studies must be undertaken.

TECHNICAL PROGRESS

Summary

Pressureless-Sintering of Titanium Carbide Composites

Recent work has demonstrated the feasibility of sintering TiC/Ni_3Al cermets to high densities (>97% of theoretical). Initial investigation of this processing technique focused upon the use of standard 'ball milling' routes for mixing and milling of the relevant powders necessary for composite fabrication. It was immediately apparent that this approach was difficult to reproduce, and sintered densities typically varied between 80 and 95 % of theoretical, for samples prepared with 20 vol. % Ni_3Al binder. Also, the microstructure of many of the sintered samples was clearly inhomogeneous, with both 'binder rich' and 'binder

deficient' regions. Consequently a range of variations on the standard ball-milling route were investigated, together with attritor milling. This latter approach was the one that was found to give the most reproducible results, and this technique is now employed exclusively.

Powder mixtures are now prepared by attritor milling with tetragonal zirconia (TZP) media, 3 mm in diameter, for a total duration of 4 h (compared to typical ball-milling times of 24 h). After milling the powder mixtures are dried and sieved to -200 mesh (<75 μm), followed by uniaxial cold-pressing (at 10,000 psi) and then cold-isostatic-pressing (at 40,000 psi). Samples were sintered under vacuum at temperatures between 1475 and 1525°C for one or two hours. A typical sintering schedule is shown in Fig. 1. TiC/Ni_3Al samples have been prepared with Ni_3Al contents from 15 to 40 vol. %. The effects of Ni_3Al content upon the densities of cold-pressed compacts (green density) is shown in Fig. 2. As expected the green density increases slightly with decreasing TiC content, due to plastic deformation of the ductile metallic phase. The green densities observed are actually slightly lower than for similar composition samples prepared by ball milling, which may be indicative of a finer particle size and narrower size distribution in the attritor milled samples.

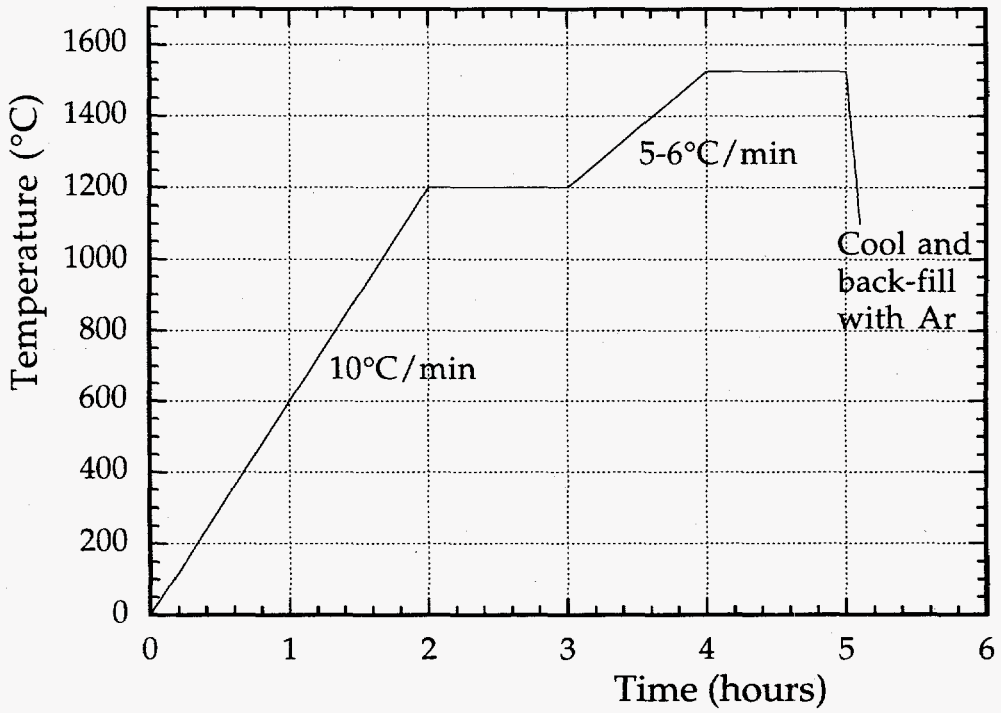

Figure 1. Typical vacuum-sintering cycle used for the densification of TiC/Ni_3Al cermets. Furnace is back-filled with argon during the initial part of the cooling cycle (at 25°C below the sintering temperature).

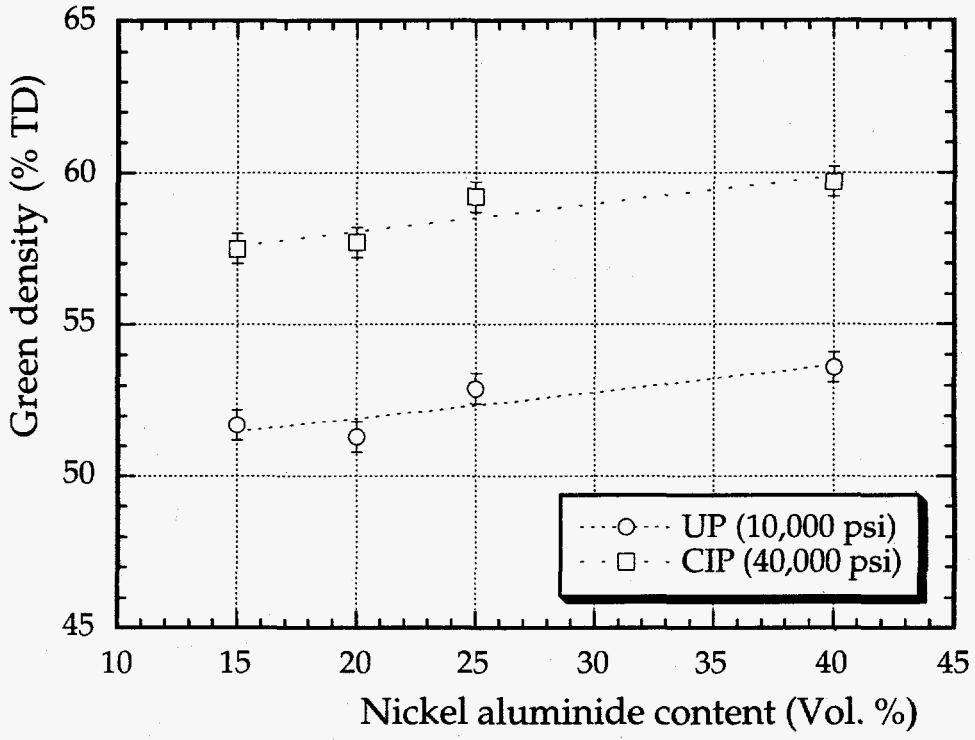

Figure 2. The effects of Ni_3Al content upon green density for uniaxially pressed (UP) and cold isostatically pressed (CIP) powder mixtures. Cold isostatically pressed samples were first uniaxially pressed at 10,000 psi.

The effects of sintering temperature upon density for samples prepared with various Ni_3Al contents is shown in Fig. 3. Sintered densities greater than 94 % of theoretical are observed for all combinations of sintering temperature and composition. Note that this assumes a TiC density of 4.93 $g.cm^{-3}$ and a Ni_3Al density of 7.43 $g.cm^{-3}$. Actual theoretical densities may change slightly due to compositional change during sintering. The sintered densities obtained compare favorably with the best densities observed for the initial 'ball-milled' material. Typical weight losses for these samples were between 0.75 and 1.0 wt. %, and were greatest for the intermediate compositions (20 and 25 vol. % Ni_3Al), although the reasons for this are not clear at present. This low level of weight loss is acceptable for processing of TiC based cermets, and is likely due to a combination of evaporated moisture and CO (or CO_2) evolution. The latter arises due to reaction between carbon in the TiC powder and any surface oxide present. The relatively short processing time (4 h for attritor milling) may result in this low weight loss relative to the 'ball-milled' materials prepared earlier (which exhibited weight losses of 1.5-2.0 wt. % for 20 vol. % Ni_3Al, compared to 1.0 wt. % for attritor milled mixtures of identical composition). As noted in the previous report, sintering of these materials can be performed at temperatures below 1600°C, typically the maximum for industrial viability.

(a)

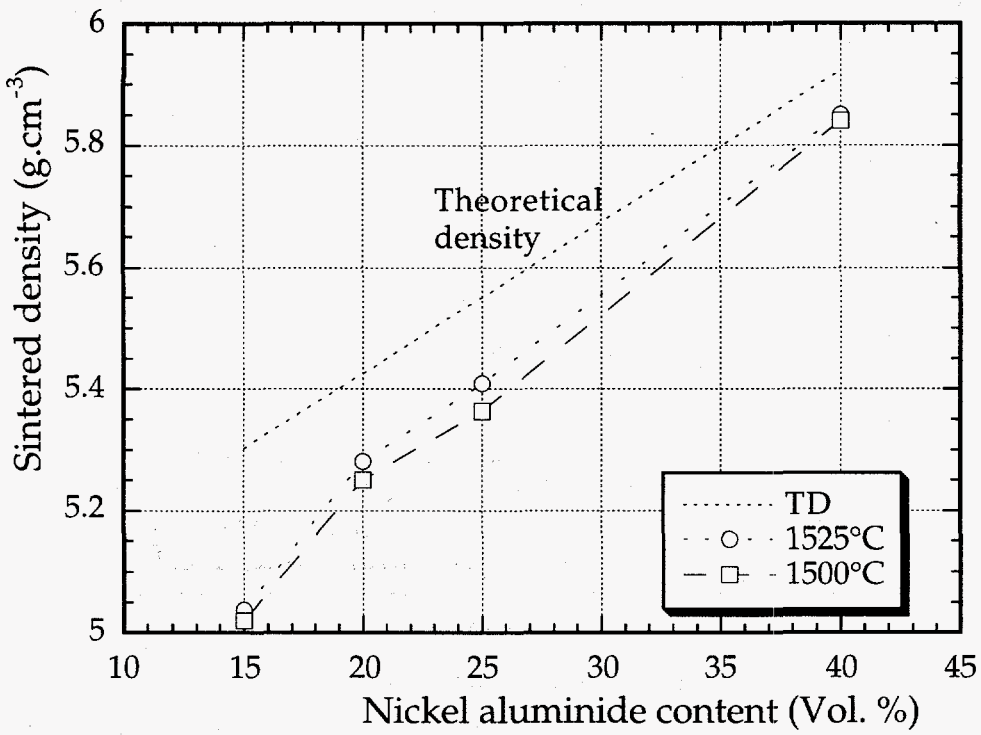

(b)

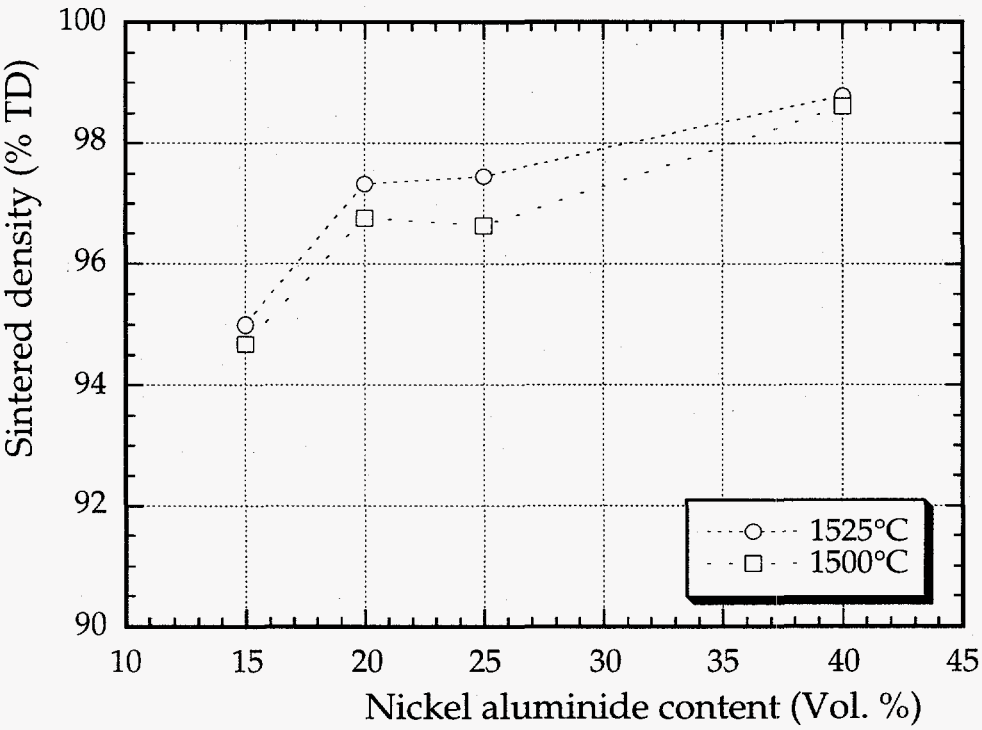

Figure 3. The effects of sintering temperature (held for 1 h) and composition on (a) bulk density and (b) percent of theoretical density for vacuum sintered TiC/Ni_3Al cermets.

It was noted that a combined sinter-HIP cycle might be used to obtain sintered densities close to theoretical. However, metallographic examination of these samples demonstrated regions of coarse, interconnecting porosity were formed during the pressurization segment of the sinter-HIP cycle. This was not initially detected due to rapid infiltration of the porosity by water during the density measurements. However, a number of these samples had already been sent out for test bar machining, and the mechanical performance of these materials will be described in a subsequent section of the present report. This de-wetting phenomenon was even noted when the initial sintered density, prior to gas pressurization, was greater than 99% of theoretical. The mechanism of de-wetting is not clear at present, however it seems that the gas/liquid (i.e. argon/ nickel aluminide) interfacial energy is similar to that of the solid/liquid interface (i.e. titanium carbide/nickel aluminide). This may arise due to the 'titanium rich' nature of the nickel aluminide binder, which will affect the wetting characteristics. This hypothesis is presently being assessed using simple wetting studies.

Due to the occurrence of this unusual de-sintering phenomenon continued emphasis has been placed on straight vacuum sintering. The effects of sintering duration (at 1500°C) upon sintered density, for compositions with 15 to 40 vol. % nickel aluminide, are shown in Figure 4. It is apparent that for the highest nickel aluminide contents significant densification (> 99 % of theoretical) is achieved in very short times (i.e. < 15 minutes). Conversely, samples with the lowest nickel aluminide content appear to reach a maximum density of ~95 % of theoretical after 60 minutes, with minimal change noted for extended sintering times. The apparent de-sintering of the 20 vol. % nickel aluminide sample after 120 minutes is believed to be an artifact, as this sample exhibited an unusually low weight change after sintering.

Mechanical Behavior of Titanium Carbide Composites

As noted in the previous section, an initial property survey has been performed upon a series of sinter-HIP processed samples. These materials contain regions of coarse porosity, which are likely to have a significant effect on the measured mechanical properties. However, it was felt that testing of these materials would give a property baseline for the assessment of future pressureless-sintered materials. Flexure strength has been obtained in four-point bending, with typically 20 plus tests for each composition. Fracture toughness has been determined using the applied moment double cantilever beam (AMDCB) geometry, with crack growth under loading monitored by optical microscopy. This latter approach allows determination of the materials 'R' curve. The materials that were tested had a 'pure' nickel aluminide binder phase, with no alloying additions.

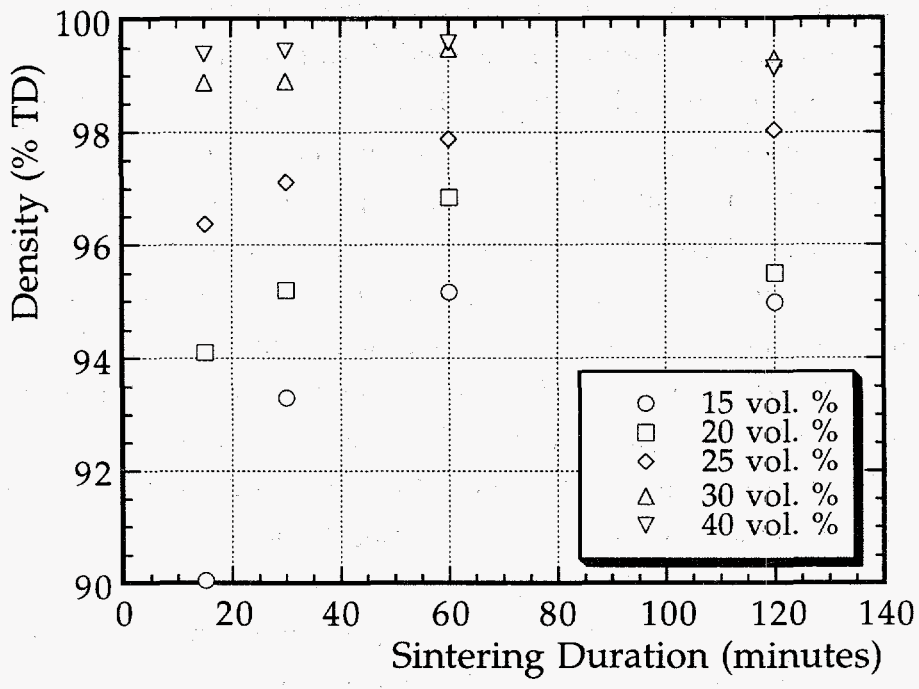

Figure 4. The effects of sintering duration upon sintered density for various nickel aluminide contents at 1500°C.

The strengths of the sinter-HIP samples are shown in Figure 5. It is clear that there is considerable scatter of the data, and that the low strength samples arise due to the presence of large porosity regions (as noted in the previous section). However, the higher recorded strengths indicate the promise of these compositions, with the 40 vol. % binder samples showing consistent values in the range 1.2 to 1.3 GPa. It is important to note that these values are significantly lower than those observed for tungsten carbide based materials (primarily due to the reduced modulus of titanium carbide), however they are consistent with recorded values for titanium carbide based cermets. A plot of the Weibull modulus for selected compositions is shown in Figure 6.

It is clear that high strengths can be achieved with the higher binder contents (1.2-1.3 GPa in 4 pt. flexure), in combination with a high Weibull modulus. Plateau fracture toughness values for cermets with 25 and 40 vol. % of 'pure' nickel aluminide binder were 9-10 and 11-12 $MPa.m^{1/2}$ respectively. These materials show a pronounced 'R' curve behavior (Fig. 7).

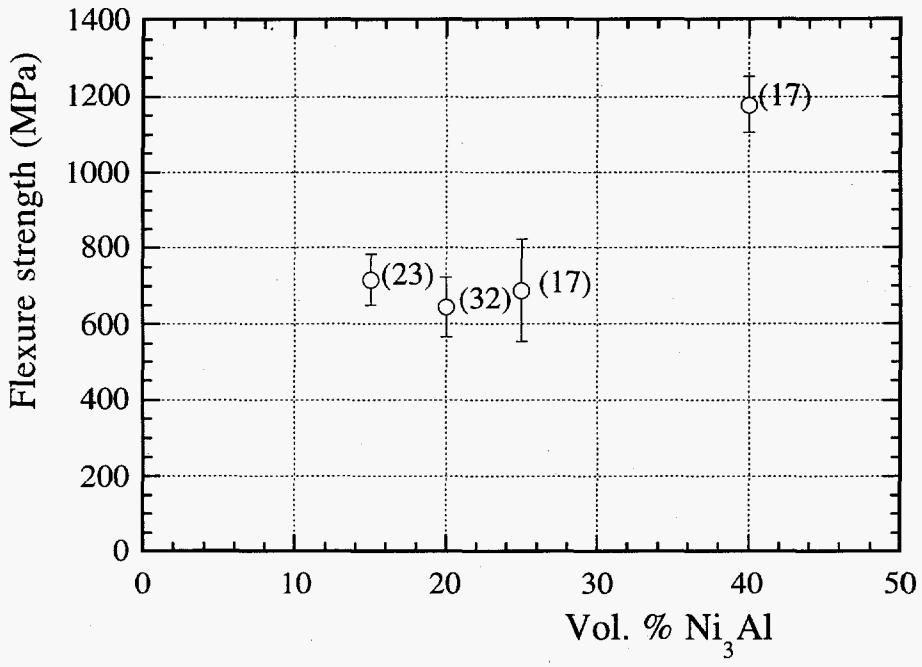

Figure 5. Flexure strength of titanium carbide/nickel aluminide cermets with various nickel aluminide contents. The number of tests performed for each of the compositions is shown in parenthesis.

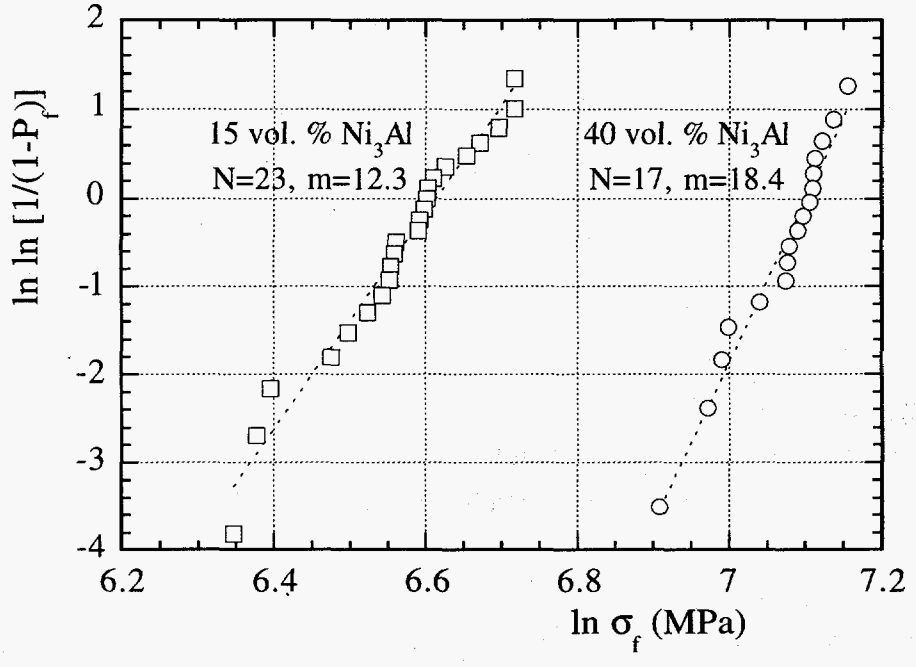

Figure 6. Weibull modulus plots for titanium carbide/nickel aluminide cermets with 15 and 40 vol. % binder phase.

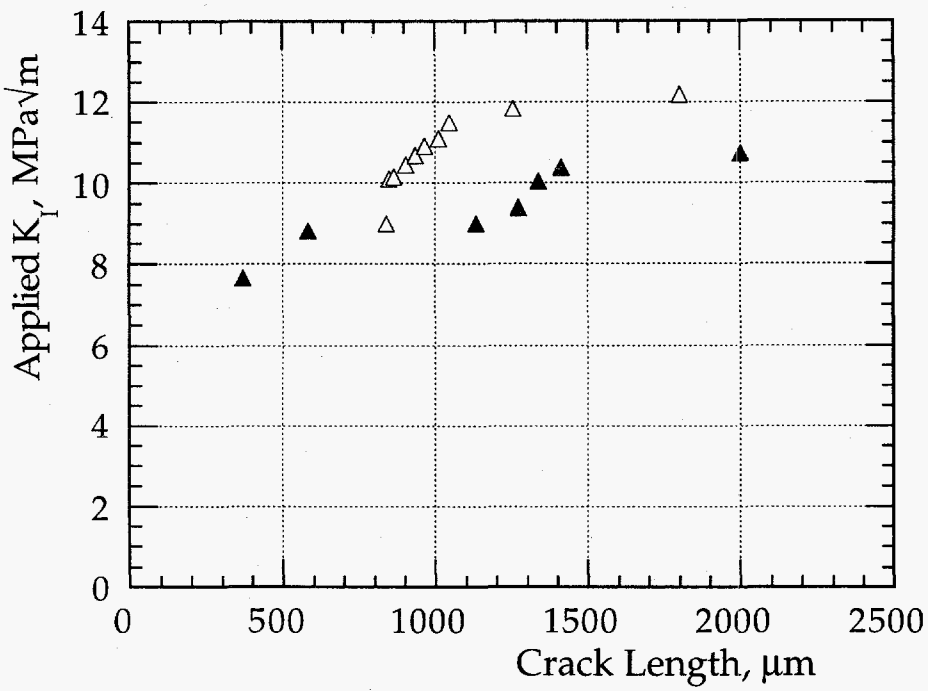

Figure 7. 'R' curves for titanium carbide/nickel aluminide cermets with 40 vol. % binder. The different symbols refer to two different AMDCB specimens.

Pressureless-Sintering of WC/Ni_3Al Cermets

Pressureless sintering and low gas pressure sintering are currently in progress. A series of samples of various composition were fabricated by conventional powder processing and cold pressed and iso-pressed into ~2.5 cm diameter discs. The specimens were then sintered at either 1550°C or 1600°C and 0.1 MPa gas pressure. The discs were then given a heat treatment at 1450°C and 1.7 MPa gas pressure to increase the densities. The compositions and sintered densities after each step are shown in Table I. As indicated, high densities were achieved for most of the samples. Poor densification was observed with the use of fine WC powder. This powder had an oxygen content about twice that of the standard powder normally used. The high oxygen content most likely indicates a substantial oxide coating on the particle surfaces and would result in the non-wetting of the particles by the Ni_3Al liquid.

Good densification was observed with the additions of Fe or W, however, lower densities were obtained by the addition of Ti to the binder phase. Poor sintering was also found when an addition of 5 wt. % TiC was made. These samples will be analyzed by x-ray to determine if any secondary phases are promoting or inhibiting the densification. As expected,

the sample with 30 vol. % binder phase achieved high density in all cases. All of the sintered samples will be tested for flexural strength , fracture toughness and hardness.

Table I. Summary of results on pressureless (vacuum) sintering behavior of various WC-Ni_3Al composites.

	Density after low pressure sintering (% T.D.)		Density after gas pressure treatment (% T.D.)	
Composition	1550°C	1600°C	1550°C	1600°C
WC-20 vol. % Ni_3Al	96.8	96.9	98.6	98.3
WC-20 vol. % Ni_3Al (5% Fe)	96.0	98.3	98.9	99.5
WC-20 vol. % Ni_3Al (5% W)	96.0	97.1	98.2	98.3
WC-20 vol. % Ni_3Al (5% Ti)	92.0	92.9	95.7	95.4
WC- 5 wt. % TiC-20 vol. % Ni_3Al	90.0	92.1	93.0	94.4
WC (Fine)-20 vol. % Ni_3Al	84.3	85.6	83.7	85.7
WC-30 vol. % Ni_3Al	98.4	97.9	98.7	98.1

Hot-Pressed Intermetallic-Bonded Carbide Matrix Composites

To examine the effects of processing on the densification and mechanical properties of WC-Ni_3Al and TiC-Ni_3Al composites a series of tests was performed. A Taguchi experimental array was formulated to assess the impact of variables, such as use of an annealing/grain growth step, powder-milling medium and powder-milling time on the composite properties (Tables II and III). Some mechanical properties from this array are also summarized in Tables II and III. The analysis of the results for this second array are currently in progress.

In addition to the work on developing pressureless-sintering routes, further investigation of the properties of hot-pressed Ni_3Al based cermets has been performed. The elevated temperature strengths of several hot-pressed carbide-nickel aluminide cermets are presented in Figure 8. Room temperature strengths are shown for comparison, together with similar data for a WC/Co cermet with comparable binder volume. The WC/Co material was a commercial grade product. It is apparent that the materials prepared with an Ni_3Al binder phase show significantly better high temperature strength retention than the equivalent WC/Co material. This observation is particularly important when considering the high temperatures that can be attained during machining (of the order of 1000°C).

Table II. Taguchi experimental design array for TiC-Ni_3Al composites for examination of hot-press temperature versus time at temperature, graphite die coating type, use of an annealing/ grain growth step, powder milling medium and powder milling time. The design is a L_9 (4^3).

Test	Temperature /Hold Time (°C / min)[a]	Powder Milling Medium	Milling Time (h)	Graphite Die Coating Type	Hardness (GPa)	Indent Toughness (MPa√m)[b]
1	A	Isopropanol	16	Al_2O_3	14.2	7.0
2	A	Hexane	4	BN	12.1	6.1
3	A	Argon	1	ZrO_2	9.8	5.5
4	B	Isopropanol	4	ZrO_2	16.0	6.2
5	B	Hexane	1	Al_2O_3	13.8	6.5
6	B	Argon	16	BN	13.4	7.4
7	C	Isopropanol	1	BN	14.4	6.0
8	C	Hexane	16	ZrO_2	14.3	6.7
9	C	Argon	4	Al_2O_3	14.0	7.8

[a] Conditions to be selected based on results from the initial Taguchi experimental design array.
[b] G. R. Anstis *et al*, *J. Am. Ceram. Soc.*, **64** [9] 533-38 (1981).

Table III. Taguchi experimental design array for WC-Ni_3Al composites for examination of hot-press temperature versus time at temperature, graphite die coating type, use of an annealing/ grain growth step, powder-milling medium and powder milling time. The design is a L_9 (4^3).

Test	Temperature/ Hold Time (°C / min)[a]	Powder Milling Medium	Milling Time (h)	Graphite Die Coating Type	Hardness (GPa)	Indent Toughness (MPa√m)[b]
1	A	Isopropanol	16	Al_2O_3	13.7	11.3
2	A	Hexane	4	BN	13.3	16.0
3	A	Argon	1	ZrO_2	13.9	9.5
4	B	Isopropanol	4	ZrO_2	13.8	10.4
5	B	Hexane	1	Al_2O_3	13.8	13.4
6	B	Argon	16	BN	12.4	12.6
7	C	Isopropanol	1	BN	13.4	12.4
8	C	Hexane	16	ZrO_2	11.0	9.3
9	C	Argon	4	Al_2O_3	14.0	11.5

[a] Conditions to be selected based on results from the initial Taguchi experimental design array.
[b] G. R. Anstis *et al*, *J. Am. Ceram. Soc.*, **64** [9] 533-38 (1981).

One reason for the selection of Ni_3Al binders as potential replacements for Co based binders, is the superior corrosion resistance of Ni_3Al over Co. A series of preliminary screening tests designed to assess the corrosion resistance of WC/Ni_3Al cermets has been

performed, and a comparison has been made with two commercial WC/Co materials (Figure 9). The Ni_3Al based materials show excellent resistance to corrosion by both nitric and sulfuric acids, in comparison to the commercial WC/Co hardmetals. It is also important to note two features; (1) the volume percentage of the Co binder is lower for the two commercial materials, and (2) the corrosion resistance of WC/Co decreases with increasing Co content. Both of these factors emphasize the improvement in corrosion resistance which can be attained by substituting Co binders with Ni_3Al. The effect of corrosion in hydrochloric acid appears to be similar for the two systems. A similar observation of improved resistance to corrosion has been noted when Ni is substituted for Co.

It is therefore clear that substitution of Ni_3Al based binders for Co results in a significant improvement in both retained high temperature strength and resistance to corrosion in aqueous acidic environments. Future work will be focused on the assessment of these properties for the most recent pressureless (vacuum) sintered materials. This work will be performed in combination with the determination of oxidation resistance at elevated temperatures, with comparison to current 'state of the art' WC/Co cermets provided by commercial vendors.

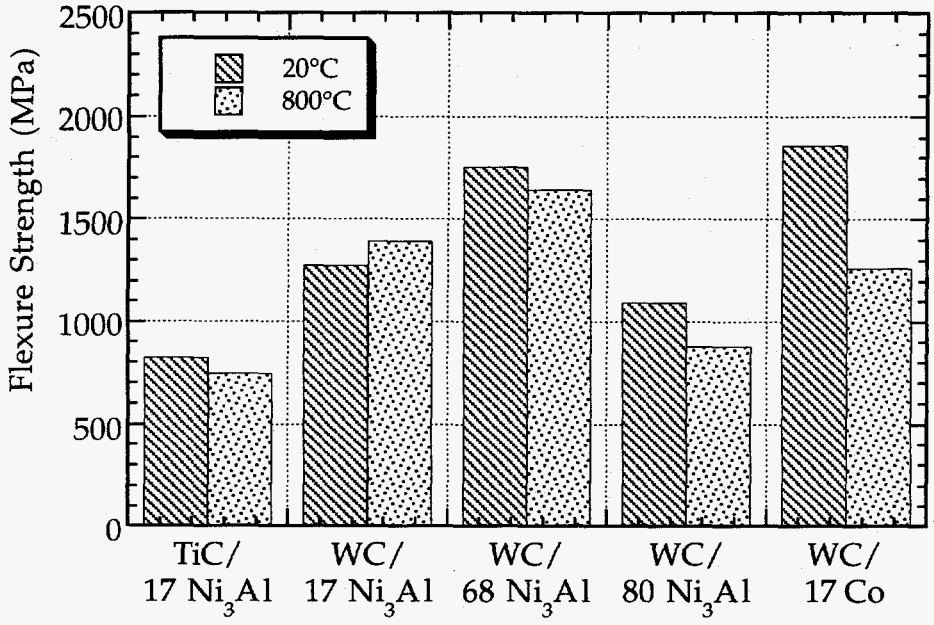

Figure 8. The effects of temperature upon the flexure strength of various carbide/Ni_3Al cermets (from 17 to 80 vol.% Ni_3Al). Data for a commercial WC/Co material is shown for comparison. Samples were tested in four point flexure, with test jig dimensions of 40 mm outer span and 20 mm inner span.

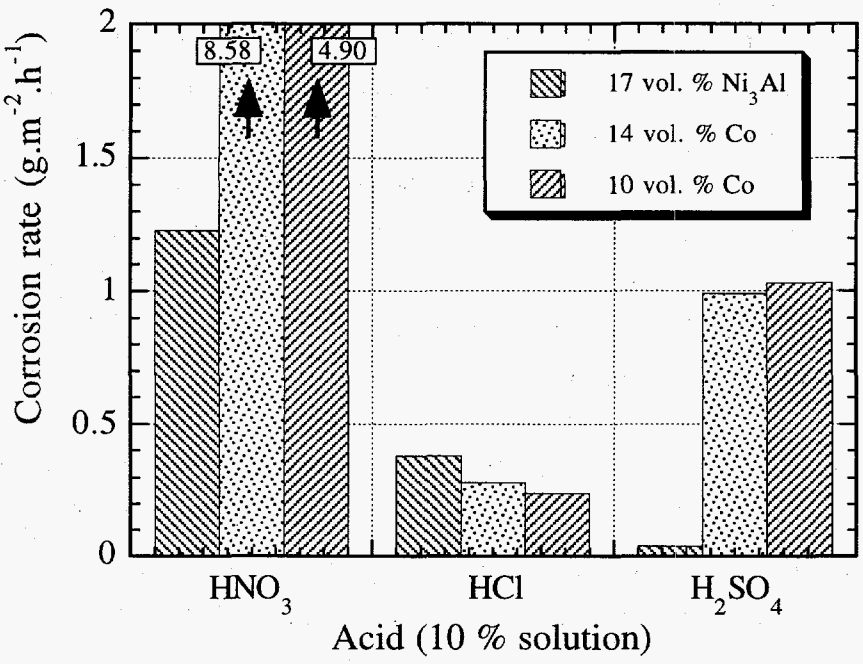

Figure 9. Corrosion rates, as measured by weight loss, of a WC/Ni_3Al (17 vol. %) cermet immersed in 10% acid solutions for 48 h (at 25°C). The WC/Co materials were commercial grade products.

PATENT/DISCLOSURES

Method to Fabricate Ductile Intermetallic Bonded Ceramic Composites by Sintering and Articles Resulting Therefrom, K. P. Plucknett, T. N. Tiegs, and P. F. Becher, Invention Disclosure ESID #1751X.

PUBLICATIONS

T.N. Tiegs, K.B. Alexander, K.P. Plucknett, P.F. Becher, P.A Menchhofer, S.B. Waters and J.H. Schneibel, 'Ceramic Composites with a Ductile Ni_3Al Binder Phase', accepted for publication in *Mat. Sci. Eng.A*, special issue; Proc. 5th Int'l Conf. on the Science of Hard Materials (Feb. 1995).

T.N. Tiegs, P.A. Menchhofer, K.B. Alexander, K.P. Plucknett, P.F. Becher, S.B. Waters and J.H. Schneibel, 'Hardmetals Based on Ni_3Al as the Binder Phase', to be published in the *Proceedings of 4th Int'l. Conf. on Powder Metallurgy in Aerospace, Defense and Demanding Applications*, Anaheim, California, May 1995.

K.P. Plucknett, T.N. Tiegs, K.B. Alexander, P.F. Becher, J.H. Schneibel, S.B. Waters and P.A. Menchhofer, 'Intermetallic Bonded Ceramic Matrix Composites', pp. 511-520 in the *Proc. of the CIM Int. Symp. on Advanced Ceramics for Structural and Tribological Applications*, Vancouver, British Columbia, August 1995.

PRESENTATIONS

None.

LICENSES

None.

INDUSTRIAL INPUT AND TECHNOLOGY TRANSFER

A recently published news release brought inquires from over 30 companies, both domes and foreign, that have interest an in the technology. These companies represent most of t hardmetals industries in the world.

Informal discussions are also proceeding with several companies that are either; manufa urers of hardmetal powders or components, users of hradmetal components or involved in therm spraying of hardmetal type coatings.

COST SHARING

NEW METHOD FOR SYNTHESIS OF METAL CARBIDES, NITRIDES AND CARBONITRIDES

R. Koc, J. S. Folmer, S. K. Kodambaka, H. Shin, P. F. Becher*, V. Nehring†

Department of Mechanical Engineering and Energy Processes,
Southern Illinois University
Carbondale, IL 62901
*Oak Ridge National Laboratory, Oak Ridge, TN 37831
† 3M Ceramic Technology Center, St. Paul, MN 55144

ABSTRACT

The purpose of this research is to develop a novel synthesis method for producing high purity, submicron, non-agglomerated and low cost metal carbide and nitride powders. The synthesis route utilizes a carbothermic reduction reaction of novel coated precursors that has potential as a low cost powders synthesis route. During the first quarter of the project, steps were taken to apply the process towards producing submicron TiC powders. The precursor is derived from a titania (TiO_2) and a hydrocarbon (C_3H_6) gas and provides high contact area between the reactants. This yields a better distribution of carbon within the titania and results in a more complete reaction and a purer product at a comparatively low temperature. The TiC powders produced at 1500°C for two hours under argon gas flow have oxygen content of about 2 wt.%, a very fine particle size (0.1-0.3 μm), non-agglomerated and are low cost. 3M Ceramic Technology Center has shown a special interest in these powders for their Al_2O_3 - TiC composite products.

TECHNICAL PROGRESS

I. Background

Titanium carbide is a ceramic with many applications in key high technologies from mechanical to chemical and microelectronics [1]. Titanium carbide has a high melting point (3260°C), high hardness (Knoop's = 32.4 GPa), high electrical conductivity ($30x10^6$ 1/ohm.cm), high chemical and thermal stability, high wear resistance, and high solvency for other carbides.

Titanium carbide can be used as a substitute for tungsten carbide, a common machining material, due to its similar properties of high hardness, melting point, and wear resistance. Currently 10 % of the world's consumed cobalt is used as binder material for tungsten carbide components [2]. Because of the lack of domestic ore reserves, cobalt must be imported to the U.S. from foreign and occasionally politically unstable sources. Titanium carbide compounds use nickel as a binder which has a more stable source and costs only half as much. Titanium carbide is also used in coated steel press tools, grinding wheels, wear resistant coatings, high temperature heat exchanger, magnetic recording heads, turbine engine seals, and bullet proof vests. Titanium carbide and carbonitride are also utilized in the production of Al_2O_3-TiC and ZrO_2-Ti(C,N) composites [3]. In addition, a promising field of application comprises plasma and flame spraying process in air, where titanium carbide-based powders show higher phase stability than that of tungsten carbide-based powders [4]. For all these applications, the synthesis of titanium carbide powders with a homogeneous chemical composition, fine particle size, a narrow particle size distribution, and a loose agglomeration is of great importance.

Methods that have been used to synthesize TiC powders can be classified into three categories:

i). The direct carbonization of titanium metal or titanium hydride, or combustion synthesis of TiC.

ii). The gaseous pyrolysis of titanium halide, such as $TiCl_4$, in a carbon containing atmosphere.

iii). The carbothermal reduction of TiO_2 with carbon in controlled atmospheres at high temperatures.

Metallic titanium as a starting material is relatively expensive, and furthermore, the oxygen contained in the metal can hardly be reduced, so that the product is generally characterized by a high oxygen content [4]. Titanium chloride as a precursor is of importance in the field of chemical vapor deposition, but it is very expensive. An inexpensive method for producing titanium carbide involves the reaction between titania (TiO_2) and carbon particles:

$$TiO_2 + 3C === TiC + 2\ CO\ (g) \text{----------(1)}$$

Because the reactants exists in separate particles, the extent of this reaction is limited by the contact area between the reactants and the distribution of the carbon within the titania. These limitations result in a TiC product that contains unacceptable quantities of unreacted TiO_2 and carbon. This is due to the interruption of intimate contact of TiO_2 and C in the reduction reactions. Also, the reaction rate is extremely slow and a complete reaction is practically impossible by this method.

The process being developed avoids the expense of the first two methods while surmounting the inability of the third to make a suitable product. It exploits the reaction between TiO_2 and C in a way that improves the contact area between the reactants and yields a better distribution of carbon within the titania.

The Gibbs free energy change of reaction (1) as a function of temperature for various carbon monoxide partial pressures (P_{CO}) is shown in Figure 1. Reaction (1) is thermodynamically favorable above 1289°C unless (P_{CO}) is lowered in the system. An argon gas flow during the carbothermal reduction is required to take the produced CO gas away, lowering the thermodynamic onset temperature of the overall reaction. On the other hand, the reaction (1) is the sum of a more complex set of reactions. The initial stage of the reactions is the reduction of TiO_2 to lower metal oxides.

$$TiO_2(s) + C(s) === TiO(s) + CO\ (g) \text{----------(2)}$$

$$TiO_2(s) + CO(g) === TiO(s) + CO_2\ (g) \text{----------(3)}$$

Carbon dioxide is then reduced by carbon that is present in the system.

$$CO_2(g) + C(g) === 2\ CO(g) \text{----------(4)}$$

In these reactions, carbon is either a CO_2 reducer or a CO generator which keeps the CO_2/CO ratio low enough to make the reduction of TiO_2 possible by gas phase reduction. Because the extent of the reactions is limited by the contact area between the reactants and continuous supply of CO, the intimate contact of carbon with TiO_2, TiO and CO_2 is essential during the reduction for complete conversion of TiO_2 into TiC.

In the present work, the minimization of the kinetic barriers is aimed by a new synthesis method [5], composed of a two step processes. The first step consists of coating TiO_2 powders with carbon by decomposing a hydrocarbon gas (C_3H_6) at temperatures of 400-600°C. This provides intimate contact between reactants and an even distribution of carbon within titania. The second step involves the formation of TiC powders by promoting a carbothermal reduction reaction within the carbon coated TiO_2 particles, in an inert atmosphere at temperatures of 1200-1550°C.

In this report, the effectiveness of the carbon-coating by the pyrolysis of propylene (C_3H_6), the phase evolution of the carbon coated TiO_2 precursor in the subsequent firing conditions, and the characteristics of the resultant TiC powders are presented.

II. Experimental Procedure

As a preliminary step, the formation of the condensed phase of carbon by the pyrolysis of C_3H_6 was studied by obtaining equilibrium composition with one mole of C_3H_6 gas using computer software[1] based on Gibbs free energy change as a function of temperature. Figure 2 shows the equilibrium composition of major products out of 1 mole of C_3H_6 gas at 1 atm. pressure. As shown in the figure, the reaction:

$$2\ C_3H_6(g) = 3C(s) + 3\ CH_4(g) \quad \text{----------(5)}$$

is dominant at low temperatures while the formation of high purity condensed phase of carbon is accelerated at high temperatures according to the reaction:

$$C_3H_6(g) = 3C(s) + 3\ H_2(g) \quad \text{----------(6)}$$

[1]HSC Chemistry, Outokumpu Research Oy, Pori, Finland

Based on these calculations the pyrolysis of hydrocarbon (C_3H_6) gas was determined to be 600°C for the carbon coating step.

A rotating coating apparatus, consisting of a 10 cm ID x 35 cm long stainless steel vessel was used for preparing low density, pyrolytic carbon coated titania particles utilizing propylene (C_3H_6) as the coating gas. About 20 grams of titania[2] powder were placed in the vessel and the vessel was evacuated to a moderate vacuum level using a rotary vacuum pump. Then the propylene gas was filled into the vessel until pressure reached 40 psi. The vessel was then heated to 600°C, while it was rotating. Thermal cracking of propylene increased the internal vessel pressure upon initiation of the carbon coating. The coating step was continued until about 33.7 wt.% carbon was deposited, which required about 18 cycles (each cycle was 20 minutes). The weight percentage of the carbon in the precursor was determined using thermogravimetric analysis in air.

The carbon coated titania precursors with carbon content greater than 32 wt.% were subjected to a second step. TiC powders were produced by promoting a reaction within the carbon coated titania particles at temperatures of 1200 to 1550°C for two - four hours under flowing argon gas (1 liter per minute, 1LPM). This step was performed in an atmosphere controlled tube furnace with ID 70mm.

The precursor material and TiC powders produced at 1200 - 1550°C were characterized using X-ray diffraction (XRD) with Cu-Kα radiation, BET surface area analyzer, and transmission electron microscopy (TEM). Oxygen and total carbon content of the produced powders was determined by 3M Ceramic Technology Center. Oxygen was analyzed by infrared detection in a LECO induction furnace while total carbon content was determined by ignition in a LECO induction furnace analyzing the evolved CO_2 colurimetrically.

III. Results and Discussion

Figures 3 and 4 show TEM and XRD pattern of the carbon coated titania precursor, respectively. As shown in the Figures, very uniform coating (see Figure 3) of pyrolytic carbon (see Figure 4, phases consists of anatase and rutile no graphitic carbon) on titania is apparent. These results showed that uniform, highly porous and low density carbon coating can be deposited on titania particles by using C_3H_6 gas.

---

[2] Degussa Corparation, Ridgefield Park, NJ.

The XRD patterns in Figure 5 show the formation of the TiC powders as a function of reaction temperature. Phases in the XRD pattern of the powders at 1200°C is determined to be Ti_3O_5 and TiO - TiC solid solution. At 1300°C lower oxides of titanium disappeared and TiC-TiO solid solution formation was completed. From 1300°C, no appreciable oxide phase was identified while TiC peak intensities increased with temperature. The increase in the TiC peak intensity was accompanied by the increase in weight loss and the decrease in oxygen content with reaction temperature as shown in Figures 6 and 7.

From equation (1), the percentage weight loss for the stoichiometric reaction was calculated to be 48.3 %. A weight loss less than this amount indicates an incomplete reaction, where as greater weight loss indicates the presence of volatile species in the titania powders. The weight loss data elucidates that a reaction temperature of 1500°C is required to accomplish the acceptable degree of reaction of two hours. Figure 6 shows the oxygen content and the total carbon in the produced TiC powders as a function of reaction temperature. The TiC powders synthesized from the precursors containing 33.7 wt.% carbon had about 2 wt.% oxygen and 18.4 wt.% total carbon when they were fired at 1500°C for two hours in 1 LPM argon flowing atmosphere. Lattice parameters are being calculated from the XRD data to determine the position of oxygen content in the powders.

The BET surface area measurements were made to obtain information about the reaction mechanism and the particle size of the resulting powders as a function of the reaction temperature. As can be seen from Fig. 7, the BET surface area of the resulting powders increases with reaction temperature to maximum at 1300°C and then linearly decreases as the reaction temperature increases. The decrease in the BET surface area above 1300°C implies the particle growth of the resulting powders while the increase in BET below 1300°C may be related to the formation of lower oxides of titanium. Further study is underway to uncover the detailed reason for the increase in the BET surface area below 1300°C.

Figure 8 shows a dark field image of TEM micrograph of synthesized powders at 1550°C for four hours under 1LPM argon flowing gas. As it can be seen from Fig. 8, the produced TiC powders have fine particle size, narrow particle size distribution (0.1-0.2μm), and are loosely agglomerated.

IV. Conclusion

The developed process was capable of producing high quality TiC powders suitable for making ceramic materials and composites - highly pure powder with submicron particles. There are three

advantages of using TiO_2 powders coated with carbon instead of a simple mixture of carbon black and TiO_2 powder. First, carbon coated TiO_2 forms an intimate mixing of the reactants. Second, it provides high-surface contact between TiO_2 and carbon. Third, it produces a high-purity TiC at a comparatively low temperature, because the carbon source is a hydrocarbon gas. Consequently, the new process results in a very complete reaction and yields a high quality TiC powder that meets the exacting requirements for the manufacture of ceramic materials and composites: the powder has very fine, uniform particles; contains very few impurities (particularly oxygen, iron, and free titanium) and low cost.

REFERENCES

1. I. N. Mihailescu, M. L. De Giorge, C. H. Boulmer-Leborgne and S. Udrea, "Direct Carbide Synthesis by Multipulse Exciter Laser Treatment of Ti Samples in Ambient CH_4 Gas at Superatmospheric Pressure", *J. Appl. Phys.*, 75, 5286-5294 (1994).

2. D. D. Harbuck, C. F. Davidson and B. Monte, " Gas Phase Production of TiN and TiC Powders", *J. of Metals*, 38, 47-50 (1986).

3. V. Gross, J. Haylock, and M. V. Swain, *Mater. Sci. Forum*, 34-36, 555-559 (1988).

4. L. M. Berger, " Titanium Carbide Synthesis from Titanium Dioxide and Carbon Black", *J. Hard Materials*, 3, 1, 3-15 (1992).

5. R. Koc and G. Glatzmaier, "Process for Synthesizing Titanium Carbide, Titanium Nitride and Carbonitride", *U.S. Patent* No: 5,417,952 (1995).

PATENT DISCLOSURES

U.S. patent granted on May 23, 1995, No: 5,417,952.

PRESENTATIONS

R. Koc, J.S. Folmer, H. Shin, P.F. Becher and V. Nehring, " New Method for Synthesis of Metal Carbide, Nitrides and Carbonitrides", poster presentation at the Annual Meeting of the Office of Industrial Technologies and Energy Efficiency and Renewable Energy, U.S. Department of Energy, Advanced Industrial Materials (AIM) Program-Laboratory/Industry Partnerships for New and Improved Materials, Washington, D.C. (June 1995).

LICENSES

None

INDUSTRIAL INPUT AND TECHNOLOGY TRANSFER

3M Ceramic Technology Center has shown a special interest in these submicron TiC powders for their Al_2O_3 - TiC composite products since there is no submicron size TiC powders available in the world market.

LIST OF THE FIGURES

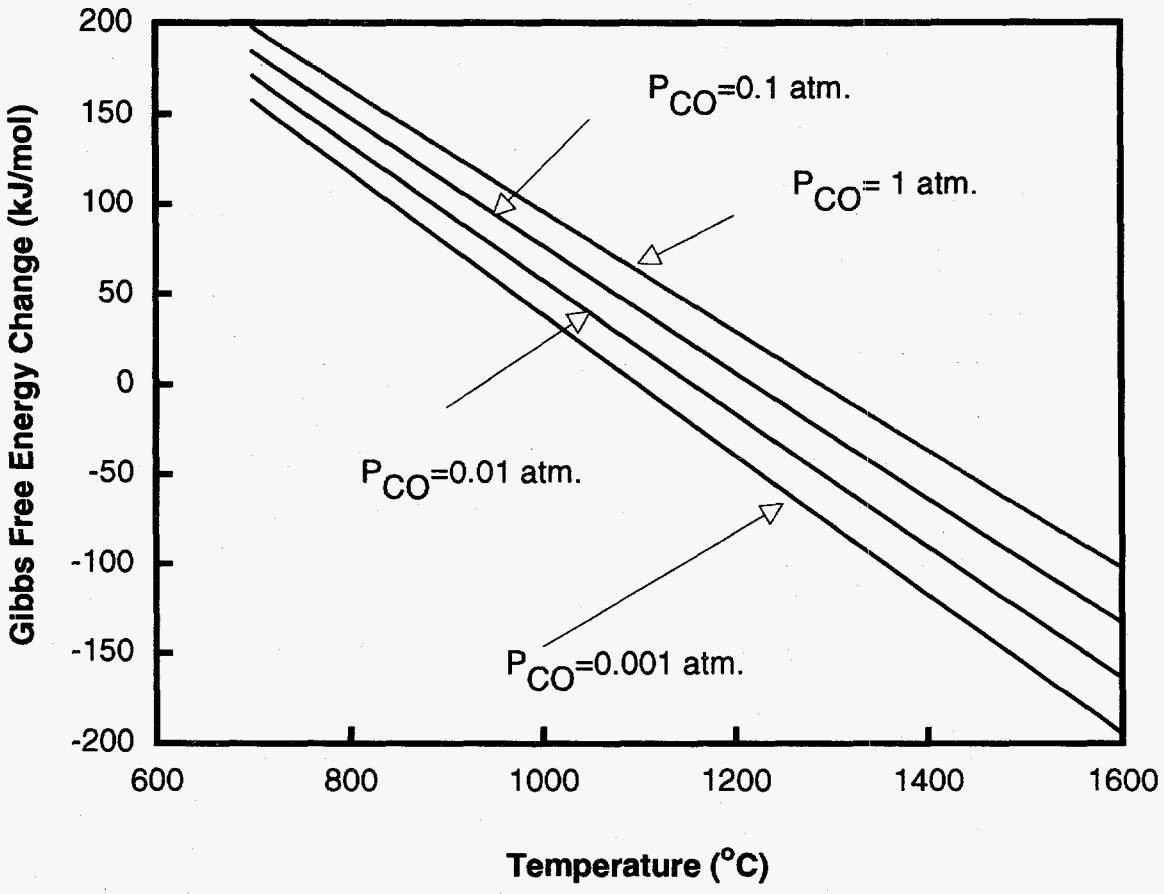

Figure 1. Gibbs free energy change of reaction (1) for various partial pressure of carbon monoxide gas (P_{CO}).

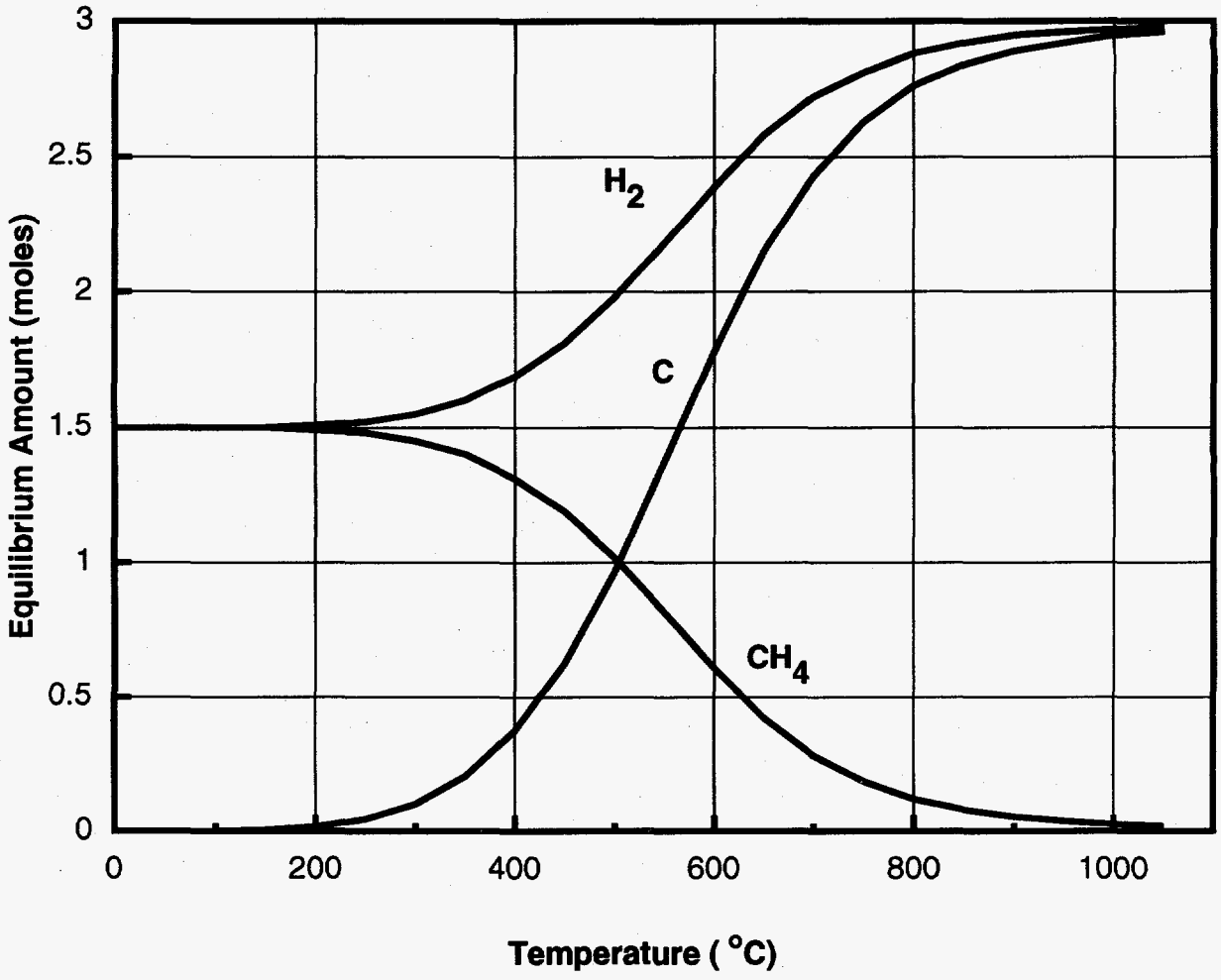

Figure 2. Equilibrium composition of major products out of 1 mole of C_3H_6 gas at 1atm. pressure.

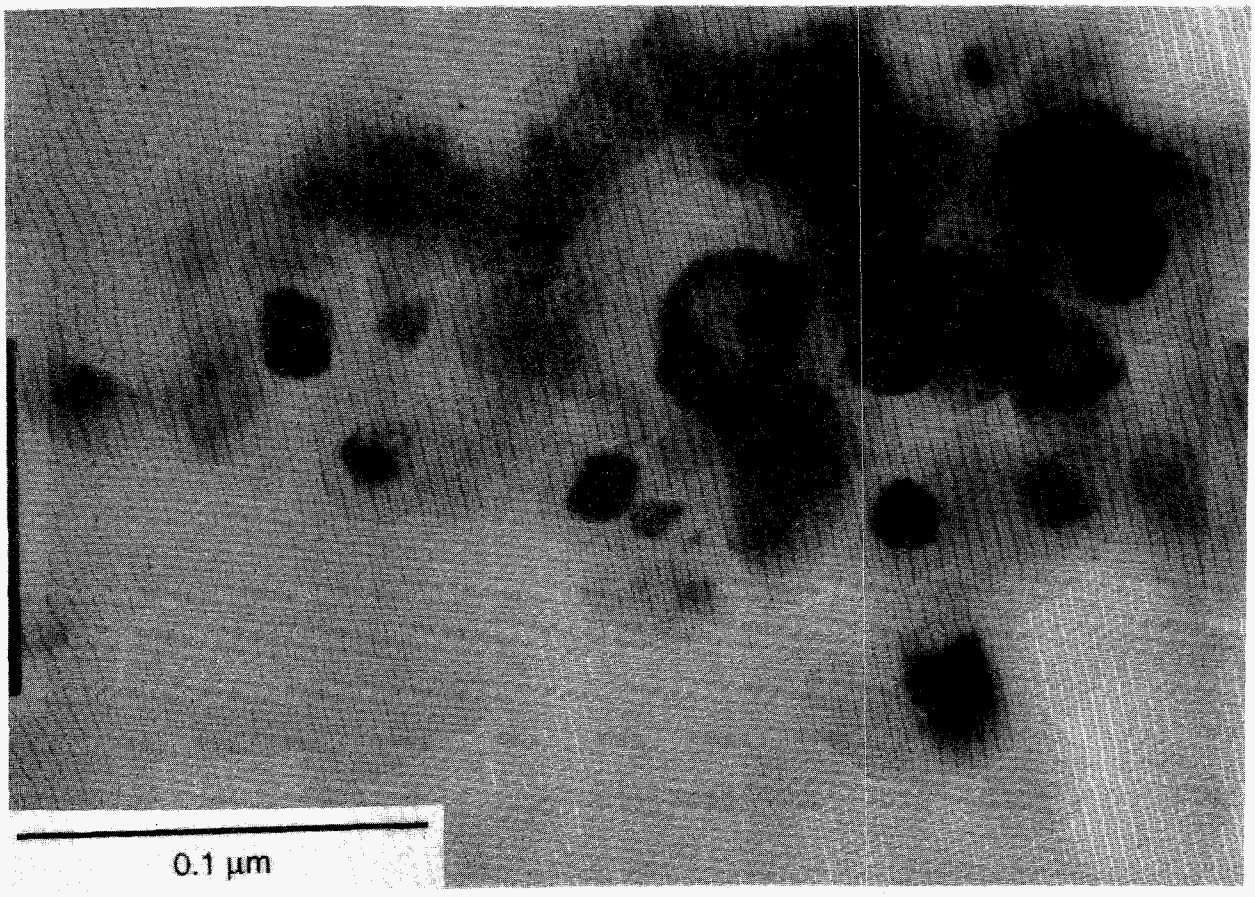

Figure 3. TEM of carbon coated TiO_2 precursor by the pyrolysis of C_3H_6 at 600°C.

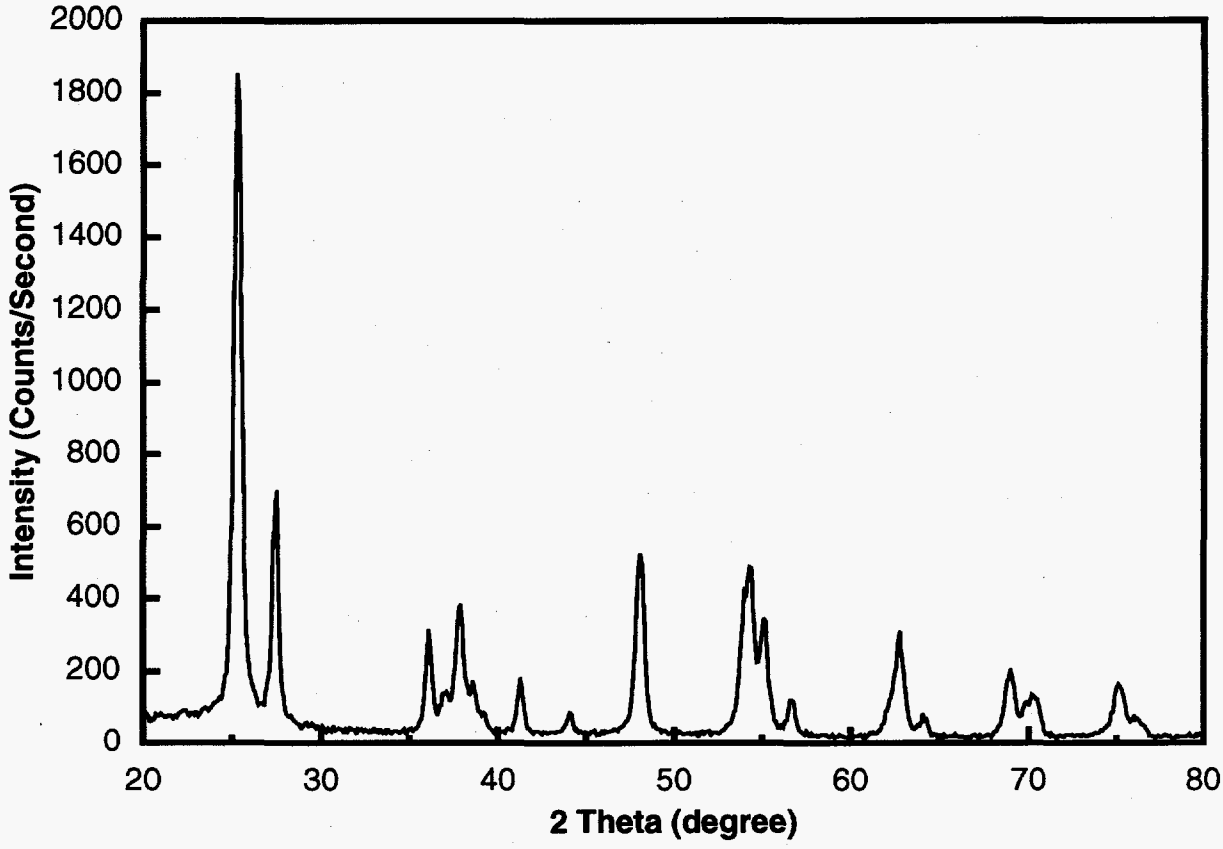

Figure 4. XRD result of carbon coated TiO_2 precursor by the pyrolysis of C_3H_6 gas at 600°C. All peaks correspond to TiO_2 phase, implying pyrolytic form of carbon is deposited.

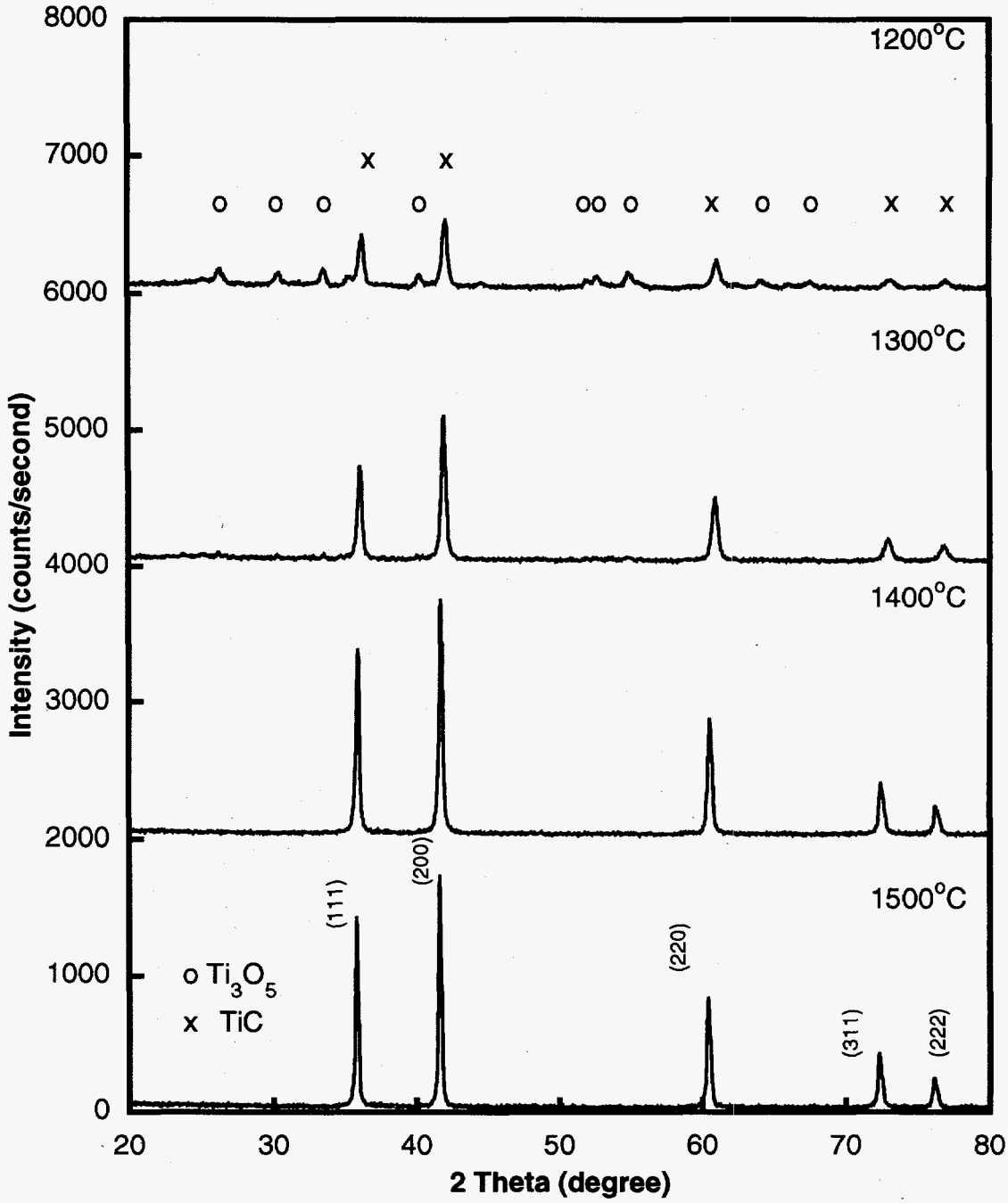

Figure 5. XRD results of reaction products produced at 1200-1500°C for two hours in flowing argon of 1atm.

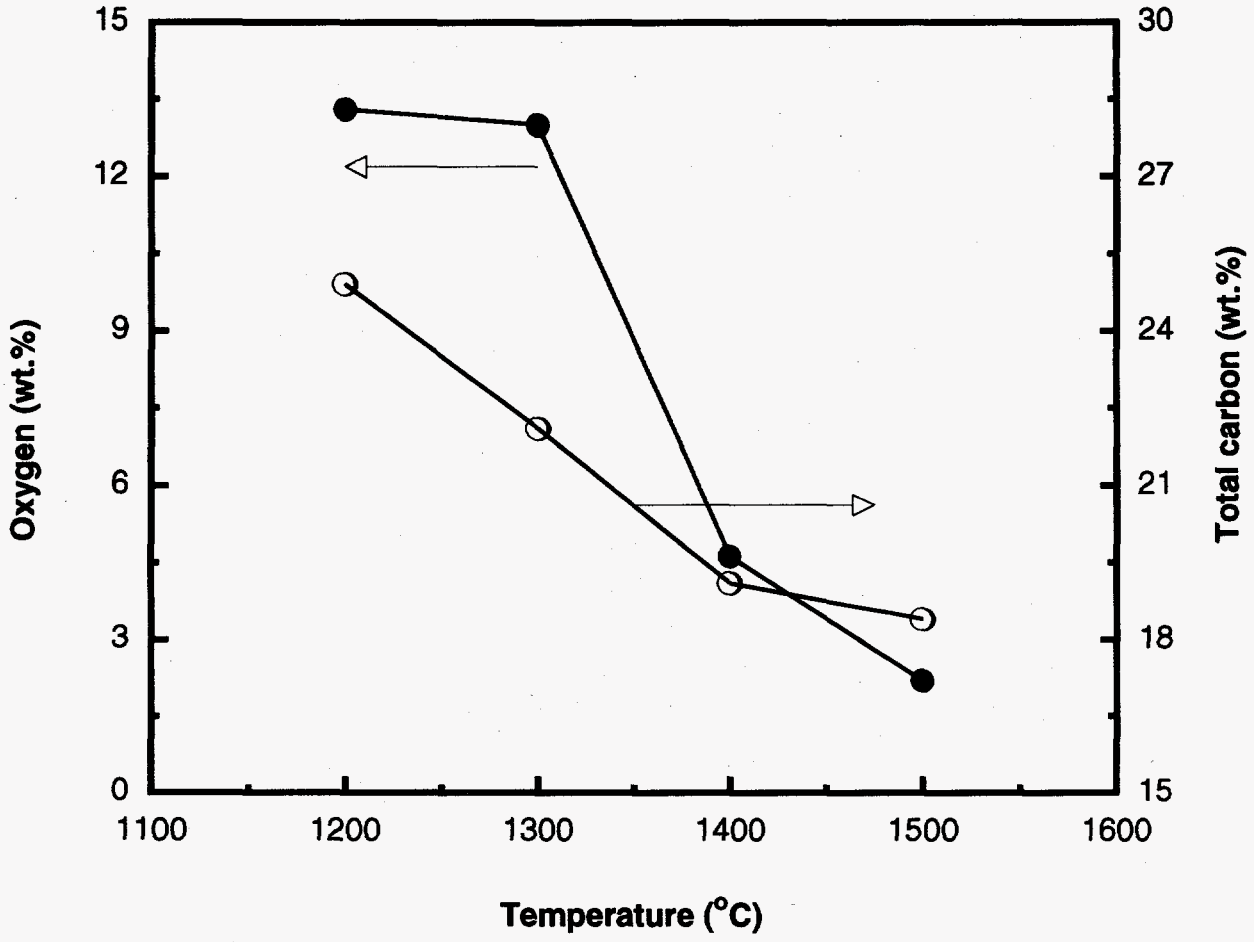

Figure 6. Change in oxygen and total carbon content as a function of reaction temperature.

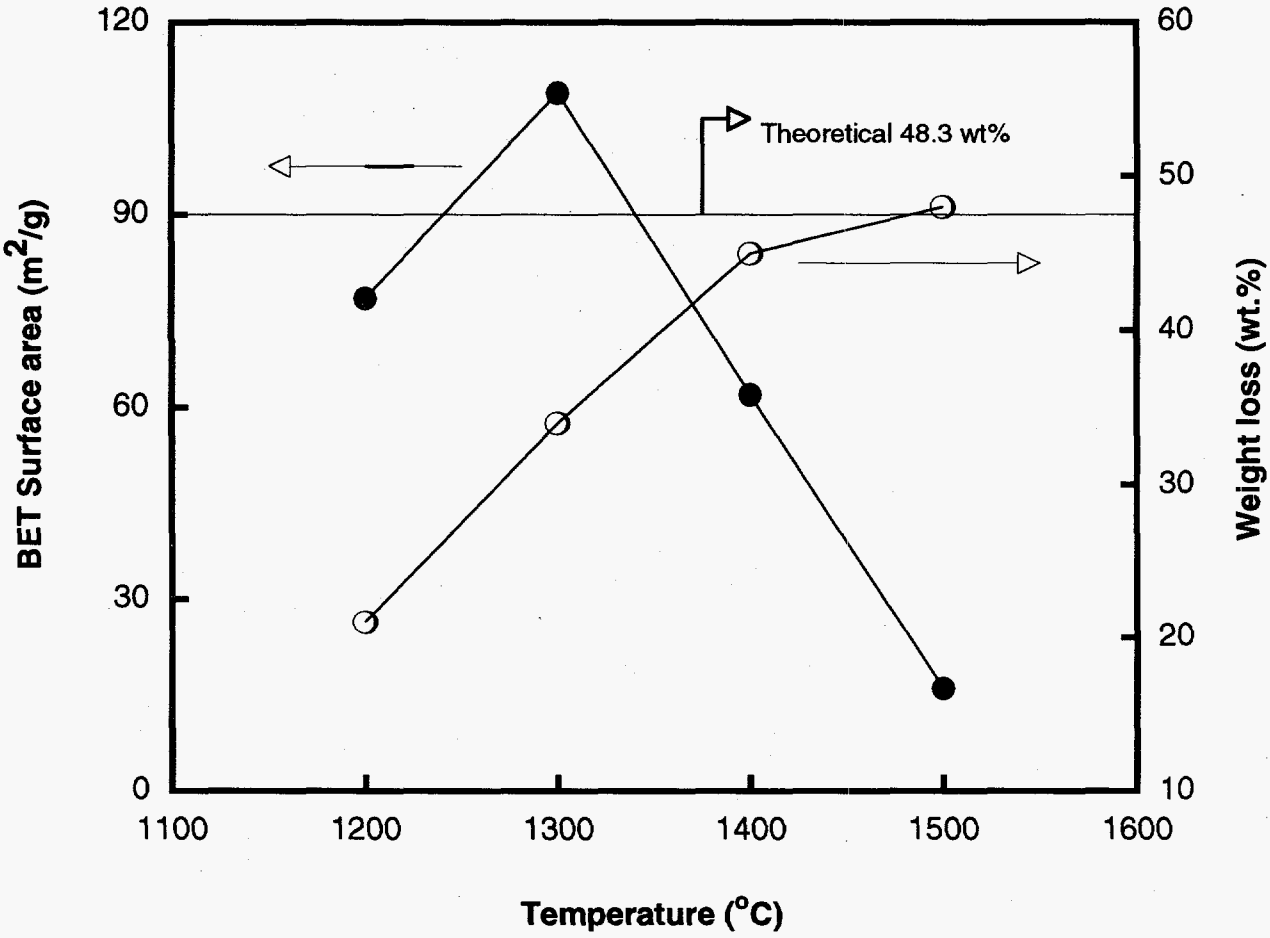

Figure 7. Change in BET surface area and weight loss as a function of reaction temperature.

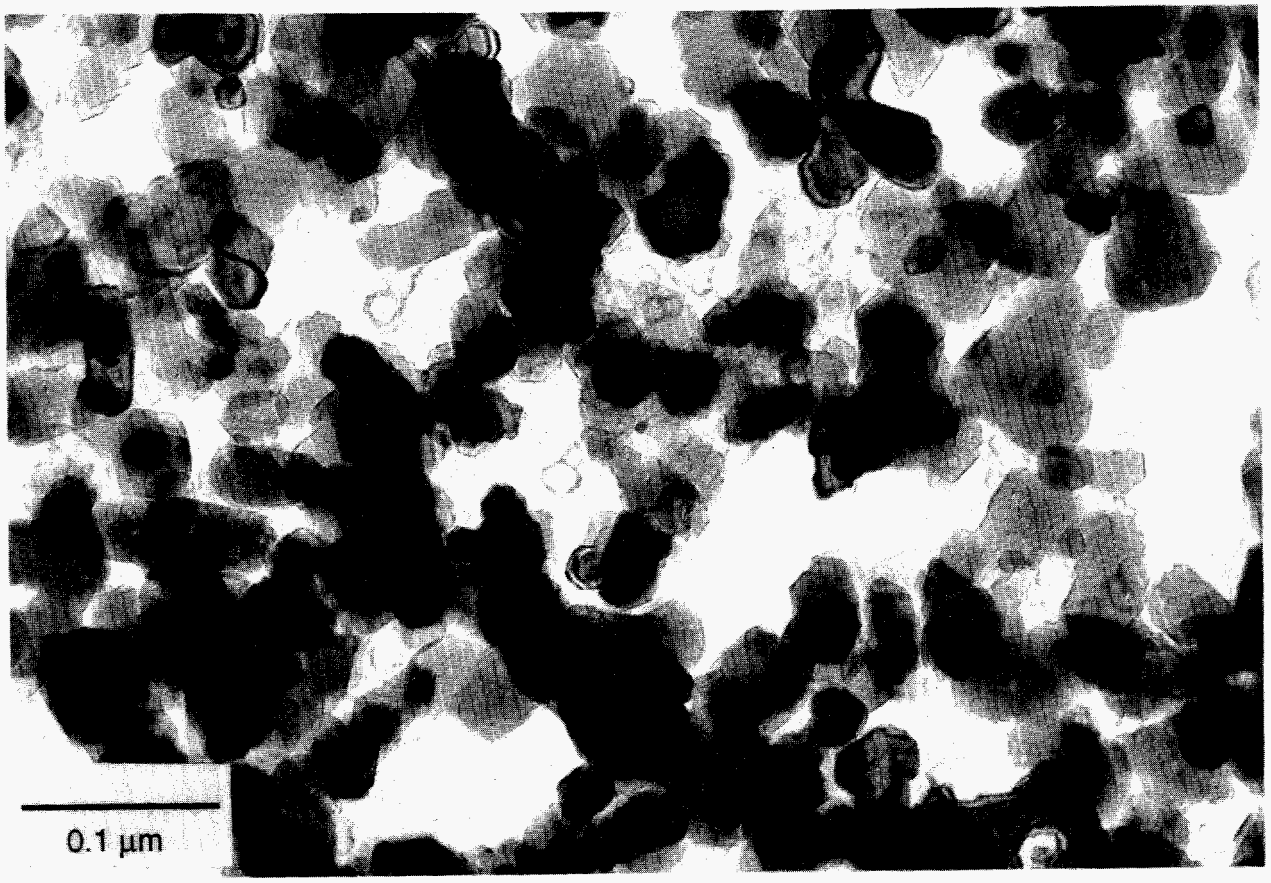

Figure 8. TEM micrograph of reaction product produced at 1550°C for four hours in flowing argon at 1 atm.

PROCESS SIMULATION FOR ADVANCED COMPOSITES PRODUCTION

M. D. Allendorf, S. M. Ferko, S. Griffiths, R. Nilson, T. H. Osterheld,
N. Yang, and D. R. Hardesty

Sandia National Laboratories
Livermore, California 94551-0969

INTRODUCTION

The objective of this project is to improve the efficiency and lower the cost of chemical vapor deposition (CVD) processes used in manufacture of advanced ceramics by providing the physical and chemical understanding necessary to optimize and control these processes. Project deliverables include: numerical process models; databases of thermodynamic and kinetic information related to the deposition process; and process sensors and software algorithms that can be used for process control. Target manufacturing techniques include CVD fiber coating technologies (used to deposit interfacial coatings on continuous fiber ceramic preforms), chemical vapor infiltration, and novel techniques such as the chemical vapor composites (CVC) process for rapid production of ceramic composites. Efforts are typically focused on the development of a specific new or existing processes, but are sufficiently generic to find application across a range of related processes.

Experimental measurements are performed under realistic processing conditions to obtain gas-phase concentrations, precursor decomposition kinetics, and deposition rates, using a high-temperature flow reactor (HTFR) equipped with mass spectrometric and laser diagnostics. In addition, advanced characterization methods such as high-resolution transmission electron microscopy and energy-dispersion spectroscopy are used to characterize the microstructure and composition of reactor deposits. Computational tools developed through extensive research in the combustion field are employed to simulate the chemically reacting flows present in typical industrial reactors.

Currently, this project is conducted in collaboration with DuPont Lanxide Composites (DLC; Newark, DE) and is directed toward development of a simulation capability for interfacial coating processes. This report only contains information of a non-proprietary nature.

Project Tasks

Two tasks for FY95 are defined as follows:

1. Characterization of reactor deposition chemistry
   a. Boron nitride deposition mechanism
   b. Characterization of the fiber-coating interface

2. Simulation of reactor fluid dynamics and mass transport: application of a 1-D infiltration model to boron nitride fiber coating processes

TECHNICAL PROGRESS FY95

Summary

This year we significantly advanced our understanding of the role of gas-phase chemistry in the formation of boron nitride (BN) interfacial layers. A database of thermochemical data for chlorinated boron compounds was compiled, a gas-phase reaction mechanism describing the reaction between BCl_3 and NH_3 as well as their unimolecular decomposition was constructed, and experimental and modeling investigations were conducted to determine the temperature and pressure dependence of gas-phase and surface reactions occurring during the deposition. These results were incorporated into a new preform coating model developed this year that predicts BN coating rates and thickness profiles in ceramic-fiber preforms used in the manufacture of CFCCs. The model is simple to apply and can be used to optimize reactor operating conditions (temperature, pressure, and precursor concentration) to produce coatings with the desired thickness and uniformity. Model predictions were verified by comparison with boron nitride (BN) coating thicknesses measured by scanning electron microscopy, which shows that both the coating thickness and uniformity across the preform can be predicted with reasonable accuracy.

Milestones and Progress

Task 1: Characterization of reactor deposition chemistry

a. Boron Nitride deposition mechanism. Boron nitride layers are deposited on continuous-fiber preforms prior to densification to form ceramic composite structures. This creates a debonding mechanism, so that when the composite is placed under load, the fibers can take up the load by pulling out of the matrix. Before summarizing our results, we present a brief overview of the reaction conditions for this process, using information obtained from studies of BN CVD in the literature.

BN can be deposited from a variety of precursors, but the ones most commonly used for ceramic applications are boron trichloride (BCl_3) and ammonia (NH_3), both of which are relatively inexpensive and easy to handle. The overall reaction for the process is:

$$BCl_3 + NH_3 \rightarrow BN(s) + 3HCl \qquad (1)$$

A carrier gas such as hydrogen or helium may be used but is not required. In either case, excess ammonia is necessary to achieve stoichiometric material. Deposition temperatures as low as 450 °C and as high as 1600 °C and reactor total pressures from a few torr to one atmosphere have been reported. Recent investigations, however, have focused on the lower end of this range (450-1100 °C), since either the substrate or preform fibers (such as Nicalon) can be damaged by high temperatures. The crystalline phase obtained from these methods is either turbostratic or a mixture of the turbostratic and hexagonal forms, although a third form, known as "pyrolytic" boron nitride, can be obtained at very high temperatures (above 1900 °C). Note that these phases are different from the ultra-hard cubic form, which is metastable and cannot be obtained by ordinary thermal CVD techniques.

In determining a mechanism for BN deposition, it is important to establish whether or not homogeneous (i.e., gas-phase) reactions play any role in the process. This year we significantly advanced our understanding of the role of gas-phase chemistry in the formation of boron nitride (BN) interfacial layers. Major results of these investigations are summarized below:

- Thermochemical data for chlorinated boron compounds were estimated using *ab initio* electronic-structure calculations. Calculations were performed for a total of 36 compounds in the B-N-H-Cl system. The predicted values of, for example, heats of formation, are in good agreement with previous calculations and the available (although scanty) experimental data from the *JANAF Tables*. In addition to providing data for both stable and radical species, the energetics of several transition-state structures were determined to allow rate constants to be estimated for suspected key gas-phase reactions. Application of these computational methods to other chemical systems indicate that heats of formation are generally accurate to $\pm$ 3 kcal mol^{-1}. These data permit a realistic assessment of the role of gas-phase chemistry in the BN CVD process to be made.
- The calculated thermochemical data show that gas-phase chemical reactions between BCl_3 and NH_3 are likely under CVD conditions. Figure 1 is a potential energy diagram for this reaction, which shows that a stable complex $Cl_3B{:}NH_3$ can be formed when the two BN precursors react. Further reactions, in which HCl is removed from the complex to form Cl_2BNH_2 and ClBNH can also occur.
- A gas-phase reaction mechanism describing the reaction between BCl_3 and NH_3 as well as their unimolecular decomposition, was constructed that includes 23 species and 65 reactions. Rate constants for several uncharacterized reactions were calculated or estimated from flow-reactor experiments. The mechanism was combined with a plug-flow reactor code to evaluate the importance of various gas-phase processes under realistic BN CVD conditions. The results show that: (1) BCl_3 is a highly stable molecule that does not decompose at routine CVD temperatures (1100-1400 K) (Figure 2, left); and (2) NH_3 may undergo decomposition to form N_2 and H_2, but the extent of decomposition is highly dependent upon the reactor temperature, pressure, and gas residence time (Figure 2, right).

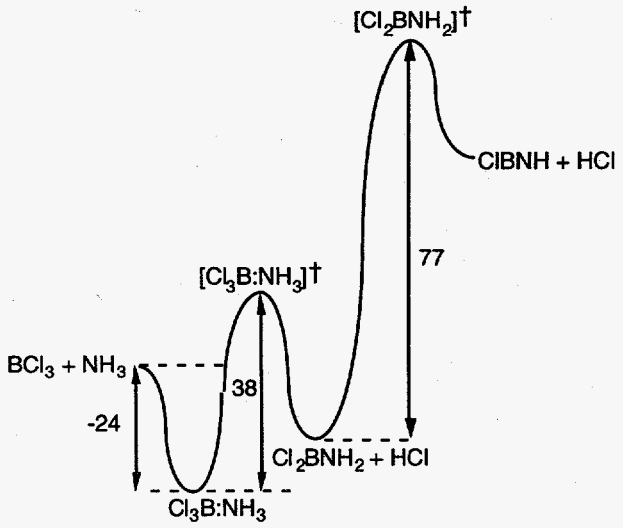

Figure 1. Potential-energy diagram for the reaction of BCl_3 with NH_3. Energies on the diagram are given in kcal mol^{-1}.

- Plug-flow calculations using the gas-phase mechanism also show that the reaction of BCl_3 with NH_3 is rapid under CVD conditions and yields species containing both boron and nitrogen. One of these compounds, Cl_2BNH_2, is likely to be a key gas-phase precursor to BN, since it is the immediate product of the reaction and forms in substantial amounts at residence times as

short as 50 msec. The composition of the gas-phase is also predicted to vary widely as a function of reactor temperature (Figure 3).

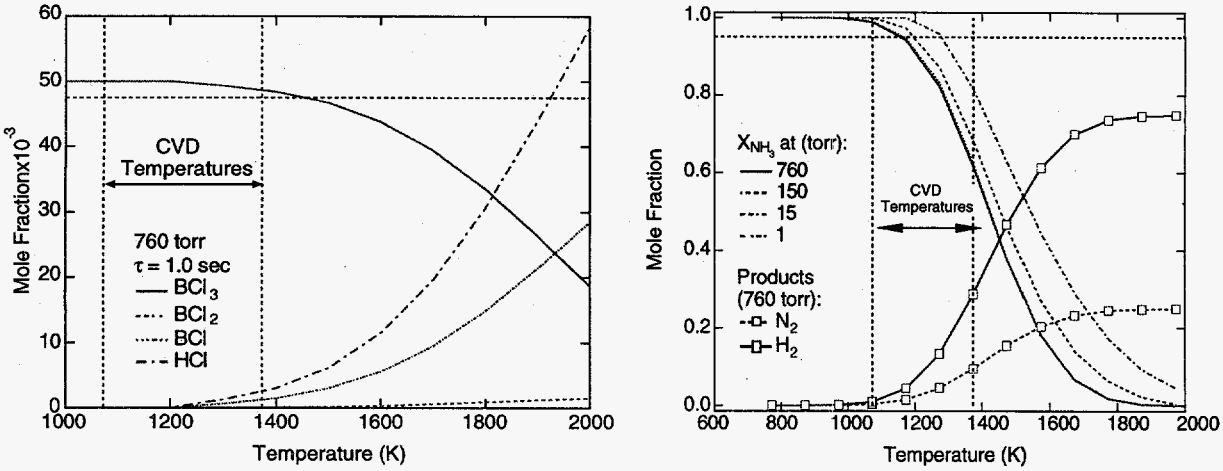

Figure 2. Plug-flow predictions of the decomposition of BCl_3 (left) and NH_3 (right) as a function of temperature. Residence time for all calculations is 1 second. Left: 5% BCl_3 in H_2, 760 torr. Right: 100% NH_3. Decomposition of NH_3 is shown as a function of reactor pressure.

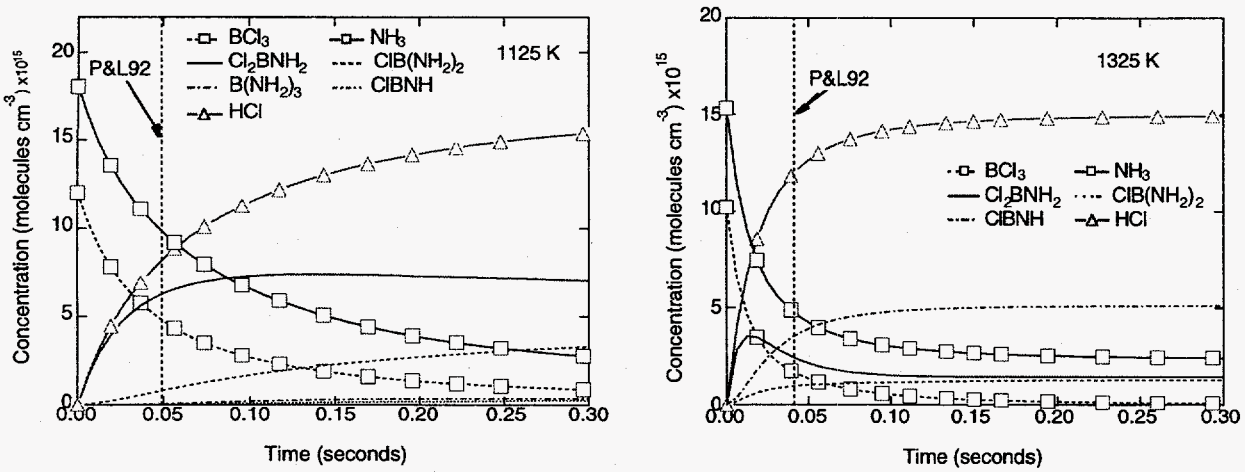

Figure 3. Plug-flow predictions of gas-phase concentrations at 1125 K and 1325 K. All calculations were performed for a total pressure of 2.0 torr and a 40% BCl_3, 60% NH_3 mixture. Dashed vertical lines indicate the estimated residence times for one set of experimental BN deposition-rate measurements in the literature (N. Patibandla and K. L. Luthra, *J. Electrochem. Soc.* **12**, 3558 (1992).

- HTFR experiments confirm that BCl_3 and NH_3 react and that one of the predicted products, Cl_2BNH_2, is formed. This is illustrated in Figure 4, which shows mass spectra obtained with the reactor operating at 20 torr, 690 °C, and a residence time of 160 msec. Spectra corresponding to two gas mixtures are shown: (1) 0.9% BCl_3 in helium carrier gas and (2) 0.9% BCl_3 and 3.3% NH_3 in helium. In the absence of NH_3, only BCl_3 and its fragments formed in the mass spectrometer are observed (some HCl is also seen; this is due to reaction with adsorbed water in the gas-transfer lines). Addition of NH_3 produces dramatic changes in

the spectrum. The peaks associated with BCl_3 disappear almost entirely and new peaks corresponding to Cl_2BNH_2 and $(BClNH)_3$ (a cyclic compound analogous to benzene) appear. In addition, the concentration of HCl increases. However, no peaks associated with $Cl_3B{:}NH_3$ or ClBNH are seen.

- The combination of calculations and experiments allow us to conclude that gas-phase chemical reactions are important on the timescales and at the temperatures and pressures employed in BN CVD. Except at the shortest residence times, these reactions produce a mixture of species that contain both boron and nitrogen. The relative efficiency with which these species deposit BN is unknown, although the similarity of the BN deposition kinetics obtained by various research groups suggests that there may not be great differences.

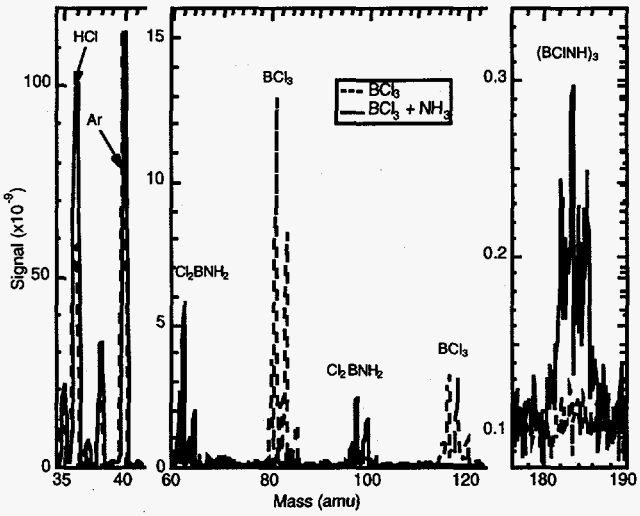

Figure 4. Mass spectra illustrating the reaction of BCl_3 with NH_3, showing the formation of the Cl_2BNH_2 and $(BClNH)_3$ products.

b. Characterization of the fiber-coating interface. Measurements of BN coating thickness are necessary to provide data to validate models predicting deposition rates within fiber preforms (see Task 2 below). To address this need, samples of 2-D Nicalon™/Al_2O_3 composite provided by DuPont Lanxide Composites Inc. (DLC) were subjected to evaluation by scanning electron microscopy (SEM). Fibers on these preforms were coated with BN followed by a layer of silicon carbide (SiC). Results for two representative samples, henceforth referred to as Samples 095 and 142, are described here. The samples were in the form of plates from which a 6-mm long section was cut to provide a sample with dimensions appropriate for microscopy.

Figures 5A and B show SEM micrographs at two magnifications. The figures show that both the SiC and BN coatings around a given fiber are remarkably uniform and appear to be fully dense. The SiC coating in Sample 095 is about 1.6 μm thick, while that in Sample 142 is thinner, about 1.1 μm thick, based on a measurement 1.4 - 1.5 mm from the surface of the sample.

Figure 6 shows a comparison of the predicted BN deposit thickness profile with measurements of the thickness obtained from SEM images similar to those in Figure 5B. The thickness varies by roughly a factor of two from the surface of the sample to the center, with

roughly the same parabolic shape the model predicts (see discussion under Task 2). The measured BN coating thicknesses are significantly smaller than those estimated from a weight-gain calculation.* The average thickness obtained by the calculation is 0.41-0.42 μm, while the measured thickness varies from about 0.15 to 0.35 μm. It should be noted that SEM will, if anything, overpredict the thickness, since a non-perpendicular orientation of the sample with respect to the electron beam will cause the coating to appear to be thicker than it actually is. Additional samples will be provided by DLC in FY96 to provide further information concerning BN deposition rates as a function of reactor size.

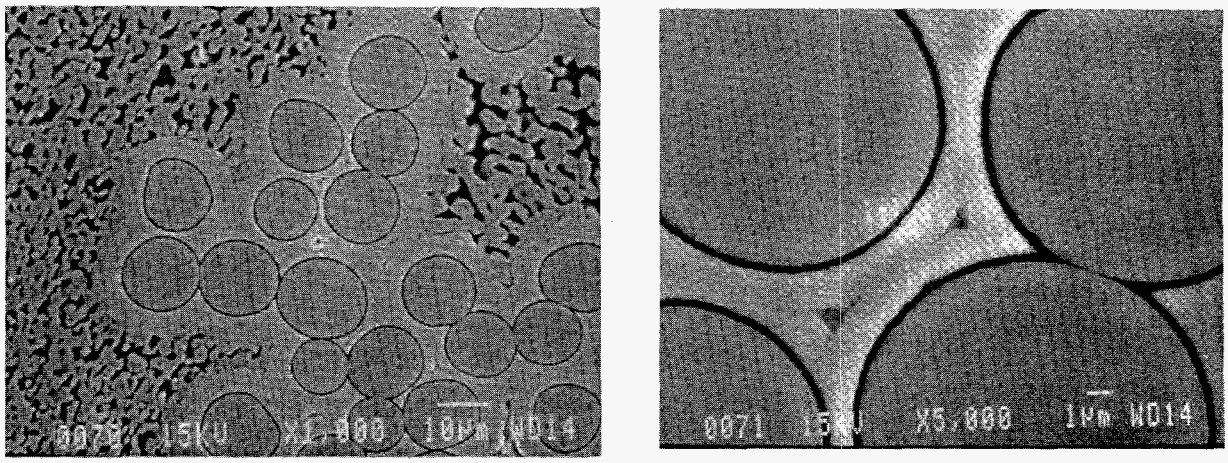

Figures 5A/B. SEM micrographs of SiC-fiber-reinforced alumina composite at A) 1,000X (left), taken roughly 200 μm below the sample surface and B) 5,000X magnification, taken roughly 100 μm below the sample surface (right).

Task 2: Simulation of reactor fluid dynamics and mass transport

Efforts this year focused on the development of mathematical models that predict BN deposition rates and cross-part coating uniformity within a continuous-fiber preform as a function of processing conditions and preform geometry. A one-dimensional model of gas flow, species diffusion, and chemical reaction in a representative preform slab has been formulated. The resulting "continuum" equations are locally averaged over an elementary volume that is small compared to the preform thickness, but large enough to contain many fibers. The model includes both diffusive and advective transport of reactant and product gases, as well as a deposition reaction that is governed by the collision rate of the precusor molecules with the surface and a temperature-dependent sticking coefficient. In the absence of measurements, molecular diffusion coefficients were estimated from known gas properties, fiber diameter and packing, and preform porosity, taking into account the effects of collisions between gas molecules, as well as the collisions with fibers that become dominant at the low pressures used for fiber coating. Owing to the relatively fast kinetics of gas-phase reactions (see Task 1), it is presently assumed that the deposition precursor Cl_2BNH_2 is formed outside the preform. Finally, processing conditions were assumed to be isothermal and quasisteady, the latter assumption justified by the fact that the BN coatings are far too thin to significantly alter the porosity or transport properties.

* Provided by Dr. Ali Fareed, DuPont Lanxide Composites Inc.

Two different approaches were used to solve the quasisteady transport equations: one numerical, the other purely analytical. Both yield profiles of reactant concentration and deposition rate as a function of position within the preform. These solutions depend on only two dimensionless parameters. The first parameter characterizes the relative rates of reaction and diffusion, while the second incorporates the influence of the net gas outflow that occurs when the deposition reaction releases more moles of gas than it consumes. By comparing calculated deposition rates at the edge and center of the preform, the nonuniformity can be obtained as a function of these two parameters. The analytical approach yields this relationship as a closed-form perturbation expansion that accurately predicts small to moderate nonuniformities. This limit is of great practical importance, since larger nonuniformities will degrade the mechanical properties of the finished product.

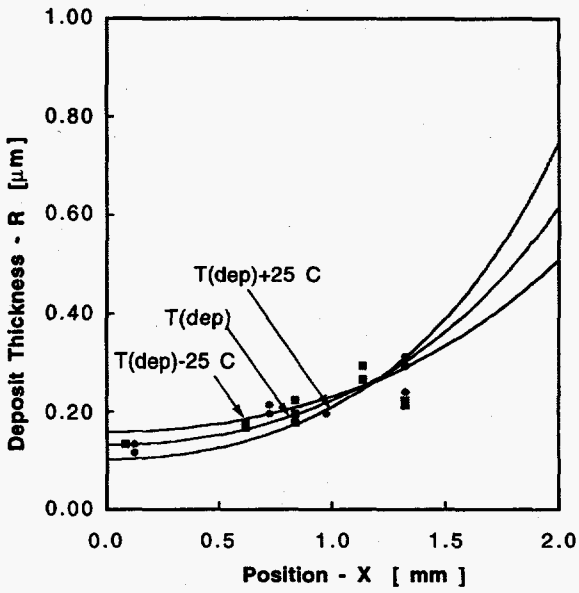

Figure 6. Depth profiles of the predicted BN deposit thickness (solid lines) compared with measurements of coating thickness for each of the two samples (points). The part thickness assumed in the model was 2.65 mm. T(dep) is the reactor temperature.

Predictions of the BN coating thickness were compared with electron micrograph measurements (see Task 1) of deposit thickness for two preforms processed by DLC. As is apparent in Figure 6, the agreement in both coating thickness and uniformity is quite encouraging. The three predictions (solid lines) bracket the temperature range corresponding to the data. These results were obtained by coupling the preform transport model with a one-dimensional analysis of gas transport through the perforated plates that constrain the preform during processing. This analysis showed that the thickness of the plates is large enough to severely inhibit reactant transport and substantially reduce deposition rates within the preform. Comparisons between theory and experiment will be expanded in FY96, both to improve our understanding of the DLC process and to increase our confidence in model predictions.

The primary value of process models lies in their ability to predict operating conditions (temperature, pressure, reactant concentrations, and fixture geometry) needed to produce a desired coating thickness and uniformity in minimum processing time. Thus, modeling efforts in FY96 will be directed toward process optimization and a number of other issues suggested by our colleagues at DLC. These include development of strategies for simultaneous processing of preforms having different thicknesses and geometries as well as extension of the technology to much thicker parts.

PUBLICATIONS

1. M. D. Allendorf, C. F. Melius, P. Ho, and M. R. Zachariah "Theoretical Study of the Thermochemistry of Molecules in the Si-O-H System," accepted, *J. Phys. Chem.*, 1995.

2. M. T. Schulberg, M. D. Allendorf, and D. A. Outka "The Adsorption of Hydrogen Chloride on Polycrystalline β-Silicon Carbide," accepted, *Surf. Sci.*, 1995.
3. T. H. Osterheld and M. D. Allendorf "The Decomposition of Methyltrichlorosilane in Hydrogen and Helium," in *Chemical Vapor Deposition of Refractory Ceramics and Metals III*, M. A. Pickering, B. M. Gallois, and W. Y. Lee, 1995, Eds. vol. 363, (Mat. Res. Soc. Symp. Proc., Pittsburgh), p. 27.
4. M. D. Allendorf and T. H. Osterheld "Modeling the Gas-Phase Chemistry of Silicon Carbide Formation," in *Chemical Vapor Deposition of Refractory Ceramics and Metals III*, M. A. Pickering, B. M. Gallois, and W. Y. Lee, Eds., 1995, vol. 363, (Mat. Res. Soc. Symp. Proc., Pittsburgh), p. 39.

PRESENTATIONS

1. T. H. Osterheld and M. D. Allendorf "Gas-Phase Kinetics of Methyltrichlorosilane Decomposition: Experiment and Modeling," Annual Meeting of the AIChE, San Francisco, November, 1995.
2. T. H. Osterheld and M. D. Allendorf "The Decomposition of Methyltrichlorosilane in Hydrogen and Helium," Fall Meeting, Materials Research Soc., Boston, November, 1995.
3. M. D. Allendorf and T. H. Osterheld "Modeling the Gas-Phase Chemistry of Silicon Carbide Formation," Fall Meeting, Materials Research Soc., Boston, November, 1995.
4. M. T. Schulberg, M. D. Allendorf, and D. A. Outka "The Reaction of HCl with Polycrystalline β-SiC: Implications for the CVD of SiC from Chlorine-Containing Precursors," presented at 1995 March meeting, Division of Materials Physics Focused Sessions, American Institute of Physics.
5. T. H. Osterheld and M. D. Allendorf "The Gas-Phase Chemistry of Titanium Boride Formation. The Decomposition of $TiCl_4$ and BCl_3 in Hydrogen and Helium," presented at the Spring Meeting of the American Chemical Society, Anaheim, April 1995.
6. M. D. Allendorf, S. Griffiths, D. R. Hardesty, T. Headley, C. F. Melius, R. Nilson, T. H. Osterheld, N. Yang "Materials Processing by Design: Optimization of CVD Processes," Annual Review Meeting of the DOE/Advanced Industrial Materials Program, Washington, D. C., June, 1995 (poster and presentation).

HONORS AND AWARDS: None during this reporting period.

PATENTS/DISCLOSURES:

1. M. D. Allendorf, D. A. Outka, and M. T. Schulberg, "The Adsorption of Hydrogen Chloride by Polycrystalline β-Silicon Carbide," Disclosure of Technical Advance, 6/9/95.

LICENSES: None during this reporting period.

INDUSTRIAL INPUT AND TECHNOLOGY TRANSFER: Technical discussions were conducted with ceramic materials manufacturers and potential end-users in the float-glass, fiberglass, and paper industries to provide an understanding of Sandia capabilities in process simulation and materials science. Discussions resulted in a short-term research project funded by Libbey Owens Ford Glass Company (Toledo, OH) to investigate the high-temperature behavior of precursors used in the manufacturing of float-glass coatings. This interaction is expected to continue in FY96 at higher funding levels. In addition, extensive interactions with DuPont Lanxide Composites, Inc. (Newark, DE) are continuing and will address both generic and proprietary aspects of fiber-coating processes.

COST SHARING: None.

SYNTHESIS AND PROCESSING OF COMPOSITES BY REACTIVE METAL PENETRATION

Ronald E. Loehman and Kevin G. Ewsuk
Sandia National Laboratories
Albuquerque, New Mexico 87185

Antoni P. Tomsia
Pask Research and Engineering
Berkeley, California 94720

William G. Fahrenholtz
University of New Mexico
Albuquerque, NM 87106

INTRODUCTION

Ceramic-metal composites are being developed as engineering materials because of their high stiffness-to-weight ratios, good fracture toughness, and because their electrical and thermal properties can be varied through control of their compositions and microstructures. Wider use of ceramic-metal composites requires improvements in synthesis and processing so that high-performance parts can be produced more economically. Over the past three years reactive metal penetration has been shown to be a promising technique for making ceramic and metal-matrix composites to near-net-shape with control of both composition and microstructure. It appears that reactive metal penetration could be an economical process for manufacturing many of the advanced ceramic composites that are needed for light-weight structural and wear applications for transportation and energy conversion devices. Near-net-shape fabrication of parts has the additional advantage that costly and energy intensive grinding and machining operations are significantly reduced, and the waste generated from such finishing operations is minimized.

The goals of this research and development program are: 1) to identify compositions favorable for making composites by reactive metal penetration; 2) to understand the mechanism(s) by which these composites are formed; and 3) to control and optimize the process so that composites and composite coatings can be made economically.

TECHNICAL PROGRESS: FY 1995

Summary

This work is based on the discovery by R.E. Loehman of SNL and A.P. Tomsia of Pask Research and Engineering that when molten aluminum is placed in contact with a dense mullite preform it infiltrates the ceramic and converts it to a composite. Analysis showed that their composite consisted of a co-continuous network of Al_2O_3 ceramic and Al-Si alloy. Further work revealed that this technique is a general route to composite synthesis with the prospect for near-net-shape processing.

Generally, reactions between Al and oxides are of the form;

$$(2 + x)\ Al + (3/y)\ MO_y \rightarrow Al_2O_3 + Al_xM_{3/y} \qquad (1)$$

where MO_y can be either a simple binary or complex oxide, and the residual metal phase can take a variety of forms as determined by the phase equilibrium relations of the given system. Reactive penetration has been shown to produce composites in a number of oxide-metal systems for which there is both favorable wetting of the oxide by the molten metal (i.e., contact angle $\theta < 90°$) and a negative Gibbs energy for reaction.

In the Al/mullite system, molten aluminum reduces mullite to produce alumina and elemental silicon according to the reaction,

$$3\ Al_6Si_2O_{13} + (8 + x)\ Al \rightarrow 13\ Al_2O_3 + 6\ Si + x\ Al \qquad (2)$$

For the reaction with x=0, $\Delta G_r(1200K) = -1014$ kJ and $\Delta G_r(1600K) = -828$ kJ.
With excess aluminum present (i.e., $x > 0$), a composite of alumina, silicon, and aluminum is formed. When the mullite preform is in contact with a large external source of molten Al, the Si produced from the reaction diffuses outward into the Al source, leaving only a small concentration in the composite. Thus, the process naturally avoids leaving significant amounts of Si that could embrittle the composite.

Ceramic-metal composites have been produced by reactive penetration of dense and porous ceramic preforms with molten metal and by reactive sintering or hot pressing mixtures of ceramic and metal powders. Experimental results on different compositions of ceramic-metal reaction couples indicate that reactive metal penetration can be a general route to composite synthesis. Additionally, in many systems, reactive metal penetration affords near-net-shape forming capability. Ceramic-metal composite coatings can be made by controlling the penetration time.

Making composites with physical properties optimized for particular applications is one of the potential benefits of the reactive metal penetration process. For composites in the Al_2O_3/Al/Si system, improvements in Young's modulus, fracture strength, density, hardness, fracture toughness, and specific modulus are apparent as compared with the pure mullite preform, as shown in Table 1. The fracture toughness of reactively-formed ceramic-metal composites increases with increasing Al concentration, while modulus and density remain relatively constant, making it possible to make materials that are both tough and have a high specific modulus (i.e., modulus/density).

Table 1. Properties of Ceramic-Metal Composites Formed by Reactive Metal Penetration Compared to the Properties of the Ceramic Preform

Property	**Mullite**	**Al_2O_3-Al-Si Composite**
Bend Strength(MPa)	180	250-320
Hardness (GPa)	11.2	10-11
Toughness (MPa • $\sqrt{m}$)	1.7	6-9
Density (g/cc)	3.16	3.6
Young's Modulus (GPa)	200	274
Specific Modulus(GPa•cm^3/g)	63	76-86

Mechanical and physical property data, as well as microstructural evidence, indicate a three-dimensional, alumina skeletal structure is formed during reactive penetration. For higher Al concentrations the Al phase also is continuous, resulting in a composite with mutually-interpenetrating metal and ceramic phases. Results also indicate that, relative to the ceramic preform, the composites are more flaw tolerant; that is, the strength degradation from crack formation and propagation appears to be less severe in the ceramic-metal composite than in the mullite preform. With further development, improvements in strength and fracture toughness can be expected.

Milestones:

Work this year has focused on Tasks 1, 2, 3, and 5 of the Field Work Proposal.

Task 1. Evaluate Mechanisms of Composite Formation in the Al/Mullite System

We have continued our experiments to understand the mechanism for reactive metal penetration. By combining TEM results on microstructural development with previously obtained thermodynamics and kinetic data, we have been able to develop a likely reaction mechanism for reactive metal penetration. As reported previously, the concentration of oxygen in the system (P_{O_2}) during reaction plays a critical role. At 1200K, there is a large thermodynamic driving force for reaction (2) to proceed as written (i.e., ΔG_r = -1014 kJ). However, there is also a large thermodynamic driving force for reaction of aluminum with atmospheric oxygen to form alumina at 1200K (i.e., ΔG_r = -1163 kJ/mole). The Ellingham diagram for Al/Al_2O_3 indicates that Al and alumina will be in equilibrium at a P_{O_2} of $10^{-28.5}$ atm., which is a condition favorable for wetting. Thus, to limit Al oxidation by atmospheric oxygen and to ensure the Al/mullite reaction proceeds as written in reaction (2), a system P_{O_2} of $\leq 10^{-28.5}$ atmospheres is required. It seems likely that the molten Al itself acts as an O_2 getter during the reaction to reduce the P_{O_2} of the mullite grain boundaries to $\leq 10^{-28.5}$ atmospheres, which will make conditions favorable for wetting and reaction. The optically-visible reaction layer formed during partial penetration can be attributed to the localized oxygen deficiency and initial precipitation of metal particles at the grain boundaries. The time required to reduce grain boundary oxygen concentration to $\leq 10^{-28.5}$ atmospheres can explain the 5 - 10 minute delay in penetration at the start of an experiment. Finally, localized grain boundary reduction also explains the difference in penetration of dense and porous mullite preforms. It appears that, because oxygen diffusion through an interconnected pore structure is faster than along grain boundaries, it is more difficult to achieve a favorable P_{O_2} condition for wetting and reaction in a porous mullite body.

To characterize wetting and penetration in the Al/mullite system, sessile drop experiments were conducted with high purity, molten aluminum on dense mullite at 900, 1000, and 1100°C. Contact angles decrease with time at 900°C and above. Because of metal penetration and reaction, the molten Al drop decreases in volume during the experiment. The absence of a steady-state contact angle is indicative of an on-going chemical reaction. XRD analysis shows the infiltrated specimens contain Al_2O_3, Al, and, usually Si, demonstrating that

the reaction is the same whether the product is formed by reaction of mixed powders or by penetration of Al into the dense ceramic. Sessile drop experiments conducted on nominally 100%, 99.5%, and 99% pure, dense mullite (with the remainder as SiO_2) at 1100°C reveal no significant differences in wetting behavior with minor compositional variations in the ceramic preform. Wetting (i.e., $\theta < 90°$) is not observed at 900°C and it occurs only after ~30 minutes at 1000°C in the Al/mullite system. Aluminum penetration and composite formation are sluggish below ~1000°C, indicating that both wetting and a negative Gibbs energy of reaction are required to make ceramic-metal composites by reactive metal penetration.

To more quantitatively determine the kinetics of ceramic-metal composite formation in the Al/mullite system, an apparatus was designed and constructed for making ceramic-metal composites by controlled dipping of ceramic preforms in molten aluminum. Reaction times were accurately controlled by dipping a dense ceramic preform into molten aluminum at 900-1500°C for a prescribed time, and then removing it. The reacted samples were sectioned, and the thickness of the composite layer formed was measured by optical microscopy. There is a 5-10 min. induction time for Al penetration and reaction with mullite. The rate of ceramic-metal composite formation in the Al/mullite system is proportional to the square root of time for short reaction times (<1 hr) and is linearly proportional to time for longer reaction times. As expected, composite formation rate also increases with temperature up to 1150°C but then exhibits a surprising decrease with increasing temperature between 1150 and 1500°C. The exact temperature of the maximum rate of composite formation depends on the preform density. Based on the measured penetration distances at given times for different temperatures, an activation energy for composite formation of ~200 kJ/mole was calculated. Although the exact mechanism has yet to be determined, the rate controlling step for reactive metal penetration appears to be the interface reaction.

Scanning and transmission electron microscopic analysis of Al/mullite reaction couples revealed that silicon diffuses out of the mullite ceramic during reactive metal penetration. This observation is also supported by X-ray diffraction analysis and scanning electron microscopy with electron dispersive spectroscopy, which indicated that composites produced by reacting aluminum with mullite are silicon deficient.

In summary, TEM, thermodynamic, and kinetic analyses suggest the following 4-stage reaction mechanism for reactive metal penetration: 1) the metal melts and wets the ceramic preform surface; 2) oxygen diffuses out of the ceramic preform grain boundaries to lower the P_{O_2} to a favorable wetting condition; 3) molten metal penetrates the ceramic preform grain boundaries; and 4) the metal on the grain boundaries reacts with and reduces the individual grains of the ceramic preform.

Impact: By evaluating reactions to understand the mechanisms of composite formation by reactive metal penetration, we are establishing guidelines to control composite formation, and to control the structure and properties of composites formed by reactive metal penetration. These guidelines will be the basis for developing a commercial process for manufacturing ceramic-metal composites with tailored properties.

Task 2. Evaluate Other Ceramic-metal Systems

As discussed briefly above, the reactions other than Al/mullite that may produce ceramic-metal composites by reactive metal penetration include:

$$Al_6Si_2O_{13} + 3\,Mo + (8 + x)\,Al \rightarrow 13\,Al_2O_3 + 3\,MoSi_2 + x\,Al$$
$$Al_6Si_2O_{13} + 8Mg \rightarrow 4MgO + 2Mg_2Si + 3Al_2O_3$$
$$(4 + 3x)\,Al + 3\,TiO_2 \rightarrow 2\,Al_2O_3 + 3\,TiAl_x$$
$$(2 + 3x)\,Al + 3\,NiO \rightarrow Al_2O_3 + 3\,NiAl_x$$

We, as well as others, have proposed that refractory ceramic-metal composites can be synthesized in-situ in the Al/TiO_2 and Al/NiO systems according to the reactions listed above. Ti or Ni formation is predicted when x = 0 in the third and fourth reactions above. For x = 1, TiAl or NiAl formation is expected. According to equilibrium thermodynamics, when Al reacts with TiO_2 or NiO, the reactions proceed as written above. However, little is known about the kinetics or microstructural mechanisms of the reactions between Al and either TiO_2 or NiO. Likewise, the possibility of using these reactions to form refractory ceramic-metal composites by melt penetration or reactive hot pressing has not been explored in detail.

The contact angle of Al on TiO_2 was determined as a function of temperature. Figure 1 shows that the contact angle decreases as temperature increases from 1000°C to 1400°C. At 1200°C the contact angle approaches 90° while at 1400°C it reaches 80°, indicating that aluminum partially wets the ceramic. After an equilibration time of less than 10 minutes, the contact angle varies little with time, indicating no further significant reaction at the interface. Figure 2 shows the cross-section of an Al drop on TiO_2 after heating at 1400°C for 75 minutes. No reaction layer was observed for any of the Al/TiO_2 reaction couples, indicating that reactive metal penetration of TiO_2 by Al does not occur under these conditions. Despite not forming a discernible reaction layer, the Al drop strongly adhered to the surface of the substrate. This was true even for contact angles above 90°.

No contact angles were observed for Al on NiO because the aluminum did not become fluid enough to form a uniform sessile drop. Apparently, contact with Al reduced the NiO substrate, and then, due to reaction with the oxygen liberated during the NiO reduction, a thick, stable oxide layer formed on the Al drop during the wetting experiment. The Al, however, did penetrate and react with the NiO. As shown in Figure 3, an appreciable reaction layer developed during the 1400°C contact angle experiment. Samples heated at 1000°C, 1100°C, and 1200°C also showed distinct reaction zones, though penetration depth decreased slightly with decreasing reaction temperature. The reaction layer at the ceramic-metal interface shows that reactive metal penetration is possible in the Al/NiO system; however, much more work needs to be done to develop sufficient understanding for process control.

Al/TiO_2 and Al/NiO powder mixtures were reactively hot-pressed at 1200-1300°C and 34.5 MPa (5000 psi) for 1/2 hr in graphite dies. A compositionally homogeneous, but porous composite of Al_2O_3 and Ti was produced by hot pressing an Al/TiO_2 powder mixture containing x = 0 Al at 1200°C. Preliminary results indicate that it may be possible to produce a dense composite with a higher hot-pressing temperature.

A phase-segregated composite consisting of a central metallic core surrounded by a ceramic shell was produced by reactively hot pressing Al/NiO powder mixtures containing x = 0 and x = 1 Al at 1200°C and 1300°C. X-ray diffraction analysis showed that the metallic core was Ni and NiAl for the x = 0 and x = 1 samples, respectively. The ceramic shell was Al_2O_3 in both cases. The phase segregation of the ceramic and metal phases indicates poor wetting of the Al_2O_3 by the metallic and intermetallic reaction products. A temperature/pressure program was

designed to minimize phase segregation and produce a more favorable condition for wetting so that interpenetrating ceramic-metal composite microstructures can form.

The extension of reactive metal penetration and reactive hot pressing to systems that form alumina-intermetallic composites allows for the preparation of novel composites for a variety of high temperature applications. The advantages of these techniques over existing technology include lower raw material and fabrication costs and a finer-scale, interpenetrating microstructure.

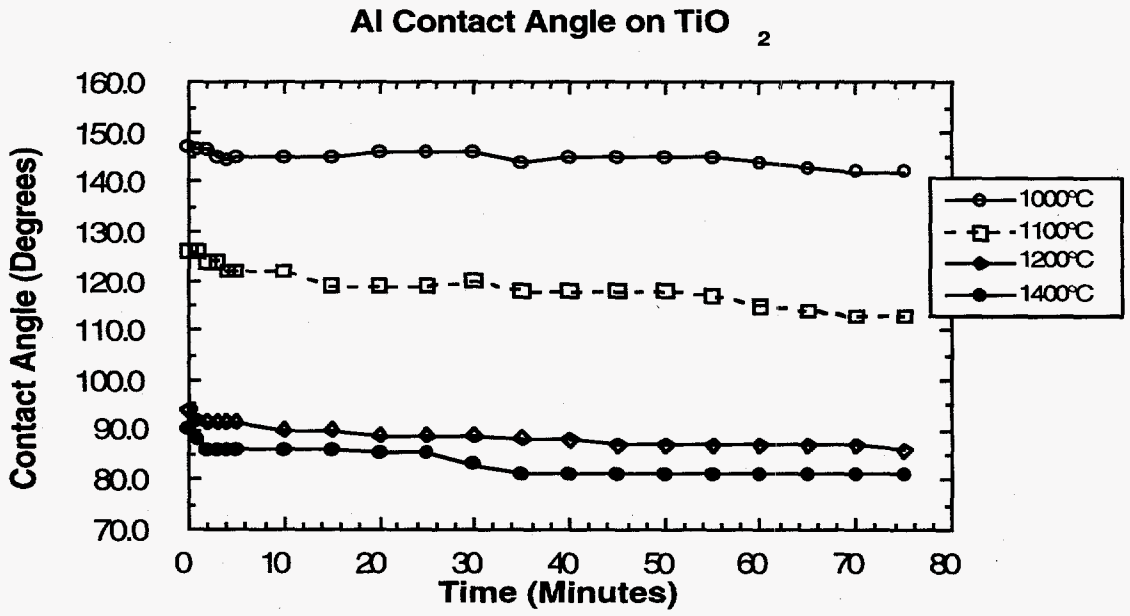

Figure 1. Contact angle as a function of time for Al in contact with TiO_2 at 1000°C, 1100°C, 1200°C, and 1400°C.

Figure 2. Optical micrograph of the cross-section of an aluminum drop on TiO_2 after heat treatment at 1400°C for 75 minutes, note the absence of a reaction layer.

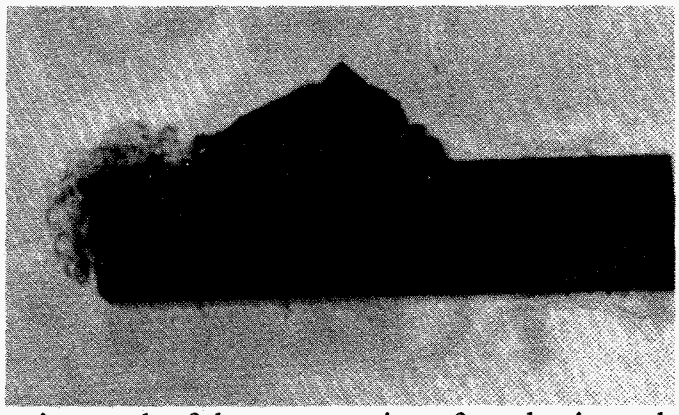

Figure 3. Optical micrograph of the cross-section of an aluminum drop on NiO after heat treatment at 1400°C for 75 minutes, note the presence of a reaction layer.

Cost is perhaps the most important factor in determining the commercial potential of new materials. Advanced composites may offer marked improvement in performance and reliability, but any increase in cost as compared to traditional materials usually prevents significant market penetration. One potential barrier to commercialization that so far has not been addressed in detail in our program is that of raw material cost. Due to the availability, purity, and batch-to-batch consistency of mullite powder as compared to other aluminosilicates, the majority of our work on reactive metal penetration has been carried out using phase-pure mullite preforms. The absence of second phases and trace impurities greatly simplifies the study of reaction mechanism and kinetics as well as the volume and mass balance calculations and thermodynamic predictions. Typically, phase-pure mullite powder sells for ~$25/kg. In a previous technical advance, SD5484 at Sandia, we discussed the advantages of using kaolin, ~$0.10/kg, as a low-cost alternative to mullite.

As with the Al/mullite reaction, initiating the Al/kaolin reaction depends on first forming a ceramic-metal interface. Recent results show that aluminum wets dense kaolin better than mullite, as indicated by a reduced contact angle. The lower contact angle should produce a more uniform ceramic-metal interface and, therefore, a more stable reaction front as the metal reacts with and penetrates into the preform. One indication that the Al/kaolin reaction is kinetically more favorable is that complex shapes are more easily formed from kaolin preforms as compared to mullite. For porous preforms, aluminum must physically infiltrate the pores prior to reaction with the matrix. In this case, the reduced contact angle in the Al/kaolin system means that physical infiltration of the pores can proceed at much lower temperatures than in the Al/mullite system.

Kaolin, $Al_2Si_2O_5(OH)_4 \cdot 2H_2O$, dehydrates to meta-kaolin, $Al_2Si_2O_7$, when heated to 800°C. When heated to the sintering temperature, crystalline mullite, $Al_6Si_2O_{13}$, nucleates and grows within a glassy matrix. A fired kaolin preform is similar to a mullite preform but with a continuous glassy grain boundary phase. The sequential conversion of kaolin to meta-kaolin and then to mullite/silica is detailed in Reactions 3 and 4.

$$Al_2Si_2O_5(OH)_4 \cdot 2H_2O \rightarrow Al_2Si_2O_7 + 4\ H_2O \quad (3)$$
$$3\ Al_2Si_2O_7 \rightarrow Al_6Si_2O_{13} + 4\ SiO_2 \quad (4)$$

Fired kaolin preforms react with aluminum in much the same way as does phase-pure mullite. The reaction is near-net-shape and silicon diffuses away from the reaction front and out of the preform/composite, to produce an Al_2O_3/Al composite. Due to the higher silica content of the preform, composites prepared from kaolin preforms contain more aluminum than those prepared from mullite. The Al/kaolin reaction can be represented as the reaction of aluminum with mullite and silica:

$$(8 + x)\ Al + Al_6Si_2O_{13} + 4\ SiO_2 \rightarrow 7\ Al_2O_3 + 6\ Si + x\ Al \quad (5)$$

Mass and volume balance equations show that stoichiometric reaction of dense kaolin with aluminum produces a composite that contains approximately 30 vol.% Al and 70 vol.% Al_2O_3. This corresponds to an x value of ~ 7 in Reaction 5. The predicted composite density is 3.62 g/cm^3.

As in the Al/mullite reaction, aluminum reacts with porous kaolin to produce dense ceramic-metal composites through a combination of physical infiltration and reactive penetration. Kaolin preforms fired at 1100°C for 3 hours are ~ 61% of theoretical density. After reaction with aluminum, the resulting composite contains 56 vol.% Al, 13 vol.% Si, and 31 vol.% Al_2O_3 . The predicted composite density is 3.05 g/cm^3. The volume and density calculations for reaction of aluminum with dense and porous kaolin are summarized and compared to mullite in Table 2.

Table 2. Al Content and Density of Composites Prepared by Reacting Aluminum with Dense and Porous Mullite and Kaolin.

	Dense Mullite	Porous Mullite	Dense Kaolin	Porous Kaolin
Al Content (vol.%)	17	54	28	56
Density (g/cm^3)	3.75	3.15	3.62	3.05

Figures 4 and 5 plot the contact angle of aluminum as a function of temperature on dense and porous kaolin, respectively. As shown in Figure 4, the contact angle for aluminum on dense kaolin generally decreases with increasing time and temperature, except at 1100°C. At 1100°C, the aluminum drop rapidly penetrates the preform, indicating a maximum in reaction rate near this temperature. Increased reaction is often accompanied by a decreased contact angle. For aluminum on dense kaolin at T ≥1100°C, the contact angle is less than 90°, indicating partial wetting. In comparison, the aluminum contact angle on mullite between 1100 and 1400°C is around 140°. The implication is that aluminum forms a stable interface more rapidly with kaolin than with mullite.

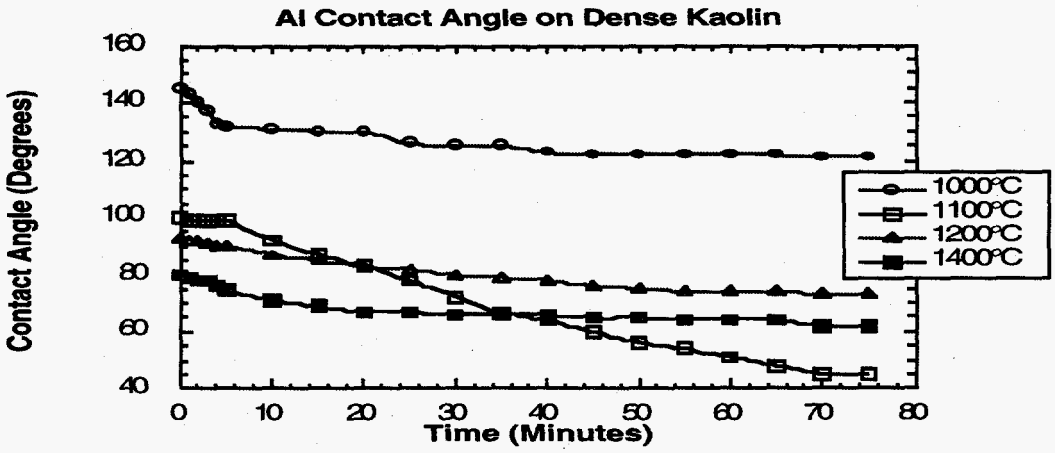

Figure 4. Contact angle of aluminum on dense kaolin.

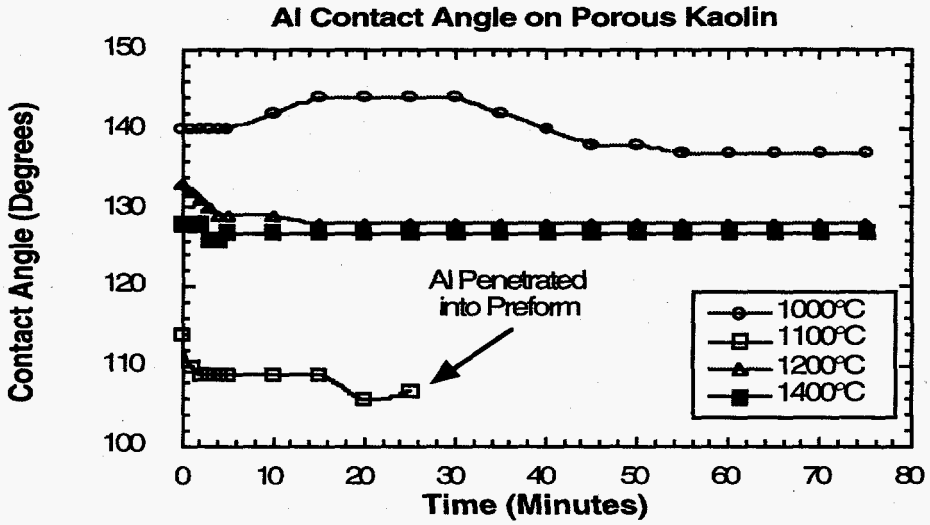

Figure 5. Contact angle of aluminum on kaolin preforms containing 39 vol.% porosity.

The contact angle of aluminum on kaolin increases with increasing preform porosity. Figure 5 shows that the contact angle of aluminum on kaolin containing 39 vol.% porosity (61% dense) is significantly higher than on dense kaolin. As with dense kaolin, the contact angle decreases with increasing temperature except at 1100°C. At 1100°C, aluminum only partially wets porous kaolin, but it rapidly infiltrates the preform and completely within 30 minutes. For porous mullite, the aluminum contact angle is ~ 140° at 1100°C, with no penetration or reaction. A temperature of at least 1500°C is required for aluminum to wet and infiltrate porous mullite.

The 400°C reduction in processing temperature using a kaolin preform will result in significant energy savings during processing, as well as a process more favorable for commercialization.

It is curious that wetting and penetration are best at 1100°C for both dense and porous kaolin. Generally, contact angle decreases with increasing temperature. The fact that contact angle increases above 1100°C for both dense and porous kaolin may be due the formation of a reaction layer between aluminum and kaolin above 1100°C. . Further study is required to determine why 1100°C is such a favorable temperature.

Impact: The discovery that kaolin can be used as a raw material may have enormous impact on the commercialization of ceramic-metal composites. Kaolin, the main mineral constituent of common clay, is a low-cost raw material that is available in nearly unlimited quantities. The ceramic industry prepares huge quantities of clay-based products at a nominal cost per piece. In raw material cost alone, there is nearly a three order-of-magnitude savings for kaolin as compared to mullite, with additional savings due to the fact that kaolin is easier to handle, requires fewer organic processing aids, and requires lower firing temperatures. Combined with the ease of conversion from preform to ceramic-metal composite, the low raw material and processing costs suggest that Al_2O_3/Al composites will be cost-competitive with traditional materials, while offering superior strength and fracture toughness. We are extremely excited about the potential of the Al/kaolin reaction system and are actively pursuing its development.

Task 3. Assess Near-Net Shape Formation by Reactive Metal Penetration

Reaction of Al with mullite can be written as stated in Reaction 2 in the Summary section. The change in volume, ΔV, on reaction can be calculated from the molar volumes, V_m, of reactants and products. In the Al/mullite system, the relevant values in cm^3/mol are: $Al_6Si_2O_{13}$ (135.26), Al (9.99), Al_2O_3 (25.62), and Si (12.00). For the above reaction, assuming $x = 0$ and a dense mullite preform, the predicted volume change after Al penetration, ΔV, is -0.72 cm^3/mole. The fractional volume change on reaction, as calculated below, is -0.0018.

$$\frac{\Delta V}{3\,V_m(Al_6Si_2O_{13})} = \frac{13\,V_m(Al_2O_3) + 6\,V_m(Si) - 3\,V_m(Al_6Si_2O_{13})}{3\,V_m(Al_6Si_2O_{13})} = -0.0018$$

The volume change on reacting Al with commercial mullite-SiO_2 ceramics can be calculated in a similar way by assuming that the molar volumes of the mullite and silica phases in the preform are additive.

With excess Al (i.e., $x > 0$), reactive metal penetration produces a composite of Al_2O_3, Al, and Si whose molar volume depends on the x value in Reaction 2. Net-shape composites also can be obtained with $x > 0$ compositions by adjusting the porosity of the ceramic preform to accommodate the increased volume of Al present in the composite after reaction. For x excess moles of Al, the relative density, ρ_r, of the mullite preform required for no volume change on reaction is

$$\frac{3V_m(Al_6Si_2O_{13})}{13V_m(Al_2O_3) + 6V_m(Si) - xV_m(Al)} = \frac{40.62}{40.55 + x}$$

The aluminum content of ceramic-metal composites prepared by reactive metal penetration of dense preforms is controlled by the silica to alumina ratio of the preform. The predicted aluminum content of the composite as a function of the silica content of the preform is given in Figure 6. This model has been validated by reacting dense aluminosilicate preforms with 28 to 50 wt.% silica and then determining metal content by quantitative stereology and density measurements. Some of the preform compositions tested and their corresponding composite metal contents are shown in Figure 6. By calculation, the upper limit of metal content for reacting a dense silica preform with Al is ~40 vol.%; however, experimentally, 35 vol.% was found to be the upper limit.

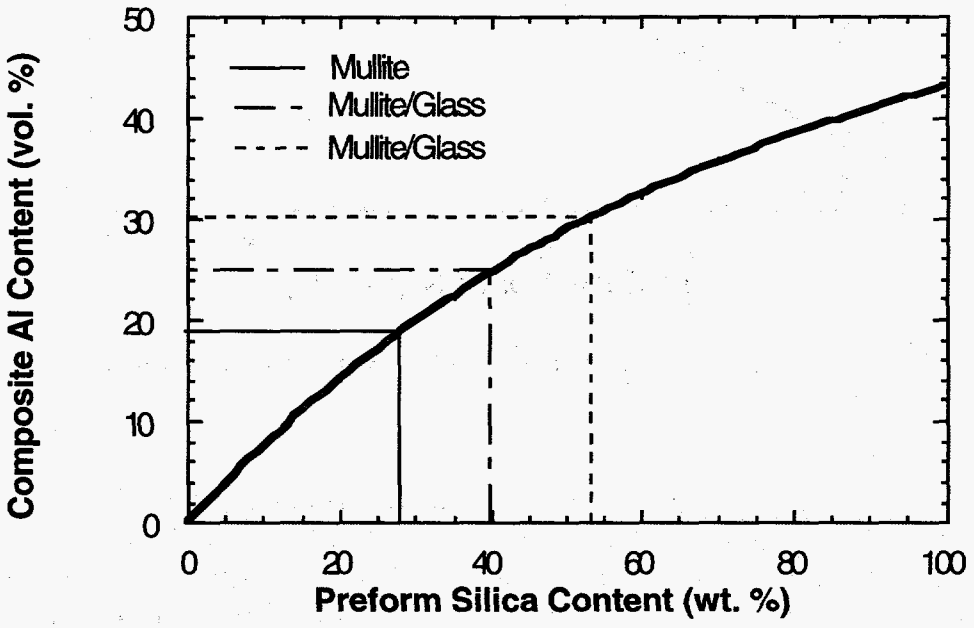

Figure 6. Predicted composite metal content as a function of preform silica content.

Reaction of porous preforms was explored in order to produce composites with higher metal content. Aluminum physically infiltrates the pores of porous mullite preforms and then reacts with the ceramic matrix. The predicted composite metal content increases as the porosity of the preform increases, as shown in Figure 7. This calculation assumes that the reaction is net-shape and that the pores are completely filled with metal. The bulk of our experimental work has been carried out with mullite preforms of 62% relative density, which produce composites that contain 55 vol.% metal. Examination of composite cross-sections by scanning electron microscopy shows that much of the silicon generated during reaction is retained in the composite. This case contrasts with reactive metal penetration of dense preforms in which the silicon diffuses out of the composite during processing.

Impact: The ability to react porous preforms allows us to prepare ceramic-metal composites with controlled metal content, ranging from near 0 to 55 volume percent. This compositional flexibility

will allow the design of composites with properties tailored to specific applications. The compositional range demonstrated for reactive metal penetration is far greater than for other reactive forming techniques used to prepare ceramic-metal composites.

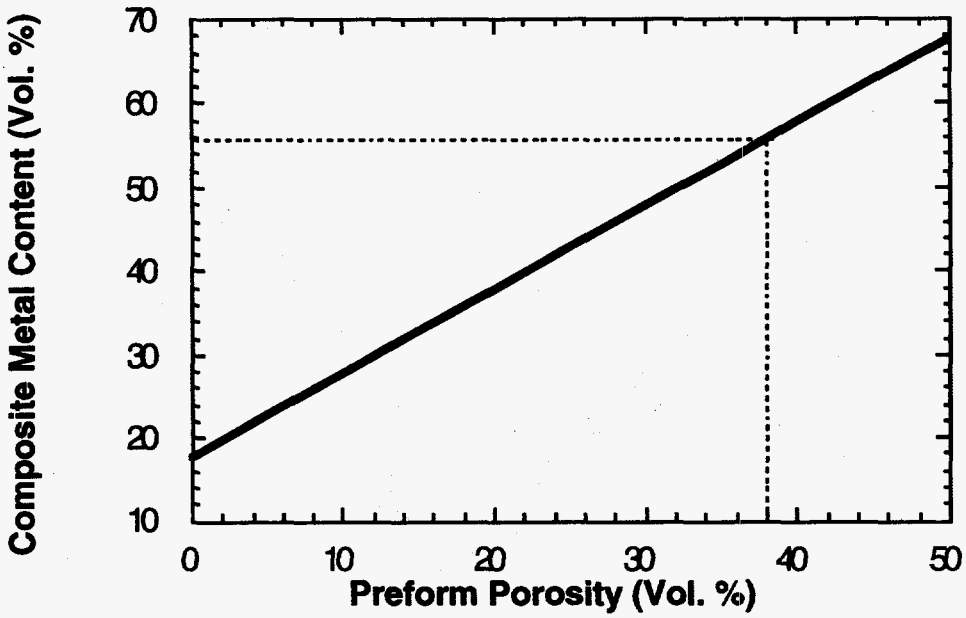

Figure 7. Predicted composite metal content as a function of preform porosity for reaction of aluminum with mullite.

Task 5. Evaluate Ceramic-metal Composite Microstructure and Properties.

The average four-point bend strength for composites with 55 vol.% metal is ~300 MPa, and the Young's modulus is 160 GPa. The strengths of these high metal-content composites are comparable to those of other, lower metal-content composites prepared by reactive metal penetration of dense preforms. The strength is impressive for a composite with such a high metal content, and is attributed to the continuous alumina skeleton. The modulus is significantly lower than the lower metal content composites due to the increased size of the metal ligaments. The increased connectivity of the metal phase can be seen when comparing the fracture surface of a composite containing 55 vol.% metal to one with a lower metal content, as shown in Figure 8. The metal phase is continuous on the fracture surface of the higher metal content composite whereas isolated metal ligaments are seen in the 25 vol.% metal material. In both microstructures, knife-edging is evident, indicating that the toughness of these composites is enhanced by ductile metal toughening. A toughness as high as 9.0 ± 1.1 has been calculated from work of rupture measurements on ceramic-metal composites containing 30 vol.% Al. Work is in progress to determine more precise toughness values for both types of composite.

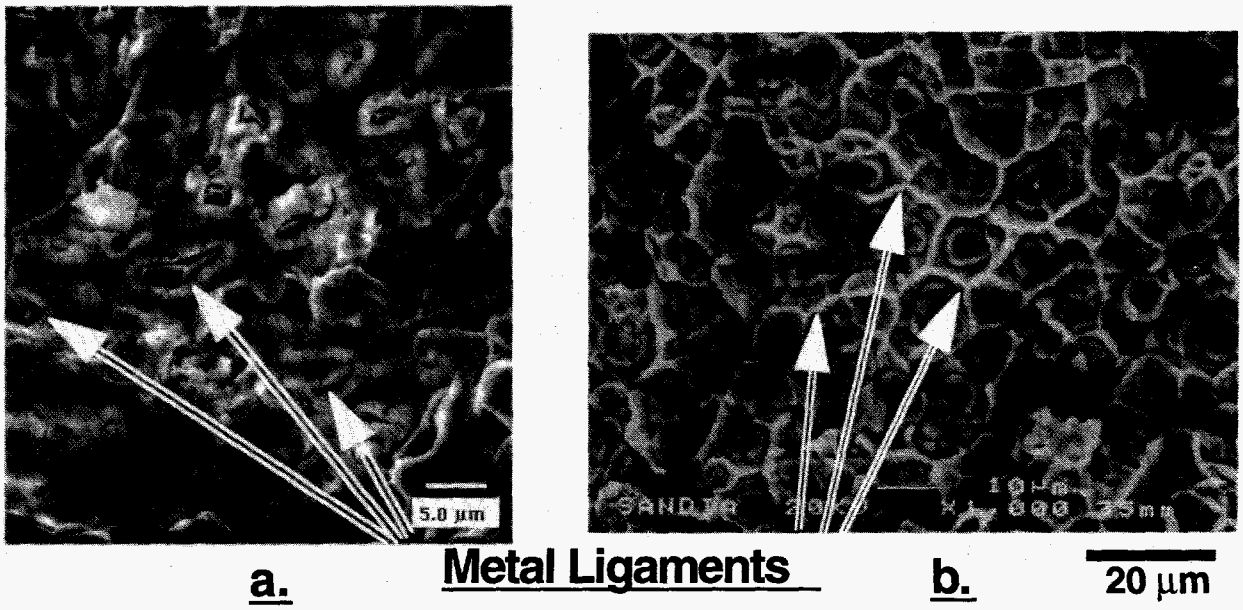

Figure 8. Fracture surface of ceramic-metal composites containing a) 25 vol.% and b) 55 vol.% metal.

The wear properties of a ceramic-metal composite prepared by reactive hot pressing were evaluated by the U.S. Bureau of Mines. The composite was found to have a wear rate of 1.94 x 10^{-3} $mm^3/N•m$, which is slightly less than the values for alumina and silicon nitride. Additionally, the reactively-formed ceramic-metal composite exhibits less brittle microfracture on the abraded surface. These are very positive results since many of our proposed applications require good abrasion resistance.

Impact: We have established a property data base for ceramic-metal composites prepared by reactive metal penetration that will be useful for making comparisons to composites formed by other techniques. The property data base also will be useful in demonstrating the versatility of the reactive metal penetration process for making composites for commercial application.

PUBLICATIONS AND PRESENTATIONS (1/1/95 - 12/1/95)

Journals

1. Y. Gao, J. Jia, R. E. Loehman, and K. G. Ewsuk, "TEM Studies of Ceramic-metal Composite Fabricated by Reactive Metal Infiltration," *J. Matls. Res.* **10** [5], (1995).

2. Ronald E. Loehman, Kevin Ewsuk, and Antoni P. Tomsia, "Synthesis of Al_2O_3-Al Composites by Reactive Metal Penetration," in press, J. Amer. Ceram. Soc.

3. E. Saiz, A. P. Tomsia, R. E. Loehman, and K. G. Ewsuk, "Formation of Al_2O_3-Al Composites by Reactive Metal Infiltration of Mullite," in press, Journal of the European Ceramic Society.

4. W.G. Fahrenholtz, K.G. Ewsuk, R.E. Loehman, and A.P. Tomsia, "Formation of Structural Intermetallics by Reactive Metal Penetration of Ti and Ni Oxides and Aluminates," submitted to Metallurgical and Materials Transactions, March 1995.

5. W. G. Fahrenholtz, K. G. Ewsuk, R. E. Loehman, "Near-Net Shape Processing of Ceramic-metal Composites by Reactive Metal Penetration," submitted for publication, J. Am. Cer. Soc.

6. Kevin G. Ewsuk, S. Jill Glass, Ronald E. Loehman, Antoni P. Tomsia, and William G. Fahrenholtz, "Microstructure and Properties of Al_2O_3-Al Composites Formed by In Situ Reaction of Aluminum and Mullite," submitted for publication in Metallurgical and Materials Transactions, April 1995.

7. Y. Gao, J. Jia, R. E. Loehman, K. G. Ewsuk, and W. G. Fahrenholtz "Microstructure and Composition of Al_2O_3-Al Composites Made by Reactive Metal Penetration," submitted to *J. Matls. Sci.*, July 1995.

Proceedings

1. W.G. Fahrenholtz, K.G. Ewsuk, R.E. Loehman, and A.P. Tomsia, "Synthesis and Processing of Al_2O_3/Al Composites by In Situ Reaction of Aluminum and Mullite," pp. 99-109 in In-Situ Reactions for Synthesis of Composites, Ceramics, and Intermetallics, ed. by E.V. Barrera, et al., The Minerals, Metals, and Materials Society, Warrendale, PA, 1995.

2. D. Ellerby, W. Scott, R. Bordia, K. Ewsuk, and R. Loehman, "Investigation of the Effect of Microstructure on the R-Curve Behavior of Ceramic-metal Composites," Proc. ICCM-10, Whistler, BC, August 14-18, 1995.

3. Y. Gao, J. Jia, R. E. Loehman, and K. G. Ewsuk, "TEM Characterization of Al_2O_3-Al Composites Fabricated by Reactive Metal Infiltration," to be published in "Ceramic Matrix Composites - Advanced High-Temperature Structural Materials," MRS Symp. Proc., **Vol. 365**, Materials Research Society, Pittsburgh, PA (1995).

Presentations

1. K.G. Ewsuk, S.J. Glass, R.E. Loehman, W.G. Fahrenholtz, and D.T. Ellerby, "Microstructure and Properties of Al_2O_3/Al Composites Formed by In Situ Reaction of Al and Mullite," presented at the 124th Annual Meeting of the Metal, Minerals, and Materials Society, Las Vegas, NV, February 15, 1995.

2. W.G. Fahrenholtz, K.G. Ewsuk, R.E. Loehman, and A.P. Tomsia, "Synthesis and Processing of Al_2O_3/Al Composites by In Situ Reaction of Aluminum and Mullite," Presented at the 124th Annual Meeting of the Metal, Minerals, and Materials Society, Las Vegas, NV, February 15, 1995.

3. W. G. Fahrenholtz, S. J. Glass, K. G. Ewsuk, and R. E. Loehman, "Mechanical Properties Al_2O_3/Al Composites Prepared by Reactive Metal Penetration," presented at the 1995 Annual Meeting of the American Ceramic Society, Cincinnati, OH, April 30 - May 4, 1995.

4. B. P. Hansen, W. G. Fahrenholtz, R. E. Loehman, and K. G. Ewsuk, "Influence of Process Variables on Composition and Microstructure of Reactively Formed Composites," presented at the 1995 Annual Meeting of the American Ceramic Society, Cincinnati, OH, April 30 - May 4, 1995.

5. E. Saiz, A. P. Tomsia, R. E. Loehman, and K. G. Ewsuk, "The Effect of Reactive Penetration of Al Into Porous Mullite," presented at the 1995 Annual Meeting of the American Ceramic Society, Cincinnati, OH, April 30 - May 4, 1995.

6. R. E. Loehman (invited), "Ceramic-Metal Interfaces in Reactively Formed Composites," presented at the 1995 Annual Meeting of the American Ceramic Society, Cincinnati, OH, April 30 - May 4, 1995.

7. R. E. Loehman, K. G. Ewsuk, W. Fahrenholtz, and A. P. Tomsia, "Processing and Properties of Al_2O_3/Al Composites formed by Reactive Metal Penetration," presented at the DOE/Advanced Materials Concepts Annual Review, Washington, DC, June 15-16, 1995.

8. D. Ellerby, W. Scott, R. Bordia, K. Ewsuk, and R. Loehman, "Investigation of the Effect of Microstructure on the R-Curve Behavior of Ceramic-metal Composites," presented at ICCM-10, Whistler, BC, August 14-18, 1995.

9. K. G. Ewsuk, R. E. Loehman, W. G. Fahrenholtz, and A. P. Tomsia, "Processing Advanced Ceramic-Metal Composites by Reactive Metal Penetration," presented at Sintering 1995, State College, PA, September 24-27, 1995.

10. B. P. Hansen, W. G. Fahrenholtz, R. E. Loehman, and K. G. Ewsuk, "Composite Formation by Reactive Metal Penetration of Mullite Ceramic Preforms with Al Alloys," presented at the 7th Annual New Mexico ACerS/MRS Advanced Materials Symposium, Albuquerque, NM, October 30, 1995.

11. W. G. Fahrenholtz, K. G. Ewsuk, and R. E. Loehman, "Processing and Microstructure of Ceramic-Metal Composites prepared by Reactive Hot Pressing," presented at the 7th Annual New Mexico ACerS/MRS Advanced Materials Symposium, Albuquerque, NM, October 30, 1995.

12. B. B. Lakshman, W. G. Fahrenholtz, K. G. Ewsuk, and R. E. Loehman, "Reactivity and Microstructures at Mg-Ceramic Interfaces," presented at the 7th Annual New Mexico ACerS/MRS Advanced Materials Symposium, Albuquerque, NM, October 30, 1995.

13. W. G. Fahrenholtz, K. G. Ewsuk, R. E. Loehman, "Processing and Properties of Reactively-Formed Alumina-Metal and Alumina-Intermetallic Composites," to be presented at the 1995 American Ceramic Society Pacific Coast Regional Meeting, Seattle, WA, November 1-3, 1995.

14. W. G. Fahrenholtz, K. G. Ewsuk, R. E. Loehman, "Processing and Properties of Reactively-Formed Alumina-Metal and Alumina-Intermetallic Composites," to be presented at the 1995 American Ceramic Society Pacific Coast Regional Meeting, Seattle, WA, November 1-3, 1995.

15. S. J. Glass, K. G. Ewsuk, and W. G. Fahrenholtz, "Mechanical Properties and Reliability of Al_2O_3/Al Composites Formed By Reactive Metal Penetration," to be presented at the 1995 American Ceramic Society Pacific Coast Regional Meeting, Seattle, WA, November 1-3, 1995.

16. D. Ellerby, W. Scott, R. Bordia, K. Ewsuk, and R. Loehman, "Investigation of the Effect of Microstructure on the R-Curve Behavior of Ceramic-metal Composites," presented at the 1995 American Ceramic Society Pacific Coast Regional Meeting, Seattle, WA, November 1-3, 1995.

17. K. G. Ewsuk, W. G. Fahrenholtz, R. E. Loehman, and A. P. Tomsia, "A Comparison of Reactive Processes for Forming Ceramic-Metal Composites," to be presented at the 1995 American Ceramic Society Pacific Coast Regional Meeting, Seattle, WA, November 1-3, 1995.

18. E. Saiz, A. P. Tomsia, R. E. Loehman, and K. G. Ewsuk, "Al-Al_2O_3 Composite Formation by Reactive Penetration of Different Silicon-Based Ceramics," to be presented at the 1995 American Ceramic Society Pacific Coast Regional Meeting, Seattle, WA, November 1-3, 1995.

19. B. B. Lakshman, W. G. Fahrenholtz, A. P. Tomsia, K. G. Ewsuk, and R. E. Loehman, "Synthesis, Composition, and Microstructures of Composites Made by Reactive Penetration of Ceramics by Mg," presented at the American Ceramic Society Basic Science Division Meeting, New Orleans, LA, November 5-8, 1995.

HONORS AND AWARDS

None this reporting period

PATENTS/DISCLOSURES

None this reporting period

LICENSES

None this reporting period

INDUSTRIAL INPUT, TECHNOLOGY TRANSFER, AND OTHER INTERACTIONS

Collaboration with other researchers

We are continuing our collaboration with A.P. Tomsia of Pask Research and Engineering. Dr. Tomsia is the co-discoverer of reactive metal penetration and is contributing significantly to

its understanding and development. Dr. Eduardo Saiz is a visiting scientist working with Dr. Tomsia on the project, supported by Pask Research and Engineering. Dr. Y. Gao of Pacific Northwest Laboratories has continued to collaborate on TEM analysis of composites formed by reactive metal penetration. Professor Ping Lu of New Mexico Institute of Mining and Technology is also providing TEM analysis of reaction zones, supported on a subcontract to the project. Bala Lakshman is a graduate student at the University of New Mexico who is doing a Master's thesis on reactive metal penetration under the direction of Dr. Ronald Loehman. Professor Raj Bordia of the University of Washington provided a graduate student to work on the project during the summer of 1995 at the Advanced Materials Laboratory and throughout the year at U. WA. One of UT (El Paso) Professor Art Bronson's graduate students is working on the project as a co-op student for his MS thesis. We also continued our collaboration with researchers at the U.S. Bureau of Mines to study the wear properties of ceramic-metal composites made by reactive metal penetration. Additionally, John Kaniuk Of Zircoa, Inc. Conducted corrosion tests this year on some of our high metal content composites.

HIGHLIGHTS

The discovery that kaolin can be used as a raw material for the preparation of ceramic-metal composites may have enormous impact on the commercialization of such materials. Kaolin, the main mineral constituent of common clay, is a low-cost raw material that is available in nearly unlimited quantities. In raw material cost alone, there is nearly a three order-of-magnitude savings for kaolin as compared to mullite, with additional savings from the fact that kaolin is easier to handle, requires fewer organic processing aids, and requires lower firing temperatures. The reaction of Al with kaolin is similar to that with mullite, except that kaolin has a higher silica content, which is reflected in the reaction product:
$(8 + x)\ Al + Al_6Si_2O_{13} + 4\ SiO_2 \rightarrow 7\ Al_2O_3 + 6\ Si + x\ Al.$ Thus, kaolin can produce composites with higher Al contents than does mullite, which extends the range of available metal contents using dense preforms. The ease of conversion from preform to ceramic-metal composite and the lower raw material and processing costs using kaolin suggest that Al/Al_2O_3 composites will be cost-competitive with traditional materials, while offering superior strength and fracture toughness.

POLYMERS AND BIOBASED MATERIALS

Chemical Recycling of Mixed Waste Plastics by Selective Pyrolysis

K. Tatsumoto, R. Meglen, and R. Evans

Process Research Branch
Industrial Technologies Division
National Renewable Energy Laboratory
1617 Cole Blvd., Golden, CO 80401

INTRODUCTION

The goal of this work is to use selective pyrolysis to produce high-value chemicals from waste plastics mixtures. Selectivity is achieved by exploiting differences in reaction rates and by the use of catalysis and coreactants. Target wastes are molecular mixtures, such as blends or composites, or mixtures from manufactured products, such as carpets, and post-consumer mixed-plastic wastes.

The experimental approach has been to use small-scale experiments using molecular beam mass spectrometry (MBMS), which provides rapid analysis of reaction products and permits screening of process parameters. These screening experiments permit exploration of many potential waste stream applications for the selective pyrolysis process. After screening, small-scale, fixed-bed and fluidized-bed reactors are used to provide products for conventional chemical analysis, to determine material balances, and to test the concept under conditions that will be used at a larger scale. Computer-assisted data interpretation and intelligent chemical processing are used to extract process-relevant information from these experiments. An important element of this project employs technoeconomic assessments and market analyses of durables, the availability of other wastes, and end-product uses to identify target applications that have the potential for economic success.

TECHNICAL PROGRESS - FY 1995

Summary

Recovery of ϵ-caprolactam from waste nylon-6 carpet is currently the most advanced application under study. A cooperative research and development agreement (CRADA) with AlliedSignal was signed in 1994 because of the successful results of work done from 1992-1993. AlliedSignal is the major North American

producer of caprolactam and nylon-6 fiber. **Work sponsored by the Advanced Industrial (AIM)** Materials Program since 1990 has lead to a patent which was issued in June 1993 and is the basis for this CRADA. As a result of the AIC work, a complimentary project to develop the engineering-scale of this process was undertaken with the Waste Materials Management Division (WMM) in 1993. The WMM project includes optimizing the process at the small engineering-scale level using a 10-cm fluidized-bed reactor and obtaining data for the design and construction of a 25-50 kg/h circulating fluidized-bed reactor. The WMM project is the major DOE contributor to the CRADA. This new NREL/DOE facility will be available for subsequent applications of the AIC selective pyrolysis recycling technology.

Two years ago a major chemical impurity was identified. Product containing excessive amounts of this impurity failed the accepted industrial standard. Therefore, efforts have been focussed on reducing this impurity to acceptable levels, and thereby minimizing the number of steps for caprolactam purification. The use of CO_2 as a carrier gas was found to reduce the production of the impurity. Also, a purification method to remove this impurity using CO_2 was discovered. At the same time, more emphasis was placed on improving the catalyst, and also the catalyst composition and performance were studied in detail. Progress has been made using more realistic process feedstocks. Experiments using clean post-industrial carpet and dirty, post-consumer carpet have been completed. The yield and purity of caprolactam have improved greatly. The forms in which carpet is feed to the reactor were found to affect kinetics, yields, and product purity. Therefore, studies were undertaken to explore the impact on process chemistry of the varying feedstock forms and feeding techniques. New robust feeding technique and system were established that would handle any variations of the feedstocks. Because of the current budget uncertaintity, technoeconomic evaluations were done on our process and a competing hydrolysis process. The fate of waste nylon-6 carpet recycling project will be decided based on this result and the decision of AlliedSignal, whether to continue the CRADA.

Although considerable time was spent on the support of AlliedSignal CRADA, progress was made in FY 1995 in the other major areas: recovering diamines from the isocyanates and high-value oxygenates from the polyols in waste polyurethane (PU); recovering dimethylterephthalate from wastes containing polyethylene

terephthalate (PET); and recovering bisphenol A from waste containing polycarbonate (PC). In the PU process, there are significant safety considerations in this process because one of the products is toxic. Procedures to eliminate possible chemical exposure and to periodically test for the exposure were developed. Bench scale testing has begun so that conventional chemical analysis and material balances can be done. More catalysts were tested to improve the yields of diamines from the isocyanates. Also, studies to improve process selectivity to produce high-value oxygenates from the polyol were emphasized. A discussion with General Motors and the American Plastics Council about the application of selective pyrolysis to both autoshredder residue and to potential dismantling streams continues. In the PET application, experiments were performed to test the feasibility of recycling polyester fibers for the textile industry. The discussions with Angelica Uniform Group and the American Apparel Manufacturer's Association were held on recycling polyester fiber from their cutting wastes. The PC research continues to improve the bisphenol A yield from plastic mixtures containing polycarbonate that come from the electronics industry. Several plastic samples from the post-consumer computer were obtained and evaluated.

The second component to this work is the development of the intelligent chemical processing system. The primary goal of this project is to provide researchers with a suite of multivariate data analysis tools which can be used for computer-assisted interpretation of our growing MBMS database. One difficulty in multivariate data analysis has been that several steps are required to apply these tools to MBMS spectra. The objective has been to create a seamless graphical interface that would afford non-expert users easier access to these data analysis tools. A single module program to perform principal component analysis and display the graphical results has been written. A graphical user interface has been written to take a newly-acquired spectrum of an unknown substance and display its multivariate similarity to other previously stored spectra. These advances have brought us closer to the objective of a seamless on-line multivariate data analysis system. A data set of 500 experiments has been built to demonstrate quantitative analysis of carpet mixtures and to screen catalysts for converting nylon-6 to caprolactam.

Milestones

1. Assessment of the Recovery of Chemicals from Polyurethane Foam, (December 1994).

The goal of this project was to use the temperature programmed, catalytic thermal processes to convert polyurethane foams from automobile seat cushions into useful monomers or chemicals. Polyurethane comprises a major fraction of autoshredder residue. The flexible foam chosen for this study was a blend of toluene-based diisocyanates and simple polyols. The products were directed toward the diamine rather than the diisocyanate because of the lower toxicity of the diamine. The primary focus of the work has been selection of a catalytic agent, catalyst support and coreactant. Additional work has been undertaken to identify a processing temperature which maximizes yields of the diamine monomer and high-value oxygenated hydrocarbons. The results from the temperature-programmed pyrolysis showed that in the presence of a catalyst/support with steam, the diamine is recovered without any contamination from the polyol. The remaining or unreacted polyol is then recovered when the temperature is raised. A bench scale study showed that approximately 80% of the potential toluenediamine was recovered. The propylene oxide based polyol produced mostly allyl alcohol. Work continues on the selectivity study on the polyol and to further improve the yield of diamine.

2. Assessment of Recycling Plastic Components from Cotton Fabric Blends, (April 1995).

Experiments were designed to identify the conditions to produce the monomer, dimethyl terephthalate (DMT), through a transesterification process, from the polyester of polyester/cotton fabrics. Two approaches were examined: our selective pyrolysis process, and a high temperature and pressure transesterification process. The selective pyrolysis process produced esters of terephthalate, dimethyl terephthalate and monomethyl terephthalate, and terephthalic acid as the main products. Under the best conditions, approximately 75% conversion to dimethyl terephthalate was possible without pyrolyzing the cotton. The cotton was turned to char and the second monomer of polyester, ethylene glycol, could not be recovered as a glycol due to further degradation. The high pressure process converted PET to DMT at >85% yield at a temperature of 225°C and pressure greater than 40 atm by transesterification with methanol. Although the cotton was untouched, some

dyes were extracted into the methanol. Futher study on dyes are planned to determine which dyes are extractable in our process. A preliminary technoeconomic assessment based on Angelica Uniform Group waste polyester/cotton mill cuttings was evalutated. Chemical recycling of their waste was showned not to be economical due to not enough waste being generated and the cost of transporting waste to a central processing site. Because of the interest shown by the American Apparel Manufacturer's Association, which has more cotton waste than cotton/polyester, work continues with emphasis to recover valuable chemicals from the cotton.

3. Demonstration of Quantitative Analysis Robustness, (May 1995).

Previous test have shown that MBMS can be used to obtain quantitative estimates of mixed plastics. Several experiments were done to test the accuracy and day-to-day variability of multivariate calibration models for mixed plastics quantitative analysis. Multivariate modeling was performed using the technique of Projection to Latent Structures (PLS). Mixtures of seven analytes were used to calibrate the instrument over several months. Calibration models constructed on different days are capable of quantifying with accuracy of 7-10%. Experiments performed on separate days over several months indicate that separate calibrations must be performed each day. In addition, instrumental performance changes can have a significant adverse effect on the model accuracy.

4. Assessment of the Recovery of Bisphenol A from Polycarbonate Blends, (September 1995).

This milestone assessed the feasibility of recycling polycarbonate from engineering blends and epoxies. The objective was to identify and improved the conditions to produce the monomer, bisphenol A, from polycarbonate/polystyrene or polycarbonate/acrylonitrile-butadiene-styrene blends. The general conditions to produce the highest yields of bisphenol A from the polycarboante were determined. The conditions involved the use of low concentrations of acid or base with steam or ammonium hydroxide. To improve the selectivity and kinetics of the process, transition metal salts and oxides were tested. A process involving the transition metal oxides was found to produce bisphenol A from polycarbonate at yields greater than 85%. This process required ammonia as a coreactant to lower the pyrolysis temperature of polycarbonate

so that the bisphenol A was produced without pyrolyzing the second component containing the styrene. Enginering experiment of this process showed promissing results. The preliminary technoeconomic assessment based on a large available and collectable feedstock scenario showed that the cost to manufacture bisphenol A from the selective pyrolysis process is lower than the equivalent commercial manufacturing cost.

PUBLICATIONS

Detailed publications in this project have been delayed because U.S. and foreign patents are still in progress, and because of CRADA-protected information. Technical briefs were issued on this work by the Office of Industrial Technology, DOE, and NREL.

K. Tatsumoto, C.C. Elam, M.J. Looker, and R.J. Evans, "Tertiary Recycling of Waste Polyurethane Car Seat Foam," Proc. of the Polyurethane 1995 Conferences, September 1995, pp 270-274.

PRESENTATIONS

S. Kelley, R. Evans, K. Tatsumoto, C. Elam and H. Chum, "Innovative Approaches to the Chemical Recycling of Mixed Waste Plastics." An oral presentation by S. Kelley at the IEEE Workshop, Yorktown Heights, NY, October 1994.

C.C. Elam, R.R. Meglen, K. Tatsumoto, R.J. Evans and H.L. Chum, "The Application of Molecular Beam Mass Spectrometry to the Problem of Plastics Recycling Through Intelligent Chemical Processing." A paper and poster presentation at the MBMS Workshop, Estes Park, CO, October 1994.

S. Kelley, R. Evans, K. Tatsumoto, C. Elam and H. Chum, "Innovative Approaches to the Chemical Recycling of Mixed Waste Plastics." An oral presentation by S. Kelley at the Electronic Products Disposition Workshop, Austin, TX, January 1995.

K. Tatsumoto, C.C. Elam, M.J. Looker, and R.J. Evans, "Chemical Recycling of Mixed Waste Plastics by Selective Pyrolysis." An oral by S. Kelley and poster presentation by K. Tatsumoto at the AICD Materials Program Annual Review, Washington, D.C., June 1995.

K. Tatsumoto, C.C. Elam, M.J. Looker, and R.J. Evans, "Selective Pyrolysis of Mixed Waste Plastics" An poster presentation by K. Tatsumoto at the Frontiers of Pyrolysis Conference, Breckenridge, CO, June 1995.

R.R. Meglen, C.C. Elam, and R.J. Evans, "Chemometrics, Information Extraction and Pyrolysis,." A oral presentation at the Frontiers of Pyrolysis Conference, Breckenridge, CO, June 1995.

R.J. Evans, "Innovative Approaches to the Chemical Recycling of Plastics." An invited oral presentation at the 1995 Gordon Research Conference on Fiber Science, New London, NH, July 1995.

K. Tatsumoto, C.C. Elam, M.J. Looker and R.J. Evans, "Tertiary Recycling of Waste Polyurethane Car Seat Foam," A poster presentation by K. Tatsumoto, Chicago, IL, September 1995.

PATENTS/DISCLOSURES

Patent applications have been filed which are directed to the following embodiments:
Controlled catalytic and thermal sequential pyrolysis and hydrolysis of polymer waste comprising of:

I. A process of producing caprolactam from nylon 6.
II. A process for producing caprolactam and hydrocarbons from mixtures of nylon 6 and polyolefins.
III. A process for producing terephthalic acid or its esters along with by-products from PET and PE.
IV. A process for producing amines, isocyanates, etc. from polyurethanes.
V. A process for producing terephthalic acid, styrene or mixtures of these two from PVC, PET, polystyrene and polyethylene.
VI. A process for producing amines, isocyanates, HCl or mixtures of the same from PVC and PU.
VII. A process for producing styrene, phenols, etc., from polystyrene and polyphenylene oxide.
VIII. A process for producing phenols, hydrocarbons, etc. from polycarbonates and acrylonitrile butadiene-styrene polymers.

Patents were issued for I (U.S. Patent 5,216,149) and VII (U. S. Patent 5,300,704). The rest are pending.

INDUSTRIAL INPUT AND TECHNOLOGY TRANSFER

The CRADA agreement with AlliedSignal has been the major technology transfer activity this year. Metings were held quarterly to discuss progress, accomplishments and future works. The CRADA has helped to better define the goals of this work sponsored by the AIM Materials Program, the complimentary work sponsored by the Polution Prevention Program, and the work that will be done by AlliedSignal. AlliedSignal's efforts involve waste carpet collecting, sorting, and feed preparation methods, the product purification process, and the technoeconomic analysis of the process.

A meeting was held at Angelica Uniform on the polyester recovery from their cotton/polyester fabrics. Subsequently a meeting was held with the representatives from the American Apparel Manufacturer's Association on a possible research agreement. Other technology transfer activities have come from the meetings listed above. Computer part samples were obtained from AT&T and Mike Biddle & Associates to study the polycarbonate to bisphenol A process. GM has continued to express interest in using this technology for their autoshredder wastes problem. Additionally, NREL researchers have discussed this technology with representatives of the American Plastics Council in a broader context.

ESTIMATED ENERGY SAVINGS

An economic impact is expected from this AIM nylon 6 carpet recycling technology. About 2 million tons of carpet waste is generated annually in the United States and about one-fourth of the total waste carpet is made of nylon-6. When successfully implemented through the year 2010, the selective pyrolysis of waste carpet could result in reducing electricity consumption by approximately 1,650 billion BTUs and reducing petroleum consumption by 340,000 billion BTUs because up to 500 million pounds of caprolactam will not have to be produced from imported oil.

HIGHLIGHTS

In FY 1995, several major accomplishments were achieved:

1) improvement in the waste nylon-6 carpet recycling process which lead to reduction in the impurity and possible alternate purification process;

2) demonstrate the robustness of the 10-cm fluidized-bed reactor to handle varying carpet feedstock;

3) demonstrate the production of high value chemicals from PU foam;

4) demonstrate the ability to produce high value monomer from polycarbonate; and

5) discussions with the American Apparel Manufacturer's Association which might lead to a possible research agreement.

This project continues to attract a high level of interest from industry. Future collaborations between OIT, or other DOE offices, and relevant industrial partners, such as the American Plastics Council, will likely be based on this work for the Advanced Industrial Materials (AIM) Program.

Composites and Blends from Biobased Materials

Stephen S. Kelley, Principal Investigator
Industrial Technologies Division
National Renewable Energy Laboratory
1617 Cole Blvd.
Golden, CO 80401

INTRODUCTION

The program is focused on the development of composites and blends from biobased materials that are useful as membranes, high value plastics, and lightweight composites. Biobased materials include: cellulose derivative microporous materials, cellulose derivative copolymers, and cellulose derivative blends. This year's research focused on developing an improved understanding of the molecular features that control the permselective properties of gases through cellulose derivatives. Additional efforts were also focused on understanding the solubility and phase behavior of cellulose esters that are typically used for membrane applications. Understanding these molecular level features of the polymers allows for the preparation of gas separation membranes with improved properties. Some efforts were also devoted to understanding the permselective properties and molecular motions of a novel class of ultra-high permeability polymers, poly(1-trimethylsilyl-1-propyne).

TECHNICAL PROGRESS

An improved understanding of the fundamental features that control gas permeation and polymer phase behavior has allowed for the preparation novel cellulose ester membranes. This work was conducted in collaboration with researchers at the National Science Foundation's Center for Separations Using Thin Films at the University of Colorado at Boulder. Additional work on novel membrane systems was also conducted in collaboration with researchers at Los Alamos National Laboratory (LANL).

I. Microporous Cellulose Ester Membranes.

Microporous cellulose esters membranes, primarily cellulose acetate (CA), are currently viewed as the standard polymeric material used for the preparation of microporous gas and liquid separation membranes. Cellulose acetates have a good combination of high selectivity1, reliable processing, good mechanical properties, and relatively low cost. This combination of properties is the basis of two significant commercial membrane applications, gas separation membranes, primarily for the separation of carbon dioxide/methane CO_2/CH_4, and reverse osmosis membranes. In spite of these desirable properties, CA membranes also have some limitations. A primary limitation is the long term stability of microporous CA membranes that are subjected to high use pressures.

At the high pressures (800-1,000 psi) found in a typically found in natural gas separation applications, microporous CA membranes slowly collapse from an open, spongy structure into a dense low porosity film. This collapse, or compaction, lowers the flux of CO_2 and decreases the effectiveness of the membrane system.

Research efforts in the preparation and characterization of novel cellulose derivative microporous materials have focused on organic/inorganic hybrid (OIH) composites and cellulose ester blends.

---

1 Selectivity is defined as the ratio of the permeabilities of two components exposed to the membrane under identical conditions.

We have prepared a number of homogeneous blends from a variety of cellulose esters and phenolic polymers. We have also demonstrated the ability to prepare CA OIH materials with wide variations in morphologies by controlling the chemical reactions and film preparation conditions. These morphologies include microscale (nanometers) phase-separated and macroscale (microns) phase-separated materials.

Ia. CA OIH Membranes - The goal of this research is to develop a fundamental understanding of the relationships between the inherent properties of a material, e.g., mechanical strength and solubility properties, the processes used to form a microporous membrane, and the long-term performance of membranes under realistic use conditions, e.g., high pressure and plasticizing gases.

To assist with the characterization of CA-OIH materials, researchers at Dow Chemical evaluated the mixed gas permselective properties of a series of crosslinked CA-OIH membranes. (The solvent resistance and improved mechanical properties of these membranes was demonstrated in 1994.) Dow used 50/50 mixtures of methane and carbon dioxide at 250 psi for these tests. The CA-OIH membranes prepared at NREL showed a significant increase in selectivity (from 25 to 35) and a moderate decrease in flux (from 3.5 barrers to 2 barrers) as compared to the unmodified CA. These results demonstrate the improved selectivity of the crosslinked CA-OIH membranes, which is related to the purity of the gas produced from the membrane system is one of the major limitations of the current CA membrane technology.

Research collaborators at the University of Colorado at Boulder have successfully demonstrated the ability to measure the instantaneous and long-term compaction of CA membranes. Researchers have used very high frequency acoustical reflectometry, a unique analytical technique developed at the University of Colorado, to measure micron level changes in the thickness of the microporous membrane while simultaneously measuring the permselective properties of the membranes under an variety of experimental conditions. This work will allow for the long-term compaction of the membranes to be followed for a variety of CA-OIH membranes prepared with different reaction chemistries and membrane porosities.

Improved permselective properties, along with the increased solvent resistance and mechanical properties highlight the potential for using these materials for membrane applications. In 1994 to assist with the evaluation of the potential commercial utility of these CA OIH materials, NREL entered into a collaborative research agreement with Dow Chemical Company. Dow currently sells CA membrane systems that are used for upgrading natural gas that contains high levels of carbon dioxide and water. Unfortunately, in the middle of 1995 Dow made business decision to stop all research support for their membrane products. Thus, in spite of the initial promising results Dow is not in a position to evaluate additional CA-OIH membranes. In response to this setback NREL as conducted initial discussions with W. R. Grace Membrane Systems to determine their interest in this technology. These discussions confirmed Dow view that compaction resistance and improved selectivity are the keys to increases the effectiveness of CA membrane systems.

Discussions with researchers at Grace, Chevron, and UNOCAL, all confirmed the value and limitations with the current generation of CA membranes. These researchers pointed out that there are three major, new CA membrane-based projects currently underway. One, in India, has been completed and is under-going start-up. This plant will process 400 MMSCF of natural gas with high levels, greater than 30%, of CO2. This plant cost several billion dollars and will double the amount of CA membrane area in service. Two other plants being designed, one by Chevron, and should be in the 100 MMSCF of natural gas size range.

The real advantage of CA membranes for these very large plants appears to be it's low cost and adequate performance properties. It major limitation is compaction and it's ability of handle higher hydrocarbons. These systems operate at 1,000 to 1,200 psi, with 20-30 % CO2, which is very

close to super critical CO2, and depending on the site the natural gas can have significant quantities of non-volatile hydrocarbons. Thus, CA membranes with improved compaction resistance and selectivity would greatly enhanced the cost effectiveness of these plants.

Ib. Cellulose Acetate/Phenolic Polymer Blends

A second approach for increasing the compaction resistance of CA membranes is to increase the mechanical strength, modulus, of the CA material. This approach is similar to that take by membrane manufacturers who have gradually switched from weaker cellulose diacetate to stronger cellulose triacetate. However, the strength of cellulose triacetate is still lower than the membranes manufacturers would like. The approach taken here at NREL has been to increase the strength of the membranes by the addition of a small amount of a second strong polymer. To derive benefits from this approach the mixture of CA and the second polymer must be homogeneous or single phase.

To test this approach a series of homogeneous, single-phase, cellulose ester based blends have been prepared. A wide range of cellulose mixed esters (CME), e.g., cellulose acetate, cellulose acetate propionates and cellulose acetate butyrates, can be mixed with both polyvinyl phenol (PVP), and linear novolac resins. Polyvinyl phenol and novolac resins have very similar chemical compositions, but differ in their free volume and accessibility around the phenolic hydroxyl. Thermal and spectroscopic analysis demonstrated that the CA/PVP blends are all single-phase. These analyses show that the CME/phenolic polymer blends are single phase. Infrared spectra that show shifts in the CA carbonyl stretching vibrations for all of the single phase blends, indicate that hydrogen bonding between the CME carbonyl group and the hydoxyl on the phenolic polymer is responsible for the homogeneous nature of the blends.

The permselective properties of some of these homogeneous blends have been measured with the pure gas system at NREL. These measurements indicate the permselectivity of the membranes is only marginally improved by the addition of up to 30 % of the phenolic polymer. Additional experiments have focused on methods to crosslink the blend components, as was done in the case of the CA-OIH materials, and determine the effect on permselective properties.

II. Preparation of Organic-Inorganic Polymer Membranes.

Building on their experience in the use of OIH materials, researchers at NREL have conducted an initial investigation into the properties of poly(1-trimethysilyl-1-propyne) (PTMSP). This polymer has a silicone side-group attached directly to the carbon polymer backbone. This initial work has resulted in a research collaboration between at Los Alamos National Laboratory (LANL) and the Topchiev Institute (TIPS) in Moscow. Initially this research work will concentrate on the development of pervaporation membranes, using polymeric materials developed at TIPS for the recovery of ethanol from biomass fermentation reactors. This work will is now being funded by the Newly Independent States-Industrial Partnership Program. This work also leverages on-going research at NREL that is focused on the evaluation of pervaporation membranes to improve the performance of bioreactors used to produce ethanol from biomass.

PRESENTATIONS

Kelley, S. S., Myers, M. D, Reinsch, V. P., Miscibility of cellulose acetate/phenolic polymer blends, presented at the International Chemical Conference of Pacific Basins Societies, December 17-22, 1995.

Kelley, S. S., Reinsch, V. P., Characterization of semi-crystalline of poly(hydroxy-alkanoate)/ wood fiber composites, presented at the IUFRO XX World Congress, Tampere, Finland, August 6-12, 1995.

Kelley, S. S., Unique permselective properties of poly(1-trimethylsilyl-1-propyne), invited lecture presented at the A. V. Topchiev Institute, Moscow, Russia, August 1-3, 1995.

PUBLICATIONS

Kelley, S. S., Reinsch, V. P., Characterization of semi-crystalline of poly(hydroxy-alkanoate)/ wood fiber composites, submitted to the Journal of Applied Polymer Science, December, 1995.

Jorgensen, G., Pern, J., Kelley, S., Czanderna, A., Schissel, P., Polymers for Solar Energy Devices , In Functional Polymers for Emerging Technology, R. Arshady, Ed, in press, 1995.

Shojaie, S. S., Rials, T. G., Kelley, S. S., Preparation and characterization of cellulose acetate organic/inorganic hybrid films, J. Appl. Polym. Sci. 1995, 58(8), 1263-1274.

Rivard, C., Moens, L., Roberts, K., Bigham, J., Kelley, S., Starch Esters as Biodegradable Plastics: Effects of Ester Group Chain Length and Degree of Substitution on Anaerobic Biodegradation, Enzyme. Microbial Tech., March, 1995.

HONORS AND AWARDS - In 1995 Dr. Kelley was elected to served as the chairman of the Industrial Board for the NSF Industry/University Cooperative Research Center for Separations Using Film Films at the University of Colorado at Boulder.

PATENTS/DISCLOSURES - None

LICENSES - None

INDUSTRIAL INPUT AND TECHNOLOGY TRANSFER - Researchers at Dow Chemicals, W. R. Grace, Chevron, and UNOCAL, have all confirmed the value and limitations with the current generation of CA membranes. Even with these limitations there are three major, new CA membrane-based natural gas upgrading projects currently underway. One in India is complete and is under going start-up. This plant will process 400 MMSCF of natural gas with high levels, greater than 30%, of CO2. This plant cost several billion dollars and will double the amount of CA membrane area in service. Two other plants being designed, one by Chevron, and should be in the 100 MMSCF of natural gas size range.

A joint research agreement was signed in 1994 with researchers at NREL, the University of Colorado's NSF University/Industry Cooperative Research Center for Separations Using Thin Films, and Dow Chemical to study the effects of membrane material properties and the performance of microporous CA membranes subjected to mechanical creep and compaction. Initial evaluations of the CA-OIH membranes were conducted by Dow. While the initial results look promising, Dow has made a business decision close it's membrane research laboratory and has withdrawn from the Center for Separations Using Thin Films.

POTENTIAL ENERGY BENEFITS - The United States annually uses about 17,500 billion standard cubic feet (bscf) of clean burning natural gas to heat homes, produce chemicals, and for industrial power generation. To supply this energy need the United States has 95,000 bscf of known, domestic reserves of natural gas. In addition, there are an estimated 357,000 bscf of reserves of low grade, natural gas that contains carbon dioxide (CO2) contaminates that can not be economically removed with current technology. Improved cellulose ester membranes that would

allow the use of only 5 percent of the low grade natural gas in known domestic reserves, and new fields would provide more than 22,000 bscf of new domestic energy resources.

HIGHLIGHTS - Cellulose ester organic inorganic hybrid (CA OIH) materials with improved solvent resistance and mechanical properties have been prepared. Homogeneous CA/phenolic polymer blends have been prepared and show an increase in selectivity. Other organic-inorganic membranes have been prepared from substituted polyacetylenes. This work has resulted in a collaborative research project with Los Alamos National Laboratory and the Topchiev Institute in Moscow, Russia.

The permselective properties of the CA-OIH materials have been evaluated for a series of pure and mixed gases by Dow Chemical. Initial results indicate that these CA OIH materials may be useful for natural gas upgrading. A collaborative research agreement has been signed with Dow Chemical Company to allow them to assist with the evaluation of these CA OIH materials for mixed gases at high pressure.

THE ADVANCED INDUSTRIAL MATERIALS (AIM) PROGRAM ANNUAL REPORT, FY 1995

CONDUCTING POLYMERS: SYNTHESIS AND INDUSTRIAL APPLICATIONS

S. Gottesfeld, Principal Investigator

Electronic and Electrochemical Materials and Devices, MST-11
LOS ALAMOS NATIONAL LABORATORY
Los Alamos, NM 87545

The Conducting Polymer project funded by the AIM Materials Program is developing new methods for the synthesis of electronically conducting polymers and is evaluating new industrial applications for these materials which will result in significant reductions in energy usage or industrial waste. The applications specifically addressed during FY 1995 were electrochemical capacitors and membranes for gas separation. As an active material in electrochemical capacitors, conducting polymers have the potential of storing large amounts of electrical energy in low cost materials. Such devices are needed in electronics for power failure back-up and peak power applications, and in electric vehicles for peak power and load leveling. Potential energy savings estimated at 1 quad/yr. would result from introduction of electrochemical capacitors as energy storage devices in power trains of electric and hybrid vehicles, once such vehicles reach 20% of the total transportation market in the US . As a gas separation membrane, conducting polymers offer high selectivity and the potential to chemically or electrically adapt the membrane for specific gas combinations. Potential energy savings in the US. for this application are estimated at 1 to 3 quads/yr.

MILESTONES:

I. Electrochemical Capacitors (Ultracapacitors) Based on Conducting Polymer (CP) Films

We continued this year the development and testing of conducting polymer (CP) materials tailored for electrochemical capacitor applications. In our past work, we have shown that capacitors of three types (named by us Type I, II and III) can be designed with conducting polymer active materials, with the Type III material having the highest potential energy and power densities. Type III capacitors are based on unique conducting polymer materials which can be both p- and n- doped reversibly. The material of this type synthesized and most intensively researched by us to date is poly-3-(4-fluorophenyl)-thiophene (PFPT). The advantages of such an ideal conducting polymer are a larger voltage window and highly conducting active material on both plates at full charge. We have targeted this year the following specific milestones for Type III ultracapacitors:

* Demonstration of Enhanced Power and Energy Densities in a model device of a Type III capacitor with PFPT active material:

* Enhanced cycle life in Type III capacitors with PFPT active material

Additionally, an important development during this year has been the interest expressed in our electrochemical capacitor technology by a major US industry. This industry has, among other large scale activities, a substantial capacity in both manufacturing and development of electrochemical power sources for telecommunications. Following several interactions at both technical and programmatic levels, an agreement on a LANL effort, to be devoted to the development of Type III ultracapacitors with conducting polymer active

materials for needs of that industry, is expected early in 1996. This project will rely on our previous developments achieved within the AIM project, addressing some specific needs in the advancing technology of electrochemical power sources for telecommunication. Future extension for transportation applications has also been considered.

Demonstration of Power and Energy Densities in Model Type III capacitor with PFPT active material: A model Type III electrochemical capacitor, based on the conducting polymer PFPT as charge storage material, was tested by us during this year to demonstrate power and energy densities. Unlike previous tests, this one addressed not just active material (or single electrode) characteristics, but, rather, the performance of a complete small model device. The model capacitor was built using the technology developed previously at LANL as part of this AIM program, based on electrodeposition of the active conducting polymer material onto a carbon paper substrate from a non-aqueous solution of the monomer (FPT), to form the ultracapacitor electrode. A model cell was built with two such electrodes and an electrolyte comprising a non-aqueous solution of tetra-alkyl ammonium salts in acetonitrile. Figure 1a demonstrates complex impedance plots measured for this model cell prior to charge-discharge cycling. In it's highest state of charge, corresponding to a cell voltage of 3V, the high-frequency resistance of the cell is seen to be around 1.5 ohm cm^2. This is a relatively low value considering the non-aqueous electrolyte involved, enabling relatively fast discharge of such Type III capacitors. Moreover, the overall resistance associated with complete discharge of this device (low-frequency impedance) is seen from such measurements to be in the range of 3-5 ohm cm^2. This translates to an ability to tap an overall capacitance of the order of 1 Farad/cm^2 of (geometric) electrode area within periods of 3-5 seconds. This is corroborated by the measured dependence of capacitance on perturbation frequency, depicted in figure 1b. The latter figure shows that: (a) tapping the total energy content of this capacitor is possible within about 10 seconds, as required for transportation applications, and (b) a significant part of the energy of the capacitor is available within much shorter discharge times, as required for some telecommunication applications.

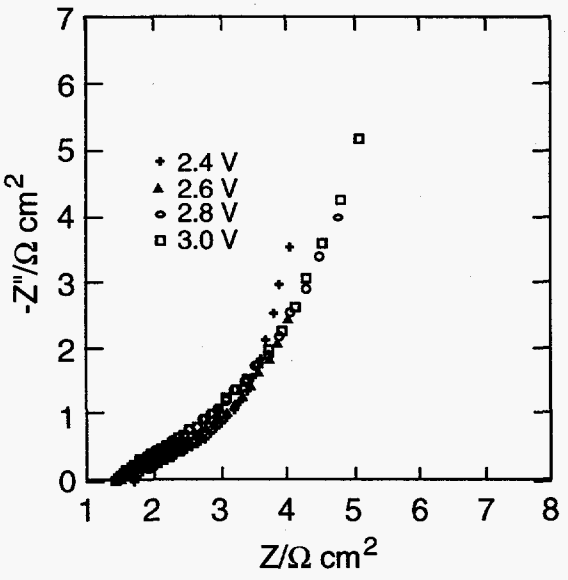

Figure 1a

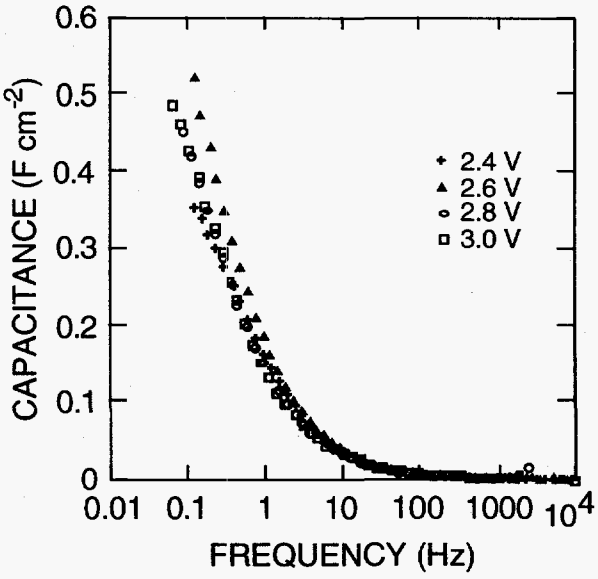

Figure 1b

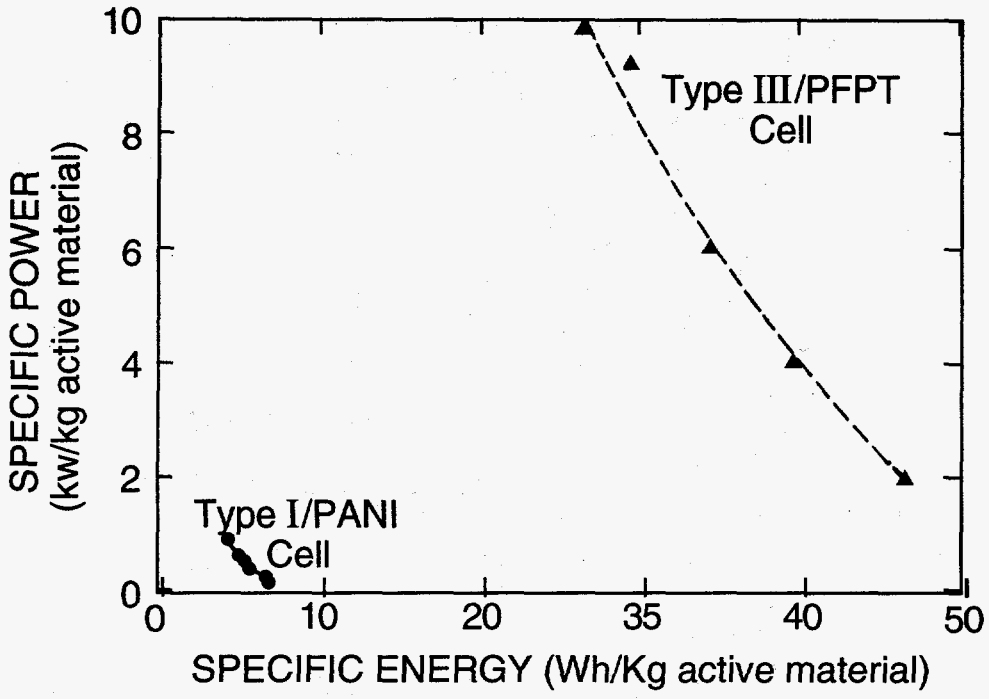

Figure 2

Charge-discharge tests of this model ultracapacitor were performed with a range of discharge currents. The overall energy released during discharge was measured at each of the corresponding discharge power levels, and is presented as a specific energy vs. specific power plot in Figure 2. Figure 2 also includes a similar plot for a Type I (aqueous electrolyte, 1V) capacitor based on polyaniline active material , developed and tested earlier in this AIM project. Considering the non-optimized nature of the model Type III capacitor, the performance obtained in the initial (short-term) test of this device was impressive. Assuming a typical weight fraction of 25% for the active material in a final device, this Type III capacitor, based on our novel conducting polymer active material, should enable an energy density/power density combination of: 10 Wh / 3.6 kW per kg of total device -- highly desirable for automotive applications and significantly better than present day demonstrated ultracapacitor technologies.

Enhanced cycle life in Type III capacitors with PFPT active material: As specified above, we demonstrated this year in tests of model Type III ultracapacitors exceptionally high values for the key merit parameters of energy density and power density. A remaining hurdle that needs to be surmounted to implement Type III ultracapacitors, is the limited stability of the active material, exhibited following prolonged charge cycling. Accordingly, in the work performed this year we investigated a range of electrolyte solution compositions in an attempt to extend the cycle life of PFPT-based ultracapacitors. In this recent investigation, we have subjected electrodes, prepared by electrodeposition of PFPT onto metal foils, to three different cycling modes: p-charge/discharge, n- charge/discharge, and complete cycles which involved both p- and n- charge/discharge processes in each cycle.

We found that the nature of the anion of the salt used in the electrolyte had a clear effect on the conducting polymer stability for p- charge/discharge cycles, with the stability varying with the anion as:

toluene sulfonate $< PF_6^- < BF_4^- < CF_3SO_3^-$

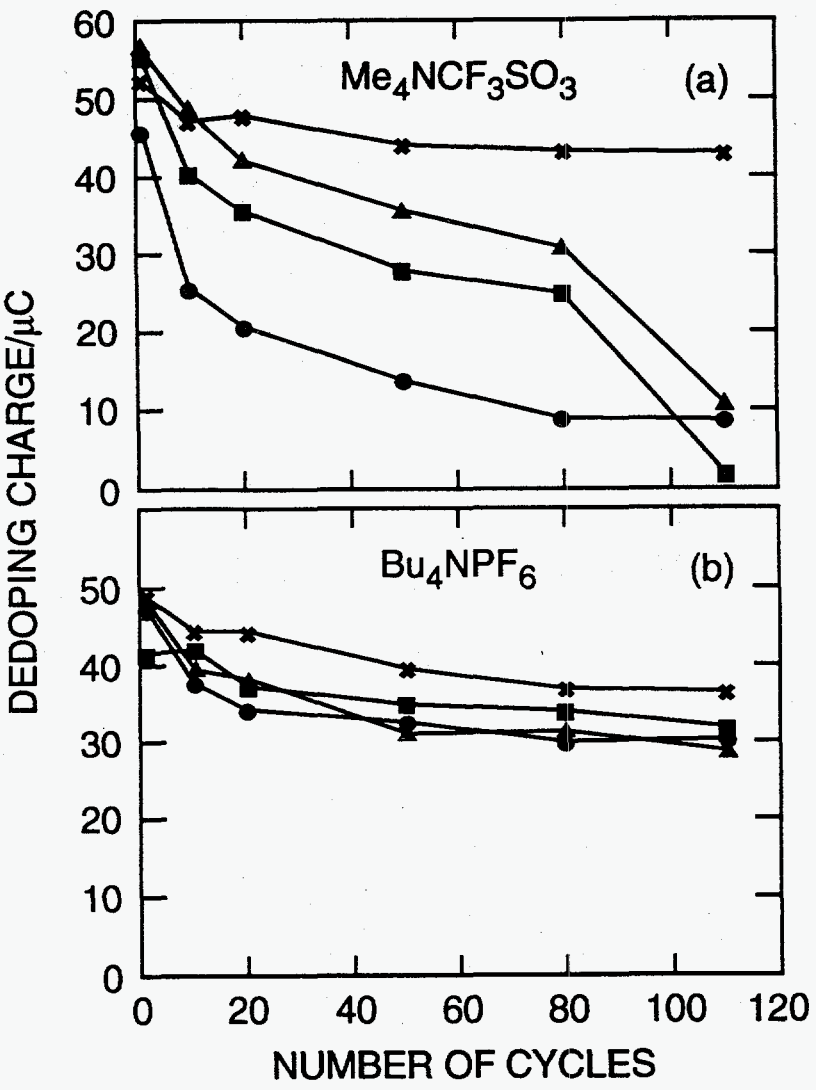

Figure 3

Similarly, the nature of the cation of the salt used had a clear effect on the stability during n- charge/discharge cycles, with this stability varying with different cations used as:

$$Me_4N^+ < Et_4N^+ < Bu_4N^+$$

The PFPT active material exhibited the strongest tendency to lose charge capacity during n- charge/discharge cycles.

Figure 3 demonstrates effects of electrolyte composition on charge/discharge cyclability of the PFPT active material. Shown here are the charge losses for four different cycling modes, applied to the PFPT active material in two different electrolytes containing the salts $Me_4NCF_3SO_3$ and Bu_4NPF_6, respectively. Clearly, use of the Bu_4NPF_6 salt lowered significantly the rate of charge loss during cycling.

The stability trends described above have provided us with a basis for enhancing the long term stability of Type III capacitors under multicycling conditions, showing the need for future efforts in two directions: (i) identification of possible contaminants (mainly water) in the salts, that limit material stability under cycling conditions, and (ii) using salts based on the best possible cation-anion combination revealed by this systematic investigation, i.e., $(Bu_4N^+)(CF_3SO_3^-)$. These efforts are now underway, and should result in further improvement in cyclability of high-performance Type III ultracapacitors.

II. Conducting Polymer Membranes For Gas Separation

Our FY-95 goals for this research activity have been:

* Develop techniques for the fabrication of asymmetric membranes of polyaniline, aiming at a combination of high selectivity and high throughput

* Analyze fundamental gas transport properties in membranes of polyaniline (PANI), aiming at clarification of effects of molecular structure and doping level on selectivity.

Asymmetric membranes of Polyaniline for gas separation: We have advanced significantly during this year in our work on the fabrication of asymmetric membranes of polyaniline for gas separation. About 40 μm thick, dense membranes of polyaniline (PANI) have been demonstrated by us previously to posses high selectivity in the separation of gas pairs like oxygen/nitrogen and hydrogen/carbon dioxide. What has been clearly required for commercial viability in industrial gas separation processes, is the fabrication of asymmetric membranes, consisting of a dense very thin "skin" (1 μm thick, or less) on top of a porous base layer (e.g., 40 μm thick). Such a structure should enable a vast increase in gas permeability, while maintaining a high selectivity by the dense "skin".

A preferable method of fabrication, established for other membranes for gas separation, is based on an integrally-skinned membrane, with both "skin" and porous base made of PANI. This approach is most effective for larger scale fabrication of industrial modules. It requires, however, development of highly refined solution chemistry for the asymmetric membrane fabrication process which, for the case of asymmetric PANI membranes, is a highly non-trivial task. The fundamental reason is the limited solubility of PANI in most solvents and the tendency of PANI solutions to spontaneously coagulate when prepared at high concentrations.

The process of asymmetric PANI membrane fabrication developed by us involves the steps of:

(i) film casting from a concentrated solvent/non-solvent mixture ("dope"),

(ii) formation of dense skin by enhanced controlled solvent evaporation from the top surface of the film,

(iii) formation of porous base by a "coagulation" process in an appropriate solvent, and

(iv) washing with methanol and drying

During our work this year we achieved the following:

(1) The mechanical properties of such membranes have been substantially improved by increasing significantly the molecular weight (MW) of the PANI starting material

(2) the microstructure of the porous, base layer of the asymmetric integrally skinned PANI membrane, has been significantly improved by optimization of the coagulation process

The following are some of the specific improvements in the process for fabrication of asymmetric PANI membranes implemented this year:

* The emulsion polymerization process for the production of PANI starting material has been further optimized. The combination of "reactant confinement" with low bath temperature has resulted in PANI product of molecular weight (MW) close to 1,000,000 (estimated from comparative viscosity measurements). Enhanced MW is key for improved mechanical properties of films recast from solution, particularly films with a highly porous structure as required for the base of the asymmetric PANI membrane.

* Highly concentrated (20% by weight) "dopes" for PANI have been developed, based on novel specific mixtures of solvents (NMP + "solvent X"), non-solvents and added components. This is a very high dope concentration, as required to achieve good mechanical properties. Development of this dope composition with high MW PANI, provides an important basis for fabrication of the asymmetric membrane.

* The "art" of the coagulation step is based on the nature (particularly, the polarity) of the coagulation solvent which determines the rate of casting solvent extraction. The replacement of water by other, less polar coagulation solvents, has resulted this year in significant improvements in the nature of base porosity.

In summary, significant advances towards the fabrication of asymmetric membranes of PANI have been made this year. A remaining element to achieve is reproducible fabrication of perfectly flawless thin selective layers at the surface of these porous membranes. We are focusing our efforts now on the fabrication of such flawless "skins", using a newly built environmental chamber which enables better control of the duration of membrane exposure to well defined gas streams, of known relative humidity or evaporated solvent content. Such well controlled desolvation of the top surface of the PANI film should enable generation of the desirable selective layers.

Evaluation at Praxair (New York) of polyaniline membranes for gas separation based on a novel form of doping: During this year, PANI membranes which employ a new type of dopant have been tested at Praxair, New York. The first target of these tests has been to establish good agreement between gas separation parameters measured at LANL and at Praxair, and evaluate PANI membranes prepared at LANL for applications of interest to Praxair. The evaluation of our PANI membranes has been carried out under a non-disclosure agreement between Praxair and LANL. The measurements at Praxair have demonstrated a separation factor of 1100 for He/N_2, and of 12.4 for O_2/N_2. These numbers are in good agreement with the corresponding separation factors measured by us at LANL for the same two pairs of gases, and are superior to separation factors obtained with other polymeric membranes. Dialogue with Praxair continues at this point.

Investigation of oxygen and nitrogen solubilities in various forms of polyaniline: Work performed by Dr. John Pellegrino (NIST, Colorado), during a sabbatical visit at LANL devoted to this AIM project, was completed and summarized. Pellegrino's effort was devoted to the investigation of nitrogen and oxygen solubilities in polyaniline (PANI), and focused primarily on differences in such solubilities as function of the form of the conducting polymer sample and of treatments applied to it. These are fundamental issues that need to be resolved to establish understanding of the parameters which determine oxygen/nitrogen separation factors in these membranes-- a central target of our effort in developing novel membranes for gas separation. The results obtained can be briefly summarized as follows:

(a) Gas solubility dynamics in PANI membranes contains some very slow components. Variations in gas uptake over several weeks(!) could be observed in some cases. This suggests slow variations in membrane nano-morphology following an increase in the activity of the penetrant gas molecule. Such slow effects may influence the reproducibility of measured gas permeabilities and could be an important reason for discrepancies between permeabilities reported from experiments performed previously by various groups on shorter and on longer time scales. Only the latter serve as appropriate gauge for the quality of the membrane in an industrial gas separation process.

(b) Pellegrino's experiments showed that, following a complete acid doping/undoping cycle, the overall free volume of a PANI sample increases, as evidenced by a measured overall decrease of sample density, but gas access to the additional free volume is apparently restricted, as evidenced by very similar solubilities of oxygen in PANI before and after such a doping/undoping cycle. Such a cycle has been shown earlier (x-ray scattering investigation) to generate more uniform molecular chains in PANI during doping, while subsequent undoping yields irreversible changes in local interchain structure including larger interchain gaps and narrow "pinch points". These observations seem to explain the apparent discrepancy between an increased free volume and an unchanged gas solubility following a doping/undoping cycle. They also suggest that some of the selectivity in oxygen/nitrogen separation achieved in PANI is due to nano-structural "bottlenecks", which discriminate against the somewhat larger molecule (N_2), thus increasing the relative permeability ratio O_2/N_2.

Industrial Input and Technology Transfer

Electrochemical Capacitors

(1) We have recently advanced in our negotiations with a major US electronics /electrochemical power source company, on a project devoted to adaptation of the LANL electrochemical capacitor technology for specific applications in power sources for telecommunications.

The interest of this US Industry was expressed earlier this year (Feb. 95) during a two-days visit to our lab by technical staff from an electrochemical power sources division of the company. The technical staff have been specifically interested in Type III ultracapacitors of the highest power/energy density, developed by us as part of the AIM project on industrial applications of conducting polymers. During that visit, they obtained detailed information on our capabilities and on the state-of-the-art of the technology, while describing some special needs in power sources for telecommunications. The main tasks in a joint project were agreed upon during that

visit. The tasks include improved cyclability under special charge-discharge cycling regimes relevant to telecommunications applications, and development of alternative components for Type III ultracapacitors to ensure a perfectly environmentally benign system and a solid basis for manufacturability.

Following this technical discussion, a recommendation was made by the visiting technical team to their management to pursue a collaboration with LANL on ultracapacitors based on conducting polymer active materials. This has been an encouraging vote of confidence in the ultracapacitor technology developed at LANL under the AIM program, coming from a major US industry in relevant fields of advanced technology. We were visited subsequently by a Vice President of the company, and finalized a draft agreement. We expect that the agreement (most probably funds-in) will be signed early in 1996.

(2) Our CRADA agreement with Evans Finding Co., Rhode Island has come to it's formal ending this year. We are still maintaining contact with Evans, attempting to achieve together the first demo capacitor stack based on our Type I (polyaniline, aqueous electrolyte, 1V) technology. The most significant barrier to date has been an appropriate bipolar plate material for the stack, and we are about to experiment with some unique carbon/plastic composite sheets (source identified very recently) which could be hopefully adapted for this need in the Type I stack. It seems that Type III capacitors based on conducting polymer active materials provide the better potential for exceptional energy and power densities, and, therefore, deserve the stronger focus in our future work (see item (1) above).

Conducting Polymer Membranes for Gas Separation

Polyaniline membrane with a novel type of dopant have been tested by Praxair (New York). Praxair have obtained high selectivity factors for the separation of the pairs He/N_2 and O_2/N_2, in accordance with previous results obtained by us at LANL

Conducting Polymer Films: Application in Electronics Microfabrication

We have demonstrated this year the potential applicability of a technology developed and patented earlier in this AIM project -- the chemical polymerization of conducting polymer films on insulating substrates -- , for new needs in electronics microfabrication. A US company in the field of advanced chemical materials & processes for the electronics industry, provided us with samples for initial testing. In these tests, we managed to demonstrate conducting polymer films of high quality on substrates of interest to that industry, that could serve effectively for this new specific application. Films of polypyrrole of surface resistivities under 2000 ohms/square could be readily applied to substrates of interest to the industry within ten minutes, or less, satisfying both conductivity and industrial process duration requirements. Further development of our process for this new industrial application is being negotiated with the company Microlithography Chemical, Inc.

PUBLICATIONS

(1) Ultracapacitors based on Conducting Polymer Active Materials , Invited Talk and Proceedings Paper (X. Ren, J. Davey, S, Gottesfeld, J. Ferraris and D. Belanger) at the International Seminar on Double Layer Capacitors and similar Energy Storage Devices, Deerfield Beech, Florida, December 1994.

(2) Ultracapacitors with Conducting Polymer Active Materials, X. Ren, J. Davey, S. Gottesfeld and J. Ferraris, Abstract No. 53, The book of Abstracts of the Electrochemical Society Meeting in Chicago, Oct., 1995

(3) Ultracapacitors Using p- and n-dopable Poly (3-arylthiophene), X. Ren, J. Davey, S, Gottesfeld and J. Ferraris, Abstract No. 55, The book of Abstracts of the Electrochemical Society Meeting in Chicago, Oct., 1995

(4) Ultracapacitors Using p- and n-dopable Poly (3-arylthiophene), X. Ren, J. Davey, S, Gottesfeld and J. Ferraris, in Supercapacitors, a Proceeding Volume of the Electrochemical Society, F. Delnick, Editor, in press.

(5) Winokur, M. D., Maron, J., and Mattes, B.R. "Processing Induced Changes in the Local Structure of Amorphous Polyaniline using RDF Analysis." Macromolecules, v. 28, 13, p. 4475-4486 (1995).

(6) Pellegrino, J.P., Radebaugh, R. Gottesfeld, S., and Mattes, B.R. "Oxygen and Nitrogen Adsorption in Electrically Conducting Polymer Membranes." Macromolecules. (in press).

PRESENTATIONS:

Mattes, B. R. " Advanced Analytical Equipment for Measuring Gas Permeabilities". A.V. Topchiev Institute of Petrochemical Synthesis, Moscow, Russia, Sept. 15, 1994.

Mattes, B. R. "Opportunities for Joint Technical Collaborations Between Russia and the USA in the Field of Gas Separations". Kurchatov Institute, Moscow, Russia, Sept 22, 1994.

Mattes, B.R. "Transport Properties of Conducting Polymers". August 24, 1995. Washington University, Department of Chemistry, St. Louis, MO.

Mattes, B. R. " Correlations in Conductive Polymer Films between Structure and Charge & Mass Transport Behavior." August 25, 1995. Monsanto, St. Louis, MO

Mattes, B. R. "Synthetic Routes to Polyaniline". CST Division Synthesis Group. September 6, 1995

PATENTS:

Metallization of Electronic Insulators-- S. Gottesfeld and F. Uribe, US Patent No 5,368,717 issued Nov. 1994.

HIGHLIGHTS

1. An important development during this year has been the interest expressed in our electrochemical capacitor technology by a major US industry. Following interactions at both technical and programmatic levels, an agreement on a LANL effort devoted to the development of Type III ultracapacitors with conducting polymer active materials is expected in the near future. This project will rely on our previous achievements in the AIM and will address some specific needs in the technology of electrochemical power sources for telecommunications. Future extension for transportation applications has also been considered.

2. We demonstrated this year the potential applicability of a technology developed and patented earlier in this AIM project -- the chemical polymerization of conducting polymer films on insulating substrates -- , for specific needs in electronics microfabrication. A US company in the field of advanced chemical materials& processes for the electronics industry, provided us with samples for initial testing. In these tests, we managed to demonstrate conducting polymer films of high quality on substrates of interest to that industry, that could serve effectively for a new application. Further development of our process for this new industrial application is being negotiated.

PROJECT INVESTIGATORS

NAME	ACTIVITIES
Gottesfeld	Principal Investigator
Ren*	Conducting Polymers for electrochemical capacitors
David Mosley**	Gas Separation
Ben Mattes	Gas Separation
UT subcon.***	Conducting Polymers For electrochemical capacitors
Davey	Tech., Conducting Polymers for electrochemical capacitors

* Postdoctoral Fellow **GRA ***John Ferraris + Ph.D student

MAGNETIC FIELD PROCESSING OF INORGANIC POLYMERS THE ADVANCED INDUSTRIAL CONCEPTS (AIC) MATERIALS PROGRAM

D. C. Kunerth

E. S. Peterson

Idaho National Engineering Laboratory

P. O. Box 1625

Idaho Falls, Idaho 83415-2209

Introduction

The purpose of this project is to investigate, understand, and demonstrate the use of magnetic field processing (MFP) to modify the properties of inorganic-based polymers and to develop the basic technical knowledge required for industrial implementation. Polyphosphazene membranes for chemical separation applications are being emphasized by this project. Previous work demonstrated that magnetic fields, appropriately applied during processing, can be used to beneficially modify membrane morphology. MFP membranes have significantly increased flux capabilities while maintaining the same chemical selectivity as the unprocessed membranes.

Technical Progress in FY-1995

The MFP membrane gas separation studies initiated in FY-1994 were completed. The emphasis of this work was to fabricate MFP membranes, having improved flux characteristics, in geometries suitable for industrial applications. A tube-in-shell membrane module was chosen in which membranes were cast on the inner surface of tubular ceramic supports surrounded by an external shell. Functionally, permeate from the feed stream on the inside of

the tube migrates through the membrane and porous ceramic substrate to the interior of the shell where it is transported to a collection point. A number of tube-in-shell membrane modules were fabricated and tested for their gas/gas and liquid/liquid separation characteristics. Tables 1, 2, and 3 provide the results of the separation studies for CO_2, H_2S, and SO_2 from CH_4.

A CRADA between the INEL and ChromatoChem, Inc., Missoula, Montana, to jointly develop a chemical separation system having extended capabilities demonstrated the ability to fabricate and use MFP membranes for industrial applications. ChromatoChem's current system is very efficient at separating metal ions from aqueous process streams but cannot separate trace organics. Mating MFP membranes (having improved flux capabilities) with ChromatoChem's current technology produced a hybrid separation system with expanded capabilities. The test results for the second generation hybrid magnetically-processed membrane/column system are provided in Table 4.

Publications

1. R. C. Boehm, "MNDO Model Structure for Poly(diphenoxyphosphazene) Derived from Cluster of Several Related Phosphazenes," Journal of Physical Chemistry, 1993, 97, pp. 13877-13886.

2. E. S. Peterson, K. R. Arehart, D. C. Kunerth, M. L. Stone, and R. F. Hammen, "Selective Separations of Trace Metals and Organics from Water," Proceedings of the 124th TMS Annual Meeting, Las Vegas, Nevada, February 1995.

Presentations

AIC Annual Program Review, June 1995

124th TMS Annual Meeting, Las Vegas, Nevada, February 1995

Honors and Awards

None

Patents/Disclosures

None

Licenses

None

Industrial Input and Technology Transfer

ELF ATOCHEM, N.A., King of Prussia, Pennsylvania, supplied some of the polyphosphazene materials used in the experiments. Triton Systems and ,Technically, Inc. Boston, Massachusetts, are jointly custom-manufacturing polyphosphazene materials. The CRADA between the INEL and ChromatoChem, Missoula, Montana, developed and demonstrated a chemical separation system having extended capabilities.

Estimated Energy Savings

Improvement of polymer properties using magnetic processing has potential to achieve significant energy savings. If membranes having superior properties could be fabricated, their industrial implementation would become feasible, and energy could be saved. For example, a recent DOE study (DOE/NBM-80027730) states that an annual energy savings of over one quad (equivalent to 170 million barrels of oil) could be achieved if membrane separations were fully utilized in only one application, liquid-to-vapor separations.

Highlights

The efforts of FY-1995 demonstrated that a second generation hybrid magnetically processed membrane/column system with extended capabilities can be fabricated and implemented in a geometry that is suitable for industry. Additionally, it has been shown that such a system can be economically feasible.

Table 1. Magnetically Processed Membranes vs. Conventional Membranes--

10% Carbon Dioxide (CO_2) in Methane (CH_4)

Permeability (Barrers)

	30°C		50°C		70°C	
	CO_2	CH_4	CO_2	CH_4	CO_2	CH_4
Magnetic Process	1.182	0.259	3.042	0.994	5.100	2.389
Conventional	0.528	0.125	1.250	0.398	2.459	1.149

Separation Factor

	30°C	50°C	70°C
Magnetic Process	4.502	2.980	2.062
Conventional	4.223	3.108	2.098

Flux (l/m^2hr)

	30°C	50°C	70°C
Magnetic Process	1.02	1.13	1.30
Conventional	0.79	0.90	1.18

Table 2. Magnetically Processed Membranes vs. Conventional Membranes--

10% Hydrogen Sulfide (H_2S) in Methane (CH_4)

Permeability (Barrers)

	30°C		50°C		70°C	
	H_2S	CH_4	H_2S	CH_4	H_2S	CH_4
Magnetic Process	17.848	1.811	33.235	7.726	44.15	41.22
Conventional	0.982	0.090	2.813	0.337	4.913	0.824

Separation Factor

	30°C	50°C	70°C
Magnetic Process	7.920	3.178	1.041
Conventional	10.845	8.037	5.608

Flux (l/m^2hr)

	30°C	50°C	70°C
Magnetic Process	1.81	4.30	>317
Conventional	0.68	0.68	1.36

Table 3. Magnetically Processed Membranes vs. Conventional Membranes--

10% Sulfur Dioxide (SO_2) in Methane (CH_4)

Permeability (Barrers)

	30°C		50°C		70°C	
	SO_2	CH_4	SO_2	CH_4	SO_2	CH_4
Magnetic Process	10.46	0.305	18.03	1.617	22.02	2.894
Conventional	3.003	0.112	5.854	0.368	7.001	1.234

Separation Factor

	30°C	50°C	70°C
Magnetic Process	29.62	8.944	5.913
Conventional	25.70	14.67	5.209

Flux (l/m^2hr)

	30°C	50°C	70°C
Magnetic Process	1.88	1.88	3.85
Conventional	1.15	1.47	2.94

Table 4. Hybrid System Capabilities

Metal Ion Removal

Metal	Initial Concentration (ppm)	Final Concentration (ppm)	Break Through (Bed Vols.)	Percent Metal Recovery
Cu	2700	No Detect	12	73
Ni	500	No Detect	150	97
Zn	510	No Detect	180	89

Methylene Chloride Removal

Percent MeCl in Feed	Percent MeCl in Permeate	Percent MeCl Recovery	MeCl Flux L/m-Hr	Separation Factor
0.5	99.5	93	0.07	3800

Membrane Systems for Energy Efficient Separation of Light gases

David J. Devlin, Kerry N. Siebien,
Thomas Archuleta and Robert Barbero

Los Alamos National Laboratory
MS E549, MST-7
PO. Box 1163
Los Alamos NM 87545

INTRODUCTION

Ethylene and propylene are two of the largest commodity chemicals in the US. and are major building blocks for the petrochemicals industry. These olefins are separated currently by cryogenic distillation which demands extremely low temperatures and high pressures. Over 75 billion pounds of ethylene and propylene are distilled annually in the US. at an estimated energy requirement of 400 trillion BTU's. Non-domestic olefin producers are rapidly constructing state-of-the-art plants. These energy-efficient plants are competing with an aging US. olefins industry in which 75% of the olefins producers are practicing technology that is over twenty years old. New separation opportunities are therefore needed to continually reduce energy consumption and remain competitive. Amoco has been a leader in incorporating new separation technology into its olefins facilities and has been aggressively pursuing non-cryogenic alternatives to light gas separations. The largest area for energy reduction is the cryogenic isolation of the product hydrocarbons from the reaction by-products, methane and hydrogen. This separation requires temperatures as low as -150°F and pressures exceeding 450 psig. This CRADA will focus on developing a capillary condensation process to separate olefinic mixtures from light gas byproducts at temperatures that approach ambient conditions and at pressures less than 250 psig; this technology breakthrough will result in substantial energy savings. The key technical hurdle in the development of this novel separation concept is the precise control of the pore structure of membrane materials. These materials must contain conically-shaped channels in the 20-40A range to provide the driving force necessary to remove the condensed hydrocarbon products. In this project, Amoco is the technology end-user and provides the commercialization opportunity and engineering support. LANL provides the material development expertise that is critical for achieving the desired product separation. LANL has over 35 years of experience in developing novel materials using chemical vapor deposition (CVD) and chemical vapor infiltration (CVI) techniques. These techniques allow for controlled porosity and the development of mesoporous materials for capillary condensation.

TECHNICAL PROGRESS-FY 1995

Summary

A number of experiments to investigate the controlled pore closure of substrates were under taken. Two approaches based on vapor deposition techniques have been investigated. Due to the desired pore shape and required surface chemistry for this separation application we have focused our attention on the closure of anodized aluminum substrates with carbon. Other substrate systems will be investigated in the future. Anodized aluminum substrates are made up of straight pores with uniform dimensions. Filters available from Whatman contain channels 200 microns in diameter and 60 microns in length with a 0.02 micron diameter membrane layer approximately 100 nm thick on one side. The pore size distribution is uniform (Figure 2) and the pores as shown in figure 3 are straight. This structure is ideal for the development of a tapered pore system. Our approach is to use vapor deposition techniques to further close pores with carbon and produce a membrane surface capable of capillary condensation.

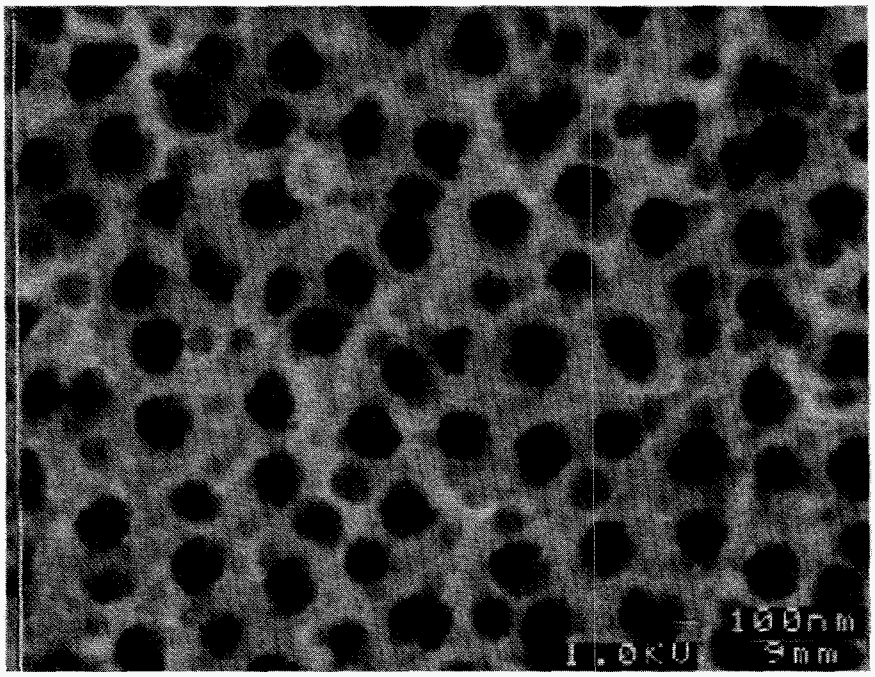

Figure 1. Uniformly distributed 200 micron pores in a an anodized aluminum membrane.

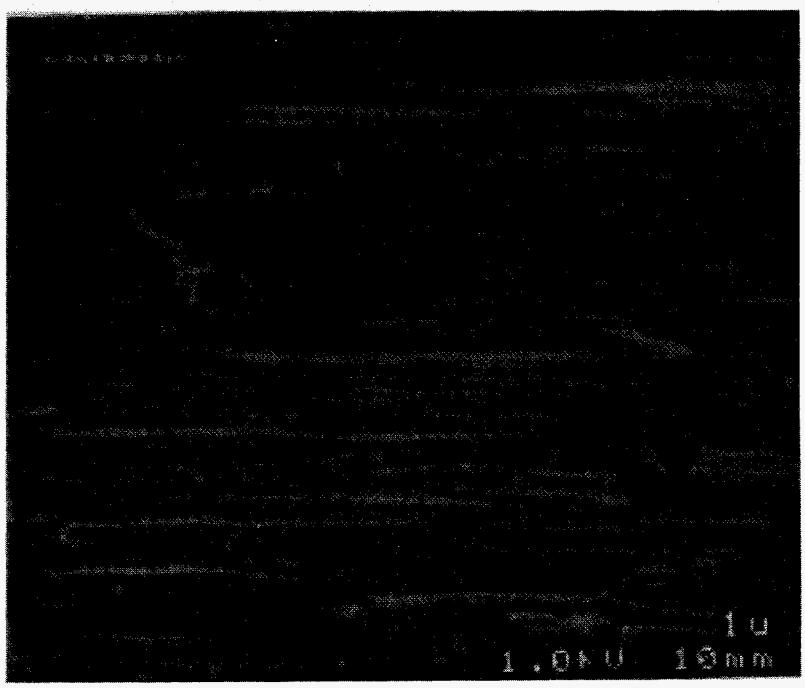

Figure 2. Anodized aluminum membrane showing straight pores through the thickness.

Chemical Vapor Infiltration:

Our initial experiments investigated chemical vapor infiltration, CVI as a means of depositing carbon on the interior of pores. Figure 4, illustrates the process for a carbon deposit within a cylindrical pore. In this approach advantage is taken of the preferential deposition near the outer regions of the pore typical of CVI processes.

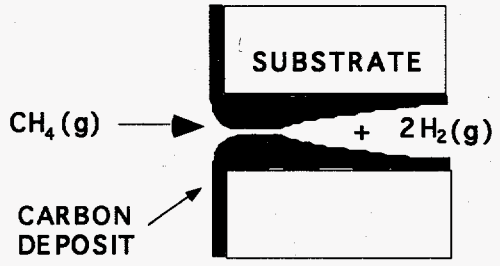

Figure 4. Pore closure by the chemical vapor infiltration of carbon.

An experimental reactor for this purpose was assembled and is schematically shown in figure 5. The system is a forced flow CVI reactor. The substrate/membrane is fixed to the inner

tube of the reactor with a glass seal. Reactant gas can enter the top of the reactor in the outer tube and are forced through the substrate via a pressure gradient where deposition occurs. The product gases are exhausted through the inner tube. A differential pressure gauge monitors the pressure gradient across the membrane.

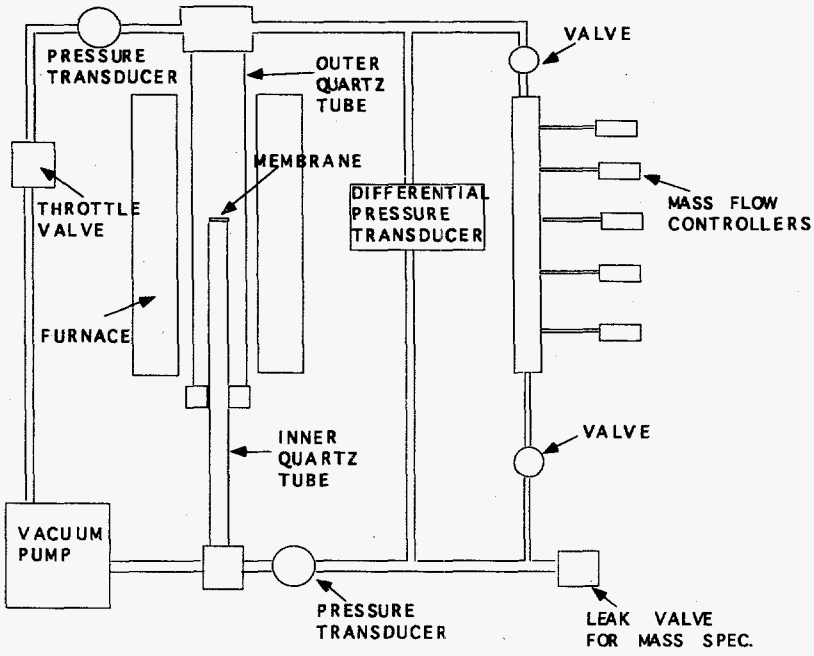

Figure 2. Schematic of FFCVI reactor for membrane preparation

The throttle valve at the high pressure side of the reactor is used to control the pressure gradient and allow for a high feed flow relative to the permeate flow, reducing concentration gradients. The direction of flow in the reactor can be in either direction. This allows for back etching of pores with, for example oxygen to reopen pores that have been completely sealed. The reactor may also be used for the measurement of permeability and selectivity at elevated temperatures.

In our initial infiltration experiment we ran the reactor at conditions of constant reactant flow, thus the pressure differential was allowed to increase to 350 torr. This resulted in a rapid sealing of the substrate in the final stages of deposition. Figure 5 shows the evolution of pressure with time.

A rapid abrupt increase in pressures occur in the final stages. As a result a top layer of carbon on the membrane is deposited. Initially we believed this caused residual stress due to

thermal expansion mismatch between the substrate and carbon. This in turn resulted in cracking of the membrane. Further investigation showed the cracking phenomena to be associated with the thermal stability of the membrane itself. Free standing membranes heated in vacuum to 400°C showed signs of warping and higher temperatures resulted in cracking. The infiltration of pyrocarbon requiring temperatures in excess 800 °C will not be possible with these substrates. Silica aerogels will be investigated for this purpose. An alternative approach using sputtering techniques for the lower temperature deposition is described below.

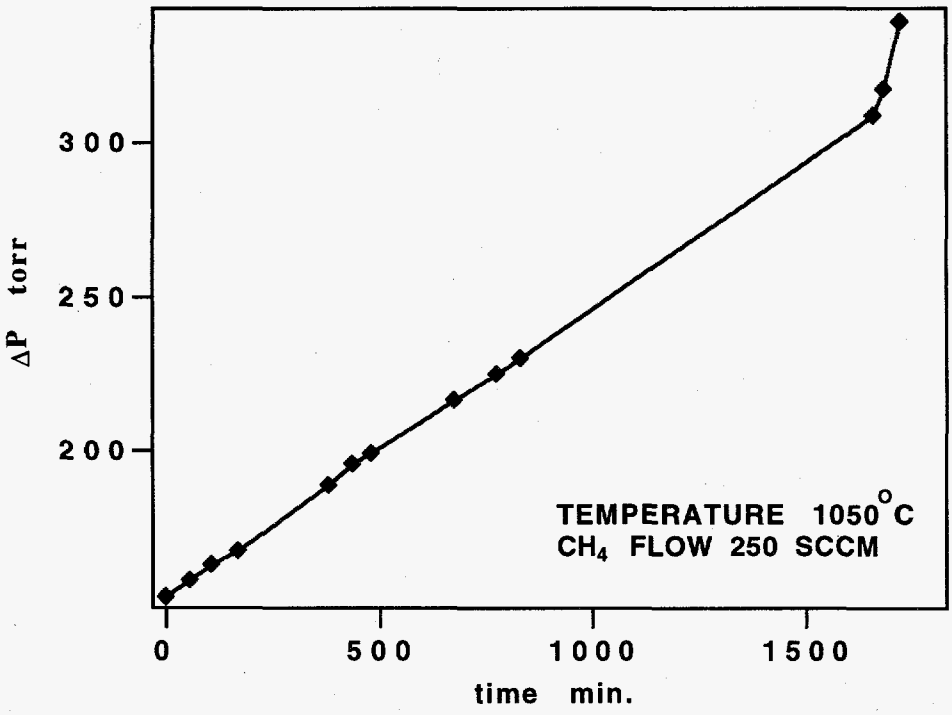

Figure 5. Pressure drop across the alumina membrane during CVI of pyrocarbon

Sputter deposition

It has long been recognized that thin film deposition by evaporation and sputtering at oblique angles and low adatom mobility leads to a porous columnar microstructure. The development of this microstructure has been shown to be the result of self-shadowing effects. Numerous examples and simulations of this effect exist in the literature. A revised version of the Thorton zone model for microstructural development describes porosity on the nanometer scale for thin films 10 to 100 nanometers thick. Advantage can be taken of this effect to develop highly porous carbon films with the required pore sizes.

Using the anodized aluminum membrane as a substrate and a combination of sputtering with substrate rotation, and oblique angle deposition, pore closure is possible. Figure 6, illustrates the approach to closing pores by a magnetron sputtering technique.

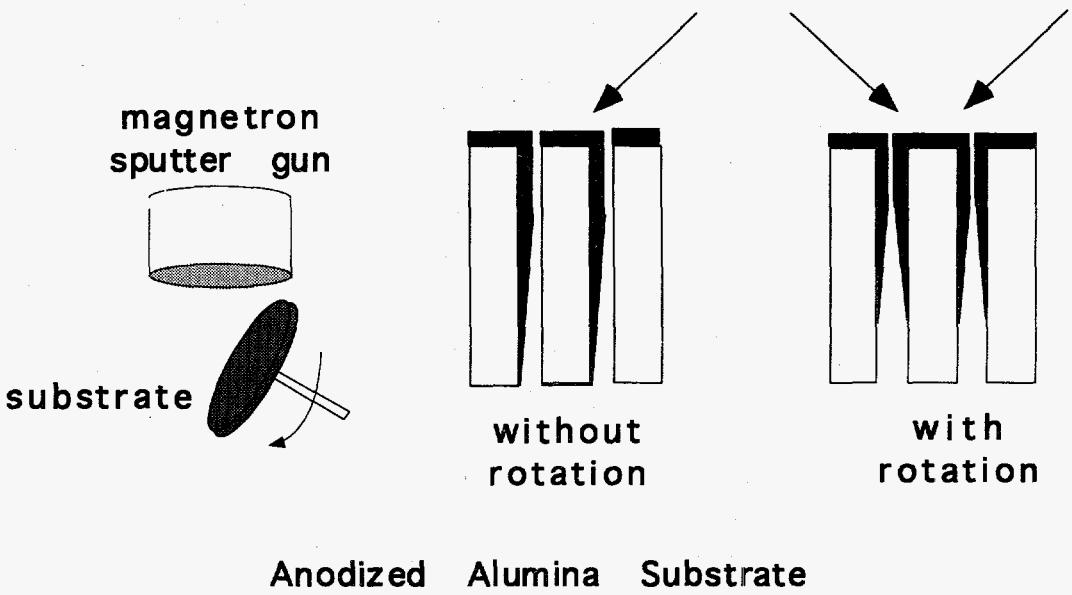

Figure 6. Illustration of pore closure by sputtering at an angle with substrate rotation

By rotating the substrate and depositing at an angle inclined to the beam direction, deposition within the pores is possible. With variation of the deposition angle a wide range of pore shapes can be achieved. The partially closed pore structure can than be over coated with an obliquely sputtered film leading to a nanoporous structure (see Figure 7). Tapered pores with an obliquely deposited carbon membrane suitable for capillary condensation should be possible by this approach.

Experiments under various sputtering conditions were performed to evaluate the potential of filling pores by rotation at an angle to the beam. Figure 8 shows the early stages of deposition into 200 micron pores. The sample was inclined with its surface normal at an angle of 75° to the beam direction. Tapering of pores is clearly evident. Similar effects are possible on the 0.02 micron diameter pores. We have not yet established the smallest pore size possible by this approach. Future experiments are aimed at establishing these limitations and the range of pore shapes possible.

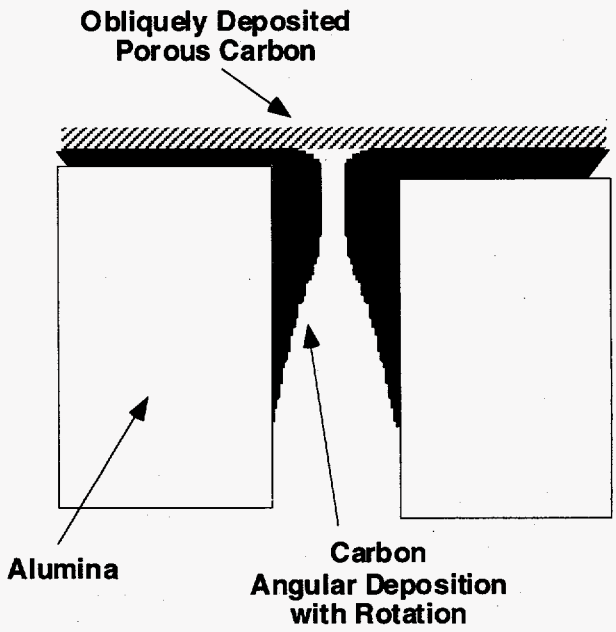

Figure 7. Tapered pore with obliquely deposited porous carbon film.

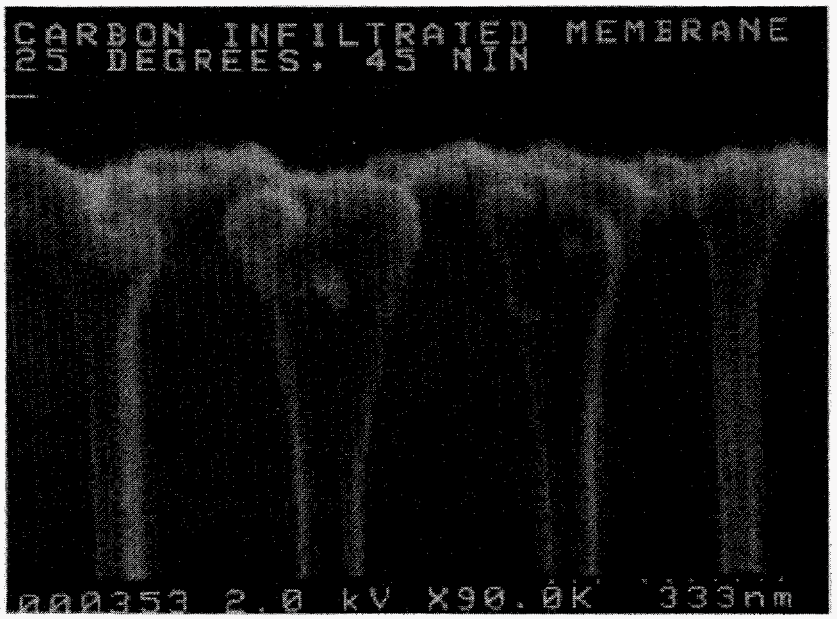

Figure 8. Pore tapering by magnetron sputtering of carbon

We have looked at oblique angle sputtering of carbon films onto the 0.02 micron diameter pore membrane. Samples were not rotated but inclined with the surface normal 85^{o} to the beam direction. To examine the microstructural features TEM samples were prepared. Figure 9 shows

one such sample with a 100 nm carbon coating. Evident in the micrograph are regions of low density material inclined at an angle of approximately 65° to the surface. These are very likely pores resulting from self shadowing effects due to the oblique angle of deposition.

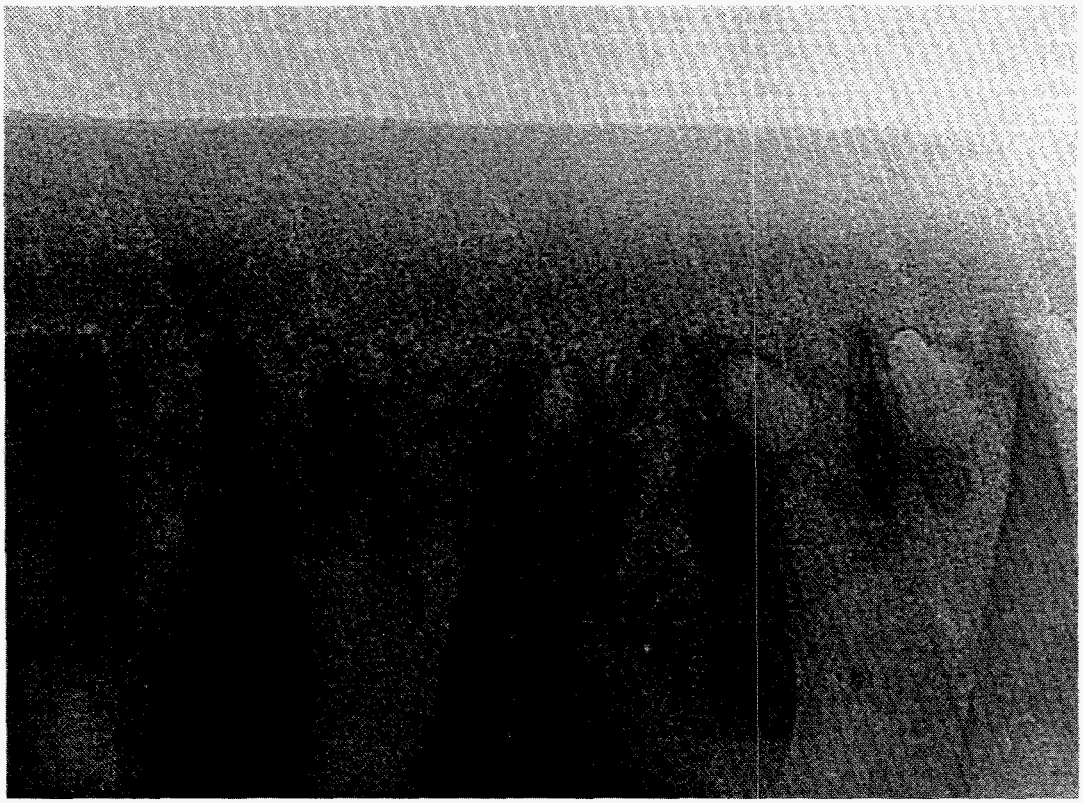

Figure 9. TEM micrograph of obliquely sputtered carbon film on anodized aluminum substrate.

The sputtering approach appears to have potential for fabricating the pore structure required in this application. Future work will be aimed at developing the desired porous columnar microstructure utilizing the self shadowing effect. This will include measurements of permeability, surface area, hydrocarbon adsorption and microstructural examination (SEM/TEM). Processing parameters such as angle of incidence, pressure, power and biasing for the sputter deposition will be investigated. Oblique angle deposition of electron beam evaporated films will also be examined and parameters such as pressure, substrate temperature, and angle of incidence will be evaluated.

MILESTONES DURING FY 95:

A method for developing tapered carbon pores for capillary condensation of hydrocarbons has been devised. Initial experiments demonstrate the feasibility of this approach. A joint work statement with Amoco was prepared and approved by the DOE. The CRADA has been reviewed by Amoco's legal department and some minor changes have been requested. These are now being processed and we expect to have the CRADA in place by January of 96.

PUBLICATIONS

"Dynamics of Chemical Vapor Infiltration in Carbon Fiber Bundles", R.P. Currier, D.J. Devlin and J. Morziski. submitted to Advanced Materials.

"Carbon Based Prosthetic Devices" D.J.Devlin, J. Cowie and D. Carrol. Proceedings of International Mechanical Engineering Congress. Advances in Bioengineering , Vol. 31, 1995.

"Radio Frequency Assisted Chemical Vapor Infiltration", D.J. Devlin, R.S Barbero, K.N. Siebein, To be published: Proc. of the 13th International Conference on Chemical Vapor Deposition 1996.

PRESENTATIONS

(Related to earlier work on RF and Microwave Assisted CVI)

"Chemical Vapor Infiltration." D.J. Devlin, R.S. Barbero, K.N. Siebien, Advanced Industrial Materials Program Annual Review, june 95, Washington D.C.

"Carbon Based Prosthetic Devices", D. J. Devlin, J. Cowie, D Carrol, American Society of Mechanical Engineers, Annual Winter Meeting, November 1995.

"Radio Frequency Assisted Chemical Vapor Infiltration", D.J. Devlin, R.S Barbero, K.N. Siebein, 13Th International Conference on Chemical Vapor Deposition, April 1996

HONORS AND REWARDS

None

PATENTS/DISCLOSURES

None

LICENSES

None

None

INDUSTRIAL INPUT and TECHNOLOGY TRANSFER

This effort will continue in '96 as a joint research effort with Amoco's Olefins R&D group. Amoco will develop characterization capabilities and design criteria for the membrane systems. With their guidance we will develop the materials and processing for the fabrication of these membranes. Amoco's goal is a materials system capable of scaling for use in a pilot plant system.

ESTIMATED ENERGY SAVINGS:

Initial economic analyses have shown that the commercialization of this novel separation concept could result in an energy reduction potential of 5 trillion BTUs per year for an olefins complex: this corresponds to a potential annual savings of nearly $8 million.

HIGHLIGHTS

A method for developing tapered carbon pores for capillary condensation of hydrocarbons has been devised. Initial experiments demonstrate the feasibility of this approach. A joint work statement with Amoco was prepared and approved by the DOE. The CRADA has been reviewed by Amoco's legal department and has requested minor changes. These are now being processed and we expect to have the CRADA in place by January of 96.

Polymerization and Processing of Organic Polymers in a Magnetic Field

Annual Report for FY95

Elliot P. Douglas
Polymers and Coatings Group
MST-7, E549
Los Alamos National Laboratory
Los Alamos, NM 87544

Introduction

Liquid crystalline thermosets (LCT's) have become recognized over the past few years as an important new class of materials. Numerous reports from our laboratory and others have described their synthesis and phase behavior.[1-10] In particular, we have described important effects due to the orientation of the rodlike molecules in a liquid crystalline phase. We have found that curing rates are enhanced compared to reaction in an isotropic phase,[3] and that the glass transition of the fully cured material can be significantly higher than the final cure temperature.[4]

For structural applications, orientation of LCT's will allow maximum improvement in mechanical properties. A few studies have described use of magnetic fields to orient LCT's.[8,9] However, the maximum reported field strength was 13.5 T and no measurements were made of the tensile properties. In this report we provide the first description of the field strength dependence of orientation in LCT's, as well as the first report of tensile properties for both unoriented and oriented LCT's. The LCT we have chosen for study is the diglycidyl ether of dihydroxy-α-methylstilbene (DGE-DHAMS) cured with the diamine sulfanilamide (SAA). We have cured this thermoset at field strengths of up to 18 Tesla in order to evaluate the effects of very high magnetic fields on the properties of the system.

Technical Progress

Summary

In this report we provide the first description of the orientation of liquid crystalline thermosets (LCT's) in field strengths of up to 18 T, as well as the first report of tensile properties for both unoriented and oriented LCT's. The LCT we have chosen for study is the diglycidyl ether of dihydroxy-a-methylstilbene cured with the diamine, sulfanilamide. Orientation in magnetic fields leads to an increase of almost three times the modulus compared to the unoriented material. These values are much greater than can be obtained with conventional thermosets. The strain at break is also significantly affected by the chain orientation. The coefficient of thermal expansion and x-ray diffraction of oriented samples show high degrees of anisotropy, indicating significant chain alignment in the magnetic field. We are working to further understand the field dependence of orientation and properties plus the mechanisms of the alignment process.

Milestones

1.0 Magnetic Field Processing

Magnetic Field Processing: The thermoset formulation was prepared by dissolving 0.25 equivalents of SAA and 2 milliequivalents of an organophosphonium catalyst into 1 equivalent of DGE-DHAMS at elevated temperatures. This mixture was then poured into a mold for the magnetic field experiments. This mold consisted of a Teflon cup into which was placed two aluminum heater blocks, with the thermoset formulation filling the space between the blocks. Temperature control was maintained with a PID controller. Magnetic field experiments were conducted at the National High Magnetic Field Laboratory using both a 20 T superconducting magnet using a special high temperature probe we designed and built and a 20 T variable field electromagnet. Curing was done in the field for 1 hr at 150° C. The sample was then removed from the mold by cutting the Teflon cup and separating the aluminum plates. The final cure was done in a conventional oven, and consisted of an additional 3 hrs at 150° C, 1 hr at 175° C, and 4 hrs at 200° C. Plaques approximately 2" x 1.5" x 0.125" were obtained.
Thermal Expansion: Thermal expansion measurements were performed parallel and perpendicular to the field direction using an Omnitherm TMA 1000 with a heating rate of 5° C/min and a mass of 10 g. Values of CTE reported are calculated by linear extrapolation of the displacement-temperature curve over the temperature range 30 to 60° C.
Tensile Properties: Tensile properties were measured on ASTM Type V dogbones using an Instron 4483 testing machine and an MTS 632.26E extensometer. The results given here are the average of three different samples for each field strength.
X-ray Diffraction: X-ray diffraction was performed using a rotating anode generator and a two dimensional position sensitive detector. Calculation of the orientation parameter was done using the equation

$$f = \frac{1}{2}\left(3\left\langle \cos^2 \phi \right\rangle - 1\right)$$

where the average value of $\cos^2 \phi$ is given by

$$\left\langle \cos^2 \phi \right\rangle = \frac{\int_0^{\pi/2} I(\phi) \sin\phi \cos^2 \phi \, d\phi}{\int_0^{\pi/2} I(\phi) \sin\phi \, d\phi}$$

Results and Discussion

The DGE-DHAMS/SAA system forms a smectic phase upon curing. Curing is done at 150° C, which is initially in the isotropic phase. Upon curing a smectic phase is formed due to the increase in aspect ratio of the rodlike molecules as the reaction proceeds. Under these conditions, the smectic phase forms after approximately 20 minutes of cure, and the gel point is reached in approximately 45 minutes. Curing in the magnetic field was done for 1 hour in order to ensure that any orientation induced by the field was locked into the network structure.

Tensile properties of the cured LCT at 0, 15, and 18 T are shown in Table I. Numbers in parentheses are the standard deviations. The tensile properties of the unoriented material are similar to those obtained with epoxies based on bisphenol A cured under the same conditions. The unique advantages of the liquid crystalline epoxy are realized when the material is oriented in magnetic fields. Particularly noteworthy is the increase in tensile modulus. Orientation in magnetic fields leads to an increase of almost three times over the modulus of the unoriented material. The strain at break is also significantly affected by the chain orientation. The reduction in strain at break and the increase in the modulus are due to the decreased elasticity of chemical bonds in the direction of orientation, as compared to the interchain interactions which dominate the stress-strain behavior in the unoriented sample.

Measurements of the coefficient of linear thermal expansion, shown in Table II, also indicate a high degree of anisotropy in samples prepared in magnetic fields. Again, the CTE values of the unoriented sample are similar to those of conventional epoxy thermosets. Alignment in magnetic fields causes a significant decrease in the thermal expansion parallel to the field direction and a significant increase in the thermal expansion perpendicular to the field direction. This is also consistent with the molecules being aligned parallel to the direction of the field.

In order to quantify the orientation, x-ray diffraction measurements were performed. The orientation parameter was determined by integrating the scattered intensity around the azimuthal angle ϕ at a given value of the scattering angle 2θ according to the equations given above. The orientation parameters calculated are 0.93 and 0.90 for 15 and 18 T, respectively, where a value of 1.0 indicates complete orientation. X-ray results confirm that the molecular axes and the smectic layer normals are aligned parallel to the field direction.

Table I: Tensile Properties

	0 T	15 T	18 T
modulus (ksi)	443 (32)	1081 (93)	1174 (166)
strain at break (%)	8.9 (1.6)	0.8 (0.3)	1.0 (0.03)
stress at break (psi)	13,010 (621)	8117 (1105)	9985 (500)

Table II: Coefficients of Thermal Expansion

	0 T	15 T	18 T
CTE parallel to field (μm/m/°C)	54.1	4.7	4.3
CTE perpendicular to field (μm/m/°C)	----	99.6	111.2

2.0 Kinetics of Orientation

The deuterium NMR measurements to determine the kinetics of orientation in the magnetic field require deuterated samples. We have completed synthesis of the deuterated materials. The reactions schemes below describe the reaction approach used. Scheme I, direct deuterium exchange, is the simplest approach. However, due to electronic interactions exchange does not occur in the meta position. Instead, Scheme II can be used, in which the Raney/nickel provides a substrate for heavy water to react with the chlorinated positions on the ring, resulting in exchange of deuterium for chlorine. Unfortunately, on the scale needed the first step of the reaction requires an excessive quantity of sodium metal. Therefore, Scheme III was developed. The starting material is commercially available. In order to avoid the waters of hydration from exchanging a proton with the chlorine substituents, the starting material is first dried in an azeotropic distillation with toluene. The remainder of the reaction is the same as Scheme II.

Using this approach, the synthesis of deuterated phenol has been scaled up to the quantities needed. This material been supplied to our industrial partner for synthesis of the materials that will be used in the NMR experiments.

Scheme I

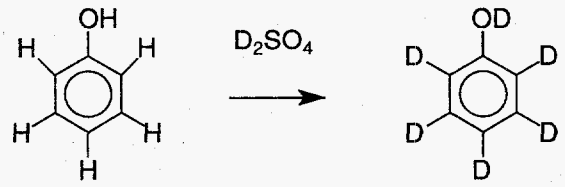

Scheme II

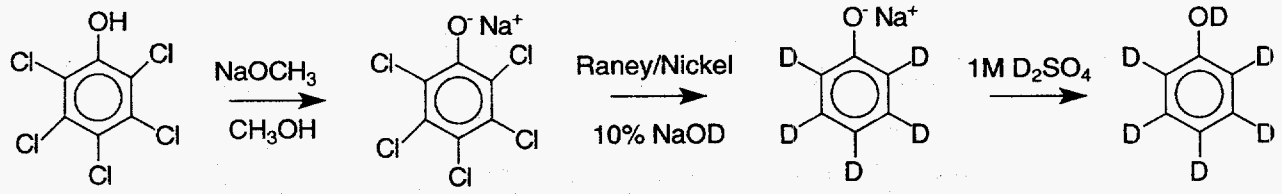

Scheme III

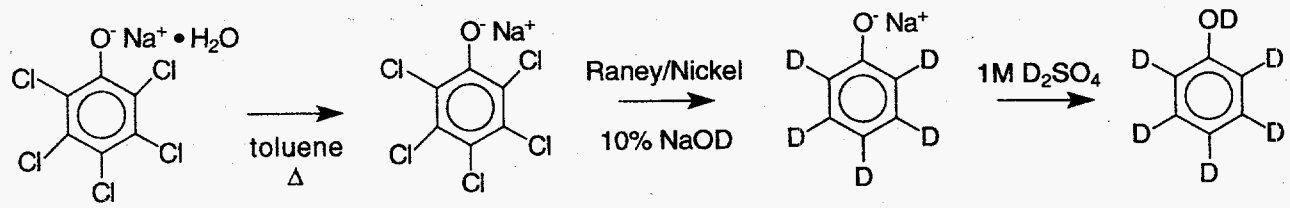

3.0 Industrial Collaboration

As part of our program on magnetic processing of polymers, a CRADA was executed with an industrial partner. The purpose of this CRADA is to investigate magnetic field

processing of liquid crystalline thermosets. Compared to conventional processing techniques such as injection molding or extrusion, magnetic field processing has the advantages of acting on the bulk of the sample, as well as providing a high amount of control over the structure through the use of different field strengths and processing times within the field.

The potential benefits of this CRADA to the U.S. are significant. Several U.S. companies supply structural materials to industries ranging from construction to automotive. Successful application of our technology to manufacturing processes will result in a new class of high strength, light weight structural materials.

References

1. Hoyt, A. E., Benicewicz, B. C. *J. Polym. Sci., Part A: Polym. Chem.*, **28**, 3403, (1990).
2. Hoyt, A. E., Benicewicz, B. C. *J. Polym. Sci., Part A: Polym. Chem.*, **28**, 3417, (1990).
3. Douglas, E. P., Langlois, D. A., Benicewicz, B. C. *Chem. Mater.*, **6**, 1925, (1994).
4. Langlois, D. A., Smith, M. E., Benicewicz, B. C., Douglas, E. P. *Polym. Mater. Sci. Eng.* **74** (1996)
4. Litt, M. H., Whang, W., Yen, K., Qian, X. *J. Polym. Sci., Part A: Polym. Chem.*, **31**, 183, (1993).
5. Melissaris, A. P., Litt, M. H. *Macromolecules*, **27**, 883, (1994).
6. Melissaris, A. P., Litt, M. H. *Macromolecules*, **27**, 888, (1994).
7. Melissaris, A. P., Litt, M. H. *Macromolecules*, **27**, 2675, (1994).
8. Barclay, G. G., McNamee, S. G., Ober, C. K., Papathomas, K. I., Wang, D. W. *J. Polym. Sci., Part A: Polym. Chem.*, **30**, 1845, (1992).
9. Barclay, G. G., Ober, C. K., Papathomas, K. I., Wang, D. W. *Macromolecules*, **25**, 2947, (1992).

MILESTONES DURING FY94

Synthesis of deuterated derivatives.

This milestone was completed in May, 1995, with scale-up of synthesis. The material has been supplied to the industrial partner for further synthesis.

PUBLICATIONS

None

PRESENTATIONS

None

PATENTS/DISCLOSURES

None

LICENSES

None

INDUSTRIAL INPUT and TECHNOLOGY TRANSFER

Current work on this program is being done under the auspices of a CRADA, signed in February, 1994. The industrial partner is supplying the materials for magnetic field processing and test data on the effectiveness of the magnetic field processing.

ESTIMATED ENERGY SAVINGS

This project has the potential for energy savings through the introduction of processing techniques to create high strength, light weight structural materials. Additional energy savings could result from the use of self-reinforcing liquid crystalline polymers in manufacturing processes. Liquid crystalline polymers do not require the use of reinforcements or fillers, resulting in less wear on manufacturing equipment, elimination of compounding as a processing step, and more efficient recycling of materials.

HIGHLIGHTS

IMPROVED MECHANICAL PROPERTIES RESULT FROM MAGNETIC FIELD PROCESSING

Use of magnetic fields to orient liquid crystalline thermosets during processing has resulted in significant improvements in mechanical properties compared to materials processed in the absence of a field. The typical tensile modulus for a material processed at 18 Tesla is 1174 ksi with an orientation parameter of 0.90, compared to 443 ksi and 0.00 for the material processed in the absence of a field. These are the highest fields used to date for alignment of liquid crystalline molecules, and the degree of order obtained is higher than previously reported.

NEW MATERIALS AND PROCESSES

ADVANCED MICROWAVE PROCESSING CONCEPTS

R. J. Lauf, A. D. McMillan, and F. L. Paulauskas

Metals and Ceramics Division
Oak Ridge National Laboratory
Oak Ridge, Tennessee 37831-6087

INTRODUCTION

The purpose of this work is to explore the feasibility of several advanced microwave processing concepts to develop new energy-efficient materials and processes. The project includes two tasks: (1) commercialization of the variable-frequency microwave furnace; and (2) microwave curing of polymer composites.

The variable frequency microwave furnace, whose initial conception and design was funded by the AIM Materials Program, will allow us, for the first time, to conduct microwave processing studies over a wide frequency range. This novel design uses a high-power traveling wave tube (TWT) originally developed for electronic warfare. By using this microwave source, one can not only select individual microwave frequencies for particular experiments, but also achieve uniform power densities over a large area by the superposition of many different frequencies.

Microwave curing of thermoset resins will be studied because it holds the potential of in-situ curing of continuous-fiber composites for strong, lightweight components. Microwave heating can shorten curing times, provided issues of scaleup, uniformity, and thermal management can be adequately addressed.

TECHNICAL PROGRESS

Microwave Furnace Development

The benchtop variable frequency furnace has been modified to include an air-actuated press to enable consolidation of prepreg laminates. The press allows us to apply as much as 60 psig over a variety of sample configurations. Additionally, in collaboration with Lambda Technologies, Inc., we have designed and fabricated a plasma chamber, in which we have conducted preliminary hydrogen/methane plasma experiments.

Lambda has developed a computer model using the Finite Difference Time Domain (FDTD) to identify the cause and predict the location of hot spots. This model demonstrates the advantage of a variable frequency microwave source when compared to

a single frequency microwave source in that the simulations indicate a "well-stirred" cavity. Experiments confirm the model results.

Lambda is now actively commercializing the VFMF. As a direct result of ORNL's work on adhesive curing via variable frequency microwave irradiation, a unit was delivered to a major electronics manufacturer and additional units are pending. Lambda is continuing in-house R&D activities on diamond film growth and polymer curing under SBIR grants.

Polymer Curing

Study has continued on the glass-fiber polymer matrix composites. Thermal profiles were obtained for PMC plates heated using either fixed frequency and variable frequency microwave irradiation. Black body probes were used to more accurately measure the temperature of the plates. It was found that the variable frequency heating very closely followed the fixed frequency heating (fig. 1); however, by using the variable frequency, the post-curing time was cut from over eight hours to less than two hours while maintaining comparable mechanical properties (fig. 2).

We were the first to successfully cure a multidirectional carbon-fiber polymer matrix composite using microwaves. Thermal profiles in figure 3 illustrate that although the unidirectional carbon-fiber PMCs temperature rises at a more rapid rate, the multidirectional PMCs does reach the cure temperature. To date, curing a carbon-fiber crossply using microwaves has been unattainable; we have been the first to demonstrate that with variable frequency, carbon-fiber PMCs can be cured. It was demonstrated that not only did we homogeneously cure the laminates, but our processing actually increased the properties of the material. Differential scanning calorimetry was employed to determine the glass transition temperature of the laminate. Conventional processing results in a T_g of approximately 175°C whereas variable frequency microwave processing results in an average T_g of 184°C (fig. 4).

We are also currently exploring the use of microwave-cured adhesives for joining metal-to-metal or metal-to-polymer or metal-to-ceramic. A proprietary epoxy-based adhesive from B.F. Goodrich and a commercially available sheet adhesive manufactured by Cyanamid (FM73) have been examined individually. An invention disclosure has been filed (ESID 1812-XC).

Milestones

None this reporting period

PUBLICATIONS

Journals

None

Other Publications

1. A.D. McMillan, R.J. Lauf, F.L. Paulauskas, and Z. Fathi, "Variable Frequency Microwave Curing in Polymer Systems," presented at the 1995 ACS Meeting, Anaheim, CA; to be published in ACS proceedings.

PRESENTATIONS

1. A.D. McMillan, R.J. Lauf, F.L. Paulauskas, and Z. Fathi, "Variable Frequency Microwave Curing in Polymer Systems," presented at the 1995 ACS Meeting, Anaheim, CA; to be published in ACS proceedings.

2. A.D. McMillan, R.J. Lauf, and R.S. Garard, "Advanced Microwave Processing Concepts," presented at the Advanced Industrial Materials Annual Meeting, Washington, D.C., 1995.

HONORS AND AWARDS

None

PATENTS/DISCLOSURES

1. R.J. Lauf, A.D. McMillan, F.L. Paulauskas, and Z. Fathi, "Method for Adhesive Bonding Using Variable Frequency Microwave Heating," ESID 1812-XC.

LICENSES

1. Lambda Technologies, Inc. (successor company to Microwave Laboratories, Inc.) previously licensed the Variable Frequency Microwave Furnace covered by US Patent 5,321,222 and additional patents pending. They have now executed a Sole Commercial License for microwave curing of polymers (ESID 1378-X, patent pending).

Fixed Versus Variable Frequency Processing

(Thermal profiles for PMC plates heated using fixed and variable frequency irradiation)

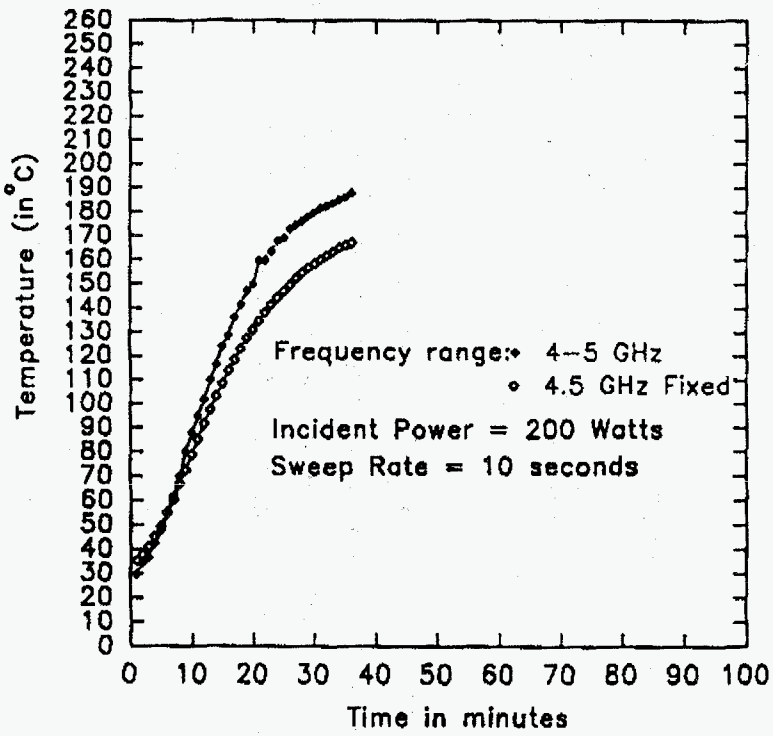

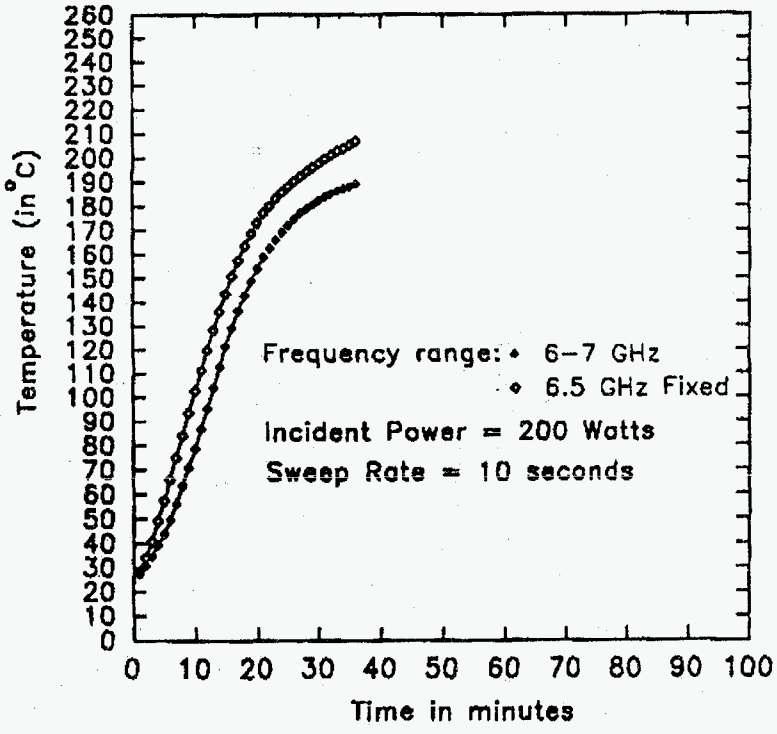

FIGURE 1

Mechanical Behavior

	Flex Modulus (GPa)	Flex Strength (MPa)	Impact Strength (KJ/m^2)
Microwave	5.77 ± 0.15	197.5 ± 15.5	5.7
Conventional	5.75 ± 0.14	195 ± 11.5	5.7

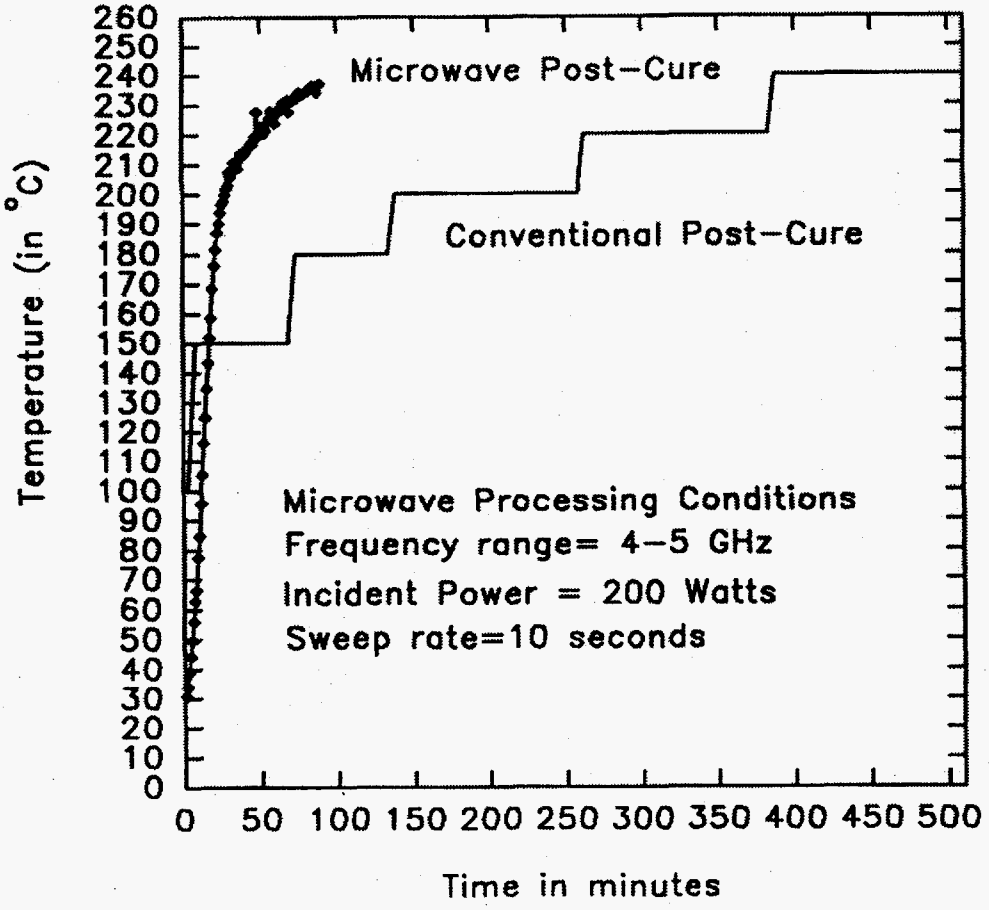

FIGURE 2

Heating profile for graphite fiber/epoxy composite

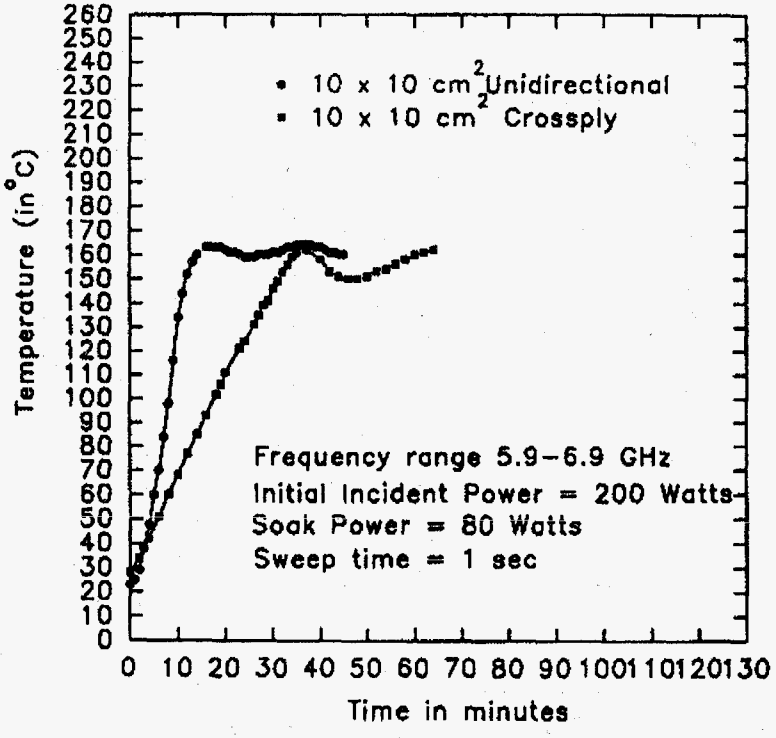

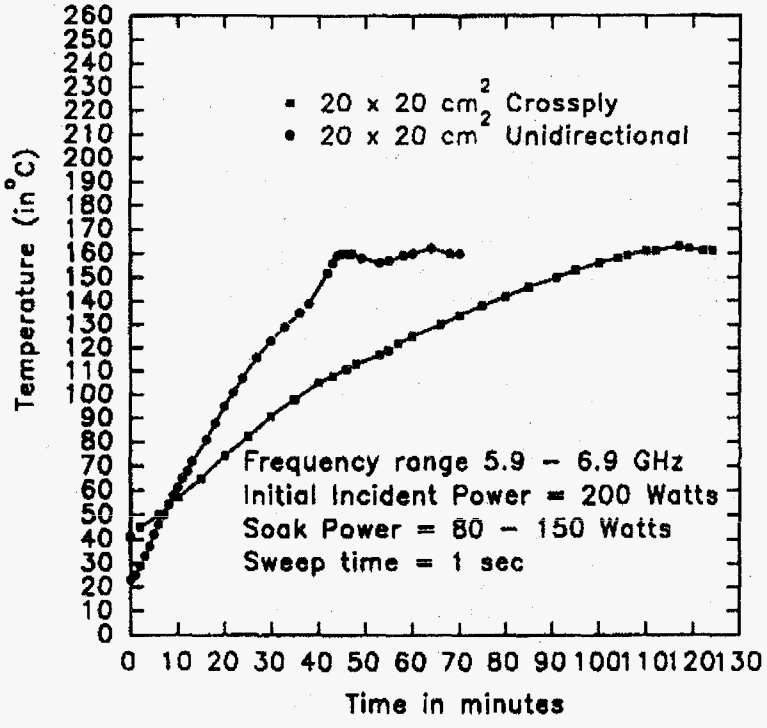

FIGURE 3

Tg measurements as a function of location in a Crossply Graphite fiber reinforced epoxy Composite

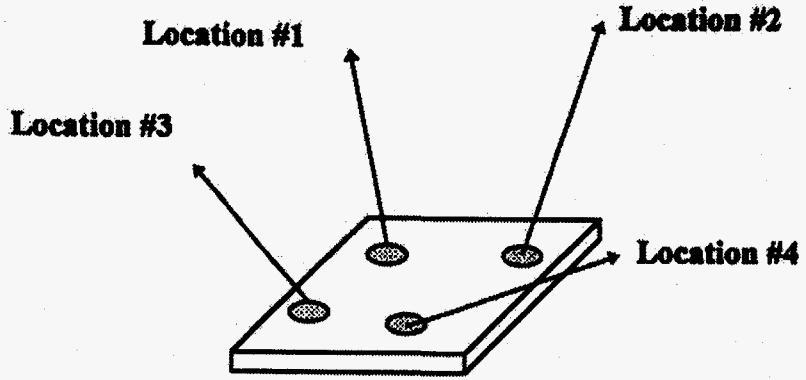

Crossply Graphite fiber reinforced epoxy at different locations	
Location#	Tg(°C)
Location#1	181
Location#2	185
Location#3	186
Location#4	181

FIGURE 4

Control Technology for Surface Treatment of Materials Using Induction Hardening

EEW-2359.7

J. Bruce Kelley and Russell D. Skocypec

Annual Report, FY 1995

INTRODUCTION

Induction hardening is widely used in the industrial and automotive industries to case harden components to provide enhanced strength, wear resistance, and toughness in components made from medium and high carbon steels. It is an energy efficient, environmentally benign, flexible in-line manufacturing process that can directly contribute to improved reliability, manufacturing agility, and the manufacture of high-performance lightweight parts. However, process and input material variations produce unacceptable product variations which cause de-rating of components, higher than desired scrap rates, and necessitate frequent inspection of product quality by destructive examination. Real-time closed-loop control of the process has eluded industry for 5 decades. Additionally, process and tooling development are experience-based activities, accomplished by trail and error. This inhibits use of the process outside the bounds of a company's historical experience.

A multidisciplinary team from Sandia National Labs and Delphi Saginaw Steering Systems has been investigating the induction hardening process under a Cooperative Research and Development Agreement (CRADA) under the auspices of the Technology Transfer Initiative (TTI) and the Partnership for a New Generation of Vehicles (PNGV). The CRADA includes research in the areas of process characterization, computational modeling, materials characterization, plus high speed data acquisition and controller development. The goal is to demonstrate the feasibility of closed-loop control for a specific material, geometry, and process, enabling savings of 2-3 million

dollars per year in scrap, inspection costs, and machine down time at the Delphi Saginaw plant. It was also desired to initiate development of process simulation tools, which could decrease product development lead times and enable optimized component processing. With success in these areas, the opportunity exists to further develop the technology and raise the level of the broad heat treatment industry.

The goal of this FY 1995 project for the Office of Industrial Technology (OIT) was to assess the potential to develop a consortium of industrial companies involved in heat treating to further develop this technology for use across a broader range of processes, components, and materials. Participants in this assessment included automotive, off-highway, aerospace, mining, petrochemical, and industrial equipment suppliers involved in the broad heat treatment market, which typically case harden a mix of wrought and cast materials. The value of applying this technology to new applications such as induction heating for paper and pulp drying and textile fiber drying was also explored.

TECHNICAL PROGRESS

Industrial Outreach: This past year we prepared and presented a paper, "Intelligent Systems For Induction Hardening Processes," at the First International Conference on Induction Hardened Gears and Critical Components (Reference 1). This conference was sponsored by the Gear Research Institute (GRI) of the American Gear Manufacturers Association (AGMA) and the American Society of Mechanical Engineers (ASME). The conference was also sponsored by ASM International, the Electric Power Research Institute (EPRI), the Society of Automotive Engineers (SAE), and a number of the induction heat treating equipment manufacturers. Representatives from over 75 companies worldwide attended this conference. An information booth was manned during the conference at which a summary of project accomplishments, a straw-man proposal for an industrial consortium, and a non-binding letter of intent were available to interested companies. The literature available at the booth is attached to this report as Appendix 1.

Approximately 50 U.S. companies reviewed this information and provided feedback on what it would take to interest them in participation. There was broad support for the technical thrust areas identified in the proposal, with considerable support for the idea that steering committees would define the range of materials and processes to be investigated. One year project agreements that defined useful deliverables were also strongly supported, but many expressed concern that a 5 year structure was too long and suggested a total life of 3 or 4 years. The number of companies willing to participate was sensitive to the straw man proposal of annual contributions of $10K in addition to equal amounts of in-kind. Feedback indicated that annual cash contribution requirements of $3K-5K, and corresponding amounts of in-kind contributions, would be much easier to obtain and sustain over the life of the project. It was explained that the companies involved would determine the actual programmatic and financial structure of the project, and that the level of company contributions would determine the size the program, and its viability. Fourteen companies expressed their intent to participate at the $10K per year cash-in level, including John Deere, Cummins Engine, Black and Decker, Caterpillar, Thompson-Saginaw Ball Screw, and Zion Industries.

Poster exhibits were displayed in Washington DC at the first Industrial Energy Efficiency Symposium and Expo in early May and at the Advanced Industrial Materials (AIM) conference held June 14-16, 1995. The Managing Director of ASM International saw our poster at the AIM conference and expressed interest in the project as a mechanism of advancing the state of the heat treating industry through precompetitive research. He arranged to have an overview of our project published in Advanced Materials and Processes (Reference 2).

Specimens of a number of materials commonly induction hardened but outside the scope of our investigation for Delphi Saginaw, were prepared for evaluation of material and process interactions. The alternative materials included 4150, 1144 , and 1141 steels. However, originally planned tests of these materials and a relevant industrial experiment were postponed when significant uncertainty in the FY96 funding for an industrial consortium became apparent. It was not appropriate to impose on an industrial facility if the potential for relevant follow-on activity is low.

Opportunities in the Casting Industry: The posters attracted the attention of additional potential industrial participants including one that routinely induction hardens wrought and cast parts for DOD applications (United Defense LP) and a company that makes cast rolls for paper making (Sandusky International). Induction hardening is already used to case harden cast parts like cast iron camshafts and spider gears, plus cast iron and cast steel valve seats in pumps and engines, all of which are subjected to moderate contact loads with relatively low structural loads. However, broader use of cast structural parts with moderate structural loads and higher levels of contact loads, components like drive sprockets and gears, requires optimized cast materials and better process controls. Depending on component geometry, applied loading, and desired production volumes, the most energy efficient and least wasteful production path may be to rapid prototype, cast near net shape, finish machine, and induction heat treat.

Opportunities in the Steel Industry: Discussions were also held with steel industry representatives who would be impacted by improving induction hardening. Optimization of the induction hardening materials and processes would broaden the market for induction hardenable grades of steel, and ultimately move the industry towards producing higher volumes of fewer materials. The research would also impact mill processing in that the effects of chemistry, deoxidation practice, finishing temperatures might be discerned and improvements in materials properties such as cold and warm formability and machinability might be improved.

Additionally, the coupled electro-magnetic and thermal models developed in this project could be used to by the steel and forging producers to support integrated product processing through model and sensor developments. For billet, bar, and strip heating in the steel mill or forge shop, induction heating enables close tolerance heating with minimum waste and energy usage for just-in-time production. Model-based production systems envisioned for these industries will require accurate thermal models and appropriate robust heat control sensors.

Opportunities in the Pulp and Paper Industry: Utilization of induction heating for pulp and paper drying and textile fiber drying were also explored. A group led by the Institute for Paper Science and Technology and an industrial company that makes paper drying equipment are already

exploring the use of induction heating as the heat source for impulse drying, a drying process reported to use one-third of the energy required by conventional drying. However, initial experiments using induction have revealed difficulty obtaining uniform heat input which is required to make impulse drying viable. Intelligent induction heating (a model-based process control scheme similar to that developed for the induction hardening process) would enable near-term implementation of impulse drying which is estimated to enable energy savings of more than 80 trillion BTUs of energy within 30 years (Reference 3).

Energy Savings Potential: Significant effort was made to quantify the potential energy savings available by substituting induction hardening for competing processes like carburizing and nitriding for a broader range of materials and components. *Direct* energy savings of 57-85% were calculated using information provided by a major furnace supplier and Delphi Saginaw. Corresponding cost savings estimates were 39-43%. The energy savings information is summarized in an internal Sandia memo by J.B. Kelley and D.R. Adkins (Reference 4). Actual savings depend on furnace efficiency, duty cycle, load utilization, and maintenance. Since induction hardening is an in-line manufacturing process which generally results in less distortion, scrap and rework, *indirect* energy savings in reduced component transportation, straightening, and hard-finishing could potentially be as great as the *direct* savings. However, these *indirect* savings are not quantifiable.

Using a *direct* energy savings estimate of 60% for the substitution of induction hardening for carburizing, in the lower range of the estimates, and an ASM International estimate that carburizing uses 105 trillion BTUs per year, it was calculated that *direct* energy savings of 630 trillion BTUs are possible over 20 years. Inclusion of *indirect* energy savings makes it appear that total energy savings of about 1 quadrillion BTUs could be realized over a 20 year period.

Environmental Impact: Induction hardening is an environmentally benign process, requiring no endothermic atmospheres, no plating tanks or paint compounds for selective carburizing, and no caustic stripping baths to remove stop-off paints or platings. Induction is an in-line manufacturing process so parts are not shipped to a separate batch heat treating facility which may

be across the plant or across the state. Significant reduction in transportaiton costs could result. Induction case hardeing generally results in less part distortion than carburizing, which reduces the amount of hard finishing, rework, and scrap generated. Replacement of carburizing, nitriding, andhard chrome or nickel plating with induction hardening will result in reduced environmental burden.

REFERENCES

1. "Intelligent Systems For Induction Hardening Processes," J.B. Kelley, D.R. Adkins, C.V. Robino, S.L. Stanton, P.M. Kahle, B.K. Damkroger, G.A. Knorovsky, and R.D. Skocypec of Sandia National Laboratories and R.P. Hoppe, D.M. Hitz, and D. Rogers of Delphi Saginaw Steering Systems, Proceedings of the First International Conference on Induction Hardened Gears and Critical Components, May 15-17, 1995, Gear Research Institute, Evanston, IL, 1995

2. "Controlling Induction Hardening," Advanced Materials and Processes, Volume 148, No. 6, pp 36O-36S, December, 1995

3. "Linerboard Drying On A Sheet-Fed Pilot Impulse Drying Shoe Press," D.I. Orloff, Paul M. Phelan, and Jere W. Crouse, Tappi Journal, Volume 78, No. 1, pp 129-141, January 1995

4. "Cost and Energy Savings Analysis for Induction Hardening Processes," J.B. Kelley and D.R. Adkins, Internal Sandia Memo, September, 1995

MILESTONES DURING FY 1995

Identify Key Tasks To Broadly Develop and Implement The Technology

This milestone was completed as described in the body of the report.

PRESENTATIONS AND PUBLICATIONS

1. Oral Presentation and Publication: "Intelligent Systems For Induction Hardening Processes," J.B. Kelley, D.R. Adkins, C.V. Robino, S.L. Stanton, P.M. Kahle, B.K. Damkroger, G.A.

Knorovsky, and R.D. Skocypec of Sandia National Laboratories and R.P. Hoppe, D.M. Hitz, and D. Rogers of Delphi Saginaw Steering Systems, Proceedings of the First International Conference on Induction Hardened Gears and Critical Components, May 15-17, 1995, Gear Research Institute, Evanston, IL, 1995

2. Oral Presentation: "Intelligent Systems For Induction Hardening Processes," J.B. Kelley, D.R. Adkins, C.V. Robino, S.L. Stanton, P.M. Kahle, B.K. Damkroger, G.A. Knorovsky, and R.D. Skocypec of Sandia National Laboratories and R.P. Hoppe, D.M. Hitz, and D. Rogers of Delphi Saginaw Steering Systems, presented at the September meeting of ASM International, Peoria Chapter, held in Peoria, IL, on September 11, 1995.

HONORS AND AWARDS

None

PATENTS/DISCLOSURES

None

LICENSES

None

INDUSTRIAL INPUT AND TECHNOLOGY TRANSFER

Discussions were held with over 50 companies that expressed interest in the technology being developed in our project. Information sheets were sent to all who asked for them. Detailed meetings and presentations were held with a smaller number of companies including Caterpillar,

John Deere, Thompson-Saginaw Ball Screw, Black and Decker, Ford Motor Company, Chrysler, and General Motors. John Deere, Black and Decker, and Thompson-Saginaw expressed interest in hosting an industrial experiment.

ESTIMATED ENERGY SAVINGS

As detailed in the body of this report, energy savings of up to 1 quadrillion BTUs could be realized over 20 years by substituting intelligent induction hardening for carburizing and other competitive case-hardening processes. The technology required to add intelligence to the large number of induction hardening machines in place in industry is easily adapted once developed. Intelligent induction hardening incorporates closed-loop process control to enable optimization of product and process parameters, minimize scrap and rework, and is an agile manufacturing process. Further development to include a virtual prototyping capability would make this process much more widely used than it is today because it would remove much of the uncertainty involved in using the process as it currently exists.

HIGHLIGHTS

COMPANIES EXPRESS INTEREST IN CONSORTIUM TO FURTHER DEVELOP INTELLIGENT SYSTEMS FOR INDUCTION HARDENING. Fourteen companies including Caterpillar, John Deere, Black and Decker, Thompson Saginaw Ball Screw, and Zion Industries expressed interest in establishing a consortium to conduct pre-competitive research on the induction hardening process to further the development of *intelligent* induction hardening processes. Induction hardening is an energy efficient, environmentally benign process used to case harden critical components like shafts, ball screws, bearings, and gears used in a wide variety of industrial equipment. *Intelligent* induction hardening uses science-based process control technology in which process physics knowledge is embedded in a neural network control framework. It incorporates closed-loop process control to enable optimization of product and process parameters, minimize scrap and rework, and provide maximum process agility. It utilizes process modeling to reduce trial and error process development and drastically reduce product development time through the use of virtual prototyping capabilities.

APPENDIX 1

INTELLIGENT SYSTEMS FOR INDUCTION HEATING & HARDENING

Intelligent Systems For Induction Heating & Hardening

Goal: **Develop And Apply Energy-Efficient Intelligent Induction Processes To Reduce Waste And Enhance Manufacturing Competitiveness.** Integrated model-based process design and control systems based on real-time knowledge of fundamental physical phenomena.

Background: **Induction Hardening Is Widely Used** in the industrial equipment and automotive equipment industries to case-harden power transmission and wear components such as shafts, gears, bearings, valve seats, and ball screws. **Induction Heating Is Used** in casting, steelmaking, and forging industries, to make glass-to-metal seals, and to cure industrial adhesives.

Advantages: **Energy Efficient:** Hardening -- direct energy savings ~40%, total energy savings up to 75%. **Environmentally Friendly:** Elimination of hazardous atmospheres, caustic and acid stripping tanks. **Less Wasteful:** less rework, hard finishing, and scrap.

Challenges: Existing practice lacks closed-loop process control and ability to compensate for material variations. Process variability leads to de-rating of components. Excessive reliance on cut-and-try for process design and development.

Accomplishments: **We Have Developed a First Generation Closed-Loop Controller** for the induction hardening process -- one material, one geometry, one type of process. Can relate characteristic process signals to fundamental physical changes occurring in parts. **We have Developed Computer Codes To Enable Virtual Process Tryout.**

Industry Impact: Near Term: **Improve Economic Competitiveness Through Manufacturing Robustness And Agility, Reducing Inspection, Waste, And Inefficiency.** Ability to change inputs, i.e., materials and geometries, without re-developing processing parameters.
Long Term: **Reduce Manufacturing Lead Time And Replace Relatively Inefficient And Environmentally Harmful Processes** such as carburizing and nitriding. Enable the manufacture of lightweight components.

Commercialization Plan: **Broaden Applicability** (materials, geometries, and processes), **And Refine The Resolution Of The Technology Through Industry-Led Consortia**. Two consortia under development -- automotive and industrial heat treating. License appropriate technology to commercial market at appropriate time.

Industry Partner: Delphi Saginaw Steering Systems (formerly Saginaw Division, General Motors)
Contact: David M. Hitz, Chief Process Engineer, (517) 757-4215, email: dmhitz@aol.com.

For Further Information:
Russell D. Skocypec, Sandia National Laboratories, (505) 845-8838, email: rdskocy@sandia.gov.
J. Bruce Kelley, Sandia National Laboratories, (505) 845-3384, email: jbkelle@sandia.gov.

Intelligent Systems for Induction Hardening Processes

Project Proposal for an Industrial Consortium

The Department of Energy (DOE) has defined 3 significant goals to improve Industrial and Manufacturing Technology. Project funding may be available for projects which demonstrate the following national benefits:

- **Significant Reduction in Environmental Burden**
- **Significant Enhancements in Energy Efficiency**
- **Significant Improvements in Manufacturing Efficiency and Flexibility**

Intelligent systems for induction hardening offer all of these benefits. Induction hardening is a fast, flexible, in-line technology for case hardening components which uses approximately 40% less direct energy than carburizing and significantly reduces environmental burden by minimizing plating operations, special gasses, and scrap. This project is designed to enable significant broadening of the range of applications for which induction hardening can be successfully used.

Induction hardening is used across a wide range of industrial sectors, including machine tools, hand tools, appliances, castings, agricultural equipment, oil field equipment, mining equipment, and recreational equipment. Most components used for power transmission, such as gears, bearings, and shafts, are case hardened for wear resistance and to achieve a balance between fatigue strength and fracture toughness. The case hardening processes used most widely are carburizing, nitriding, and induction hardening. Other processes such as hard plating, flame, laser, and electron beam hardening, also have specialized niches of use. Components hardened by these processes include camshafts and crankshafts for heavy duty diesel engines; ball screws for machine tools; gears for fractional horsepower electric motors, heavy duty industrial gearboxes, boat transmissions, and motorcycles; drive shafts for pumps and appliances; and bearings for automotive and non-automotive applications.

Induction hardening is an in-line heat treating technology, and as such enables significant productivity increases compared to off-line batch heat treating technologies. Induction hardening uses significantly less energy to case harden parts than batch processes, heating only the material intended to be hardened and having instant on/off capability which eliminates the energy consumed in furnace idling. Induction hardening produces less distortion since only the surface layers are heated, enabling reduced rework, scrap, and post-heat treat machining than carburizing. Other benefits include the elimination of special gasses, plating processes, and other environmentally burdensome processes.

Shortcomings of the process include the lack of understanding of material/process interactions, the lack of closed loop process controllers, and a lack of process modeling and visualization tools. Experience based development is required to bring the process on-line for each application. Quality control strategies require significant resources to destructively examine finished parts and ensure process stability. In summary, there is inadequate understanding of the fundamental aspects of the process.

Current work in the area of surface induction hardening at Sandia National Labs is supported through a CRADA with Delphi Saginaw Steering Systems, a wholly owned subsidiary of General Motors. The Saginaw CRADA has two primary goals aimed specifically at induction hardening axle shafts; development of closed-loop process controllers, and development of process modeling tools. Development of these tools is expected to result in significant cost savings.

A survey of ASME/AGMA Gear Research Institute members interested in induction hardening technology identified four thrust areas where pre-competitive research would be of direct benefit. These are Material/Process Interactions, Process Models, Quenching Effects, and Smart Controllers. The thrust areas are listed below, each with possible sub tasks. The specific projects to be conducted in each of these areas will be determined by the membership.

Technical Thrust Areas

1. Material/Process Interaction Research

Goal: Identify dominant issues over a broad range of materials.

Properties as a function of frequency, heating rate, temperature; develop the building blocks necessary to build process models.

- Electromagnetic Properties
- Austenitization Kinetics, heating rates similar to induction
- Transformation Temperatures, heat rates similar to induction
- Effects of cold finishing, decarburization, prior microstructure, etc.

2. Process Models

Goal: Create a PC-based software tool kit for process tryout and visualization.

- Various materials
- Frequencies
- Wave forms
- Coil geometries
- Part geometry's
- Coupling conditions
- Quenching Parameters
- Multi-Pulse heating processes

3. Quenching

Goal: Develop quenching data to assess dominant issues as they affect hardening process.

- Concentration
- Temperature
- Pressure
- Flow Rate
- Surface Condition and Contamination

4. Smart Controller Development (Closed-Loop Neural Net Controllers)

Goal: Evaluate the applicability of neural net controllers for use on alternate applications and develop controller concepts, algorithms, and prototypes.

- Range of part geometries
- Range of coil geometries
- Range of materials
- Range of frequencies
- Variations in wave forms
- Multi-pulse heating systems
- Range of applications
- Post-process inspection tools

The goal of the proposed follow-on effort will be to broaden the range of applications for induction hardening by developing an understanding of material/process interactions, creating process tryout and simulation tools, incorporating quenching effects into the simulation tools, and developing smart controllers for various types of geometries. Success in one or more of these areas will improve existing operations and enable replacement of carburizing and other case hardening processes for significant numbers of applications.

The structure of an industrial consortium, based on comments included in our survey of the Gear Research Institute membership, is outlined below.

- 20-30 Companies contributing 10K in cash each (200-300K total) and contributing an aggregate amount of PIK valued at 200-300K
- Budget Target, 800K-1.2M/year, 600-900K as cash
- Mix of industries, users, intended users, and equipment manufacturers
- Life Target, 5 years
- Steering committees to define project focus areas
- One year project agreements, meaningful deliverables building to 5 year goals
- Projects to be approved by overall membership
- Semi-annual technical review meetings
- Six-month industrial internships available as desired
- Industrial experiments integral part of the plan

Sandia National Laboratories
P.O. Box 5800
Albuquerque, NM 87185

Attn.: Russell D. Skocypec, MS 0835
Manager, Thermal and Fluid Sciences
Phone: 505-845-8838
Fax: 505-844-8251

Gentlemen:

RE: **Non-Binding Letter Of Intent**
Induction Hardening Consortium
(Please Respond By June 15, 1995)

Although _____ (hereinafter, "The Company") is not legally bound hereby, The Company presently intends to seek membership in the **Induction Hardening Consortium** for a period of five (5) years, provided that the final negotiated terms and conditions of the consortium charter agreement and the agreement between the consortium and the United States Department of Energy, DOE, are acceptable. Membership is contingent upon all final terms and conditions, but particularly with respect to consortium members rights to technical data, other intellectual property rights, and establishing a predefined scope of technical work. Presently, The Company is interested in continuing the organizational discussions for the proposed **Induction Hardening Consortium** with Sandia National Laboratories and the DOE.

Signed,
Company Officer

MATERIALS R&D — STUDENT INTERNSHIPS

R. B. Thompson, D. C. Jiles and L. S. Chumbley

Metallurgy and Ceramics Division
Ames Laboratory
Iowa State University
Ames, Iowa 50011

INTRODUCTION

This program has as an objective the conduct of programmatic research for the Advanced Industrial AIM Materials Program while training minority students in the process.

Well-known demographics indicate that minorities will constitute an increasing fraction of our future work force. Consequently, efforts have been initiated to increase the fraction of minorities and women who choose and successfully follow technical career paths. Included are a wide ranging set of programs beginning with pre-school education, progressing through efforts to retain students in technical paths in grades K-12 and undergraduate education, and ending with encouraging graduate education. The Materials R&D — Student Internships is a unique approach in the latter category. Here, we have focused on a particular area of applied materials research, the Advanced Industrial Materials (AIM) Program. Our goal, then, is to educate minority graduate students in the context of this program. The Ames Laboratory was selected as a site for this pilot project since it is a DOE national laboratory, located on the campus of a major research university, which includes in its research interest programs with a strong technological flavor. Many of the Laboratory staff hold shared faculty appointments.

More specifically, the pattern through which a student will pass involves a sequence of steps progressing through recruitment, project selection, research, mentoring, and graduation. Recruiting is being accomplished by nationally advertising " AIM Materials Technology Fellowships for Minorities." We feel that it would be desirable to offer at least one such fellowship each year to maintain continued visibility on minority campuses and to establish effective working relationships with appropriate personnel. Other factors which we believe to be essential to the success of the project include offering each student a variety of project opportunities — active choice in project selection will greatly increase the student's motivation

and likelihood of success — and continued mentoring throughout the program. The projects offered to the students are consistent with the guidelines of the AIM program.

TECHNICAL PROGRESS — FY 1995

Summary

During FY 1995, the first minority fellow, Ms. Patricia Pulvirenti, completed her third year of course work and research. She plans to complete her Masters degree in February 1996. During this period, she has made a presentation at one regional and one international meeting, had a paper accepted for publication in the Journal of Applied Physics, and submitted one patent application. Her work is concerned with the dynamic magnetostrictive response of Terfenol-D, a highly magnetostrictive material. The second student, Ms. LaVonne Carson, completed her third full year of studies. Her work concerns the preparation of nanocrystalline materials and deposition of CR layers using an inductively-coupled RF plasma. She plans to take her Ph.D. preliminary examinations in January 1996. Each student is enrolled in the Materials Science and Engineering Department of Iowa State University. Technical progress on these projects is summarized below.

Technical Details

1. Development of Magnetostrictive Materials with Enhanced Energy Transfer Efficiency for Transducers and Actuators

Introduction. The rare earth-iron magnetostrictive material Terfenol is being studied by Ms. Pulvirenti for its use in sensor and transducer applications, particularly adaptive vibration control. The conductivity of the material significantly reduces the magnetic field penetration into the material, and hence reduces the strain at kilohertz frequencies. This results in a drastically reduced energy conversion efficiency as the frequency of excitation increases. Therefore, one of the principal objectives of this work has been to study ways to alter the material to improve the performance at frequency. In addition, basic studies have been undertaken to understand and characterize the properties of the material.

A principal concern of this work has been the ac characterization of Terfenol-D. One of the important properties under consideration is complex permeability. When operating under AC conditions, permeability is a complex quantity with a real part and an imaginary part. That is, it

has an in-phase component and an out-of-phase component. The imaginary part is the component of the induction B which is out-of-phase in reference to the applied magnetic field H. It is related to the power losses in the material which result from the eddy currents that dissipate energy and limit the field penetration. In the ac characterization of a magnetostrictive material, among other factors, one is often interested in the energy conversion efficiency, that is the ratio of mechanical energy output to magnetic energy output. This is often represented by the magnetomechanical coupling coefficient, k. It may have a maximum value of 1. Conventionally, there are two accepted methods for calculating k.

The first is the resonance-antiresonance method, equation (1)

$$k^2 = \frac{\pi^2}{8}\left[1 - \left(\frac{f_r}{f_a}\right)^2\right] \tag{1}$$

where f_r is resonant frequency and f_a is the antiresonant frequency.

The other method for calculating k is using the piezomagnetic coefficient, g, permeability at constant stress, μ_s, and compliance at constant induction s_B. This is the so-called three parameter method. The value of k is obtained from equation (2).

$$k^2 = g^2 \frac{\mu_s}{s_B} \tag{2}$$

The two equations actually yield different values of k because of the measurement conditions from which they are calculated. So it is very important to specify the exact conditions under which the measurements were taken. In addition, different measurement conditions can yield different values for k, even when using the same equation, since k is very much a measure of the efficiency of the entire system, and not necessarily the material alone.

Measurements. Nine samples of polycrystalline Terfenol with various alloying additions were made by the drop cast method. These were compared with an undoped polycrystalline sample. By alloying with elements from group IIIA and IVA, it may be possible to provide additional scattering sites for the conduction electrons (since the impurity atoms will sit on interstitial sites) and thereby increase the resistivity. If this can be achieved, the penetration depth of an alternating magnetic field into the Terfenol samples may be increased. Samples were made with 1%, 2% and 3% Al, 1%, 2% and 3% Si, and 1%, 2% B, and undoped Terfenol.

The addition of elements such as aluminum, silicon or boron to Terfenol is thought to have two main effects: (i) it increases resistivity and (ii) it decreases magnetostriction. The first of these is clearly desirable for improving the frequency response of the material. The second is undesirable. It is therefore possible that the trade off between these two effects will lead to an optimum amount of alloying additions at which the energy conversion efficiency reaches a maximum. This was indeed found to be the case. The optimum level of alloying additions in the specimens that we investigated appeared to be close to 1%. We therefore report on these particular specimens. In the case of the 1% boron, the material was so brittle that we were unable to produce a suitable specimen.

Measurements have been made of the complex permeability over a range of frequencies from 10 Hz — 50 kHz. It was found that two of the doped samples showed enhanced properties at frequency. The samples with 1% each of Al or Si exhibited a 125% increase in resistivity compared to the pure Terfenol sample. This corresponds to an increase in skin depth of 80% at 1 kHz. The results are described in detail in reference.[1]

Theory: Magnetic Grüneisen Parameter. In order to better understand the conversion of magnetic to elastic energy, we have investigated some fundamental issues underlying the magnetostriction coefficient. The magnetostriction of a material, like the thermal expansion, is a result of anharmonicity in the crystal lattice. Therefore, it should be possible to develop a relationship between, on the one hand, the third order (anharmonic) terms in the crystal potential and the magnetostriction coefficient. It is known that in Terfenol and related materials the magnetostriction coefficient is very large, therefore we expect the anharmonicity to reflect this. One way of quantifying the anharmonicity is by the so-called Grüneisen parameter which is the coefficient of proportionality which relates the fractional change in vibration frequency to the fractional change in volume when subjected to pressure.

An expression for the Grüneisen parameter in terms of the force constant in the crystal lattice can be derived relatively simply. It is found that the fractional change in the vibrational

---

[1]P. P. Pulvirenti, D. C. Jiles, R. D. Greenough and I. M. Reed, to be published, Proceedings of the 40th Conference on Magnetism and Magnetic Materials, Philadelphia, November 1995, *J. Appl. Phys.* (1996).

frequency of the lattice as it is distorted gives the fundamental measure of anharmonicity. In fact, the ratio of the volume strain to the fractional change in vibration frequency is found to be linearly dependent on the third order coefficient of the interatomic potential. The Grüneisen parameter is thus a linear function of the third order (anharmonic) coefficient of the lattice potential.

We can expect that a higher Grüneisen parameter is characteristic of a material with a higher energy conversion efficiency. It remains for us to quantitatively relate this Grüneisen to the k coefficient.

The magnetomechanical coupling, and hence the energy conversion efficiency, can be related to the anharmonicity in the crystal lattice. In fact, the relationship between anharmonicity of crystals and thermal expansion is very well known. They are related by the Grüneisen parameter, γ, given by

$$\frac{\Delta v}{v} = -\gamma \frac{\Delta V}{V} \tag{3}$$

and consequently,

$$\gamma \equiv -\frac{d \ln v}{d \ln V} \tag{4}$$

where v is the vibrational frequency of the solid, and V is the volume. In this work, we have attempted to obtain a relationship between magnetostriction and anharmonicity. That is, we have defined a magnetoelastic Grüneisen parameter, analogous to the well known thermoelastic one.

A thermoelastic equation of state can be written as a function of volume and internal energy in terms of the temperature, an independent variable:

$$dT = \left(\frac{\partial T}{\partial U}\right)_V dU + \left(\frac{\partial T}{\partial V}\right)_U dV \tag{5}$$

The first term is the inverse of the specific heat at constant volume, c_v, where

$$c_v \equiv \left(\frac{\partial U}{\partial T}\right)_V \tag{6}$$

The differential of the volume as a function of temperature and pressure is:

$$dV = \left(\frac{\partial V}{\partial T}\right)_P dT + \left(\frac{\partial V}{\partial P}\right)_T dP \tag{7}$$

The first term is the coefficient of thermal expansion, β times V where β is defined as:

$$\beta \equiv \frac{1}{V}\left(\frac{\partial V}{\partial T}\right)_P \tag{8}$$

The second term is the isothermal compressibility, $-\kappa_T$ times V, where κ_T is defined as:

$$\kappa_T \equiv -\frac{1}{V}\left(\frac{\partial V}{\partial P}\right)_T \tag{9}$$

One can define the coefficient of linear expansion, α,

$$\alpha \equiv \frac{1}{l}\left(\frac{\partial l}{\partial T}\right)_P \tag{10}$$

where

$$\beta = 3\alpha \tag{11}$$

The dimensional changes discussed above, which may arise from such contributions as lattice vibrations or magnetic phenomena, occur in order to minimize free energy. Thermal expansion is therefore related to elasticity, Fermi surface, magnetostriction, etc. Grüneisen showed that the dimensionless combination

$$\frac{\beta}{\kappa_T c_V} = \frac{\beta}{\kappa_s c_p} \tag{12}$$

was found to be equal to -dlnv/dlnV. He therefore set this equal to a constant γ, known as the Grüneisen parameter.

$$\gamma = -\frac{d \ln v}{d \ln V} \tag{13}$$

where v is the vibrational frequency of the lattice, and V is the volume. The importance of this is that the gammas are (nearly) independent of temperature. For most solids γ is constant.

It is often written in terms of the linear coefficient of expansion α.

$$\gamma = \frac{3\alpha}{c_v \kappa_T} \tag{14}$$

The magnetoelastic equations of state are derived in an analogous fashion to the relevant thermoelastic equations of state written above.

The magnetoelastic analog to the volume differential is the strain (or magnetostriction) differential:

$$d\lambda = \left(\frac{\partial \lambda}{\partial H}\right)_\sigma dH + \left(\frac{\partial \lambda}{\partial \sigma}\right)_H d\sigma \tag{15}$$

or

$$d\lambda = d_\sigma dH + s_H d\sigma \tag{16}$$

where d_σ is the piezomagnetic strain coefficient at constant stress, and s_H is the elastic compliance (inverse of Young's modulus) at constant applied magnetic field.

The derivative of internal energy, U with respect to magnetic field, H at constant strain is

$$\left(\frac{dU}{dH}\right)_\lambda = B_\lambda \tag{17}$$

which is the magnetic induction at constant strain.

Now comparing each thermoelastic differential with its magnetoelastic counterpart, we can obtain a magnetoelastic Grüneisen constant.

$$c_v \rightarrow B_\lambda \tag{18}$$

$$\beta \rightarrow d_\sigma \tag{19}$$

and

$$\kappa_T \rightarrow s_H \tag{20}$$

We may now write a magnetoelastic Grüneisen gamma as:

$$\gamma_{me} = \frac{3d_\sigma}{B_\lambda s_H} = \gamma_{me} = \frac{3d_\sigma}{H\mu_\lambda s_H} \tag{21}$$

where H is the applied magnetic field and μ_λ is the permeability at constant strain. One can derive the magnetomechanical coupling coefficient, k, from the magnetoelastic equations of state.

$$k^2 = \frac{d_\sigma d_H}{\mu_\sigma s_H} \tag{22}$$

The important result is that the k^2 is proportional to γ_{me}. Assuming that $\mu_\lambda \sim \mu_\sigma$ then

$$k^2 = \gamma_{me} \frac{Hd_H}{3} \tag{23}$$

Although the thermoelastic gamma is substantially independent of temperature, it has not yet been established whether the magnetoelastic gamma is independent of applied magnetic field. Preliminary analysis of results indicate that indeed $k^2 \propto H$. This therefore provides a way of determining the field dependence of the energy conversion efficiency in magnetostrictive materials.

2. Plasma Processing of Materials Using Inductively-Coupled, RF Plasma.

Introduction. The use of an inductively-coupled, rf plasma system to deposit nanocrystalline, intermetallic films is being explored by Ms. Carson. In addition, while certain system modifications are underway, she has studied the deposition of Cr films using the system.

High Temperature Intermetallic Compounds. Intermetallic compounds, mainly Cr, Ti, and Mo silicides, were processed to produce nanocrystalline materials. The data from these experiments show that nanocrystalline material can be produced but the results have been inconsistent. It appears that, if the elemental constituents vary substantially in density, it is more difficult to produce material that is nanocrystalline, single phase intermetallic. Some idea of the reaction kinetics that occur as the feed material is first vaporized and then recombines in the chamber is needed if a theory is to be devised that explains why some materials work while others do not. To this end, the system is undergoing modifications to allow the various chemical species present in the plasma to be monitored. A monochromator is being installed to analyze

the material as it passes through the plasma plume. Decomposition and recombination of the material in the plasma plume will be analyzed.

In connecting the monochromator to the plasma unit, it was discovered that, due to storage, several pieces of the equipment were missing or damaged and needed to be replaced. Thus, progress on this part of the project has been slowed due to the equipment being shared with another project, delays in the completion of the monochromator stand, loss of several of the monochromator parts, and the unexpected death of one student assisting with the routine maintenance and operation of the plasma unit. During these slow periods, efforts on the deposition of Cr have increased.

Deposition of Cr. The deposition chrome using the plasma unit is being investigated. The precursor materials used in this process were chromium hexacarbonyl and pure chromium powder. These materials were fed through the plasma unit and deposited on different metallic substrates, mainly those of copper and mild steel. The objective was to determine the possibility of obtaining a thin layer of hard chrome on a part for wear applications. The control variables for these experiments were vertical and radial distances and length of deposition. An example of the experimental set up can be found in Figure 1.

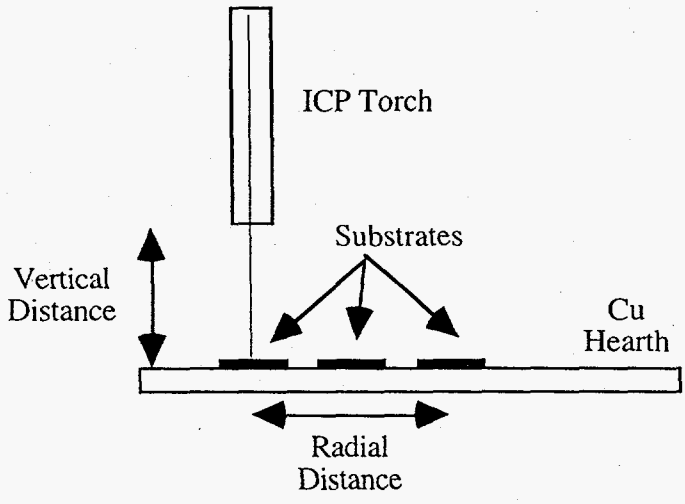

Figure 1. Schematic showing the placement of substrates and distance variables.

Each experiment was done twice for statistical purposes and design of experimental analysis. Auger analysis, along with scanning electron microscopy (SEM), was used in determining preliminary values for the coating composition. Samples generated using chromium hexacarbonyl and chromium powder as a feed material are being analyzed. The thickness of the films are being determined by sputtering through the film using the Auger spectrometer and observing the thickness at which the chromium signal falls to zero. An example of an Auger scan can be seen in Figure 2.

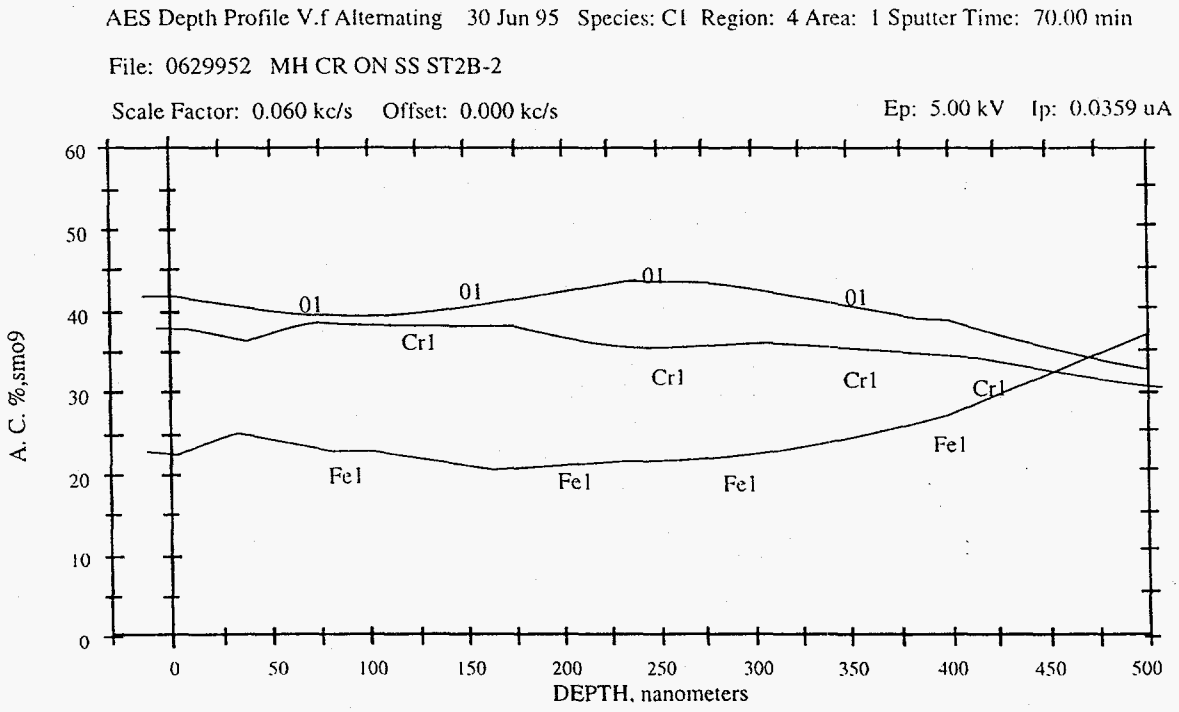

Figure 2. Typical Auger spectroscopy scan of deposited films.
This particular sample used the CR powder as the feed material.

Initial results show that the films being deposited range in thickness from 0.1 nm to 500 nm. The range in the thickness values were dependent upon the location of the substrate with respect to the torch. The composition of these coatings are chromium oxide regardless of the feed material used, with the major phase present being CrO. Samples continue to be analyzed so thickness data will be reported as it becomes available.

The design of experiment analysis was done using the software program ECHIP. ECHIP suggests that we carry out these experiments at the recommended operating parameters for both precursor materials shown in Table 1. The data obtained from these experiments will be plotted on a graph similar to that shown in Figure 3.

Table 1. Design of Experiment Results

Trial	Distance (inches)	Time (hours)
1	10	1
2	6	1.5
3	14	1.5
4	14	1
5	6	2
6	14	2
7	6	1
8	10	2
9	8.67	1.33
10	11.33	1.33
11	11.33	1.67
12	8.67	1.67
13	8.67	2
14	10	1
15	6	1.5
16	14	1.5
17	14	1
18	6	2

The design of experiments analysis using ECHIP should also be applicable to the production of nanocrystalline material. In this instance, the quantity desired will not be a coating thickness but will be the parameters that give the highest percentage of material that is single phase, nanocrystalline intermetallic.

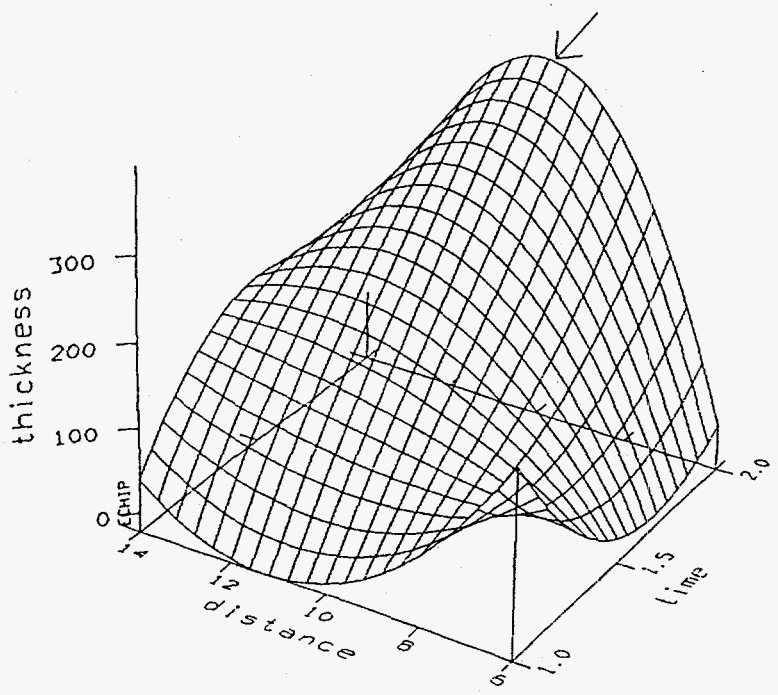

Figure 3. Results of deposition experiments using ECHIP

The information on this graph will determine the optimum operating conditions that will give the desired film thickness and composition. To date, all of the experiments for chromium hexacarbonyl has been completed and the samples are in the process of being analyzed. The experimental design will be repeated for pure chromium powder as the feed material.

ES&H studies were done to test the output of the plasma chamber for gaseous effluents and particulate matter at the exhaust point of our system. These tests were conducted for both materials at all operating conditions. The results show that for the chromium hexacarbonyl system, the amounts of CO and CO_2 detected were a little higher than the amount of these substances occurring in ambient air. The slightly higher values are believed to be due to the reaction itself since both CO and CO_2 are by-products of the reaction taking place inside of the feed container. The amount of Cr detected for this system was minimum. For the pure chromium powder system, the amounts of CO and CO_2 varied slightly from the amount present in air. The amount of Cr detected was higher, as we had expected, since there were problems in feeding the material into the system. In either case, the results show that both systems were fairly clean, i.e. the material inputs were essentially fully consumed in the reaction.

MILESTONES DURING FY 1995

Milestones included continuing the work in our first and second student while adding a third student to the program. Milestones one and two were met, as described herein. The third student was not added due to uncertainties in budget prospects.

PUBLICATIONS

1. "Enhancement of the Piezomagnetic Response of Highly Magnetostrictive Rare Earth Iron Alloys at kHz Frequencies," P. P. Pulvirenti, D. C. Jiles, R. D. Greenough and I. M. Reed. Accepted for publication in *J. Appl. Phys.* (1996).

2. "Magnetostriction and Magnetic Grüneisen Parameters in Pseudo-Binary Rare Earth Transition Metal Alloys," P. P. Pulvirenti and D. C. Jiles. Submitted to *INTERMAG 96*, Seattle, April 1996.

PRESENTATIONS

1. A presentation at the Twenty-Fourth Midwestern Mechanics Conference, Ames, Iowa, October 2-5, 1995 by P. P. Pulvirenti.

2. "Enhancement of the Piezomagnetic Response of Highly Magnetostrictive Rare Earth Iron Alloys at kHz Frequencies," P. P. Pulvirenti, D. C. Jiles, R. D. Greenough and I. M. Reed, Fortieth Magnetism and Magnetic Materials Conference, Philadelphia, November 6-9, 1995.

HONORS AND AWARDS

None.

PATENTS/DISCLOSURES

"Method for Improving the Frequency Response of Magnetostrictive Materials," P. P. Pulvirenti and D. C. Jiles. Disclosure Number AL389.

LICENSES

None.

INDUSTRIAL INPUT AND TECHNOLOGY TRANSFER

One meeting with C. Cartwright and M. Goodfriend of Edge Technologies Inc., the leading supplier of Terfenol material, to discuss possible implementation of the new method for producing highly energy efficient magnetostrictive materials for high frequency applications.

ENERGY SAVINGS

Energy savings for the improved magnetostrictive material will be a 55% improvement in conversion efficiency at kilohertz frequencies. Energy savings that would be realized should the Cr plating study lead to an industrial process would be significant since Cr plating baths could be eliminated as well as the energy costs associated with transporting the hazardous material generated by these baths and the cost of the clean-up process.

HIGHLIGHTS

Through the addition of 1% Al and Si, it has been possible to realize a 125% increase in resistivity and a 55% increase in the energy conversion efficiency of the highly magnetostrictive material Terfenol. These results are the basis for a patent disclosure that is under internal review.

MICROWAVE JOINING OF SiC

R. Silberglitt and I. Ahmad

FM Technologies, Inc.
10529-B Braddock Road
Fairfax, VA 22032

W. M. Black, R. F. Cozzens, T. A. Shan and Y. L. Tian

George Mason University
4400 University Drive
Fairfax, VA 22030

J. D. Katz

Los Alamos National Laboratory
Post Office Box 1663 Mail Stop G771
Los Alamos, NM 87545

INTRODUCTION

The purpose of this work is to optimize the properties of SiC-SiC joints made using microwave energy. The current focus is on identification of the most effective joining methods for scale-up to large tube assemblies, including joining using SiC produced in situ from chemical precursors.

TECHNICAL PROGRESS FY 1995

Summary

1. Fracture Toughness Versus Joining Temperature

During a previous performance period, specimens of Coors reaction bonded silicon carbide (RBSC) tubes with outer diameter of 3.49 cm (1.375 in), inner diameter of 2.54 cm (1 in) and length of 2.54 cm (1 in) were joined at four different joining temperatures: 1420°C, 1465°C, 1515°C and 1565°C. In each case the joining temperature was maintained to within 15°C for approximately 30 minutes. The joined specimens were sent to Los Alamos National Laboratory for mechanical evaluation. Test bend bars were machined from each specimen and Chevron

notches machined into the joint interface, as indicated in Figure 1. Figure 2 shows the fracture toughness determined from 4-point flexure tests of the notched test bend bars. The data labeled "no joint" were derived from test bend bars machined from an as-received specimen of RBSC. The average fracture toughness was determined from measurements on 6-8 specimens and the standard deviation is indicated by the shorter bars in Figure 2. The joining temperatures for each specimen were as follows: specimen 1A at 1465°C; specimen 1B at 1515°C; specimen 2A at 1565°C; specimen 2B at 1420°C. Figure 2 suggests that the optimum joining temperature is likely between 1420°C and 1500°C, and perhaps very close to 1465°C. Specimens joined near this optimum temperature have fracture toughness greater than the as-received material. The standard deviation of the fracture toughness values for the joined specimens was also smaller than that for the as-received material, except for specimen 1B, which had one data point with a fracture toughness value far different from all others. Inspection of the fracture surface of this test bar is being performed to see if its failure was caused by a defect in the material or by the specimen preparation process, rather than by failure of the joint.

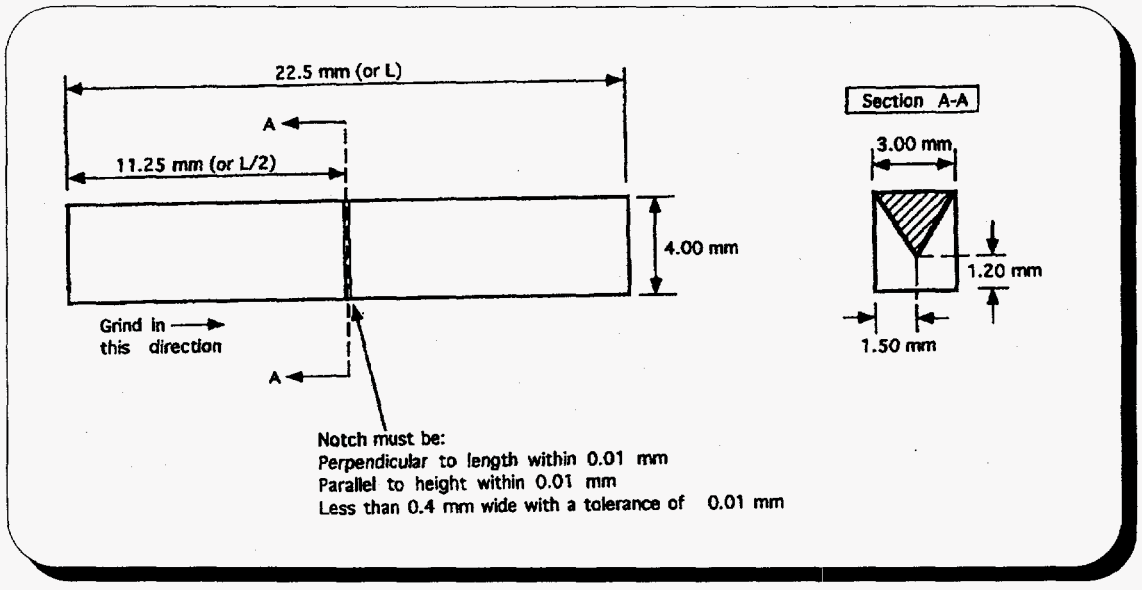

Figure 1: Schematic Illustration of Chevron Notched Fracture Toughness Specimen

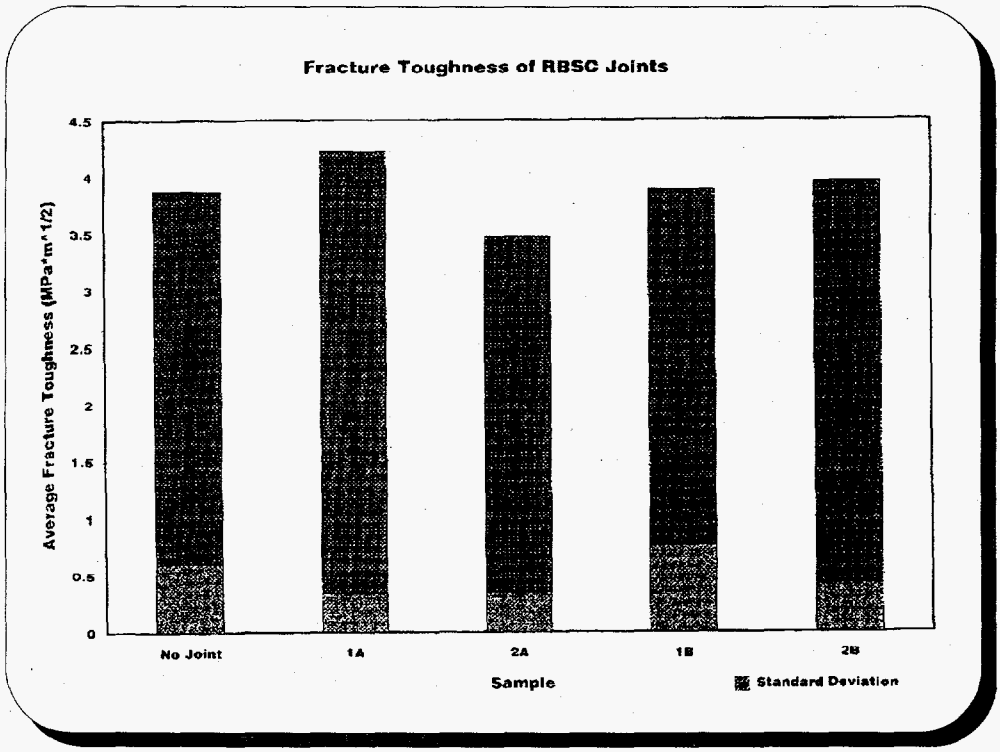

Figure 2: Fracture Toughness of RBSC Specimens (Joining Temperatures: Specimen 1A, 1465°C; Specimen 2A, 1565°C; Specimen 1B, 1515°C; Specimen 2B, 1420°C)

2. Joining Using SiC Produced In Situ From Pyrolysis of Polymer Precursor

Microwave-induced pyrolysis of Polycarbosilane (PCS) was used to join specimens of Hexoloy™ sintered SiC by forming SiC in situ at the interface. The PCS used in these experiments was Dow Corning X9-6348 (manufactured by Nippon Carbon Corporation, Tokyo, Japan), with an average molecular weight of 1400. The SiC specimens were rods 0.95 cm (0.375 in) in diameter and 0.5 cm (0.197 in) long, which were purchased from the Carborundum Company. The PCS was dissolved in hexane and applied to the surface of one sintered SiC rod, which had been polished and etched with HF. This SiC rod was then held in contact with a second SiC rod under a pressure of 30 psi (0.2 MPa), and joined in a single mode TE_{103} rectangular cavity using the configuration indicated schematically in Figure 3. Joining was accomplished in 30 minutes at a temperature of 1400°C using approximately 900 Watts of input power. Figure 4 is a representative SEM of a joined and sectioned specimen, demonstrating a smooth and homogeneous SiC interlayer a few microns in width.

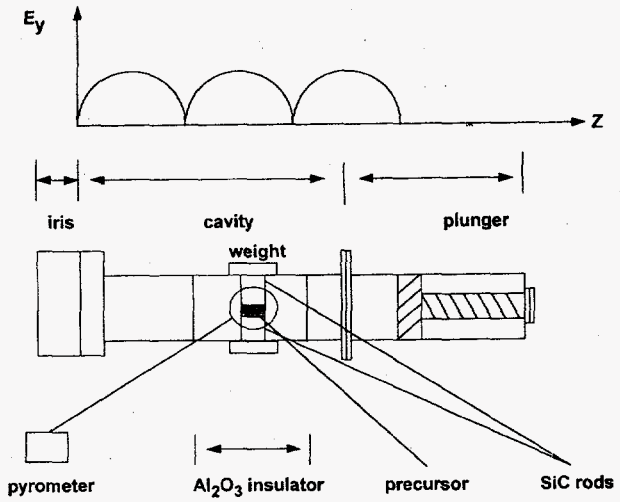

Figure 3: Experimental Setup for Microwave Joining Using Polycarbosilane Precursor

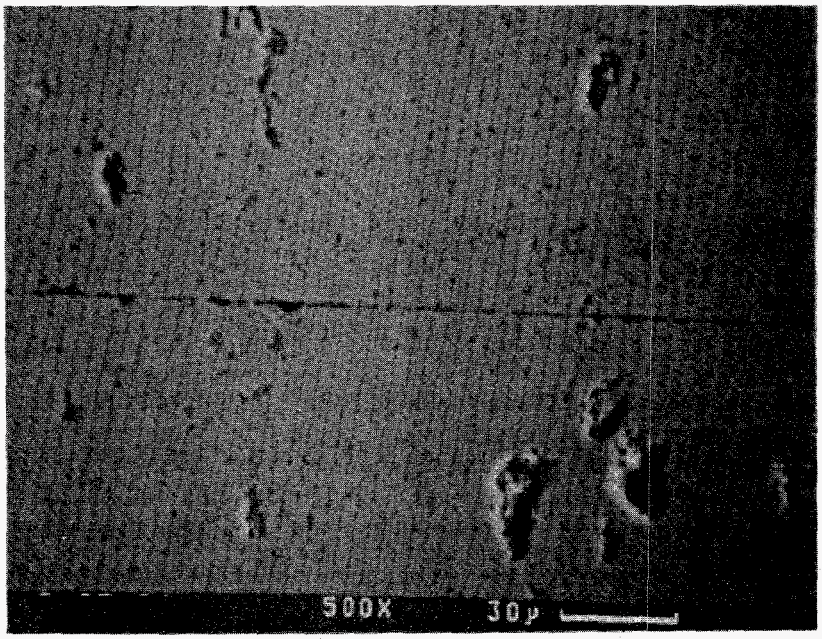

Figure 4: SEM Micrograph of Sectioned SiC Rods Joined Using Polycarbosilane Precursor

A detailed evaluation was performed of the effect of surface preparation on this type of SiC joint. Four sets of specimens were prepared using different surface treatments. All four sets of specimens were cut from as-received rods using a Buehler Low Speed Saw and a high concentration diamond blade. The PCS was again dissolved in hexane and applied to the surface to be joined. For the first set of specimens, the PCS solution was applied directly to the as-cut surface. For the second set, the surfaces to be joined were etched in 40% hydrofluoric acid before the PCS was applied. The joining surfaces of the other two sets of specimens were ground on a diamond wheel. One set of surfaces was then also etched before PCS application, while the other was not.

The specimens were placed in a TE_{103} single mode cavity applicator under a mixed reducing atmosphere of 95% nitrogen and 5% hydrogen. Microwave power was coupled to the specimens using an adjustable iris and plunger and the specimens were heated to 1400-1450°C and held in this temperature range for 30 minutes. These specimens either did not join or were weakly bonded. However, investigation of the adherence of SiC formed from the PCS on the sintered SiC surface indicated that the ground and etched surface was most favorable for joining. An additional set of specimens was then prepared using grinding and etching of the surface. In addition, a mixture of SiC powder and PCS was applied to the surface to be joined. This set of specimens was heated using the same conditions as above, resulting in a good joint.

Figures 5 and 6 are Scanning Electron Micrographs (SEMs) of the surface of the specimens which had the PCS applied to the as-cut surface and to the ground and etched surface, respectively. Both surfaces were scratched with a sharp metal point under a load of 820 grams in order to investigate the adherence of the SiC formed from the decomposition of the PCS. Comparison of the SEMs shows greatly enhanced wetting and spreading of the SiC formed from the PCS on the ground and etched surface. SEMs (not shown) of surfaces that were either ground or etched also showed improvement over the as-cut surface, but the combination of grinding and etching provided the best wetting and spreading. Figure 7 is a higher magnification of the micrograph shown in Figure 6, which indicates that larger flakes of SiC were peeled off by the metal point, but good coverage of the scratched area remained, suggesting that the smaller flakes were adherent. Figure 8 is an SEM of a cross-section of the specimen joined using the

mixture of SiC and PCS, after grinding and etching of the surfaces to be joined. A continuous joint interlayer approximately 50-60 μm in thickness was formed. In addition, a combination of the SiC introduced at the interlayer and the SiC formed from the PCS completely filled the pores near the interface of the joined specimens.

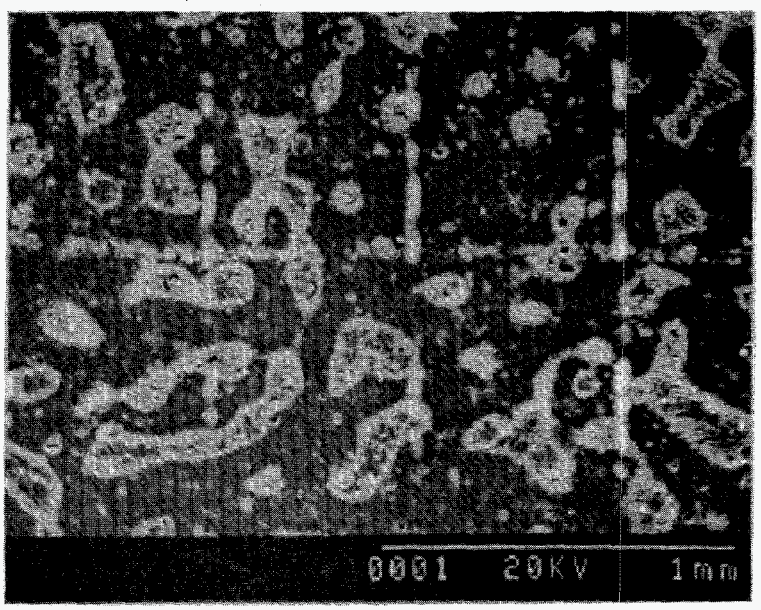

Figure 5: SEM of As-cut SiC Surface After Application of Polycarbosilane and Microwave Heating to 1400-1450°C

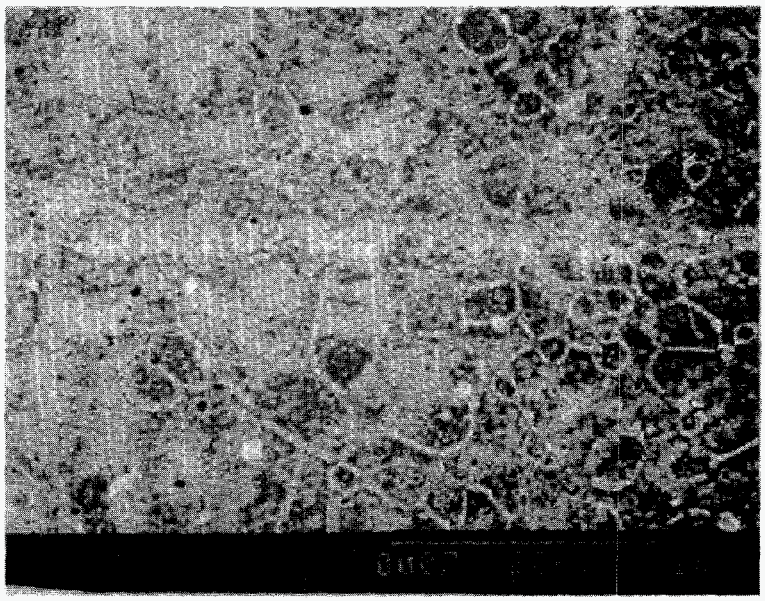

Figure 6: SEM of Ground and Etched SiC Surface After Application of Polycarbosilane and Microwave Heating to 1400-1450°C

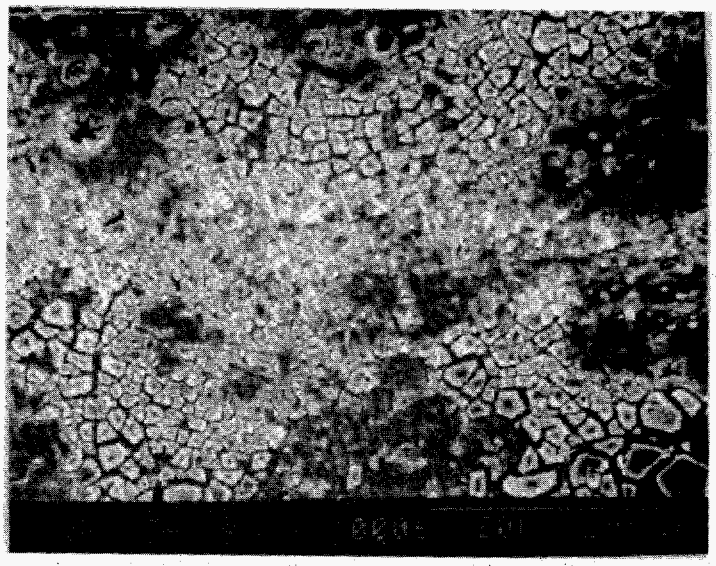

Figure 7: Higher Magnification of the SEM of Figure 6, Showing Adherence of SiC Formed From Decomposition of Polycarbosilane to the Ground and Etched Surface

Figure 8: Cross-section of Sintered SiC Joined Using a Mixture of SiC and Polycarbosilane as the Interlayer Material

MILESTONES DURING FY 1995

1. Demonstration that the fracture toughness of the microwave joints between reaction bonded SiC tube sections of 1.375" outer diameter is greater than or equal to that of the as-received material, when joined in the optimum temperature range (March 1995).

2. Joining of sintered SiC using SiC formed in situ from microwave-assisted pyrolysis of polymer precursor and investigation of the effect of surface treatment on joining (May 1995).

PUBLICATIONS

1. Y. L. Tian, W. M. Black, H. S. Sa'adaldin, I. Ahmad, and R. Silberglitt, "Dynamic Model for Electromagnetic Field and Heating Patterns in Loaded Cylindrical Cavities," Proceedings of the Symposium, Microwaves:Theory and Application in Materials Processing III, *Ceramic Transactions, Vol. 59*, American Ceramic Society, Westerville, OH, pp. 261-268 (1995).

2. I. Ahmad, R. Silberglitt, T. A. Shan, Y. L. Tian and R. Cozzens, "Microwave-Assisted Pyrolysis of SiC and Its Application to Joining," Proceedings of the Symposium, Microwaves:Theory and Application in Materials Processing III, *Ceramic Transactions, Vol. 59*, American Ceramic Society, Westerville, OH, pp. 357-365 (1995).

3. R. F. Cozzens, T. H. A. Shan, Y. L. Tian, I. Ahmad and R. Silberglitt, "Microwave Processing of Polycarbosilane and its Use as a Ceramic Joining Aid," *Proceedings of the 30th IMPI Microwave Symposium*, International Microwave Power Institute, Manassas, VA (1995).

PRESENTATIONS

1. R. Silberglitt, "Microwave Joining of SiC," presented at the Advanced Industrial Materials Program Annual Meeting, held at the J. W. Marriott Hotel, Washington, D.C., June 14-16, 1995.

2. R. Silberglitt, "Joining of Ceramics," presented as part of the ISMI Professional Development Course on Advanced Microwave Technology, International Microwave Power Institute (IMPI) Annual Microwave Symposium, Denver, CO, July 9, 1995.

3. Publications listed above were presented at the symposia referenced. The paper by I. Ahmad was an invited paper at the American Ceramic Society Annual Meeting and Exposition, April 30-May 4, 1995 in Cincinnati, OH.

HONORS AND AWARDS

None

PATENTS/DISCLOSURES

None

LICENSES

None

INDUSTRIAL INPUT AND TECHNOLOGY TRANSFER

Golden Technologies, Inc., the Coors company responsible for ceramics R&D, has provided materials and joining requirements for radiant burner tube assemblies. Technology transfer plans include fabrication and scale-up of tube assemblies, and testing by the user industry under simulated service conditions. Discussions are ongoing with manufacturers of ceramic heat exchangers and advanced turbine engines to identify subscale component demonstrations involving microwave joining.

ESTIMATED ENERGY SAVINGS

Natural gas savings estimated at $172,892 per year due to 4-7% higher efficiency of SiC radiant burner tubes. Use of SiC tube heat exchanger in externally fired combined cycle coal power plants is projected to produce a 20% increase in thermal efficiency, together with a 20% reduction in CO_2 emissions and a 90% reduction in SO_x emissions.

HIGHLIGHTS

The two major accomplishments during FY 1995 were: (1) demonstration that the fracture toughness of reaction bonded SiC tube joints with outer diameter of 1.375" is greater than or equal to that of the as-received material; and (2) microwave joining of sintered SiC using pyrolysis of a polymer precursor to form SiC in situ. These provide the building blocks necessary for scale-up of the method to joining of larger tubes for commercial applications such as radiant burners and ceramic heat exchangers.

MICROWAVE PROCESSING OF CERAMIC OXIDE FILAMENTS

G. J. Vogt

Los Alamos National Laboratory
P.O. Box 1663
Los Alamos, New Mexico 87545

INTRODUCTION

The objective of the microwave filament processing project is to develop microwave techniques at 2.45 GHz to manufacture continuous ceramic oxide filaments. Microwave processing uses the volumetric absorption of microwave power in oxide filament tows to drive off process solvents, to burn out organic binders, and to sinter the dried fibers to produce flexible, high-strength ceramic filaments. The technical goal is to advance filament processing technology by microwave heating more rapidly with less energy and at a lower cost than conventional processing, but with the same quality as conventional processing. The manufacturing goal is to collaborate with the 3M Company, a US manufacturer of ceramic oxide filaments, to evaluate the technology using a prototype filament system and to transfer the microwave technology to the 3M Company.

Continuous ceramic filaments are a principal component in many advanced high temperature materials like continuous fiber ceramic composites (CFCC) and woven ceramic textiles. The use of continuous ceramic filaments in CFCC radiant burners, gas turbines, waste incineration, and hot gas filters in U.S. industry and power generation is estimated to save at least 2.16 quad/yr by year 2010 with energy cost savings of at least $8.1 billion. By year 2010, continuous ceramic filaments and CFCC's have the potential to abate pollution emissions by 917,000 tons annually of nitrous oxide and 118 million tons annually of carbon dioxide (DOE Report OR-2002, February, 1994).

Woven textiles are used in hot gas filtration, high-temperature insulation in aircraft firewalls and engine cowls, zone dividers and furnace curtains in metal processing, oil boom covers to burn off oil spills, and many other applications. Seamless ceramic fiber filter bags can

operate up to 1100°C to remove more than 99.9% of the pollution particulates in a variety of corrosive gas environments. Annual energy savings of 0.1 quad/yr are possible from the combustion of coal alone. Hot gas filters will reduce nitrous oxide and carbon dioxide emissions by thousands of tons annually. Filtered hot gas will also help prevent erosion of turbines.

TECHNOLOGY TRANSFER

A Cooperative Research and Development Agreement (CRADA), entitled "Microwave Processing of Continuous Oxide Ceramic Filaments," was established with the 3M Company, a manufacturer of continuous ceramic oxide fibers. The agreement was signed on October 22, 1993. This agreement will be the direct means of transferring this microwave technology to 3M. In this second year, our activities focus on the controlled drying of the inorganic sol used to spin the inorganic filaments. We will also continue to develop methods for the controlled sintering of a prototype ceramic oxide filament. The samples of the starting sol and prefired test tows are provided by 3M for microwave processing at Los Alamos. The 3M company will play a critical role in the technology development by supplying the needed expertise in sol-gel filament preparation and characterization.

The three-year program will develop microwave techniques for the drying, burnout, and sintering of a proprietary prototype filament. The potential energy and economic advantages of microwave processing will be evaluated through direct comparison with conventional thermal processing.

As part of this CRADA, the 3M Company has loaned to Los Alamos a working spinneret with interchangeable extrusion plates. The 3M Company has also provided the starting sol and training needed to spin filaments for microwave drying experiments at Los Alamos.

TECHNICAL PROGRESS

Summary

Significant progress was made in FY95 toward controllable microwave sintering of 3M proprietary ceramic oxide filament tows and toward drying of extruded 3M sols. We have developed a hybrid microwave heating technique for the successful sintering of several different ceramic oxide filament tows. The technique can potentially be used as a universal method to sinter ceramic oxide filaments and filament tows. Also, we have designed, constructed, and operated a prototype microwave drying system for the drying of continuous filaments extruded from inorganic sols. We have successfully demonstrated the microwave drying system for the drying a single continuous filament, hundreds of meters in length. In the next year, we will improve the drying system by augmenting the humidity control and drying multiple filaments.

MILESTONES

1. We will demonstrate controlled microwave sintering of 3M proprietary filament tows, yielding a tensile strength comparable to the conventionally sintered filaments. This milestone will be completed by June 1, 1995. This milestone is critical for the production of strong and flexible filament tows.

We have developed a hybrid microwave technique to controllably sinter several different ceramic oxide filament tows. Microwave heating can be initiated without breaking the continuous filament tow or stopping the process. A microwave-driven heating zone can be maintained and propagated along continuous filaments moving through the microwave cavity. The technique can potentially be used as a universal method to sinter ceramic oxide filaments and filament tows.

Dielectric Measurements for Zirconia-based Filaments. In FY95, we collaborated with Dr. Wayne Tinga at the University of Alberta to measure the dielectric properties of the 3M zirconia-based filaments at high temperatures. The temperature dependence of the dielectric loss

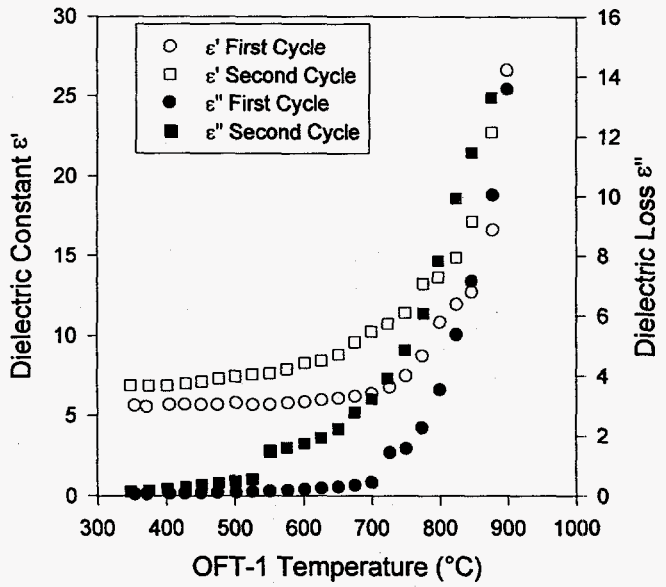

Figure 1. Dielectric constants measured at 915 MHz for a zirconia-based powder sample versus temperature measured by the control OFT. Mean sample density is 2.78 g/ml. Data for two measurement cycles are given.

as measured by Dr. Wayne Tinga appears to increase rapidly before 900°C, as seen in Figure 1. Because the temperature-dependent data do not extend beyond 900°C, we cannot speculate on how rapidly the dielectric loss increases above 1000°C.

To resolve the temperature-dependence question, dielectric measurements of fully processed zirconia-based fibers were repeated in Dr. Tinga's laboratory using a Los Alamos dual-wavelength optical fiber thermometer (OFT). Sample temperatures measured by the dual-wavelength OFT were later compared with the measured temperature from the controlling single-wavelength OFT in Dr. Tinga's dielectrometer. Figure 1 shows the temperature-dependent dielectric data for a powdered zirconia sample measured with the single-wavelength control OFT. The difference in dielectric properties between the first and second measurement cycles is due to sample sintering during the first cycle. The sample temperatures as measured by the two different OFT units are compared in Figure 2 for the powdered zirconia sample. The single-wavelength temperatures measured by the Los Alamos OFT are greater than the values from the control OFT by 100°-200°C. This variance in the temperature measurement was simply due to

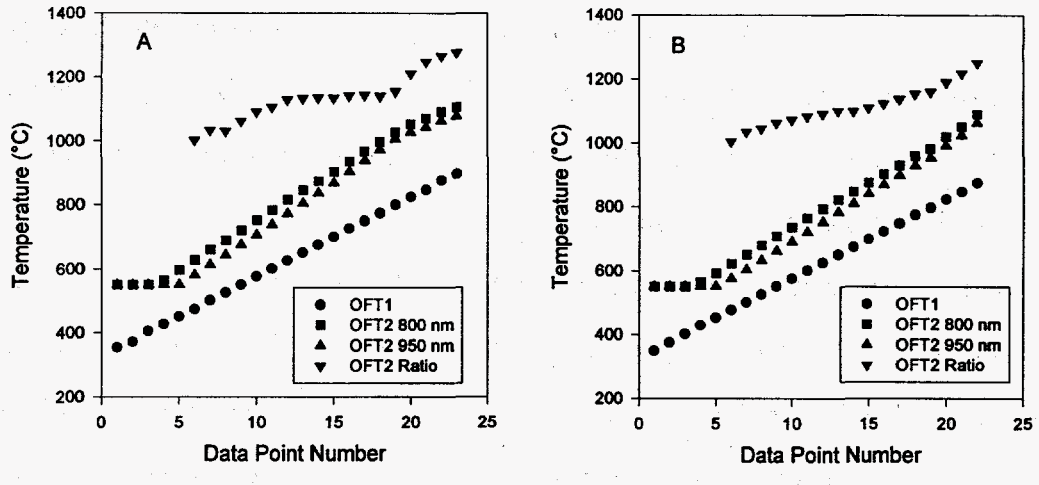

Figure 2. Measured temperatures for the zirconia-based powder sample in Figure 2 for the first (A) and second (B) measurement cycles at the same position. Data is plotted against its data point number in each measurement cycle.

distance from the hot sample to the OFT sensors. The Los Alamos sensor was closer to the hot sample than the control sensor. Whereas, the dual-wavelength temperatures from the Los Alamos OFT are even greater than the temperature values measured from the control OFT by 400°-500°C. The dielectric measurement experiment has definitely shown that the temperature from the control OFT in Dr. Tinga's dielectrometer is low by ~400C°. Analysis of the experimental setup and temperature results indicate that the temperature measurements by Dr. Tinga can be corrected by moving control OFT sensor closer to the sample or by using Accufiber pyrometer.

We cannot conclude that the dielectric data in Figure 1 should be simply shifted by ~300°-400C° to give a true picture of its temperature dependence. The dual-wavelength temperatures in Figure 2 depict a very different heating behavior for the sample than that seen from the control OFT temperatures. The dual-wavelength temperatures show little increase over the course of measurements and are nearly constant in the middle of the measurement cycle. By comparison, control OFT temperatures increased linearly and monotonically through the measurement cycle. The sample was probably experiencing non-uniform heating. The dielectrometer uses microwave power to heat the sample. Microwave heating likely began as a

small spot in the sample that grew in size with increasing power. The mean sample temperature measured by two-color thermometry would increase slowly as the spot size grew. However, the sample temperature measured by single-wavelength thermometry would increase strongly as the amount of emitted light increased with spot size.

The dielectric measurement is now difficult to interpret due to the presence of non-uniform heating. This interpretation of the sample heating behavior would suggest that the measured dielectric data is significantly less than the actual values as the dielectric measurement is designed to measure the volumetric response of the entire sample to increasing temperature. We believe that the dielectric loss data in Figure 1 corresponds to only a fraction of the entire sample.

Temperature Measurement. Routine temperature measurements of a moving filament tow are not easily made in a microwave cavity due to the presence of the electromagnetic field and to the small diameter of the heated tow. However, the Accufiber optical fiber thermometry (OFT) system has readily provided the reliable temperature measurements that we need to monitor filament heating. A sapphire OFT sensor can be precisely positioned to view the filament tow within the microwave cavity, perpendicular to the applied microwave electric field without significantly affecting the cavity resonance. Using a dual-wavelength measurement, the mean tow temperature can be measured despite the small size of the heated tow.

Late in FY94, we found a significant flaw in the Accufiber OFT system while measuring rapidly changing temperatures with the dual-wavelength mode. The Accufiber readout will drift to high temperature readings and hang up at false high temperature values while measuring rapidly changing temperatures (>100°C/min). In FY95, we shipped our OFT system to Luxtron Accufiber for hardware and software modifications to solve the system flaw. The modifications will enable the OFT unit to measure simultaneously temperatures at the 800 and 950 nm bands, rather than with the usual multiple-millisecond time delay between measurements at 800 and 950 nm. However, testing of the modified system demonstrated that the operating flaw was not

solved by the system changes. Some improvement was observed, but the problem persisted. Accufiber has no solution for this system flaw at this time.

We can still use the Accufiber OFT to measure two-color temperatures by recording the single-wavelength temperatures at the 800 and 950 nm bands during a test. The two-color temperatures can be computed from the single-wavelength temperatures after the experiment. If we should need real-time two-color temperature measurements to control heating, the temperatures can be obtained by rapidly passing the diode current values from the OFT unit to a fast personal computer that computes the two-color temperature from the OFT lookup tables.

Automatic Feedback Controller. The purpose of the electronic control system is to regulate and measure the RF power absorbed by a material placed at an electric-field maximum in a single-mode resonant cavity. The goal is to control the temperature of the fiber during processing. The controller design utilizes a traveling wave tube (TWT) amplifier as a variable frequency microwave source. Absorbed power was chosen to be the controlled variable since, in the steady state, constant absorbed power will produce a constant temperature in the fiber. To optimize RF power coupling into the fiber, a frequency control loop was also used to guarantee that the cavity remains on resonance as the fiber tow is heated. Once the feedback controller is operating correctly, we will attempt to control microwave heating of the filament tows at sintering temperatures with the feedback controller. The feedback controller can also be used with other cavity designs and heating problems.

The block diagram in Figure 3 depicts the design of the frequency control loop. A well established method is used to maintain the resonance condition in the cavity which occurs when the phase of the forward and cavity RF signals differ by $\pi/2$. A mixer is used as a phase detector which produces a DC voltage at its IF port proportional to the phase difference between its RF and LO ports. This voltage is nominally zero when the phase difference $\Delta\phi$ is $\pi/2$. A proportional, integral (PI) controller drives a voltage controlled oscillator (VCO) which shifts the output frequency of the TWT so that $\Delta\phi$ remains at $\pi/2$.

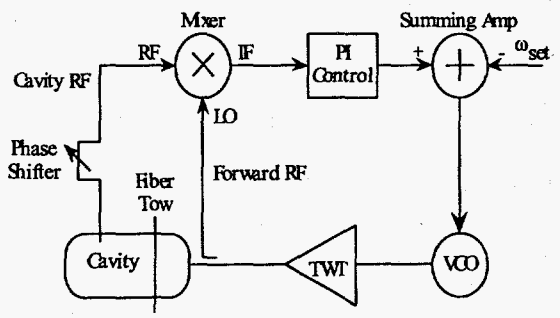

Figure 3. Control loop used to maintain cavity resonance as fiber tow is heated.

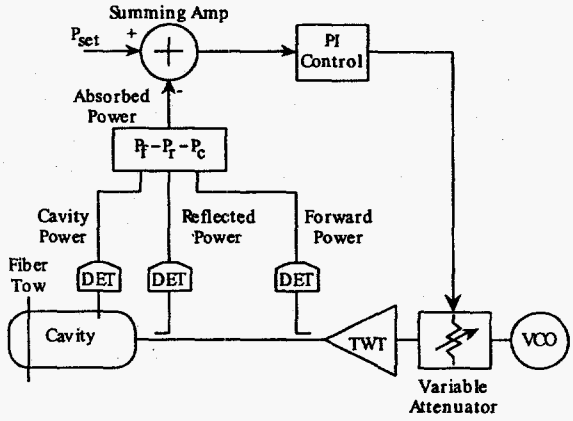

Figure 4. Control loop used to maintain constant absorbed power in the fiber tow.

The block diagram in Figure 4 shows the power control loop. Three crystal detectors (DET) are used to convert the forward (P_f), reflected (P_r), and cavity (P_c) powers to DC voltages. The signals proportional to the reflected and cavity power are then subtracted from the forward power signal. The controller circuit is calibrated to compensate for power losses to the system and cavity. The resulting signal which is proportional to the absorbed power in the fiber tow is subtracted from a set point producing an error signal. A PI controller drives a variable attenuator which modulates the forward power from the TWT so as to reduce the error signal.

A block diagram of the microwave system used to test the control loops is shown in Figure 5. The forward power (RF_f) and cavity (RF_c) signals are RF signals used for the frequency control loop. Measured by the crystal detectors (DET), the P_f, P_r, and P_c signals are DC voltages proportional to the forward power from the TWT, reflected power from the cavity, and power in the cavity, respectively. The P_f, P_r, and P_c signals are input voltages used in the power control loop. The two inputs from the control loops to the system are DC voltages used to set the VCO frequency and the forward RF power. The TWT amplifier used in the tests had an output frequency range of 2.5 to 8.0 GHz and an output power of 0-300 Watts.

The test cavity in Figure 5 was a TE_{10n} single-mode cavity, consisting of a water-cooled section of copper WR284 waveguide with a coupling iris and "beyond-cutoff" coupler at the inlet and an adjustable short. The test cavity was tuned to operate near 3 GHz. The cavity was

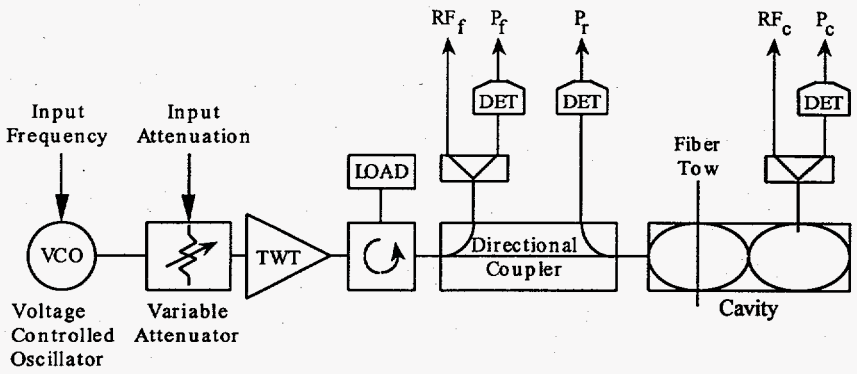

Figure 5. Block diagram of fiber tow heating system.

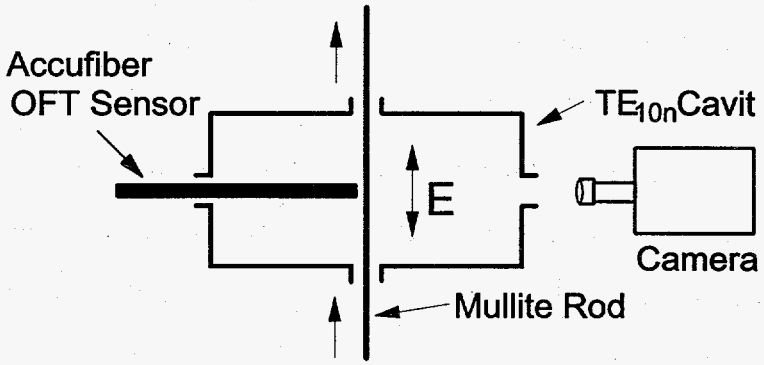

Figure 6. Cross-sectional view of the TE_{10n} cavity, showing the rod position with OFT temperature sensor and video camera.

fabricated with two pairs of opposing circular ports, as shown in Figure 6, positioned at an electric field maximum. Test samples were loaded through the paired ports aligned with the transverse electric field in the cavity. The pair of ports, perpendicular to the transverse electric field in Figure 6, provided for insertion of an Accufiber optical fiber thermometer (OFT) and for video recording of the heated sample.

The feedback controller was tested by microwave heating stationary and moving test samples to examine the ability of the controller to regulate the sample temperature. The test samples included NICALON tows, mullite rods (3-mm diameter), and mullite tubes (1.6 mm OD x 1.2 mm ID). Temperature control by the feedback controller was compared to that by manual control. Feedback controlled heating was performed with the feedback controllers outlined in

Figures 3 and 4 with rapid continual adjustment in the resonant frequency and TWT power. Manual heating conditions were set by manual control of the TWT frequency and power through a sweep generator (VCO). Manual control consisted of heating at a fixed frequency and output power from the TWT set at the beginning of the test.

The controller tested quite well with stationary NICALON tows and mullite rods. Figure 7 contrasts the time-temperature response of stationary mullite rod for feedback controlled and manually controlled heating at 2.93 GHz. As seen in Figure 7, the rod temperature under manual control drifted continually to lower values after heating the rod to temperature. The rod temperature dropped by 60°C within 10 minutes. The rod temperature under feedback control was very steady with a small drift over 8°C.

For moving samples, the controller performed poorly with no apparent improvement over manual control. Figure 8 shows the temperature-time response under feedback control for a heated NICALON tow that was pulled through the cavity at 2.0 cm/min after stationary heating for the first two minutes. The measured temperature of the moving tow varied dramatically with large swings over a 300°C range. Surprisingly, manually controlled heating produced the same large variations in measured temperature. No significant difference in the temperature variations of the moving NICALON tows were found between feedback control and manual control. Figure 9 shows the temperature-time response under manual control for a heated mullite rod that was pulled through the cavity at ~4 mm/min after stationary heating for 10 to 15 minutes. The measured temperature of the moving tow varied strongly with large changes over a 78°C range. Surprisingly, feedback controlled heating also yielded large changes in measured temperature over a 68°C range in Figure 9. Under controlled heating, the change in rod temperature was gradual without rapid swings, but still larger than the desired ±10°C range.

Video recordings of the heated samples suggest that the large variations in measured temperature could be an artifact of the temperature measurement technique. For example, video images of the 3-mm mullite rod showed that intense heating occurred only over a ~5-mm length of entire 34-mm rod length in the cavity. The heated zone on the moving rod held a roughly

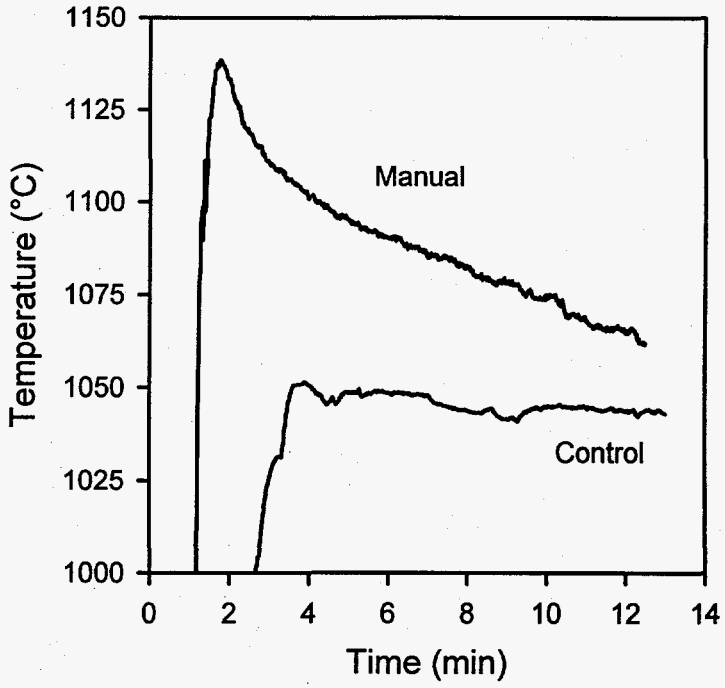

Figure 7. Mean temperature versus time for stationary mullite rod under feedback controlled heating and manual heating at 2.93 GHz.

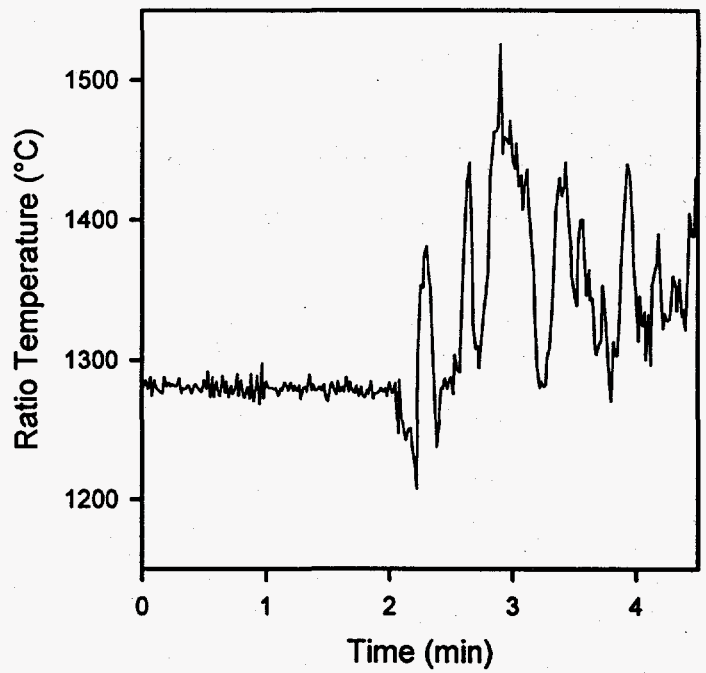

Figure 8. Measured ratio temperature versus time for a moving NICALON tow under feedback control at 2.92 GHz. Tow was pulled through cavity at 2.0 cm/min, starting at 2 minutes.

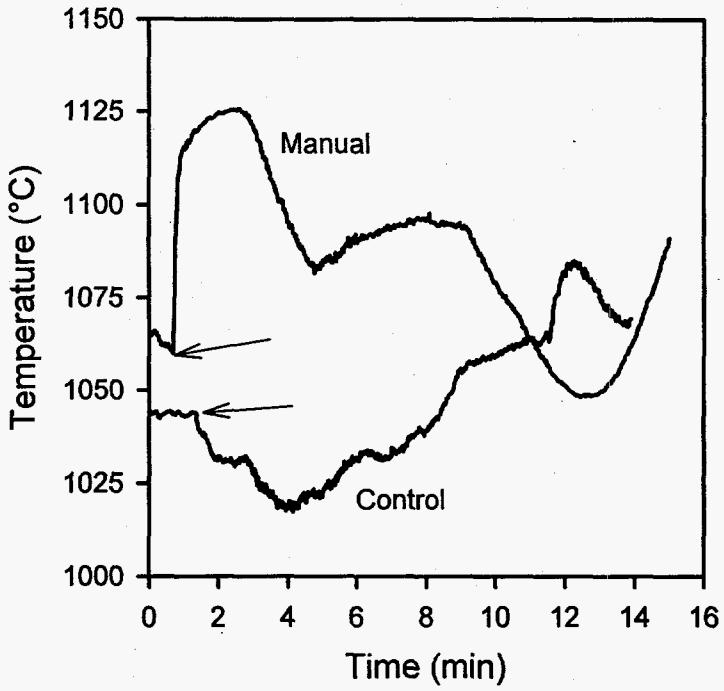

Figure 9. Mean temperature versus time for a moving mullite rod under feedback controlled heating and manual heating at 2.93 GHz. Start of pulling indicated by arrows.

steady position relative to OFT sensor with only small changes in position of ±1 mm, or less. The OFT sensor viewed only a 4-to-5 mm segment of the mullite rod and measured a mean temperature for the viewed segment. Any movement of the heated zone in or out of view by the OFT sensor could potentially induce a change in the measured mean temperature without an actual change occurring.

For the NICALON tows, only 60-70 % of the tow in the cavity was heated to radiant temperatures with no visible heating of the tow as it entered the cavity. Rapid movement of the heated zone before the OFT sensor produced large, rapid fluctuations of 200°-300°C in the measured temperature for moving NICALON tows in Figure 12. Slow movement by the heated zone in the rod experiments has certainly yielded less fluctuation in the rod temperature measurement, but did not eliminate it. For the mullite tube, only ~1-mm long segment of the tube was heated to radiant temperatures. As the tube was drawn through the cavity at 6 mm/min, the hot spot clearly traveled from out-of-view to in-view by the OFT sensor and then out again.

The measured two-color temperature of the tube correspondingly increased by 100°C and then dropped by 100°C as the hot spot moved in and out of view by the OFT sensor. The measured temperature reached a maximum when the hot spot was directly in front of the sensor.

Temperature measurements for a moving tow or rod are clearly difficult to perform with the continuous change in position of the heated zone. Therefore, we have not been able to experimentally verify that the complete control circuit performs as intended. Use of the phase lock loop in Figure 3 with another cavity has demonstrated that this part of the controller works exceptionally well. However, whether the power circuit in Figure 4 performs as designed has yet to be clearly demonstrated.

Further testing of this feedback control scheme will continue to eliminate the fluctuations in the temperature measurement. A photodiode with a large viewing angle will be used as an alternate sensor to test the feedback controller.

2. We will demonstrate controlled microwave drying of 3M proprietary filament tows to a water content comparably found in conventionally dried filaments. This milestone will be completed by September 30, 1995.

A prototype microwave drying cavity was successfully designed, built, and operated for the drying of a continuous sol fiber extruded from a 3M proprietary inorganic sol. A single fiber can be spun and continuously dried at moderate spinning rates to produce commercial lengths of fiber. Work will continue into the third year toward controlling the cavity humidity and drying multiple fibers.

3. We will develop a numerical model for thermal and mass transfer in the microwave drying of ceramic oxide filament tows. This milestone will be completed by July 1, 1995.

A simple generic drying model was constructed for a non-porous fiber, employing guesstimates of the necessary material properties. A numerical model for microwave drying can greatly aid process development by assisting experimental design and interpreting experimental

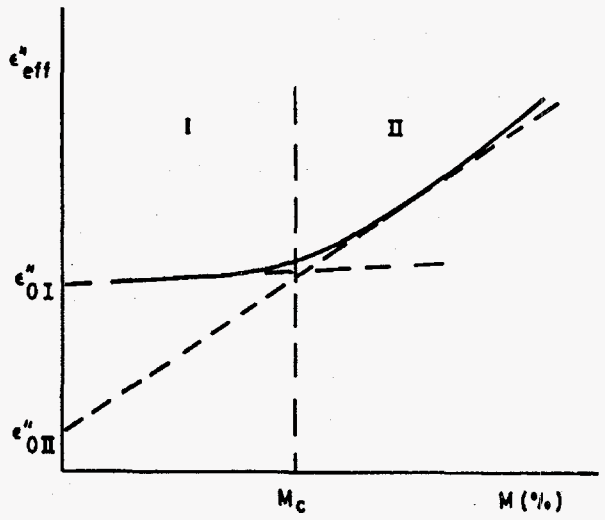

Figure 10. Typical loss factor ε″of a wet solid as a function of the water content M. Taken from Metaxas & Meredith, 1983.

results. To construct a realistic model of filament drying, we need information on the basic thermodynamic and transport properties of the sol. Several essential properties include the complex dielectric constant, thermal conductivity, diffusion coefficient of water, and sorption isotherm of the sol. Moreover, these specific properties will have a strong functional dependence on the water content of the sol. For the proprietary alumina sol, there is no available data on these thermodynamic and transport properties. We have estimated the integral diffusion coefficient of water in the starting sol by thermogravimetric experiments of the integral weight loss curve measured during evaporation of water from the sol. However, we are not able to measure other properties due to time and proprietary constraints. Approximate property values can be derived from known properties of similar materials.

A critical property needed in modeling is the dielectric loss of the sol, as microwave power absorption within the sol is proportional to the dielectric loss. Although the dielectric loss of water is well known as function of temperature and frequency, dielectric loss of absorbed water is significantly different, considerably lower than that for pure water with a strong dependence on water content. Figure 10 shows the qualitative variation in dielectric loss ε″ with water content M of a typical wet solid, taken from Metaxas & Meredith (Industrial Microwave

Heating, 1983). Above a critical water content M_c, free water resides in capillaries and pores, designated as region II in Figure 10. Here the dielectric loss decreases rapidly with M. Below M_c, water is either physically absorbed or chemically bound to the solid matrix of the sol. In this region I, the dielectric loss changes slowly with M. This typical dependence on water content is responsible for the water leveling behavior of microwave heating. Wetter regions in the wet solid will have a greater dielectric loss and a greater heating rate than drier regions. Therefore, microwave heating will level water throughout the solid matrix to a uniform distribution.

PUBLICATIONS

1. G.J. Vogt, W.R. Tinga, and R.H. Plovnick, "Dielectric Property Measurement of Zirconia Fibers at High Temperatures," in the symposium proceedings Microwaves: Theory and Application in Materials Processing III, 1995 Spring Meeting of the American Ceramic Society, April 30-May 4, 1995, Cincinnati, Ohio.
2. G.J. Vogt, A. Regan, A. Rohlev, and M.T. Curtin "Use of a Variable Frequency Source with a Single-Mode Cavity to Process Ceramic Filaments," in the symposium proceedings Microwaves: Theory and Application in Materials Processing III, 1995 Spring Meeting of the American Ceramic Society, April 30-May 4, 1995, Cincinnati, Ohio.
3. G.J. Vogt, A. Regan, A. Rohlev, and M.T. Curtin "Use of a Variable Frequency Source with a Single-Mode Cavity to Process Ceramic Filaments," in the proceedings of the International Conference on Microwave and High Frequency Heating, September 17-21, 1995, Cambridge University, Cambridge U.K.

PRESENTATIONS

1. G.J. Vogt, W.R. Tinga, and R.H. Plovnick, "Dielectric Property Measurement of Zirconia Fibers at High Temperatures," oral presentation to Symposium Microwaves: Theory and

Application in Materials Processing III, 1995 Spring Meeting of the American Ceramic Society, April 30-May 4, 1995, Cincinnati, Ohio.

2. G.J. Vogt, A. Regan, A. Rohlev, and M.T. Curtin "Use of a Variable Frequency Source with a Single-Mode Cavity to Process Ceramic Filaments," oral presentation to Symposium Microwaves: Theory and Application in Materials Processing III, 1995 Spring Meeting of the American Ceramic Society, April 30-May 4, 1995, Cincinnati, Ohio.

3. G.J. Vogt, "Microwave Processing of Oxide Ceramic Filaments," poster presentation to the First Industrial Energy Efficiency Symposium and Expo, sponsored by OIT, May 1-3, 1995, Washington, D.C.

4. G.J. Vogt, J.D. Katz, A.H Regan, and A.S. Rohlev, "Microwave Processing of Ceramic Oxide Filaments," poster presentation to the Annual Meeting for the Advanced Industrial Materials (AIM) Program, June 14-16, 1995, Washington, D.C.

5. G.J. Vogt, A. Regan, A. Rohlev, and M.T. Curtin "Use of a Variable Frequency Source with a Single-Mode Cavity to Process Ceramic Filaments," oral presentation to the International Conference on Microwave and High Frequency Heating, September 17-21, 1995, Cambridge University, Cambridge U.K.

HONORS AND AWARDS

"Recognition Of Excellence *in achieving* Industrial Partnerships" award, Los Alamos National Laboratory, Industrial Partnership Office, October, 1995.

PATENTS/DISCLOSURES

None (one in progress).

LICENSES

None.

INDUSTRIAL INPUT AND TECHNOLOGY TRANSFER

We have a CRADA with the 3M Company for the microwave processing of continuous ceramic oxide filaments. The CRADA was signed by Los Alamos and the 3M Company in October, 1993. The project is sponsored by the Advanced Industrial Materials Program, DOE-OIT.

The Los Alamos poster presented at the First Industrial Energy Efficiency Symposium and Expo generated an industrial contact with Babcock & Wilcox. We are currently performing microwave heating tests on Babcock & Wilcox filaments to evaluate the feasibility of microwave heating for the material. If the filament material can be controllably heated with microwaves, we hope to start an industrial collaboration with Babcock & Wilcox.

HIGHLIGHTS.

1. A hybrid microwave heating technique was developed for the microwave sintering of continuous ceramic oxide tows. The technique can potentially be used as a universal method to sinter many different types of ceramic oxide filaments and filament tows.

2. A prototype microwave drying system has been designed, constructed, and operated for the drying of continuous filaments extruded from inorganic sols. The prototype microwave drying system has been successfully demonstrated for the drying a single continuous filament, hundreds of meters in length.

SELECTIVE INORGANIC THIN FILMS

Mark L. F. Phillips, Lori A. Weisenbach, Teresa V. Bohuszewicz,
Phillip I. Pohl, Carol S. Ashley, and C. Jeffrey Brinker
Sandia National Laboratories
Albuquerque, NM 87185

Sinclair S. Yee and Kyle S. Johnston
Department of Electrical Engineering
University of Washington
Seattle, WA 98195

INTRODUCTION

This project is developing inorganic thin films for gas separation membranes and discriminating coatings for liquid-phase chemical sensors. Our goal is to synthesize these coatings with tailored porosity and surface chemistry on porous substrates and on optical sensors. Molecular sieve films offer the possibility of performing separations involving hydrogen, air, and natural gas constituents at elevated temperatures with very high separation factors. We are focusing on improving permeability and molecular sieve properties of crystalline zeolitic membranes made by hydrothermally reacting layered multicomponent sol-gel films, clays, and metals deposited on mesoporous substrates. We also used surface plasmon resonance (SPR) sensor elements as substrates for sol-gel films, and have used these modified sensors to determine physical properties of the films and the sensitivity and selectivity of these sensors to aqueous chemical species.

TECHNICAL PROGRESS

Molecular Sieve Films:

A porous film in which gas permeation is restricted through zeolite crystals would act as a molecular sieve membrane, separating gas molecules based on their kinetic diameters. Gas molecules smaller than the critical pore diameter in a zeolite crystal are allowed to permeate; larger molecules are completely rejected. This feature leads to obvious advantage in such processes as separation of methane from hydrogen or higher alkanes. For example, a zeolite film with a pore diameter of 4.1 Å (such as Linde Type A or LTA) would effectively separate methane (kinetic diameter = 3.8 Å) from propane or higher alkanes (C_3H_8 diameter = 4.3 Å). This type of separation is difficult in polymer membranes, in which differences in gas solubility and diffusivity among alkanes tend to cancel each other out. Also, zeolites can be stabilized to function at temperatures as high as 1000 °C, so that gas separation can be carried out in high-temperature

processes such as petroleum and natural gas refining. A membrane capable of efficiently recovering H_2 (2.9 Å) from CH_4 at 500 °C would yield very significant energy savings. Separating methane from N_2, CO_2 and H_2S at the wellhead would substantially increase natural gas production.

The choice of zeolitic phase is very important to the performance of the membrane and is specific to several parameters, particularly the molecular diameters of the gases being separated and their temperature. For separating light, "fixed" gases, the range of useful pore diameters is approximately 3-6 Å. Permeabilities, and thus separation factors, are very strongly affected by changes in pore opening within this range. For example, the 3 Å ring opening in the sodalite (SOD) structure allows significant permeability only to He (2.65 Å), while the 7.4 Å ring opening in faujasite (FAU) can reject only large, branched aliphatics or high aromatics. Examples of zeolitic phases that have been sought as films for molecular sieve membranes include LTA and ZSM-5, due to their pore sizes and high degree of internal connectivity. This project has emphasized synthesis of LTA films, principally because many methods are available for producing bulk LTA, and because the pore diameter of this phase is readily tuned through post-synthesis ion exchange. For example, the pore opening of sodium LTA is 4.1 Å in diameter, while the diameters of the pore openings of potassium- and calcium-exchanged LTA are approximately 3.3 Å and 4.5 Å, respectively.

To be industrially useful, a zeolite membrane must consist of a zeolitic film deposited onto a porous substrate, such as an alumina gas filter. Certain technical criteria must be met before such membranes will be commercially acceptable. It is believed that the zeolitic films should be very thin (500 Å or thinner) to achieve reasonable gas flow rates. Since the crystallite size of typical commercial zeolites is ca. 1-5 μm, and the films must be at least one crystal thick, such a requirement becomes a significant technical challenge. In addition, the films must completely cover a porous support in order to demonstrate any selectivity based on molecular sieving, and the films must be thermally durable enough to withstand high operating temperatures and calcination.

A number of researchers had synthesized zeolitic films prior to the initiation of this project [1]. Many of these films have been made by directly depositing zeolite crystals from a nutrient solution onto the substrate, yielding a coating that consists of layers of crystals directly adhering to one another on top the surface. Others were made by growing zeolite crystals within the voids of porous substrates. Most of these previously reported films are at least several μm thick, which limits their permeability, and they tended to crack or peel during calcination due to thermal

expansion mismatch between the film and the substrate. Much of the available data indicate that these films do not exhibit true molecular sieving character (i.e., they leak). Some attempts have been made at using organic polymers to "caulk" the films in order to inhibit leakage [2]. Caveats in this approach include permeation of gas through the polymer, obstruction of the zeolite pores, and degradation of the polymer at even moderate temperatures (>150 °C).

In FY94 we devised a new approach in which zeolite crystals are nucleated from bilayer sol-gel films rather than from solution. These films are made by sequentially spin-coating silicoaluminate and alkali alkoxide (e.g., sodium isopropoxide) sols onto an inert substrate, such as silicon. Upon exposing this bilayer film to pressurized steam, nucleation and growth of zeolite crystals occurs at the interface. The resulting composite film consists of a single layer of zeolite crystals contained within the unreacted sol-gel phase. The thickness of the crystals can be approximately limited to that of the film (ca. 0.5 μm), so that membranes can be made an order of magnitude thinner than any zeolite membranes previously reported. The flexibility of the amorphous residue allows the film to be heated (to densify the sol-gel film and calcine the zeolite) without cracking or peeling. If the residue can be densified to eliminate residual porosity, it can be used to eliminate leaks through gaps between crystals. This "brick and mortar" composite structure appears to be a unique approach to the synthesis of molecular sieve films.

In FY95 we studied experimental factors influencing crystal growth, and successfully nucleated zeolite crystals from sol-gel films deposited onto mesoporous alumina membrane tubes. We also made permeation measurements that showed selectivity better than that of the uncoated membrane (Knudsen separation via 40 Å pores), indicating that complete substrate coverage has been attained. However, these results also show residual pores too large to be attributable to zeolites, so the mortar phase has not been completely densified. We have also synthesized LTA membranes from kaolin films deposited onto porous alumina disks, and have demonstrated that these films can be calcined without cracking. In addition, we used Sandia's Intel Paragon massively parallel supercomputer to perform diffusion calculations that show LTA to be ideal for separating light gases of interest.

Sensor Coatings: The project continued to evaluate amorphous sol-gel coatings as discriminating elements in surface plasmon resonance (SPR)-based liquid phase chemical sensors intended for real-time analysis and process monitoring. Development of a method for using SPR to simultaneously determine refractive index, porosity, and thickness of sol-gel films was completed. Sol-gel coatings improved the signal stability of fiber optic SPR probes. A phase detection

technique was tested, and found to enhance SPR signal resolution. Also, a method for chemically derivatizing Au films to enhance sensor sensitivity and specificity was successfully tested on fiber optic SPR probes.

Milestones

1.1. Synthesis of continuous zeolitic films on porous supports:

The goal of this project element is to produce supported membranes with a high density (percentage of total surface coverage) of very thin (< 1 μm thick) crystals of a desirable zeolite phase, surrounded by a continuous nonporous glassy phase. This is achieved by depositing layers of aluminosilicate "nutrient" and alkali alkoxide "template" sols onto a mesoporous gas membrane tube, allowing the film to nucleate in a humid atmosphere, crystallizing the film in steam, then heating the film to calcine the zeolite and densify the residual sol-gel film to a glass. Because there are no sources of silica or alumina nutrient outside the film, the thickness of the zeolite crystals is ideally limited to approximately that of the initial film (ca. 500 nm). Synthesis of composite zeolitic membranes is made challenging by the daunting number of reaction parameters that control the quality of the films. These include, but may not be limited to, nucleation time, reaction time, nucleation temperature, reaction temperature, pH (or Na/Al ratio), concentration of mineralizer (such as F^-), substrate pore diameter, order of film layer deposition, age of sol before deposition, age of film before crystallization, and coating method (spin vs. dip).

Key results of the parameterization experiments discussed in our FY94 report are summarized here. In general, reaction parameters must be modified if the films are to be dip coated (necessary for tubular membranes) rather than spin coated (adequate for flat substrates). This is because dip-coating allows diffusion of Na ions into the aluminosilicate layer, which may inhibit nucleation by decreasing the Na concentration at the layer interface. Films must be aged in water vapor at moderate temperature (ca. 50 °C) in order to nucleate zeolite crystals. Crystallization is accomplished by heating the membranes in steam at 100 °C. Because a fluoride ion mineralizer is required to accelerate crystallization, the water supplying the steam contains a small amount of ammonium fluoride. The data obtained from these experiments allowed us to improve dip coating technique and reaction conditions to the point where thin, continuous films containing zeolite crystals were obtained on mesoporous membrane supports.

Permeability data are essential to determine if the membranes are truly continuous (leak-free), and to ensure that the zeolite crystals are free to allow gas flow from the surface to the support without obstruction from residual sol-gel material. The selectivity of the underivatized

alumina support is characteristic of Knudsen diffusion, that is, the permeabilities of different gases through the membrane are related by the square root of the ratio of their molecular weights. Separation factors greater than those of Knudsen diffusion indicate that complete coverage has been attained, and that the pore size of the membrane is smaller than that of the underivatized support (which is 40 Å). This condition has been attained in membranes made by hydrothermally crystallizing a bilayer film (Figure 1).

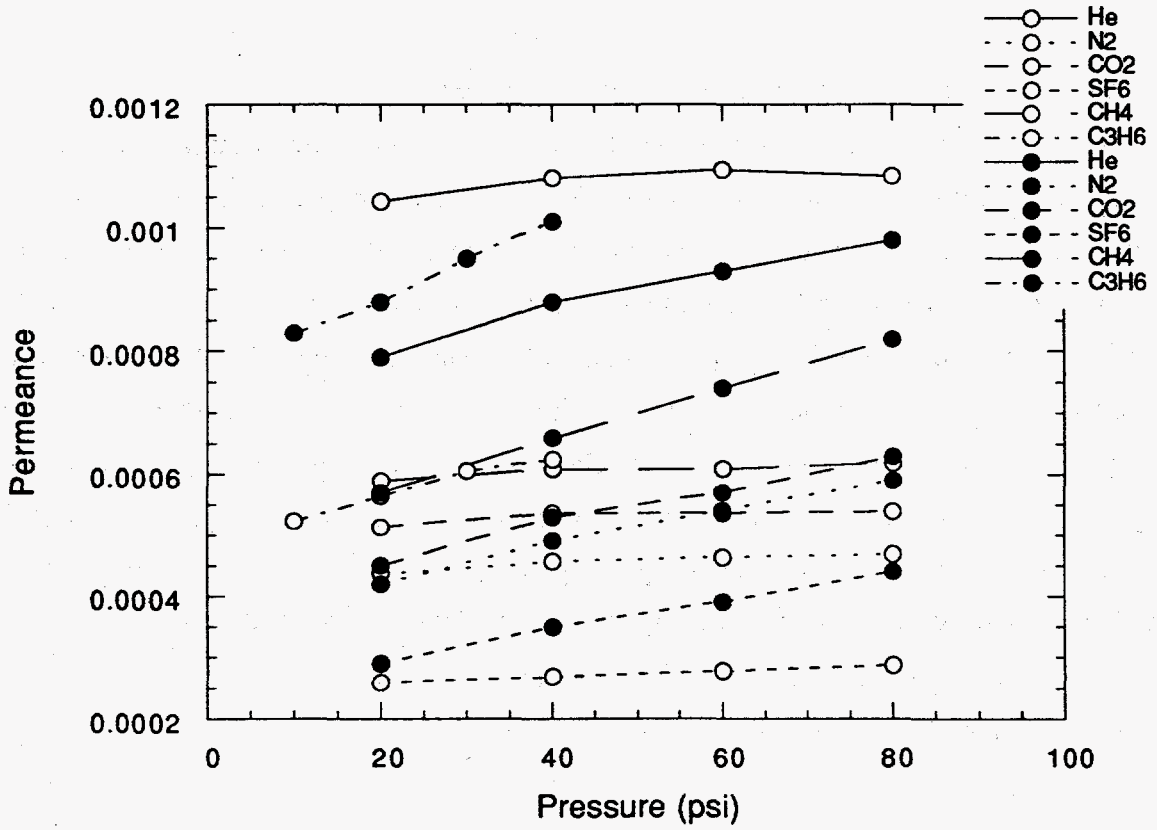

Figure 1: Permeation results for two γ–Al_2O_3 membrane tubes (U.S. Filter) coated with sol-gel derived zeolite films. The permeance values for the first tube (open circles) are characteristic of Knudsen diffusion. The values for the second tube (filled circles) reflect better separation than from Knudsen diffusion alone.

While it is possible that molecular sieving may be improving membrane performance, the data in Figure 1 are also consistent with interactions between the walls of pores in the residual sol-gel film and adsorbate gas molecules. This would indicate that this residual amorphous film is not being completely densified by the post-crystallization heat treatment (500 °C for 1 hour). The films may withstand being heated to higher temperatures without peeling, but the γ–Al_2O_3 support

begins to degrade at temperatures significantly greater than 500 °C. We are currently attempting to "caulk" mesoporosity in the amorphous phase by coating the membrane with a silica sol that is readily densified at moderate temperatures (< 400 °C).

As we obtain membranes with molecular sieving behavior, their permselectivities will be measured at elevated temperatures (up to 500 °C) at Golden Technologies. We will also continue to study the chemistry of sol-gel film crystallization to better define zeolite phase space in bilayer films.

1.2. Synthesis of zeolite membranes from supported clay films:

Zeolite A (LTA), is a very useful molecular sieve for separating light gases due to its interconncented pore structure and pore size (see Section 1.3). This phase can be made from kaolin by converting it to metakaolinite, then treating with aqueous sodium hydroxide.[3] In the most elementary process for making LTA membranes in this fashion, kaolinite is dry-pressed or slip-cast into a disc, which is then sintered to yield amorphous metakaolinite. The disc surface is then converted to LTA by aging at room temperature with aqueous NaOH, then heating to 100 °C in a steam atmosphere. The average pore size of the clay discs was determined to be approximately 15 nm, so the discs themselves are in principle sufficiently permeable to act as the porous film support. However, we have found it advantageous to use porous alumina supports prepared for us by Golden Technologies; these are made by sintering pellets of isostatically pressed α–Al_2O_3. These supports are coated with kaolinite by slip-casting; the pellets are then heated to convert the kaolinite film to metakaolinite, and hydrothermally crystallized to yield LTA films as described above.

We have constructed an apparatus for measuring gas permeabilities through underivatized and zeolite-coated metakaolinite-alumina discs. A kaolinite film with no cracks or pinholes seen in the scanning electron microscope (SEM) was subjected to permeation measurement. The gas permselectivity measurements showed no viscous flow, confirming the lack of macroscopic defects. The temperature trends and relative flow rates of the different gases indicated a combination of Knudsen diffusion and surface flow. When a similar film was fully converted to LTA, however, SEM data revealed the possibility of intercrystalline gaps; this was confirmed by permeation results. The flow through the membrane increased in proportion to the average pressure of the gas, which is characteristic of viscous flow (no gas separation).

In order to improve the selectivity of these membranes, we attempted to caulk the intercrystalline gaps with a nonporous sol-gel film. A zeolite-clay film was dip-coated with a sol

composed of 3-methacryloxypropyltrimethoxysilane (MPS) and tetraethylorthosilicate (TEOS) to yield a layer ca. 2500 Å thick. Similar films used on other membranes have shown virtually no gas permeation to 150 °C. The zeolite membrane thus coated showed no viscous flow, but the dependence of permeance on temperature appears similar to that of the pure clay film. It is possible that the sol seeped through the pores in the zeolite film, rather than filling these pores.

The composite organic-inorganic MPS-TEOS sol is probably ideal for caulking defects of an intermediate scale (10-100 nm). This sol may also caulk larger holes if sol viscosity and coating rates are increased; these experiments are in progress. Larger holes have been repaired using solutions of RTV silicone, though this method is less than ideal for membranes that will be used at high temperatures (> 200 °C). We are also attempting to repair defects and fill intercrystalline voids using successive deposition of a clay or sol-gel nutrient film, followed by hydrothermal processing. This method uses the zeolite crystals already in the membrane as seeds; growth of the seeds should narrow intercrystalline gaps to less than ca. 10 nm, where application of silica sol can completely densify the membrane surface. At this point, permselectivities of these membranes will be measured at elevated temperatures by Golden Technologies.

1.3. Diffusion modeling: In order to predict the performance of films of various zeolite phases as molecular sieve membranes, we have made preliminary calculations of the relative flow rates of permeate gas molecules through several zeolites. Phillip Pohl (Dept. 6626, SNL) and Grant Heffelfinger (Dept 1421, SNL) have calculated activation energy barriers to diffusion in order to determine the optimum zeolite ring opening diameter for separating small, fixed gases [4]. The phases considered here include sodalite (SOD), Linde Type A (LTA), Linde Type N (LTN), and faujasite (FAU), which had all been synthesized as films as part of this project. SOD was of particular interest in this study because unlike true zeolites, it can be synthesized in the absence of water. A SOD film might be synthesized by annealing a sol-gel precursor film without going through a hydrothermal step, which would greatly facilitate membrane processing.

The energy profiles of CH_4, N_2, and H_2 were determined for the 6-oxygen atom rings of sodalite (SOD) and LTN, the 8-ring of Zeolite A (LTA), and the 12-ring of faujasite (FAU). There is a barrier to diffusion for each gas through the 6-ring of SOD, with the greatest barrier for methane. In contrast, through LTA and FAU there is an energy well, which is deepest for N_2 (Figure 2). Little or no diffusion would be expected through SOD and LTN, while FAU would effect poor separation for the three gases. LTA, however, seems to have the appropriate pore size to separate the 3 gases studied via molecular sieving. In comparison with O_2, the more prolate N_2

should have greater difficulty in passing through the 8-ring of LTA, which may account for the ability of this phase to separate O_2 from N_2.

Since it is generally accepted that the chemical potential gradient is the true driving force for diffusion, diffusion driven by a chemical potential gradient was modeled in SOD, LTA and FAU using grand canonical molecular dynamics (GCMD). The fluid-fluid and fluid-wall interactions were modeled with the cut and shifted Lennard-Jones potential. The cut-off distance was taken to be $\sigma^{1/6}$ for all interactions, and the Lennard-Jones parameters were taken from the recent literature. The 184,000 wall atoms (only oxygen atoms at present, which were not allowed to move) were positioned according to the published zeolite coordinates. Using CH_4, N_2 and He as the permeate species, only He showed appreciable diffusion through the pores in SOD and LTN. A SOD film is thus probably out of the question as a molecular sieve membrane. For LTA, all three gases showed significant diffusion, with He showing the greatest movement.

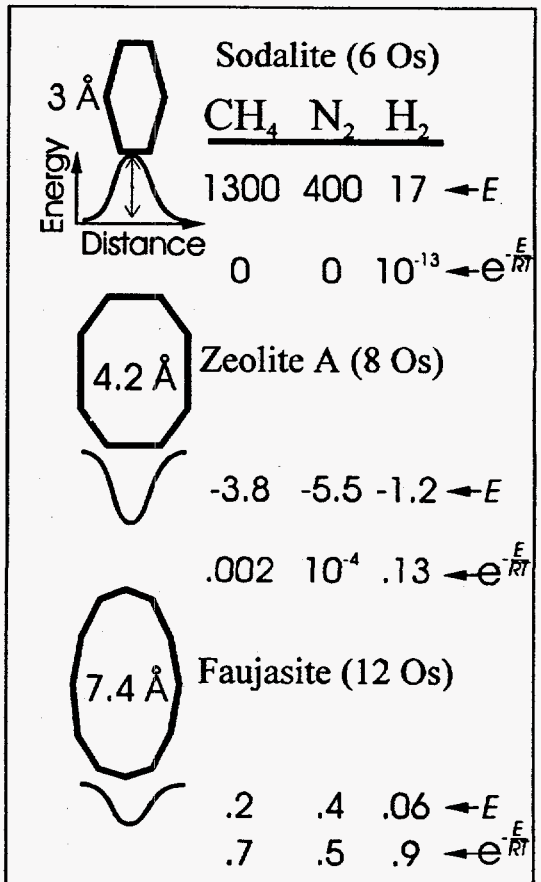

Figure 1 Energy Profile (Kcal/mol) and Exponential for Gas Diffusion [1]

These results help confirm our assumption that LTA is the optimum zeolite phase for a molecular sieve film. Further work on a 200,000 atom simulation using Sandia's Intel Paragon massively parallel supercomputer is in progress, and membrane permeability simulations containing contributions from microporosity (zeolites) and mesoporosity (uncrystallized sol-gel film) are planned for FY96.

Impact: The petroleum and natural gas refining industries would significantly benefit from high permeability molecular sieve films capable of separating light, fixed gases, particularly if the membranes can be used at high temperatures. With sufficiently high permeability and low unit area cost, energy savings of several quad/yr could be achieved.[5] We believe that with appropriate stabilization, such as dealumination or rare earth exchange, composite zeolite films such as those we are developing can be made stable up to 1000 °C.

4. Film characterization using SPR: The goals of this project are develop surface plasmon resonance (SPR) as a liquid phase sensor technique for environmental and process monitoring, and as a tool for measuring physical properties of porous thin films such as thickness, refractive index, and porosity. Environmental, industrial process, and biomedical sensor technologies based on SPR would have several practical advantages over conventional analytical methods. In particular, SPR probes can be manufactured at very low cost, they can be made environmentally robust, multiple SPR probes can be used simultaneously with a single analysis module, and most importantly, *in situ* process and environmental measurements can be made in real time.

A surface plasmon wave is a charge density wave that propagates along the interface between a metal (such as Ag or Au) and a dielectric (such as air or water). In a SPR sensor, the metal is deposited as a film upon a glass substrate, such as glass plate [6] or a fiber optic cable [7]. When light propagating through the glass is totally internally reflected from the surface supporting the metal film, the evanescent electric field associated with the beam couples with an allowed surface plasmon wavevector in the film, resulting in resonance. The allowed wavevectors, and thus the spectrum of transmitted light, are determined by the thickness and refractive index of the dielectric surrounding the metal film.

In FY95 Sandia and the University of Washington demonstrated that the sensitivity and specificity of a SPR probe can be improved by depositing a sol-gel derived film onto the metal film in which resonance occurs. A high-index film improves the sensitivity of the probe to small changes of refractive index in low-index media such as water. A film that is chemically specific to solution species of interest (e.g., metal ions) will change its index reversibly upon sorption and desorption of the species. We have also developed a technique for simultaneously determining wavelength dispersive refractive index and thickness of films using SPR measurements alone. If refractive index has been determined independently (e.g., via ellipsometry) it is possible to measure percent porosity of a film if the pores are filled with a fluid of known index. We have also determined that it is possible to optimize the sensitivity of a SPR sensor to a particular range of liquid refractive indices by coating it with a sol-gel film of the appropriate thickness or index. If several sensors are simultaneously used with films of different thicknesses or indices, a sensor array can be constructed that will be sensitive over a wide range of refractive indices.

In addition to using sol-gel films to tailor effective refractive index, improvements in SPR sensitivity were obtained by modifying the geometry of the sensor head; three Technical Advances

have been filed. This technology is being transferred to Texas Instruments, where it is being adapted for use as a gas phase sensor.

This project investigated new designs for phase-sensitive detection (PSD) of a surface plasmon resonance (SPR) signal. In principle, PSD should improve the dynamic range, sensitivity and resolution of refractive index sensors. Three different designs for PSD of the SPR signal were considered. The optical designs of each configuration are based on the use of a laser source and a single angle of incidence on a prism sensor with a Ag film. The optical signal is detected by a single photodiode or a diode array. The first and simplest design investigated is an interference configuration where the signal consists of the amplitude of the interference of the TM and TE polarization modes. The second and third configurations consist of direct measurements of the phase change between the two modes. For each design concept, mathematical models already developed were modified to predict the sensor response in both selectivity and dynamic range.

To test the performance of the new SPR configurations, varied concentrations of glycerol in water were pumped through a flow cell attached to the sensor. This caused the SPR signal to change with the refractive index of the solution. Once the thickness of the Ag film was adequately modeled, the experimental and theoretical sensitivity values coincided. The dynamic range of the interference configuration is similar to that of the standard SPR geometry (described in earlier reports), while the resolution is improved. By using a reference photodetector to measure the TE, the resolution could be improved by one-third.

Experiments in functionalizing SPR fiber-optic probes also continued in collaboration with Prof. Charles Campbell of the Department of Chemistry at UW. As a prelude to studying the cesium selectivity of crystalline silicotitanate (CST) films under development at Sandia, the sensitivity and stability of fiber-optic probes were characterized, both as bare Au probes and as probes derivatized with alkyl thiols. The main focus of studies has been to identify and analyze stability problems that exist with the fiber optic SPR probe. The probes were calibrated by immersion in ethanol-toluene solutions with known indices of refraction; these indices were then correlated with the SPR wavelength measured for each solution. The results so far show that the probe can be very stable, and gives detection limits of ca. 10^{-5} index of refraction units if the temperature is controlled to better than $\pm$ 0.1 °C and the probe is kept in the same solution for long periods. This sensitivity is sufficient to see analyte adsorption, even with very small molecules. However, serious drift problems sometimes occur whenever the probe is removed from solution even temporarily.

Additional experiments were performed to study the functionalization of the probe with thiols. So far the probe has been functionalized with 1-decanethiol, 11-mercaptoundecanoic acid and octyldecylmercaptan. The binding of these thiols to the gold surface have been analyzed with the SPR instrument, scanning tunneling microscopy (STM) and time-of-flight secondary ion mass spectrometry (TOF-SIMS). SPR results obtained after the probe was functionalized with 1-decanethiol (which binds very strongly to Au) prove that the interfacial alkyl thiol chain does not adversely affect the sensitivity or stability of the probe. Preliminary experiments also demonstrated the ability of a probe functionalized with mercaptoundecanoic acid ($HS\text{-}(CH_2)_{10}\text{-}CO_2H$) to reversibly bind and detect triethylamine ($(CH_3)_3N$) in aqueous solution. These results show that the stability and sensitivity of the SPR system is adequate for tests with antigen- and CST-derivatized fiber optic probes.

To increase the number of functional groups attached to the surface of the probe, which increases the sensitivity of the probes, we are now coating the probe surface with a highly porous sol-gel silica film. Once the SPR response of these probes is sufficiently characterized, we will apply silane coupling agents that will functionalize the surface of the SiO_2, similar to the thiol functionalization of the gold surface. We expect that the chemically bonded functional groups will be more robust (and thus more easily reused in an analytical environment) that the chemisorbed thiols.

Impact: If appropriately derivatized films for SPR sensors can be developed, this technique will have a significant impact on the markets for real-time industrial process monitoring and biomedical sensing. Energy savings resulting from use in monitoring metal concentrations in industrial processes have been estimated at 0.01 quad/yr. If SPR sensors can be used as *in situ* waste stream and environmental monitors, this technology could save millions of dollars in analytical costs.

References:

1. *a.* Anderson, M. W.; Pachis, K. S.; Shi, J.; Carr, S. W. *J. Mater. Chem.* **1992**, *2*, 255-6. *b.* Geus, E. R.; den Exter, M. J.; van Bekkum, H. *J. Chem. Soc. Faraday Trans.* **1992**, *88*, 3101-3107. *c.* Davis, S. P.; Borgstedt, E. V. R.; Suib, S. L. *Chem. Mater.* **1990**, *2*, 712-719. *d.* Tsikoyiannis, J. G.; Haag, W. O. *Zeolites* **1992**, *12*, 126-130. *e.* Suzuki, H. *U.S. Patent* 4,699,892. *f.* Ma, Y. H.; Xiang, S. *U. S. Patent* 5,258,339.

2. te Hennepe, H. J. C.; Bargeman, D.; Mulder, M. H. V.; Smolders, C. A. *J. Membr. Sci.* **1987**, *35*, 39.

3. L. V. C. Rees and S. Chandrasekhar, *Zeolites* **1993**, 524.

4. P. I. Pohl and D. M. Smith, *Mater. Res. Soc. Symp. Proc.* **1995**, *371,* 27. G. S. Heffelfinger, P. I. Pohl, and L. J. D. Frink, *Mater. Res. Soc. Symp. Proc.* **1995**, *366,* 225.

5. D. E. Fain, *MRS Bulletin* April 1994, p. 40.

6. E. Kretschmann, *Z. Phys.* **1971**, *241,* 313.

7. R. C. Jorgensen and S. S. Yee, *Sensors and Actuators B* **1995**, *12,* 213-220.

PUBLICATIONS

S. R. Karlsen, K. S. Johnston, R. C. Jorgenson, and S. Yee, "Simultaneous Determination of Refractive Index and Absorbance Spectra of Chemical Samples Using Surface Plasmon Resonance", *Sensors and Actuators B* **1995**, *24-25,* 747-749.

K. S. Johnston, S. R. Karlsen, C. Jung, and S. Yee, "New Analytical Technique for Charaterization of Thin Films Using Surface Plasmon Resonance", submitted to Materials Chemistry and Physics.

S. Karlsen, K. S. Johnston, S. Yee and C. Jung, "First Order Surface Plasmon Resonance Sensor System Based on A Planar Lightpipe", *Sensors and Actuators B*, in press.

Master's Thesis

K. S. Johnston, "Characterization of Porous Thin Films Using Surface Plasmon Resonance", University of Washington, Dec. 1994 .

PRESENTATIONS

B. G. Karle, M. L. F. Phillips, and C. J. Brinker, "Study of the Process of Conversion of Kaolin to Zeolite A", Materials Research Society (NM Section), Albuquerque, NM, Oct. 1994.

M. L. F. Phillips et al., "Selective Inorganic Thin Films", Advanced Industrial Materials Annual Review, Washington, DC, June 1995.

S. Karlsen, K. S. Johnston, S. Yee and C. Jung, "First Order Surface Plasmon Resonance Sensor System Based on A Planar Lightpipe", The 1994 International Conference on Electronic Materials (ICEM '94), National Chiao Tung University, Hsinchu, Taiwan, December 1994.

HONORS AND AWARDS: None during this reporting period.

PATENTS/DISCLOSURES

Technical Advance UW 12-94-150, "Surface Plasmon Sensors and Modulators Using Phase Detection", S. Yee, C. Jung, K. Johnston, and S. Karlsen, Dec. 1994.

Technical Advance UW 12-94-149, "Two-dimensional Surface Plasmon Resonance (SPR) Multiplexing Planar System", K. Johnston, S. Karlsen and S. Yee, Dec. 1994.

Technical Advance UW 01-94-06, "Surface Plasmon Resonance Based Dispersion Sensor", Inventors: S. Karlsen, K. Johnston, S. Yee, R. Jorgenson, Oct. 1994.

LICENSES: None during this reporting period.

INDUSTRIAL INPUT AND TECHNOLOGY TRANSFER

Golden Technologies, Inc., is providing the mesoporous gas membranes that we are using as supports for our zeolite films. They have also agreed to measure permselectivities of the resulting supported membrane at elevated temperatures (up to 600 °C). Texas instruments is developing a SPR gas sensor system in conjunction with the University of Washington.

HIGHLIGHTS

- We have deposited a continuous zeolite films onto porous membrane tubes, yielding gas permselectivities better than those available from the substrate alone. This indicates that the effective pore diameter in these films is less than 40 Å.
- We have prepared zeolite films on porous substrates from clay precursor films. These films contain no macroscopic defects even after calcination, though caulking will be required to obtain molecular sieving.
- We tested a surface plamon resonance sensor configuration with improved resolution, and demonstrated improved chemical selectivity on a fiber optic SPR device following chemical derivatization.

INTERNAL DISTRIBUTION

1-2. Central Research Library
3. Document Reference Section
4-5. Laboratory Records Department
6. Laboratory Records, ORNL RC
7. ORNL Patent Section
8-10. M&C Records Office
11. D. J. Alexander
12. K. B. Alexander
13. L. F. Allard
14. P. Angelini
15. B. R. Appleton
16. G. Aramayo
17. R. L. Beatty
18. P. F. Becher
19. T. M. Besmann
20. P. J. Blau
21. E. E. Bloom
22. C. A. Blue
23. R. A. Bradley
24. C. R. Brinkman
25. T. D. Burchell
26. G. M. Caton
27. N. C. Cole
28. K. M. Cooley
29. R. H. Cooper, Jr.
30. D. F. Craig
31. S. A. David
32. R. B. Dinwiddie, Jr.
33. J. R. DiStefano
34. D. S. Easton
35. Z. Feng
36. M. K. Ferber
37. A. T. Fisher
38. E. L. Fuller, Jr.
39. E. P. George
40. G. M. Goodwin
41. H. W. Hayden, Jr.
42. L. L. Horton
43. J. A. Horton, Jr.
44. C. R. Hubbard
45. M. A. Janney
46. D. R. Johnson
47. R. R. Judkins
48. M. A. Karnitz
49. J. R. Keiser
50. E. A. Kenik
51. H. D. Kimrey, Jr.
52. R. J. Lauf
53. E. Lee
54. C. T. Liu
55. Gail M. Ludtka
56. Gerald M. Ludtka
57. P. J. Maziasz
58. A. D. McMillan
59. P. A. Menchhofer
60. K. L. More
61. R. K. Nanstad
62. T. A. Nolan
63. A. E. Pasto
64. F. L. Paulauskas
65. S. J. Pawel
66. K. P. Plucknett
67. M. L. Santella
68. A. C. Schaffhauser
69. J. H. Schneibel
70. V. K. Sikka
71. P. S. Sklad
72. S. Spooner
73. R. W. Swindeman
74. B. Taljat
75. R. L. Thomas
76. T. N. Tiegs
77. S. Viswanathan
78. J. M. Vitek

79. M. A. Wall
80. X. L. Wang
81. S. B. Waters
82. H. W. Foglesong (Consultant)
83. E. L. Menger (Consultant)
84. J. G. Simon (Consultant)
85. K. E. Spear (Consultant)
86. T. Zacharia (Consultant)

EXTERNAL DISTRIBUTION

87-88. ABB CE Services, Combustion Engineering, Inc., 911 West Main Street, Chattanooga, TN 37402

Domenic Canonico
Mark LeBel

89. Advanced Refractory Technologies, Incorporated, 699 Hertel Avenue, Buffalo, NY 14207

Keith A. Blakely

90. Alabama Pine Pulp Company, Inc., Po. O. Box 100, Perdue Hill, AL 36470

Sunil Chandnani

91-92. Alfred University, Center for Advanced Ceramic Technology, Alfred, NY 14802

Richard M. Spriggs
Harrie J. Stevens

93. Allegheny Ludlum Steel Corporation, Research Center, Alabama & Pacific Avenue, Brackenridge, PA 15014

Gerald L. Houze, Jr.

94. Allied-Signal Aerospace Company, Garrett Ceramic Components Division, 19800 S. VanNess Avenue, Torrance, CA 90509

Maxine L. Savitz

95. Allied-Signal, Incorporated, Ceramics Program, P.O. Box 1021R, Morristown, NJ 07960

Clifford P. Ballard

96-97. Alloy Engineering and Casting Company, 1700 West Washington Street, Champaign, IL 61821

Barry L. Fritz
James R. Lytle

98. Aluminum Company of America, Government Marketing, 1615 "M" Street, NW, Washington, DC 20036

Pam Patrick

99. Andritz Sprout Bauer, Sherman Street, Muncy, PA 17756

Ronald L. Musselman

100. Argonne National Laboratory, 9700 South Cass Avenue, Argonne, IL 60439

William A. Ellingson

101. Army Materials Technology Laboratory, Watertown, MA 37919

Robert N. Katz

102. Army Research Office, P.O. Box 12211, Research Triangle Park, NC 27709

Andrew C. Crowson

103. Babcock & Wilcox, 1562 Beeson Street, Alliance, OH 44601-2196

Joan Varna

104. Babcock & Wilcox, 2302 Parklake Drive, NE, Suite 300, Atlanta, GA 30345

Robert Larsen

105-107. Babcock & Wilcox, 20 S. Van Buren Avenue, P.O. Box 351, Barberton, OH 44203-0351

Joan Barna
John Clement
J. William Smith

108. Battelle, 505 King Avenue, Columbus, OH 43201-2693

Jeffrey Colwell

109-111. Battelle Pacific Northwest Laboratories, Department of Materials Science, P.O. Box 999, Richland, WA 99352

G. L. Graff
Gary L. McVay, K2-45
B. J. Tarasevich

112. Bethlehem Steel Corporation, Homer Research Laboratories, Bethlehem, PA 18016

Charles R. Beechan

113. Bethlehem Steel Corporation, P.O. Box 248, Chesterton, IN 46304

Anthony Simola

114-115. Black & Decker, Incorporated, 701 East Joppa Road, TW 460, Towson, MD 21286

Nick Achterberg
Stephen R. Crosby

116-118. Boeing Aerospace, Material Lobby, Renton, WA 98124-2499

K. Y. Blohowiak, Building 7-20, Mail Stop 73-09
Thomas S. Luhman, Building 7-20, Mail Stop 73-09
M. S. Strasik, Building 7-20, Mail Stop 73-09

119-120. Bowater, Inc., 5020 Highway 11, South, Calhoun, TN 37309

John E. Griffey
LeRoy Hershey

121. Carpenter Technology Corporation, 92 Burning Tree Lane, Reading, PA 19607

Robert L. Caton

122-123. Carpenter Technology Corporation, 101 West Bern Street, P.O. Box 14662, Reading, PA 19612-4662

Bradford A. Dulmaine
Nicholas Fiore

124. Caterpillar, Incorporated, Engineering and Research Materials, Technical Center, Building E, P.O. Box 1875, Peoria, IL 61656-1875

Michael H. Haselkorn

125. Ceracon, 1101 North Market Street, Suite 9, Sacramento, CA 95834

Henry S. Meeks

126. Ceradyne, Incorporated, 3169 Redhill Avenue, Costa Mesa, CA 92626

Joel P. Moskowitz

127-129. Ceramatec, Incorporated, 2425 South 900 West, Salt Lake City, UT 84119

Raymond Cutler
Ronald S. Gordon
David W. Richerson

130. Champion International Corporation, W. Nyack Road, W. Nyack, NY 10994

Dave Bennett

131-132. Corning Corporation, Sullivan Park FR-02-5, Corning, NY 14831

Thomas P. DeAngelis
Frank E. Murphy, Jr.

133-135. Cummins Engine Company, Incorporated, P.O. Box 3005, Columbus, IN 47202-3005

Michael C. Brands, Mail Code 50165
Magan J. Patel, Mail Code 50183
James W. Patten, Mail Code 50183

136. Delta M Corporation, 525 Warehouse Road, Oak Ridge, TN 37830

Reginald W. McCulloch

137-138. Dow Chemical Company, Incorporated, 1776 Building, Midland, MI 48674

David A. Dalman
Richard D. Varjian

139. Dynamet Technology, Incorporated, 8 "A" Street, Burlington, MA 01803

Walter Bergler

140. Eaton Corporation, Corporate Research & Development, Milwaukee, Center, 4201 North 27th Street, Milwaukee, WI 53216

John W. Kroll

141. Eaton Corporation, 4010 North 27th Street, Milwaukee, WI 53216

Henry Kunsmann

142-143. Electric Power Research Institute, Nuclear Plant Corrosion Control, 3412 Hillview Avenue, Palo Alto, CA 94303

Ben Banerjee
Mohamad M. Behravesh

144. Electric Power Research Institute, 2000 L Street, Suite 805, Washington, DC 20036

W. Eugene Eckhart

145. Energetics, Incorporated, 7164 Gateway Drive, Columbia, MD 21046

Aziz Azimi

146. EXXON R&D Labs, P.O. Box 2226, Baton Rouge, LA 70821

R. C. Schucker

147-148. FM Technologies, Incorporated, Patriot Square, 10529-B Braddock Road, Fairfax, VA , 22032

I. Ahmad
Richard S. Silberglitt

149. Ford Motor Company, 35500 Plymouth Road, Box 13, Lovonia, MI 48150

Mark G. Shapona

150-154. Ford Motor Company, P.O. Box 2053, Dearborn, MI 48121-2053

John E. Allison, Mail Drop 3182
William E. Dowling, Jr., Room S2065
Norman A. Gjostein, Mail Drop 2247/SRL
Gorton M. Greene
Kenneth Hass, Room S3028

155. Ford Motor Company, P.O. Box 1899, Room 354, Dearborn, MI 48121

Vello Arrak

156. Foster Wheeler Development Corporation, 12 Peach Tree Hill Road, Livingston, NJ 07039

Jeffrey L. Blough

157. General Electric Company, Research & Development, Met Building, Room 263, P.O. Box 8, Schenectady, NY 12301

Alan I. Taub

158-159. General Electric Company, One Newmann Way, Cincinnati, OH 45215

Ram Darolia, Mail Drop M-89
James Williams, Mail Drop H-85

160. General Motors Corporation, 1660 L Street N.W., Suite 400, Washington, DC 20036

Bo Campbell

161-164. General Motors Corporation, AC Rochester, 1300 North Dort Highway, Flint, MI 48556

R. F. Beckmeyer
Lawrence A. Carol
W. LaBarge
Carl E. Miller

165-171. General Motors Corporation, 30500 Mound Road, Warren, MI 48090-9055

M. S. Rashid
Edward F. Ryntz
James G. Schroth
Michael M. Shea
Susan Smyth
Charles S. Tuesday
Peter Vernia

172-176. General Motors Corporation, Saginaw Division, 3900 Holland Road, Saginaw, MI, 48601-9494

Steven L. Avery
Randy P. Bal
J. Fargo
Jerry D. Jablonski
Charles R. Martin

177. General Motors Powertrain Division, 895 Joslyn Road, Pontiac, MI 48340-2920

Robert Wiltse

178-181. General Motors Powertrain Division, 1629 North Washington Avenue, Saginaw, MI, 48605-5073

Ron Cafferty
Paul N. Crepeau
Mark E. Hoover
Dennis Meyers

182. General Motors Tech Center, Composite Section Manufacturing Building, A/MD-24, 30300 Mound Road, Warren, MI 48090-9040

I. E. Poston

183-187. George Mason University, 4400 University Drive, Fairfax, VA 22030

W. M. Black
R. F. Cozzens
H. S. Sa'adaldin
T. H. Shan
T. L. Tian

188-193. Georgia Institute of Technology, School of Materials Engineering, 778 Atlantic Drive, Atlanta, GA 30332-0245

Steve Antolovich
W. Brent Carter
Joe K. Cochran, Jr.
S. Lee
Thomas L. Starr
S. R. Stock

194. Georgia-Pacific Corp., 133 Peachtree Street, N.E., 11th Floor, Atlanta, GA 30303

Karl T. Morency

195-197. Golden Technologies Company, Incorporated, Research & Development, 17750 West 32nd Avenue, Golden, CO 80401

Rick Kleiner
Dean Rulis
Jack Sibold

198. T. M. Grace Company, Incorporated, 2517 S. Harmon Street, Appleton, WI 54915

Thomas Grace

199. Herty Foundation Development, P.O. Box 7798, Savannah, GA 31418

James Anderson

200. Hoskins Manufacturing Company, 10776 Hall Road, Hamburg, MI 48139

Forrest Hall

201-203. Hughes Research Laboratories, 3011 Malibu Canyon Road, Malibu, CA 90265

Jesse Matossian
John McLendon
Robert Schumacher

204-206. Idaho National Engineering Laboratory, EG&G Idaho, P.O. Box 1625, Idaho Falls, ID 83415-2218

Elmer Fleischman
D. Kunerth
E. S. Peterson

207-211. Institute of Paper Science & Technology, Inc., 500 10th Street, N.W., Atlanta, GA 30318

Jefferey A. Colwell
Maclin S. Hall
Robert H. Horton
Thomas McDonough
Dave Orloff

212. International Paper, P. O. Box 160707, Mobile, AL 36616

Russell S. Andrews

213. International Paper, Paper Mill Road 36610, P. O. Box 2787, Mobile, AL 36652-2787

Subhash Pati

214-220. Iowa State University, Ames Laboratory, 126 Metals Development Building, Ames, IA 50011

L. Carson
L. S. Chumbley
D. C. Jiles
H. Mahmood
K. L. Pauwels
P. P. Pulvirenti
R. Bruce Thompson

221. James River Corporation, P.O. Box 2218, Richmond, VA 23217

Ronald Estridge

222-223. James River Corporation, 1915 Marathon Avenue, P. O. Box 899, Neenah, WI 54957-0899

Dave Clay
Bill Steed

224. John Hopkins University, Center for Nondestructive Evaluation, Maryland Hall 107, Baltimore, MD 21218

Robert E. Green, Jr.

225-226. Johnson Controls, Inc., 507 East Michigan Street, P.O. Box 423, Milwaukee, WI 53201

Carl F. Klein
Bryan L. McKinney

227. Kaiser Aluminum & Chemical Corporation, P.O. Box 870, Pleasanton, CA 94566

S. C. Carniglia

228-229. Kvaerner Pulping, 8008 Corporate Center Drive, Charlotte, NC 28226

Joe Barsin
Bo O. Oscarsson

230-233. Lawrence Berkeley Laboratory, 1 Cyclotron Road, Mail Stop 90-2024, Berkeley, CA 94720

M. Ayers
Arlon J. Hunt
P. Stevens
S. Zheng

234-237. Lawrence Livermore National Laboratory, P.O. Box 808, Livermore, CA 94550

M. Fluss, Mail Stop L-326
D. L. Haupt, Mail Stop L-326
John H. Kinney, Mail Stop L-356
Jeffery Wadsworth, Mail Stop L-353

238-254. Los Alamos National Laboratory, P.O. Box 1663, Los Alamos, NM 87545

P. G. Apen, D453
A. H. Bartlett, MST-6, MS K762
D. P. Butt, G755
R. G. Castro, G770
David J. Devlin, E549
Elliott P. Douglas, E549
Frank D. Gac, G756
Shimshon Gottesfeld, D429
P. J. Hay, B268
K. J. Hollis, G770
J. D. Katz, G771
H. H. Kung, K765
R. Leipens, E549
R. LeSar, K765
John J. Petrovic, G771
A. Redondo, D429
K. N. Siebien, MST-7, MS E549
Gerald J. Vogt, G771

255-256. MTCI, 5570 Sterrett Place, Suite 20, Columbia, MD 21044

Amal Mansour
Momtaz Mansour

257. MacMillan Bloedel Packaging, Inc., Hwy 10, P. O. Box 336, Pine Hill, AL 36769

Wallace Baxter

258. Metallamics, Inc., P.O. Box 1539, Traverse City, MI 49684

Robert R. McDonald, President

259. National Aeronautics & Space Administration, Materials & Structures Division, Code RM, 600 Independence Avenue, S.W., Washington, DC 20546

Samuel L. Venneri

260. National Aeronautics & Space Administration, Lewis Research Center, 21000 Brookpart Road, MS: 49-1, Cleveland, OH 44135

Joe Stevens

261. National Forge Company, Irvine, PA 16329

Ashok Khare

262-264. National Institute of Standards and Technology (NIST), Gaithersburg, MD 20899

Edwin R. Fuller, Jr., Ceramics Division, Room, A256, Building 223
Richard E. Ricker, Depart. of Commerce, Materials Bldg., Room B254
Lyle Schwartz, Director

265-270. National Renewable Energy Laboratory, 1617 Cole Boulevard, Golden, CO 80401-3393

Helena L. Chum
Robert J. Evans
Gregory Glatzmaier
Neil Kelley
Stephen S. Kelley
R. Meglen
K. Tatsumoto

271-272. National Science Foundation, Metallurgy Section, 1800 "G" Street, N.W., Washington, DC 20550

Bruce A. MacDonald
Robert Reynik

273. Naval Research Laboratory, Building 43, Room 212, Code 6000, 4555 Overlook Avenue, SW, Washington, DC 20735-5341

Bhakta B. Rath

274. North Carolina A&T State University, Department of Mechanical Engineering, Greensboro, NC 27411

V. S. Avva

275-276. North Carolina State University, Department of Materials Science and Engineering, Box 7907, Raleigh, NC 27695-7907

Carl C. Koch
Nkadi Sukidi

277. Norton Company, Goddard Road, Northboro, MA 01532-1545

Normand D. Corbin

278. Parsons and Whittemore, Inc., Atlanta Office, P. O. Box 637, Clarkston, GA 30021

Adam Melton

279. Parsons and Whittemore, Inc., Monroeville Office, P. O. Box 65, Perdue Hill, AL 36470

Adam Melton

280. Pask Research and Engineering, Berkeley, California 94720

Antoni P. Tomsia

281-282. Precision Castparts Corporation, 4600 SE Harney Drive, Portland, OR 97206-0898

David A. Chang
Larry J. Watland

283. Pulp and Paper Research Institute of Canada, Vancouver Laboratory, 3800 Westbrook Mall, Vancouver, B.C. V6S 2L9

Doug L. Singbeil

284. Rapid Technologies, Incorporated, P.O. Box 368, 170 Werz. Ind. Blvd., Newnan, GA 30264

Ed Dailey

285-286. Rennsselaer Polytechnic Institute, School of Engineering, Materials Engineering Department, 8th Street, Troy, NY 12180-3590

N. S. Stoloff

287. Reynolds Metal Company, P.O. Box 1200, Shefield, AL 35660

Nolan E. Richards

288-294. Sandia National Laboratories, Division 8361, P.O. Box 969, 7011 East Avenue, Livermore, CA 94551-0969

Mark D. Allendorf
S. M. Ferko
S. Griffiths
Donald R. Hardesty
R. Nilson
T. H. Osterheld
N. Yang

295-308. Sandia National Laboratory, 1515 Eubank, S.E., Albuquerque, NM 87185-5800

C. S. Ashley, Division 1846, Mail Stop 1405
T. V. Bohuszewicz, Mail Stop 1349
C. J. Brinker, Division 1846, Mail Stop 0607
Gary Carlson, Division 6211, Mail Stop 0710
B. Damkroger
Bob Eagan, Division 1800
Kevin G. Ewsuk, Division 1849, Mail Stop 0609
Kay Hays, Mail Stop 1709
K. S. Johnston
J. B. Kelley, Division 1833, Mail Stop 1134
Mark L. F. Phillips, Divison 1846, Mail Stop 0607
P. I. Pohl, Division 6626, Mail Stop 0720
R. D. Skocypec, Division 1513, Mail Stop 0835
Alan P. Sylwester, Division 6203, Mail Stop 0749
S. S. Yee

309-311. Sandia National Laboratory, University of New Mexico, Advanced Materials Laboratory 1708, 1001 University Boulevard, SE, Suite 100, Albuquerque, NM 87106

W. G. Fahrenholtz
Ronald E. Loehman
A. P. Tomsia

312. Sandusky International, 615 W. Market Street, Box 5012, Sandusky, OH 44871-8012

Charles W. Rainger

313. Sandvik Steel Co., P. O. Box 1220, Scranton, PA 18501-1220

Jim Noble

314-315. Stone Container Corporation, 8170 South Madison Street, Burr Ridge, IL 60521

Max Moskal
Chuck Timko

316. TRW, Incorporated, 23555 Euclid Avenue, Cleveland, OH 44117

A. L. Bement, Jr.

317. Tampella Power Corporation, 2300 Windy Ridge Parkway, Suite 1125, Atlanta, GA 30339

Markku Isoniemi

318. Tennessee Technological University, Center for Manufacturing Res. & Tech. Util. College of Engineering, P.O. Box 5014, Cookeville, TN 38505

Joseph T. Scardina

319-320. The Carborundum Company, P.O. Box 187, Keasbey, NJ 08832

Craig L. Dillman
Stanley Gursky

321. The Carborundum Company, P.O. Box 832, Niagara Falls, NY 14302

Monika O. Ten Eyck

322. The Timken Company, 1835 Dueber Avenue, S.W., Canton, OH 44706-2798

Robert L. Leibensperger

323-327. The Pennsylvania State University, Department of Materials Science and Engineering, Metals Science and Engineering Program, 221 Steidle Building, University Park, PA 16802

John Hellman
Paul R. Howell
George L. Messing
William A. Pratt
Richard E. Tressler

328-329. The University of Tennessee, Department of Materials Science & Engineering, Knoxville, TN 37996-2200

C. R. Brooks
Ben F. Oliver

330. Thermo-Chem, Incorporated, 5570 Sterrett Place, Suite 210, Columbia, MD 21044

David A. Scearce

331. Thermo Electron Technologies, 85 First Avenue, Waltham, MA 02254

Peter Reagan

332-333. U.S. Air Force, Wright Patterson AFB, Dayton, OH 45433-6533

Dennis M. Dimiduk, WRDC Material Laboratory
Allan Katz, AFWAL/MLLM Material Laboratory

334-358. U.S. Department of Energy/Headquarters, 1000 Independence Avenue, SW, Washington, DC 20585

L. Boxall, EE-234, 5F-059/FORS
B. Cranford, EE-222, 5F-043/FORS
Sidney Diamond, EE-34, 5G-064/FORS
Sara Dillich, EE-232, 5F-059/FORS
Russell Eaton, III, EE-142, 6H-034/FORS
T. D. Foust, EE-222, 5F-043/FORS
Marvin E. Gunn, Jr., EE-14, 6H-034/FORS
M. P. Hoffman, GC-62, 5F-043/FORS
Douglas E. Kaempf, EE-234, 5F-043/FORS
S. R. Leonard, EE-222, 5F-043/FORS
William P. Parks, Jr., EE-221, 5F-035/FORS
Marsha L. Quinn, EE-223, 6H-034/FORS
Scott L. Richlen, EE-221, 5F-035/FORS
V. T. Robinson, HR-422, 100 H ST
Peter H. Salmon-Cox, EE-23, 5F-059/FORS
Robert B. Schulz, EE-34, 5F-064/FORS
M. A. Smith, EE-222, 5F-035/FORS
Charles A. Sorrell, EE-232, 5F-059/FORS
Alan J. Streb, EE-20, 6B-052/FORS
Denise F. Swink, EE-20, 6B-052/FORS
B. G. Volintine, EE-233, 5F-059/FORS
Daniel E. Wiley, EE-233, 5F-059/FORS
F. W. Wilkins, EE-222, 5G-067/FORS
Stanley M. Wolf, EM-542, 413/TREV
H. Wong, EE-233, 5F-059/FORS

359-363. U.S. Department of Energy, 19901 Germantown Road, Germantown, MD 20585

James P. Carr, FE-72, 3035/270
Robert J. Gottschall, ER-131, J-322/GTN
Helen Kerch, ER-131, J-322/GTN
F. W. Wiffen, ER-533, G-258/GTN

364. U.S. Department of Energy/Albuquerque, P.O. Box 5400, Albuquerque, NM 87115

D. Morton

365. U.S. Department of Energy/Oak Ridge, Building 4500N, Mail Stop 6269, P.O. Box 2008, Oak Ridge, TN 37831-6269

Mary Rawlins

366. U.S. Department of Energy/Idaho, 785 Dow Place, Idaho Falls, ID 83402

Joanne Malmo

367. U.S. Department of the Interior Bureau of Mines, 2401 "E" Street, NW, Washington, DC 20241

Garrett R. Hyde

368. Union Camp Corporation, Research and Development Division, P. O. Box 3301, Princeton, NJ 08543-3301

Dave Crowe

369. United Technologies Research Center, East Hartford, CT 06108

Vincent C. Nardone

370. University of Alabama, Metal Casting Technology Center, P.O. Box 6374, Tuscaloosa, AL 35487

Thomas S. Piwonka

371-372. University of Cincinnati, Department of Materials Science & Engineering, 412B Rhodes Hall, Cincinnati, OH 45221-0012

J. A. Sekhar
Vijay K. Vasudevan

373-374. University of Maine, 5737 Jenness Hall, Orono, ME 04469-5737

Joseph Genco
Marquita Hill

375. University of Missouri School of Mines & Met., Ceramic Engineering, 120 Fulton Hall, Rolla, MO 65401-0249

Robert E. Moore

376. University of New Mexico, Albuquerque, New Mexico 87106

William Fahrenholtz

377. University of Pennsylvania, Department of Mechanical Engineering, 111 Towne Building, 220 South 33rd Street, Philadelphia, PA 19104-6315

David Pope

378. University of Utah, Electrical Engineering Department, Salt Lake City, UT 84112

M. Iskander

379. Vander Linden & Associates, 5 Brassie Way, Littleton, CO 80123

Carl R. Vander Linden

380-381. Virginia Polytechnic Institute and State University, Department of Materials Engineering, Blacksburg, VA 24061

J. J. Brown
K. L. Reifsnider

382. Westinghouse R&D, 1310 Beulah Road, Pittsburgh, PA 15235

Garth Clarke

383-384. Westvaco, Laurel Technical Center, 11101 Johns Hopkins Road, Laurel, MD 20723-6006

Lad Falat
W. B. A. (Sandy) Sharp

385. Weyerhaeuser Paper Company, Columbus Pulp and Paper Complex, P. O. Box 1830, Columbus, MS 39703-1830

Joe May (cc/Jim Noles)

386-387. Weyerhaeuser Paper Company, Research and Development, WTC 2H22, Tacoma, WA 98477

Peter Gorog
Dick Shenk

388. Worcester Polytechnic Institute, Department of Mechanical Engineering, 100 Institute RJ, Worcester, MA 01609

Robert N. Katz

389. 9208 Burning Tree Road, Bethesda, MD 20817

Samuel Goldberg

390. 14390 W. 30th Avenue, Golden, CO 80401

David G. Wirth

391. 3M Industrial & Electronic Sector, Research Laboratory, Building 201-4N-01, 3M Center, St Paul, MN 55144-1000

Ross H. Plovnick

392-401. Department of Energy, Office of Scientific and Technical Information, Office of Information Services, P.O. Box 62, Oak Ridge, TN 37831

For distribution by microfiche as shown in DOE/OSTI-4500, Distribution Category UC-310 [Industrial Programs (General)]